RESPONSE OF CONTINUOUS PIPELINES TO TUNNEL INDUCED GROUND DEFORMATIONS

by

Evangelia S. Ieronymaki

B.A., MSc Civil Engineering (2007),
MSc in "Analysis & Design of Earthquake Resistant Structures" (2008)

National Technical University of Athens

Submitted to the Department of Civil and Environmental Engineering
in Partial Fulfillment of the requirements for the Degree of
Master of Science in Civil and Environmental Engineering

at the

Massachusetts Institute of Technology

June 2011

Signature of Author.....
Department of Civil and Environmental Engineering
May 20, 2011

Certified by.....
Andrew J. Whittle
Professor of Civil and Environmental Engineering
Thesis Supervisor

Accepted by.....
Heidi M. Nepf
Chair, Departmental Committee for Graduate Students

RESPONSE OF CONTINUOUS PIPELINES TO TUNNEL INDUCED GROUND DEFORMATIONS

by

Evangelia S. Ieronymaki

Submitted to the Department of Civil and Environmental Engineering
on May 20, 2011 in Partial fulfillment of the
requirements for the Degree of Master of Science in
Civil and Environmental Engineering

ABSTRACT

This thesis develops analytical solutions for estimating the bending moments and axial loads in a buried pipeline due to ground movements caused by tunnel construction in soft ground. The solutions combine closed-form, analytical solutions for tunnel-induced, free-field ground deformations in a plane orthogonal to the heading (Pinto and Whittle; 2001) with Winkler models for pipe-soil interactions. The free-field ground deformations are described in terms of two parameters describing the modes of cavity deformation and the elastic Poisson's ratio of the ground. The solutions have been evaluated by others through comparisons with well-instrumented case studies for a variety of different tunneling construction methods and ground conditions. Analytical approximations for the vertical and horizontal spring stiffness coefficients in the Winkler models are interpreted from numerical finite element analyses. The proposed analyses are compared with prior solutions proposed by Vorster (2005) and Klar et al. (2005) that rely on empirical procedures to estimate the ground deformations and focus only on bending response of the pipeline. The current research provides independent validation of the vertical spring coefficient proposed by Klar et al., and derives a novel interpretation of the horizontal spring coefficient.

Results of the proposed analyses are presented graphically in design charts that show the deformations of the pipeline as functions of the pipe and tunnel geometry, tunnel cavity parameters, elastic properties of the ground and relative pipe-soil rigidity parameters. The solutions are used to re-analyze the deformations of a water main associated with a pipe-jacking procedure at an instrumented site in Chingford, London reported by Vorster (2005). The thesis also presents a hypothetical example that considers the impacts of the construction of a large-diameter sewer tunnel in soft clay using EPB construction methods (using free-field performance data from the N-2 project in San Francisco) on existing utilities. In this case, potential damage to cast-iron water pipes is clearly linked to the pipe section properties and the EPB tunnel face pressure. Data from well-documented case studies must now be obtained to validate the proposed analyses.

Thesis Supervisor: Andrew J. Whittle
Professor of Civil and Environmental Engineering

ACKNOWLEDGMENTS

By completing the current master thesis, I would like to thank those people who helped me, each in her/his own way, to achieve this goal.

First of all, I would like to thank my advisor, Professor Andrew Whittle. His in-depth knowledge and experience in civil engineering inspired me and helped me cope with several issues that arose during my research. His constant help, support and guidance throughout my studies at MIT are invaluable and I especially appreciate it.

Special thanks to Yixing Yuan and Dimitris Niarchos, for the time they spent helping and supporting me when my research progress was slower than desired. I also thank Despina Zymnis for generously giving me data from her own thesis and for making this whole process even more pleasant with her friendly and happy spirit.

Moreover, I would like to thank Dr Lucy Jen for the knowledge she passed on to me through her lectures and the advice and psychological support she offered in difficult moments.

Last but not least, I owe a big thank you to my parents Voula and Stelios and my brother Vassilis who are always by my side, loving me and supporting me in every step of my life, even though they live away.

TABLE OF CONTENTS

ABSTRACT 3

ACKNOWLEDGEMENTS 5

TABLE OF CONTENTS 7

LIST OF FIGURES 11

LIST OF TABLES 17

LIST OF NOTATIONS 19

CHAPTER 1 – INTRODUCTION 23

CHAPTER 2 – LITERATURE REVIEW

2.0 Introduction 25

2.1 Free-Field Ground Movements 25

2.1.1 Volume Loss 25

2.1.2 Empirical Methods for Distribution of the Free-Field Ground Deformations 27

2.1.2.1 Surface vertical movements 27

2.1.2.2 Surface horizontal movements 29

2.1.2.3 Subsurface ground movements 30

2.1.3 Analytical Solutions 31

2.1.3.1 Overview of different analytical approaches 31

2.1.3.2 Pinto & Whittle (2001) analytical solutions 32

2.1.4 Finite Element Analyses 35

2.2 Pipe – Soil – Tunnel Interaction 36

2.2.1 Factors Affecting Pipeline Response 37

2.2.2 Pipe – Soil Interface Shear 39

2.2.3 Analytical and Empirical Predictions of Pipeline Response 41

2.2.3.1 Attewell et al. (1986) 41

2.2.3.2 Vorster et al. (2005) 42

CHAPTER 3 – BENDING RESPONSE OF CONTINUOUS PIPELINES TO TUNNELING

3.0 Introduction 59

3.1 Free Field Settlements 59

3.1.1 Empirical Solutions (Vorster ,2005) 60

3.1.2 Analytical Solutions (Pinto & Whittle 2001) 60

3.2 Pipeline Bending Response 62

3.2.1 General Solutions Using a Winkler's Model 62

3.2.2 Pipe Strains and Stresses 68

3.3 Summary 69

CHAPTER 4 – AXIAL RESPONSE OF CONTINUOUS PIPELINES TO TUNNELING

4.0 Introduction 87

4.1 Free Field Horizontal Displacements 87

4.1.1 Empirical Solutions 87

4.1.2 Analytical Solutions 88

4.2 Axial Pipeline Response 89

4.2.1 Winkler's Model 89

4.2.2 Estimation of the Horizontal Spring Coefficient K_h 91

4.2.2.1 Proposed horizontal spring coefficient K_h 92

4.2.3 Relative Pipe – Soil Axial Rigidity Factor R_α 94

4.2.4 Axial pipe strains and stresses 95

4.3 Summary 96

CHAPTER 5 – FINITE ELEMENT ANALYSES OF PIPE RESPONSE TO TUNNELING

5.0 Introduction 109

5.1 Finite Element Model 109

5.1.1 Model Geometry and Properties 110

5.1.1.1 Boundary conditions and mesh 110

5.1.1.2 Tunnel cavity deformations and Pipeline representation 111

5.2 Comparison Between Analytical and FE Solutions 112

5.3 Summary 113

CHAPTER 6 – APPLICATION OF THE PROPOSED ANALYSES

6.0 Introduction 123

6.1 Application To Chingford Pipe-Jacking Case 123

6.1.1 Site Description and Geology 124

6.1.2 Free-Field Pipe and Soil Response 124

6.2 Application to N-2 Sewer Tunnel Project 128

6.2.1 EPB Tunneling Method 129

6.2.2 Measured Free-Field Movements 130

6.2.3 Interpreted Free-Field Movements 131
6.2.3.1 Empirical solutions 131
6.2.3.2 Analytical solutions 132
6.2.4 Response of Hypothetical Pipelines 132
6.2.4.1 Pipelines characteristics 133
6.2.4.2 Vorster method (2005) 133
6.2.4.3 Proposed method 134
6.2.5 Possibility of Pipeline Failure 135
6.2.5.1 Cast -Iron strength 135
6.2.5.2 Estimation of the possibility of pipeline failure 137
6.3 Summary 137

CHAPTER 7 – SUMMARY, CONCLUSIONS RECOMMENDATIONS

7.1 Summary and Conclusions 159
7.2 Recommendations for Future Research 161

REFERENCES 163
APPENDIX I 169
APPENDIX II 179
APPENDIX III 193

LIST OF FIGURES

CHAPTER 2 – LITERATURE REVIEW

2-1 3D settlement trough caused by tunnel advance (Attewell et al., 1986)

2-2 Sources of ground movements associated with tunneling (after Moller, 2006)

2-3 Dependence of the critical stability number N_c on the unsupported heading length (Kitamura and Mair, 1981)

2-4 Critical stability number N_c for fully lined tunnel headings with thin clay cover (Mair and Taylor, 1997)

2-5 Field and laboratory monitoring data for overconsolidated clays (after Macklin, 1999)

2-6 Empirical function for transversal surface settlement trough (Whittle & Sagaseta, 2003)

2-7 Variation in surface settlement trough width parameter *xi* with tunnel depth for soft ground tunneling (Mair & Taylor, 1997)

2-8 Modified Gaussian curve describing the settlement distribution (Vorster, 2005)

2-9 Horizontal ground movement and strain (Mair et al., 1996)

2-10 Variation of Trough width parameter K with normalized depth (y/H) for tunnels in clay (Mair et al, 1993)

2-11 Assumption of ovalization and distribution of ground movement

2-12 Comparison of elastic solutions for shallow tunnels (Whittle and Sagaseta, 2001)

2-13 Deformation modes around tunnel cavity (Whittle and Sagaseta, 2001)

2-14 Effect of input parameters on surface settlement distribution (Whittle and Sagaseta, 2001)

2-15 Display of the grout pressure method (Moeller, 2006)

2-16 Step-by-step simulation of open-face, NATM tunneling (Moeller, 2006)

2-17 Step-by-step simulation of closed-face, shield tunneling (Moeller, 2006)

2-18 Comparison between continuum solution and Winkler model using a)Vesic analogue and b) new proposed analogue (Klar et al., 2005) ($S_{max} = u_y^o$)

2-19 Normalized bending stiffness and settlements of a pipe relative to the pipe-soil stiffness ratio (Vorster et al., 2005)

CHAPTER 3 – BENDING RESPONSE OF CONTINUOUS PIPELINES TO TUNNELING

3-1 Vorster (2005) method to describe the free field settlements

3-2 Pinto and Whittle (2001) method to describe free field settlements

3-3 Comparison between surface free-field normalized settlements computed by empirical and analytical ground models

3-4 Comparison between subsurface free-field normalized settlements computed by empirical and analytical ground models

3-5 Winkler model for representing a buried continuous pipeline in the ground

3-6 Bending response of a pipeline represented by a Winkler analogue of a beam lying on elastic foundation (Hetenyi, 1946)

3-7 Vertical loading of a pipeline with infinite pointed loads dP

3-8 Defining the location of an arbitrary point C, where pipe displacements are computed due to vertical loading at parts α and b

3-9 Effect of pipe radius and relative pipe-soil bending rigidity factor, $R_b=EI/E_s r_o x_i^3$, on normalized pipe settlements

3-10 Effect of relative distortion, ρ and relative pipe-soil bending rigidity factor, $R_b=EI/E_s r_o x_i^3$, on normalized pipe settlements

3-11 Effect of pipe embedment depth, y and relative pipe-soil bending rigidity factor, $R_b=EI/E_s r_o x_i^3$, on normalized pipe settlements

3-12 Effect of soil Poisson's ratio, v and relative pipe-soil bending rigidity factor, $R_b=EI/E_s r_o x_i^3$, on normalized pipe settlements

3-13 Effect of pipe radius and relative pipe-soil bending rigidity factor, $R_b=EI/E_s r_o x_i^3$, on normalized pipe bending moments

3-14 Effect of relative distortion, ρ and relative pipe-soil bending rigidity factor, $R_b=EI/E_s r_o x_i^3$, on normalized pipe bending moments

3-15 Effect of pipe embedment depth, y and relative pipe-soil bending rigidity factor, $R_b=EI/E_s r_o x_i^3$, on normalized bending moments

3-16 Effect of soil Poisson's ratio, v and relative pipe-soil bending rigidity factor, $R_b=EI/E_s r_o x_i^3$, on normalized pipe bending moments

3-17 Sign notation of pipe strain and stresses due to bending

3-18 Effect of the relative pipe-soil bending rigidity factor, $R_b=EI/E_s r_o x_i^3$, on normalized axial pipe strains and stresses

CHAPTER 4 – AXIAL RESPONSE OF CONTINUOUS PIPELINES TO TUNNELING

4-1 Vectors of ground displacements pointing at the tunnel centerline as suggested by several empirical solutions (e.g. Mair et al., 1993)

4-2 Pinto and Whittle (2001) method to describe free-field lateral displacements

4-3 Pipeline connected to the soil with horizontal springs and Winkler analog assuming that a pipe loaded axially is equivalent to a pile loaded axially

4-4 Axial loading of a pipeline with infinite pointed loads dP_x assuming P&W (2001) analytical solutions for the free-field horizontal displacements u_x.

4-5 Comparison between numerical and analytical solutions for horizontal

pipe displacements, using Scott (1981) recommendation for K_h

4-6 Characteristic length x_j for axial pipe deformations distortion of two different relative distortion (ρ) values

4-7 Comparison between numerical and analytical solutions for axial pipe displacements, using the proposed pipe-soil coefficient K_h

4-8 Comparison between numerical and analytical solutions for axial pipe displacements, using the proposed pipe-soil coefficient K_h

4-9 Comparison between Plaxis and analytical solutions for axial pipe displacements for v=0.5, ρ=0 and y_p=-3.5m

4-10 Comparison between Plaxis and analytical solutions for axial pipe displacements for v=0.5, ρ=1.5 and y_p=-3.5m

4-11 Comparison between Plaxis and analytical solutions for axial pipe displacements for v=0.4, ρ=1 and y_p=-2m

4-12 Effect of pipe radius and the relative axial pipe-soil rigidity factor $R_a=EA/E_s r_o x_j$ on normalized horizontal pipe displacements

4-13 Effect of relative distortion, ρ and the relative axial pipe-soil rigidity factor $R_a=EA/E_s r_o x_j$ on normalized horizontal pipe displacements

4-14 Effect of the embedment depth of the pipe, y_p and the relative axial pipe-soil rigidity factor $R_a=EA/E_s r_o x_j$ on normalized horizontal pipe displacements

4-15 Effect of the soil Poisson's ratio, v and the relative axial pipe-soil rigidity factor $R_a=EA/E_s r_o x_j$ on normalized horizontal pipe displacements

CHAPTER 5 – FINITE ELEMENT ANALYSES OF PIPE RESPONSE TO TUNNELING

5-1 Schematic representation of the problem in 2D

5-2 Boundary conditions and pipe representation in the 3D model

5-3 Distortion of tunnel cavity assuming a) an ellipsis, b) oval shape resulting from the exact solutions

5-4a) Comparison of free-field ground settlements computed numerically and analytically using exact solutions for tunnel cavity displacements

5-4b) Comparison of free-field ground lateral displacements computed numerically and analytically using exact solutions for tunnel cavity displacements

5-5 Comparison between numerical and analytical solutions for vertical pipe displacements for $v=0.25$, $\rho=0$, $y_p=-3.5m$ and $u_\varepsilon=-0.025m$

5-6 Comparison between numerical and analytical solutions for vertical pipe displacements for $v=0.25$, $\rho=0$, $y_p=-3.5m$ and $u_\varepsilon=-0.01m$

5-7 Comparison between numerical and analytical solutions for vertical pipe displacements for $v=0.25$, $\rho=1$, $y_p=-3.5m$ and $u_\varepsilon=-0.025m$

5-8 Comparison between numerical and analytical solutions for vertical pipe displacements for $v=0.25$, $\rho=0.5$, $y_p=-3.5m$ and $u_\varepsilon=-0.025m$

5-9 Comparison between numerical and analytical solutions for vertical pipe displacements for $v=0.25$, $\rho=0$, $y_p=-3.5m$ and $u_\varepsilon=-0.05m$

CHAPTER 6 – N2 - SAN FRANCISCO CASE WITH HYPOTHETICAL PIPELINES

6-1 Chingford geological profile and geometry

6-2 Monitoring layout of the Chingford project

6-3 Pipe jacking process

6-4 Stages and duration of ground movements (a) Line L, (b) Line R

6-5 Comparison between modified Gaussian and P&W solutions to fit free-field measured data from Line L

6-6 Analytically computed free-field settlements and comparison between measured and analytically estimated pipe settlements

6-7 Comparison between empirical and analytical solutions for estimating free-field horizontal displacements at Line L

6-8 Analytically computed pipe axial displacements with the proposed method

6-9 Axial and bending strains and stresses at lower fiber of Chingford water main

6-10 Generalized Subsurface Profile (1ft = 0.305 m)

6-11 Typical front view of EPB shield

6-12 Line 4 vertical and lateral movement vectors, 15 days after shield passage

6-13 Long term lateral deflections at Line 1-4 (1ft = 0.305m and 1in=2.54cm)

6-14 Subsurface (y=-2m) free-field settlements at Line 4

6-15 Subsurface (y=-2m) free-field horizontal displacements at Line 4

6-16 Subsurface (y=-2m) free-field horizontal & vertical movements at Line 2

6-17 Model geometry and properties for N-2 San Francisco tunnel case

6-18 Vorster method (2005) for estimating pipe response u_y^P

6-19 Proposed method for estimating pipe response

6-20 Strains and stresses of Pipe30 for soil movements at Line 2

6-21 Strains and stresses of Pipe30 for soil movements at Line 4

6-22 Typical four-point pipe bending load configuration with corresponding shear [Q] and moment [M] diagrams.

6-23 Possibility of pipe tensile failure depending on the lowest or mean tensile strength value

LIST OF TABLES

CHAPTER 5 – FINITE ELEMENT ANALYSES OF PIPE RESPONSE TO TUNNELING

5.1 Input parameters for the tunnel wall deflections

5.2 Pipe characteristics

CHAPTER 6 – N2 - SAN FRANCISCO CASE WITH HYPOTHETICAL PIPELINES

6.1 Volume Loss associated with ground movement

6.2 Earth pressure and net lateral movement

6.3 Cast-Iron pipeline characteristics used

6.4 Tensile strength of Cast-Iron pipes

6.5 Tensile strength of Cast-Iron pipes (Seica & Packer, 2004)

LIST OF NOTATIONS

A	Parameter of the modified Gaussian curve (Vorster et al., 2005) to ensure that x_i remains the distance to the inflection point
C	Depth till the tunnel crown
D_P	Pipe diameter
D_T	Tunnel diameter
E_P	Pipe Young's modulus
E_s	Soil Young's modulus
EA	Pipe axial stiffness
$E_P I_P$	Pipe bending stiffness
H	Depth of the tunnel axis
I_P	Second moment of inertia of pipe section
K	Trough width parameter
K^*	Pipe-soil axial rigidity factor (Attewell et al., 1986)
K_∞	Pipe-soil subgrade modulus (Vesic, 1969)
K_{eff}	Effective pipe-soil subgrade modulus (Vesic, 1969)
K_h	Proposed horizontal pipe-soil spring coefficient
K_s	Horizontal pipe-soil spring coefficient (Scott, 1981)
K_v	Proposed vertical pipe-soil spring coefficient
k_s	Horizontal pipe-soil subgrade modulus (Scott, 1981)
M	Pipe bending moments
M_n	Normalized pipe bending moments
N	Force stability number

N_c Critical force stability number

n Shape function parameter controlling the width of the modified Gaussian curve (Vorster et al., 2005) profile

P Unsupported length of the tunnel

R_a Relative pipe-soil axial rigidity factor

R_b Relative pipe-soil bending rigidity factor

r Tunnel radius

r_o Pipe radius

s_u Undrained shear strength of the soil

t Pipe wall thickness

u_x Lateral free-field ground displacement

u_x^o Maximum lateral free-field ground displacement

u_x^P Axial pipe displacement

u_y Vertical free-field ground displacement

u_y^o Maximum vertical free-field ground displacement

u_y^P Vertical pipe displacement

u_ε Uniform convergence of the tunnel cavity

u_δ Ovalization of the tunnel cavity

V_o Initial volume of the tunnel cavity per unit length

x_i Horizontal distance to the inflection point in the free-field settlement trough

x_j Characteristic length controlling the lateral free-field displacements

y Depth of interest in the ground

y_p Depth of the pipe axis

γ Unit weight of the soil

ΔV_g Volume change in the ground

ΔV_L Volume Loss at the tunnel cavity

ΔV_s Volume of the settlement trough

Δu_y Uniform translation of the tunnel

ε_a Axial pipe strain in the extreme fiber due to axial deformation

ε_b Axial pipe strain in the extreme fiber due to bending

$\varepsilon_{b,n}$ Normalized axial pipe strain in the extreme fiber due to bending

$\varepsilon_{sh,lim}$ Limiting axial strain due to pipe-soil interface shear

Λ Pseudo time parameter

$1/\lambda_h$ Characteristic length of the pipe for axial loading conditions

$1/\lambda_v$ Characteristic length of the pipe for bending conditions

v Poisson's ratio of the soil

ρ Relative distortion at the tunnel cavity

σ_g Grout pressure in tunnel lining

σ_o Initial ground stresses

σ_s Surface surcharge pressure

σ_T Tunnel support pressure

σ_x Axial pipe stress in the extreme fiber

$\sigma_{x,n}$ Normalized axial pipe stress in the extreme fiber due to bending

τ_{lim} Limiting pipe-soil interface shear

CHAPTER 1

INTRODUCTION

One of the great challenges that civil engineers have to face in the 21st century is the management of ageing infrastructure assets such as the networks of urban water distribution and sewer pipelines. The structural integrity of water pipes is related to many factors including material degradation (notably internal and external corrosion), fluctuations in hydraulic pressures, external loading from third party activities and deformations within the surrounding soil. This thesis considers the effects of ground movements associated with tunneling as a potential source of damage to existing water utilities.

The construction of tunnels by boring machines (TBM) or sequential excavation and support (e.g. NATM) is increasingly common in congested urban areas. Good examples are associated with the expansion of metro systems in many cities such as the Athens metro (Marinos, 1998), Bangkok underground system (Lueprasert et al., 2009), New York subway, and others. Although tunnel construction generates disruptions associated with more conventional cut-and-cover excavation projects, there are risks associated with the stress changes and ground loss around a tunnel heading. The magnitude and distribution of tunnel-induced ground movements is a challenging problem as the source of ground movements vary, according to details and methods of tunnel construction, while ground response is influenced by stratigraphy, ground water conditions etc.

There are three main methods used to estimate the tunnel-induced ground deformations: a) empirical methods based on case studies, b) analytical solutions based on simplified models of the tunneling process and constitutive

ground behavior, and c) numerical analyses that attempt to simulate the soil-structure interaction for a given tunneling process. Recent work by Zymnis (2010) shows that simplified analytical models (Pinto and Whittle, 2001) are able to describe realistically the net 2D ground deformations in a plane orthogonal to the tunnel. This thesis describes a simplified method for estimating the deformations and stresses in a pipeline to tunnel-induced ground deformations based on 2D closed-form analytical solutions proposed by Pinto and Whittle (2001).

Chapter 2 presents a literature review with background information on different methods for predicting the tunnel-induced ground deformations and the response of existing pipelines to these ground displacements.

Chapter 3 presents an analytical model for estimating the settlements and bending moments of continuous pipelines due to tunnel-induced vertical ground deformations.

Chapter 4 extends the aforementioned model to include induced lateral ground displacements.

Chapter 5 describes the 3D finite element analyses of a circular tunnel excavation that were conducted to verify the analytical solutions of free field ground displacements and deformations of the pipeline.

Chapter 6 illustrates and compares the proposed analyses with prior predictions of stress conditions in a hypothetical pipeline due to ground displacements induced by the excavation of N2 sewer tunnel in San Francisco (Clough et al. 1984).

Chapter 7 summarizes the main conclusions of the current research and presents suggestions for future advancement of this study.

CHAPTER 2

LITERATURE REVIEW

2.0 INTRODUCTION

This chapter presents a summary of the existing literature regarding two topics: a) the movements of the free-field soil mass due to tunneling, and b) the response of buried pipelines to tunneling. Three main methods exist for modeling and predicting the free-field ground movements induced by tunneling: a) empirical methods, b) closed-form analytical solutions based on simplified constitutive solutions and c) numerical analyses using non-linear FE methods. The response of buried pipelines to tunneling is investigated by reviewing results from analytical studies and observations of instrumental field tests and laboratory pipe – soil – tunnel interaction experiments.

2.1 FREE-FIELD GROUND MOVEMENTS

Tunneling in soft ground causes inevitably surface and subsurface ground deformations. Figure 2-1 illustrates the three-dimensional surface settlement trough caused by tunnel construction. The methods and the characteristic parameters for predicting the ground deformations due to tunneling are presented in the following sections.

2.1.1 Volume Loss

Volume loss refers to the over-excavation of soil around tunnel heading due to several factors. As shown in Figure 2-2, these factors include: a) stress relief at

the tunnel face, b) over-cutting and ploughing of the tunnel shield, c) deformations of the lining system and d) long term consolidation due to dissipation of excess pore pressures caused by tunnel construction. It is generally not possible to measure these sources of ground loss directly. Although Cording and Hansmire (1975) suggested measuring soil movements close to the tunnel by means of extensometers, instead most tunnel engineers assume that volume loss at the tunnel can be inferred from the deformations observed at the ground surface. This assumption is reasonable for short-term, undrained deformations in clays, but does not account for contraction or dilation that can occur due to drained shearing in more permeable soil layers.

Mair et al. (1981) proposed that in clays the volume loss is related to the load factor N/N_c, which is the ratio between the force stability number N, and the critical stability number N_c. Broms and Bennermark (1967) defined the stability number N, which provides an indication of tunnel stability for changing conditions of tunneling as follows:

$$N = \frac{\sigma_s + \gamma H - \sigma_T}{s_u} \tag{2.1}$$

where:

σ_s = surface surcharge pressure

γ = unit weight of the soil

H = depth of the tunnel axis

σ_T = tunnel support pressure

s_u = undrained shear strength of the soil

Based on laboratory testing and field observations, they concluded that the critical stability value required to prevent collapse is approximately, N_c=6. Kimura and Mair (1981) performed centrifuge tests considering a three-

dimensional tunnel heading and observed that N varies with both the soil cover to tunnel diameter ratio, C/D_T and the unsupported length to tunnel diameter ratio, P/D_T (where C is the depth till the tunnel crown, D_T is the tunnel diameter and P is the unsupported length), Figure 2-3. Mair and Taylor (1997) extended the design curves in Figure 2-3, for fully lined tunnels ($P/D_T=0$), based on field cases and model tests (Figure 2-4). They also reported that typical volume losses for stiff clays (London clay) range from 0.3% to 2% while in sand and soft clays volume losses vary between 0.5% and 1% for EPB method or up to 2% for slurry shields. For mixed face conditions, the situation can be more variable with volume losses varying between 0.3% and 4% (Mair and Taylor, 1997). Macklin (1999) observed that the values of volume loss for overconsolidated clays, based on field and laboratory data, is related to the load factor N/N_c and lie within a distinct range enclosed in the dashed lines, as shown in Figure 2-5. A linear regression line of the data is given by:

$$\Delta V_L(\%) = 0.23e^{4.4\left(\frac{N}{N_c}\right)} \tag{2.2}$$

2.1.2 Empirical Methods for Distribution of the Free-Field Ground Deformations

2.1.2.1 Surface vertical movements

The most commonly used empirical method for interpreting surface settlements, is the one proposed by Peck (1969) and Schmidt (1969). This method suggests that the transverse settlement trough due to tunneling can be described by a Gaussian curve, Figure 2-6.

$$u_y = u_y^o \cdot exp\left(-\frac{x^2}{2x_i{}^2}\right) \tag{2.3}$$

where:

u_y^o = centerline settlement

x_i = horizontal distance to the inflection point in the settlement trough

Hence, the volume of the settlement trough, ΔV_s can be found by integrating Equation 2.3:

$$\Delta V_s = \sqrt{2\pi} \cdot u_y^o \cdot x_i \quad \left(in\ \frac{m^3}{m}\right) \tag{2.4}$$

The volume loss in the region close to the tunnel is equal to:

$$\Delta V_s = \Delta V_L + \Delta V_g \tag{2.5}$$

When tunneling occurs in clays under undrained conditions, $\Delta V_g = 0$ (volume change in ground) and thus $\Delta V_L = \Delta V_s$. However, for tunneling in granular soils ΔV_s can differ from ΔV_L due to dilation or contraction within the soil mass.

In soft and stiff clays, the maximum surface settlement u_y^o, as well as the trough itself, was observed to decrease inversely linearly with increasing tunnel depth (Mair, 1979; Mair et al., 1993; Mair and Taylor, 1997). Figure 2-7 shows that x_i was generally wider in clays than in granular soils for similar geometries.

Based on data from tunnels in UK, O'Reilly and New (1982) showed that x_i changes approximately linearly with tunnel depth H, as shown in Equation 2.6.

$$x_i/H = K \tag{2.6}$$

The trough width parameter, K ranges from 0.4 for stiff clays to 0.7 for soft silty clays and between 0.2 and 0.3 for tunnels in granular soils above the water table, as reported by New and O'Reilly (1991). Mair and Taylor (1997) reported that a mean value for K should be 0.5 for all clays and 0.35 for granular soils, as

shown in Figure 2-8. Mair and Taylor (1997) also reported that consolidation will increase x_i after construction.

Celestino et al. (2000) and Jacobsz (2002) reported that, in many cases, the Gaussian curve fails to represent the ground movement. The same observation was made by Vorster et al. (2005), who conducted several centrifuge tests to simulate tunneling in sand. In order to fit better the observed soil settlements, the authors proposed a modified Gaussian curve:

$$u_y = u_y^o \frac{n}{(n-1) + \exp\left[A\left(\frac{x}{x_i}\right)^2\right]} \qquad (2.7a)$$

$$n = 1 + \frac{e^A(2A-1)}{2A+1} \qquad (2.7b)$$

where n is the shape function parameter controlling the width of the profile, with $0<n<2$, while A is defined to fix the location of the inflection point x_i. For $n=1$ and A=0.5, equation 2.7a reduces to the simple Gaussian curve. Figure 2-9, shows the effect of the shape function parameter n.

2.1.2.2 Surface horizontal movements

Based on the work of Attewell (1978) and O'Reilly and New (1982), it is often assumed that the vectors of the tunnel-induced ground movements are directed towards the tunnel axis (Equation 2.8), such that the horizontal and vertical components are related as follows:

$$\frac{u_x}{u_y} = \frac{x}{H} \qquad (2.8)$$

The above assumption leads to the following expression for the horizontal displacements corresponding to the Gaussian curve for vertical settlements (n=1 in Equation 2.7).

$$\frac{u_x}{u_x^o} = 1.65\frac{x}{x_i}exp\left(-\frac{x^2}{2x_i{}^2}\right) \tag{2.9}$$

where $u_x{}^o$=$0.61 \cdot K \cdot u_y^o$ the maximum horizontal free-field displacement at the inflection point (Attewell and Woodman, 1982).

Figure 2-9 shows the distribution of Equation 2.9, the settlement trough and the resulting horizontal strain. Mair and Taylor (1997) reported that subsurface horizontal ground movements appear to be a function of the tunneling method. More specifically, during open face tunneling, movements are believed to occur towards the tunnel axis, while in EPB tunneling, the direction of movements is related to the magnitude and control of the face pressure.

2.1.2.3 Subsurface ground movements

Mair et al. (1993) showed that the Gaussian function can also be adapted to fit subsurface settlement troughs by modifying the trough width parameter x_i:

$$\frac{x_i}{H} = K\left(1-\frac{y}{H}\right) \tag{2.10}$$

where K is a function of depth (Figure 2-10). For tunnels in clay, Mair et al. (1993) proposed the following non-linear equation for K:

$$K = \frac{0.175 + 0.325\left(1-\frac{y}{H}\right)}{1-\frac{y}{H}} \tag{2.11}$$

This equation tends to overestimate the lateral extent of the ground movement zone and underestimate the width of the surface settlement trough, close to the tunnel. Assuming that Equation 2.11 applies, Taylor (1995) showed that vectors of ground movements under undrained conditions, direct to a point *(0.175/0.325)H* below the tunnel axis, resulting in approximately 65% of the horizontal ground movement predicted by Equation 2.7.

Jacobsz (2002) conducted a series of centrifuge tests in dense sand and found that the settlement troughs were narrower than in clay. He proposed a modified expression for *K*:

$$K = \frac{0.09 + 0.26\left(1 - \frac{y}{H}\right)}{1 - \frac{y}{H}} \tag{2.12}$$

2.1.3 Analytical Solutions

2.1.3.1 Overview of different analytical approaches

Several researchers have proposed analytical approaches for estimating tunnel-induced ground deformations. These solutions make gross approximations of real soil behavior by assuming linear, elastic soil properties but require only a small number of physical input parameters.

Sagaseta (1987) proposed approximate solutions for a linear elastic, isotropic, homogeneous and incompressible undrained soil subjected to a concentrated ground loss (point sink), based on the superposition of singularity solutions to represent the uniform convergence and pure ovalization modes of a tunnel cavity. Verruijt and Booker (1996) extended these solutions to include both drained and undrained soils.

Loganathan & Poulos (1998) modified the Verruijt & Booker (1996) solutions by introducing a semi-empirical ground loss parameter, defined from non-linear soil movements around the soil-tunnel interface. They assumed an oval-shaped cavity, based on the solutions of Rowe and Kach (1983) for non-uniform radial ground movements (Figure 2-11).

Pinto (1999) extended and compared the approximate solutions of Sagaseta (1987) with the more exact conformal transformation solutions proposed by Verruijt (1997) in a planar-elastic soil. Although Verruijt's (1997) solutions are more accurate (exact), and include the physical dimensions of the tunnel cavity, the results are only derivable in an infinite series form.

Pinto and Whittle (2001) showed that the 'approximate' and 'exact' analytical solutions, produce very similar results for tunnels with radius over depth ratios $r/H<0.5$ for all the range of expected elastic Poisson's ratios (v) (Figure 2-12). Hence, the method proposed by Sagaseta (1987) can be used reliably for a wide range of tunnel geometries.

2.1.3.2 Pinto and Whittle (2001) analytical solutions

The analytical solutions proposed by Pinto and Whittle (2001) relate the ground displacements to three prescribed displacements happening at the tunnel cavity: a) uniform convergence u_ε, b) ovalization u_δ and c) uniform vertical translation Δu_y (Figure 2-13). Volume loss is uniquely defined by the uniform convergence component, as described below:

$$-\frac{2u_\varepsilon}{r}=\frac{\Delta V_L}{V_o} \tag{2.13}$$

where $V_o=\pi r^2$ is the volume of the tunnel cavity per unit length.

The complete analytical solutions proposed by Pinto and Whittle (2001) which predict the vertical and horizontal ground movements at any depth, are shown below. It should be noted that both convergence and ovalization modes produce vertical translation to the tunnel cavity.

A. *Uniform Convergence Mode*

$$\frac{u_x}{u_\varepsilon} = xr\left\{\begin{array}{c}\frac{1}{x^2+(y+H)^2}-\frac{1}{x^2+(y-H)^2}+\frac{4(1-v)}{x^2+(y-H)^2}-\cdots \\ -\frac{4(y-H)y}{[x^2+(y+H)^2]^2}\end{array}\right\} \qquad (2.14a)$$

$$\frac{u_y}{u_\varepsilon} = r\left\{\begin{array}{c}\frac{(y+H)}{x^2+(y+H)^2}-\frac{(y-H)}{x^2+(y-H)^2}+\cdots \\ +\frac{4(y-H)x^2+2H[x^2-(y-H)^2]}{[x^2+(y+H)^2]^2}-\frac{4(1-v)(y-H)}{x^2+(y-H)^2}\end{array}\right\} \qquad (2.14b)$$

Associated uniform translation:

$$\frac{\Delta u_y}{u_\varepsilon} = \frac{4r}{H}\left\{\frac{8(1-v)-(1-2v)\left(\frac{r}{H}\right)^2}{\left[4+\left(\frac{r}{H}\right)^2\right]^2}\right\} \qquad (2.14c)$$

Ovalization Mode

$$\frac{u_x}{u_\delta} = \frac{xr}{3-4v}\left\{\begin{array}{c}\frac{(3-4v)[x^2+(y+H)^2]^2-[3(y+H)^2-x^2][x^2+(y+H)^2-r^2]}{[x^2+(y+H)^2]^3}-\cdots \\ -\frac{(3-4v)[x^2+(y-H)^2]^2-[3(y-H)^2-x^2][x^2+(y-H)^2-r^2]}{[x^2+(y-H)^2]^3}+ \\ \cdots+\frac{8(1-v)\cdot(x^2+y^2-r^2)}{[x^2+(y-H)^2]^2}-\frac{8y[y(x^2+y^2)+2H(H^2-x^2)-3yH^2]}{[x^2+(y-H)^2]^3}\end{array}\right\} \qquad (2.15a)$$

$$\frac{u_y}{u_\delta}=\frac{r}{3-4v}\left\{\begin{array}{c}\dfrac{(y-H)\left\{(3-4v)\left[x^2+(y-H)^2\right]^2-\left[3x^2-(y-H)^2\right]\left[x^2+(y-H)^2-r^2\right]\right\}}{\left[x^2+(y-H)^2\right]^3}-\ldots \\ -\dfrac{(y+H)\left\{(3-4v)\left[x^2+(y+H)^2\right]^2-\left[3x^2-(y+H)^2\right]\left[x^2+(y+H)^2-r^2\right]\right\}}{\left[x^2+(y+H)^2\right]^3}+ \\ \ldots+\dfrac{\left[x^2(2H-y)-y(y-H)^2\right]\cdot 8(1-v)}{\left[x^2+(y-H)^2\right]^2}- \\ \ldots-\dfrac{8(y-H)\left\{Hy(y-H)^2-x^2\cdot\left[\left(x^2+y^2\right)+H(y+H)\right]\right\}}{\left[x^2+(y-H)^2\right]^3}\end{array}\right\} \quad (2.15b)$$

Associated uniform translation:

$$\frac{\Delta u_y}{u_\delta}=\frac{2}{3-4v}\frac{4r}{H}\left\{\frac{(1-8v)\left(\frac{r}{H}\right)^4+4(11-8v)\left(\frac{r}{H}\right)^2-32}{\left[4+\left(\frac{r}{H}\right)^2\right]^3}\right\} \quad (2.15c)$$

The input parameters used in the analytical model are: the tunnel radius r, the depth to the tunnel springline *H*, the Poisson's ratio *v*, the uniform convergence u_ε and the ovalization u_δ of the tunnel. The notation and sign convention are shown in Figure 2-13. The ratio of the ovalization u_δ to the uniform convergence u_ε is referred to as the 'relative distortion' $\rho=-u_\delta/u_\varepsilon$, and typically ranges from -0.5 to 3. Figure 2-14 illustrates the effects of the input parameters on the surface settlement distribution.

Comparison between results from the analytical solutions and from real field monitoring cases, showed generally good agreement between those two apart from the case of the Heathrow Express Trial tunnel in London. Pinto (1999) suggested that this disagreement could be due to limitations of the isotropic analytical model for heavily overconsolidated and highly fissured soils, like London clay. Subsequently, Chatzigiannelis and Whittle (2001) conducted an

extensive study on elastic anisotropic parameters reported from laboratory tests existing in the literature, for various types of soils and proposed analytical solutions for cross-anisotropy elastic soils. Zymnis (2009) studied five real tunnel cases and concluded that analytical solutions proposed by Pinto and Whittle (2001) succeed in correctly predicting the tunnel induced ground deformation, but the incorporation of anisotropic stiffness parameters significantly improves the results.

2.1.4 Finite Element Analyses

Non-linear Finite Elements are numerical methods used to simulate various forms of tunnel construction. Although 3D analyses are preferred for modeling tunnel construction, 2D analyses are more widely used for simplicity reasons. However, it has often proven difficult to reproduce the Gaussian distribution curve for modeling the transverse surface settlement trough. Clough and Leca (1989) suggested that one of the reasons is that 2D analyses try to represent a set-up which is, by its nature, three-dimensional.

Mair et al. (1981) reported that another drawback of the 2D analyses is that they require sophisticated soil models to produce a realistic surface settlement trough, especially for tunnels in heavily overconsolidated clays, since isotropic linear elastic – perfectly plastic soil models lead to wider surface settlement troughs than the simple Gaussian distribution. Lee and Rowe (1989) suggest that the introduction of anisotropic soil properties can significantly improve the FE analyses results.

Moeller (2006) reported that in finite element analyses, surface settlements due to tunneling are influenced by the value of the coefficient of earth pressure at rest (K_o), the overconsolidation ratio (OCR) and the ground stiffness E_s.

Regarding the two-dimensional analyses, he suggested that the surface settlement trough is influenced predominately by the installation procedure, rather than by the constitutive model.

For simulating shield tunneling in 2D, Moeller (2006) proposed using the grout pressure method, where the tunnel lining is considered to be surrounded by a thin grout layer with a known grout pressure σ_g (Figure2-15). During excavation, the initial ground stresses σ_o reduce to σ_g by a pseudo-time parameter Λ, which increases from 0 to 1 as shown in Equation 2.16:

$$\sigma = (1 - \Lambda)\sigma_o + \Lambda\sigma_g \tag{2.16}$$

Regarding 3D simulation, tunnel construction processes are in general difficult to model. Figures 2-16 and 2-17 illustrate step-by-step procedures, to simulate construction of open-face NATM tunnels and closed-face shield tunnels suggested by Moeller (2006).

Furthermore, parameters such as the geometry of the tunnel lining and dimensions of the tail void are often hard to define or represent. Finally, due to usual change in soil stratigraphy and tunnel elevation, multiple FE analyses are required for different sections of the tunnel.

2.2 PIPE – SOIL – TUNNEL INTERACTION

One of the main uncertainties when designing underground pipelines is their response to the induced ground movements. For this reason, pipe-soil interaction designs are relatively conservative with high factors of safety.

As reported by O'Rourke and Trautmann (1982), tunnel-induced ground movements can cause damage on existing pipelines due to three main reasons: a) tensile strains, b) joint rotation and c) joint axial pullout. They suggested that

most pipelines would behave either as perfectly flexible, where the pipe deforms as the ground, or as perfectly rigid, where the pipeline behaves as individual rigid sections rotating at the joints.

A variety of methods has been proposed for estimating the effect of ground movements on existing pipelines, by combining empirical data and simple theoretical analyses based on linear elasticity of soil and pipe (O'Rourke and Trautmann, 1982; Tagaki et al., 1984; Yeates, 1984; Attewell et al., 1986).

Attewell et al. (1986) first illustrated the importance of the relative soil-pipe rigidity in design. They reported that the soil settlement trough would be modified if the pipelines could resist to the ground movements, but the effect would be smaller for pipes less than 1m diameter. In addition, O'Rourke and Trautmann (1982) found that pipelines with diameters less than 200 mm, tend to behave as flexible structures that conform to imposed ground deformations. Fujita (1994) also pointed out the importance of the relative soil-pipe stiffness. He reported that the large variety of pipe sizes, materials, quality, strength, depth and methods of installation of pipes, may influence the pipeline response.

2.2.1 Factors Affecting Pipeline Response

Attewell et al. (1986) modeled the soil – pipe interaction problem using a Winkler-type beam on elastic foundation, where the pipe-soil stiffness is described by $\frac{1}{\lambda_v \cdot x_i}$:

$$\lambda_v = \sqrt[4]{\frac{K_{eff}}{4E_p I_p}} \tag{2.17}$$

$$K_{eff} = 2K_{\infty} \tag{2.18}$$

K_{eff} is the effective subgrade modulus, based on a soil Poisson's ratio, *v=0.5* and assuming that the pipeline is buried at infinite depth and K_{∞} is the subgrade modulus proposed by Vesic's (1961), given by the following equation:

$$K_{\infty} = 0.65 \cdot \sqrt[12]{\frac{E_s D_p^4}{E_p I_p}} \cdot \frac{E_s}{1 - v^2} \tag{2.19}$$

where D_p is the pipe diameter and E_pI_p is the pipe bending stiffness with E_p the pipe Young's modulus and I_p the second moment of inertia of pipe section.

The main conclusions of Attewell at al. (1986) research are the following:

1) Soil yielding around the pipe, decreases stress and strain compared with linear elastic analysis
2) Increasing the soil Young's modulus E_s, increases pipe stress and strain
3) Pipe yielding decreases stress but increases total strain compared with linear elastic analysis
4) Stress and strain on jointed metal pipelines are less than on continuous pipelines
5) Increasing the ratio of the tunnel depth to the tunnel radius *(H/r)*, increases the trough width and decreases the volume loss ΔV_L, the maximum settlement, the stress and strain
6) Increasing the volume loss ΔV_L at the tunnel face, increases the settlement trough volume, the maximum settlement, the stress and strain
7) Increasing the pipe elastic modulus E_p, increases the stress and decreases the strain

8) Increasing the pipe depth y_p, increases the maximum settlement at pipe level and decreases trough width resulting in increase of stress and strain

As it was also observed by Attewell et al. (1986), the trough width reduces as the proximity to the tunnel increases. Takagi et al. (1984) reported that the maximum pipe bending stress increases as the trough width decreases. Moreover, Rumsey and Cooper (1982), observing small diameter pipelines affected by surface excavations, reported that the pipe strain increases as the distance from the excavation increased. Similar effects are observed for tunneling, with shear strains decreasing in the free field soil with increasing distance from the tunnel. This leads to wider surface settlement troughs for a given tunnel position.

Another factor that affects pipeline response is the potential gap formation (loss of bending support) between pipe and soil during tunneling. Rajani and Tesfamariam (2004) reported that gap formation with continuation of external loading after tunneling (e.g. traffic), would increase pipe strain. They also found that pipelines with small bending stiffness react more flexibly than pipelines with higher bending stiffness. This leads to the suggestion that, by resisting ground movements, a stiffer pipeline would cause higher shear strains and lower soil stiffness (due to pipe-soil interaction), and hence react even stiffer.

2.2.2 Pipe-Soil Interface Shear

Attewell et al. (1986) mentioned that in a plane parallel to a pipeline, the effect of horizontal ground movement should be considered not only in the axial but also in the bending strain. They pointed out that the pipe strain depends on a)

different soil properties such as the grain size, the stiffness and the stress state, b) the problem geometry, c) the pipe properties such as its bending and axial stiffness and the joints, d) the pipe coating and e) the degree of the pipe deterioration. All the previous parameters contribute to the development of the pipe – soil interface shear.

They also reported the influence of the width of the settlement trough in relation to pipeline diameter D_p/x_i, on the axial strain built-up due to pipe-soil interface shear, for different pipe-soil axial rigidity K^*. The later is defined as:

$$K^* = \frac{E_p}{E_s}\left(\frac{4(D_p - t)t}{D_p^2}\right) \tag{2.20}$$

where:

E_p = pipe Young's modulus

E_s = soil Young's modulus

D_p = pipe diameter

t = pipe wall thickness

They showed that the larger D_p/x_i and/or K*, the smaller the axial strain induced to the pipeline. They also suggested that axial strain due to pipe-soil interface shear should be limited to the smallest value of the case where pipe-soil slippage is allowed.

$$\varepsilon_{sh,lim} = \frac{5}{K^*}\frac{x_i}{D_p}\frac{\tau_{lim}}{E_s} \tag{2.21}$$

where:

$\varepsilon_{sh,lim}$ = limiting axial strain due to pipe-soil interface shear

τ_{lim} = limiting pipe-soil interface shear strength

They mentioned that τ_{lim}/E_s would be smaller for plastic pipelines and pipes with protective sheathing, than for old pipelines where surface roughness might be more developed.

Scarpelli et al. (2003) investigated the effect of pipe coating, by performing field and laboratory testing of a 200mm and 610mm diameter pipelines buried in different granular and clayey soils, were pulled longitudinally until pipe-soil failure occurred. They found that smooth, hard coating resulted in a shear plane forming on the pipe-soil interface associated with quick maximum load mobilization and sliding of grains on the pipe-soil interface. On the other hand, with soft, rough coatings, soil grains tended to roll along and even penetrate the coating. The shear plane occurred in the surrounding soil, causing higher load mobilization and inducing larger stress on the pipe due to the larger friction angle.

2.2.3 Analytical and Empirical Predictions of Pipeline Response

Current methods for predicting the pipeline response to tunnel-induced ground movements are based on empirical observations coupled with theoretical analysis in elasticity. Below the most comprehensive and complete methods are presented.

2.2.3.1 Attewell et al. (1986)

Attewell et al. (1986) method is the most widely used method for predicting bending and axial strains, and joint rotation and pullout. This method utilizes a Winkler-type model assuming that the pipe reacts as a beam on an elastic foundation. Due to the assumption of a Winkler foundation, the pipeline and the surrounding soil are not allowed to separate.

The method considers a relative pipe-soil bending rigidity by means of Vesic's (1961) damping factor, λ_v, as described in Equation 2.17, pipe-soil rigidity factor, K^*, as described in Equation 2.20 and it provides information on the location of the bending strain. To take into account that the pipelines are buried, the authors proposed to apply twice the value of the subgrade modulus K_∞ proposed by Vesic (1961) (Equation 2.19). However, with this assumption, they have in fact modeled a pipeline buried at infinite depth.

Attewell et al. (1986) design method is based on the Gaussian curve, despite the fact that the authors indicated that the exact ground deformation is required in order to estimate accurately the bending strain in very flexible pipelines. To calculate the axial strain due to pipe-soil interface shear, they assume that ground movement vectors point towards the tunnel axis.

Attewell et al. (1986) method is overly conservative and lacks in reflecting the effect of strain distribution along the pipe length, stiffness and volumetric changes. All these effects are directly linked with the choice of the appropriate subgrade modulus, which is suggested to be obtained from laboratory or field testing.

2.2.3.2 Vorster et al. (2005)

In order to estimate the response of buried pipelines to tunneling, Vorster et al. (2005) suggested a closed-form solution based on a Winkler model, assuming that the pipe behaves as a beam on elastic foundation. The key assumptions for this model are:

1) The pipeline is buried in homogeneous soil

2) The pipe is always in contact with the soil

3) The pipe doesn't affect the tunnel

4) The soil response to loading, at the pipe level is not aware of the tunnel

5) The pipeline is continuous

6) The free field soil displacement at the pipe level is described by a Gaussian curve (Equation 2.2):

The closed form solution is in fact derived by solving analytically the differential equation which represents the pipeline behavior.

$$\frac{\partial^4 u_y^P}{\partial x^4} + 4\lambda_v{}^4 u_y^P = 4\lambda_v{}^4 u_y(x) \tag{2.22}$$

where $\lambda_v = \sqrt[4]{\frac{K_v}{4E_p I_p}}$ and $u_y{}^P$ is the vertical pipe displacement.

To enable a general solution corresponding to different soil and pipe characteristics, the results were normalized with a relative pipe-soil bending rigidity factor:

$$R_b = \frac{E_p I_p}{E_s r_o x_i{}^3} \tag{2.23}$$

Winkler models have the advantage of simplicity and allow convenient description of nonlinear pipe-soil interaction.

In order to consider the effects of the soil continuum in the predictions of the response of the pipelines, Klar et al. (2005) carried out finite element analyses of the elastic continuum solution in order to develop a more realistic representation of K_v in the Winkler model (Figures 2-18 a) and b)). The proposed subgrade modulus is given by:

$$K_v = \frac{12 E_s r_o}{x_i} \tag{2.24}$$

Vorster et al. (2005) performed centrifuge tests on model pipelines buried in sand, in order to observe the response of the pipelines to tunnel induced ground deformations and to verify the elastic continuum solution proposed by Klar et al. (2005). They also suggested a modified Gaussian curve in order to achieve a better fit of the observed surface settlement trough, as described by Equations 2.7. Figure 2-19, shows the normalized vertical displacement and bending moments of a pipeline relative to the relative pipe-soil bending rigidity factor R_b, proposed by Klar et al. (2005). It is assumed that the free-field settlements are described by modified Gaussian curves proposed by Vorster et al. (2005).

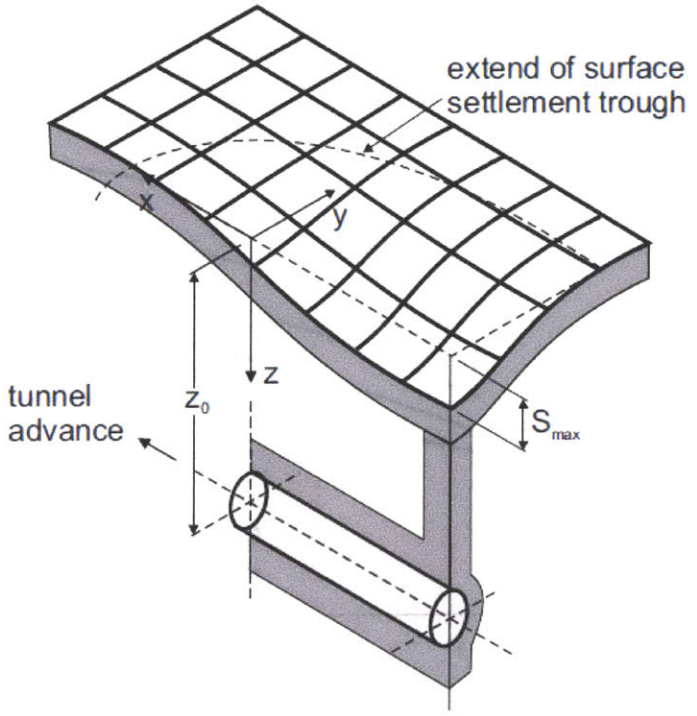

Figure 2-1: 3D settlement trough caused by tunnel advance (Attewell et al., 1986)

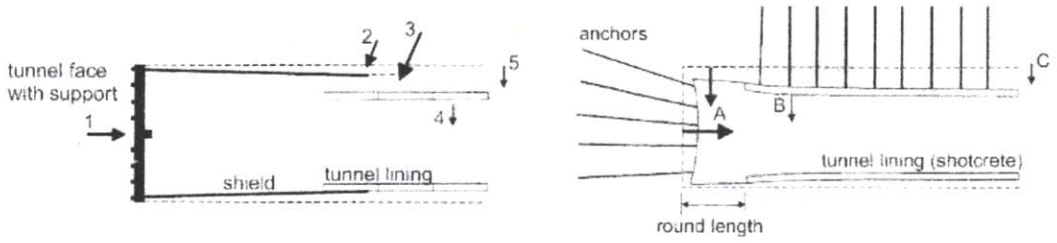

1. Stress relief at tunnel face
2. Shield over-cut & ploughing
3. Tail Void
4. Deformation of lining
5. Consolidation of soil

a) Closed-face tunnel

A. Deformation at tunnel heading
B. Deformation of lining
C. Consolidation of soil

b) Sequential excavation

Figure 2-2: Sources of ground movements associated with tunneling (after Moeller, 2006)

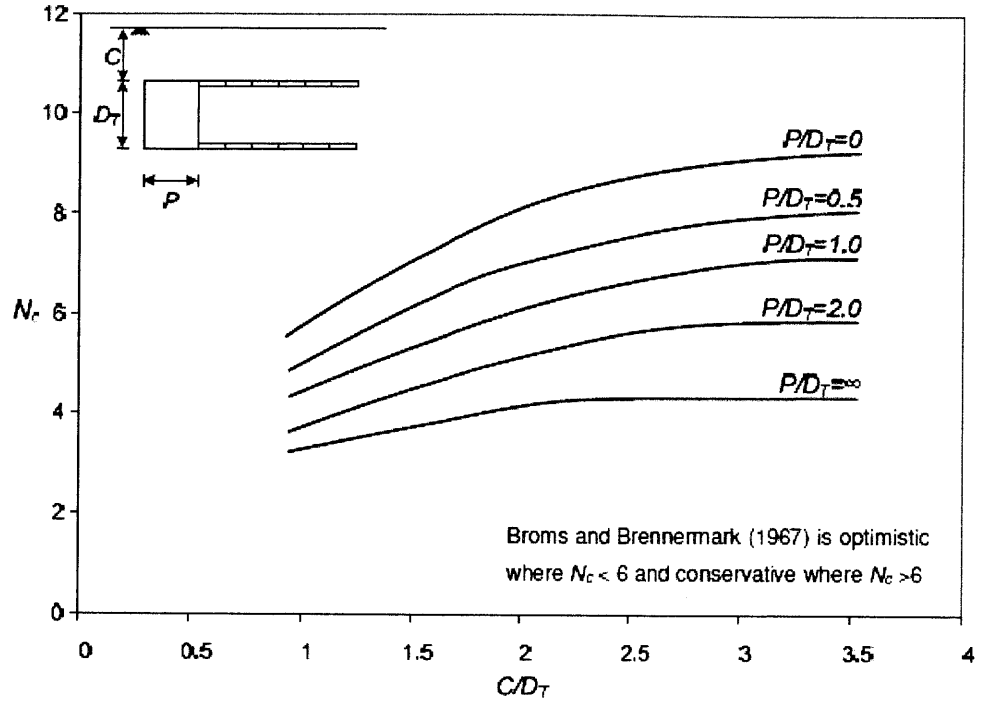

Figure 2-3: Dependence of the critical stability number N_c on the unsupported heading length (Kimura and Mair, 1981)

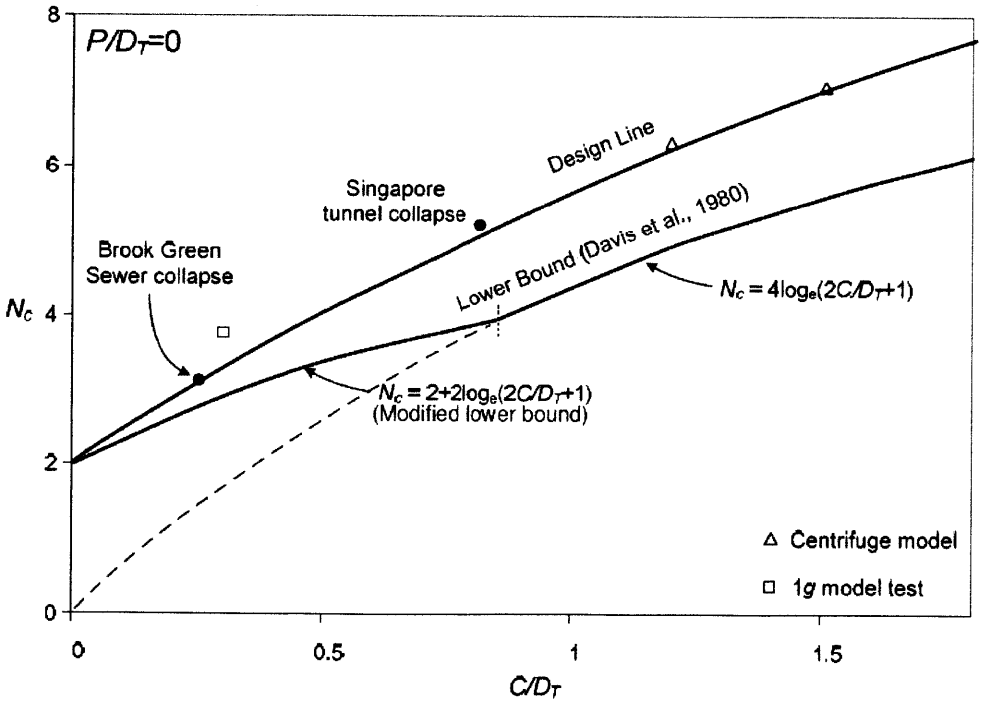

Figure 2-4: Critical stability number N_c for fully lined tunnel headings with thin clay cover (Mair and Taylor, 1997)

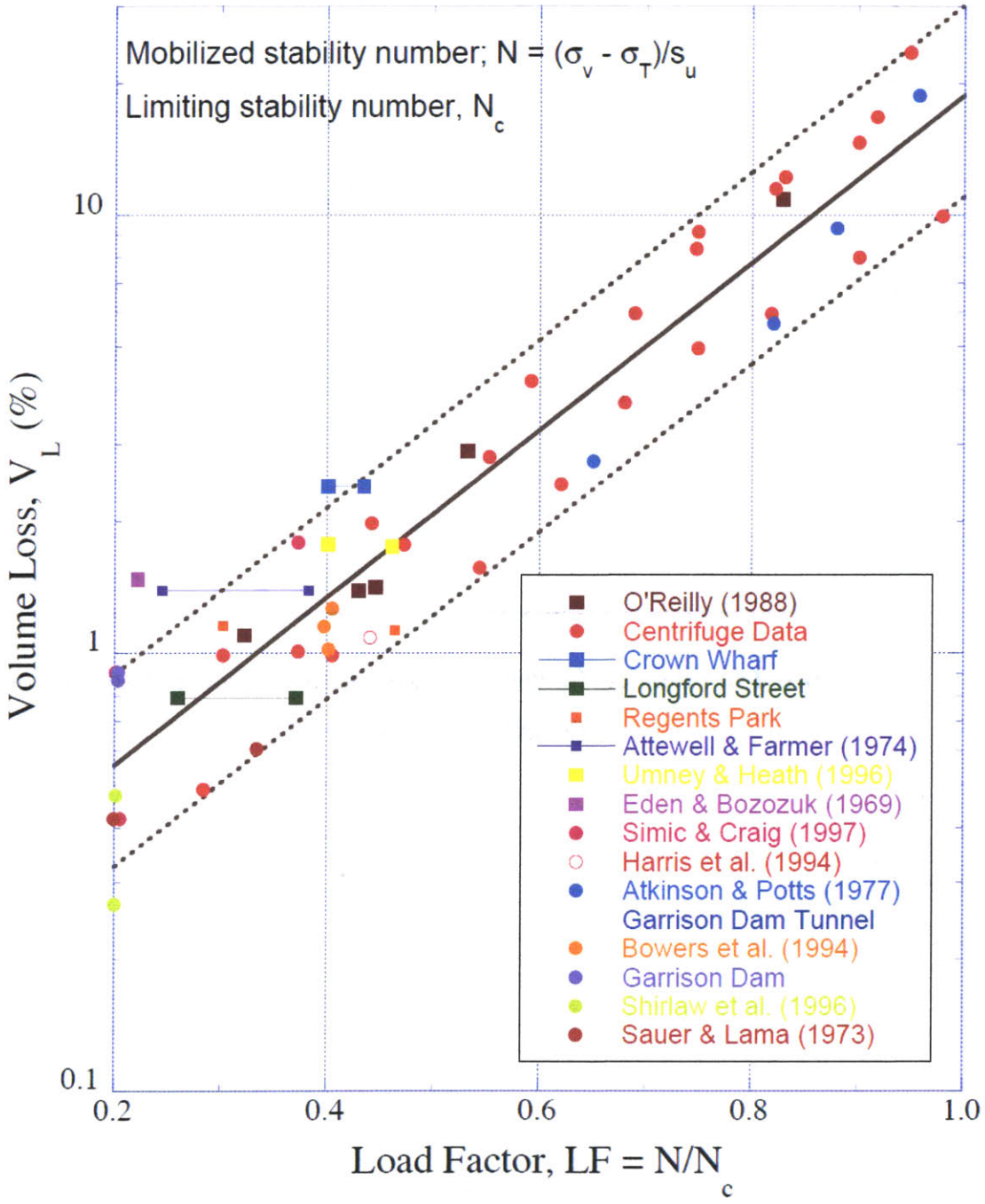

Figure 2-5: Field and laboratory monitoring data for overconsolidated clays (after Macklin, 1999)

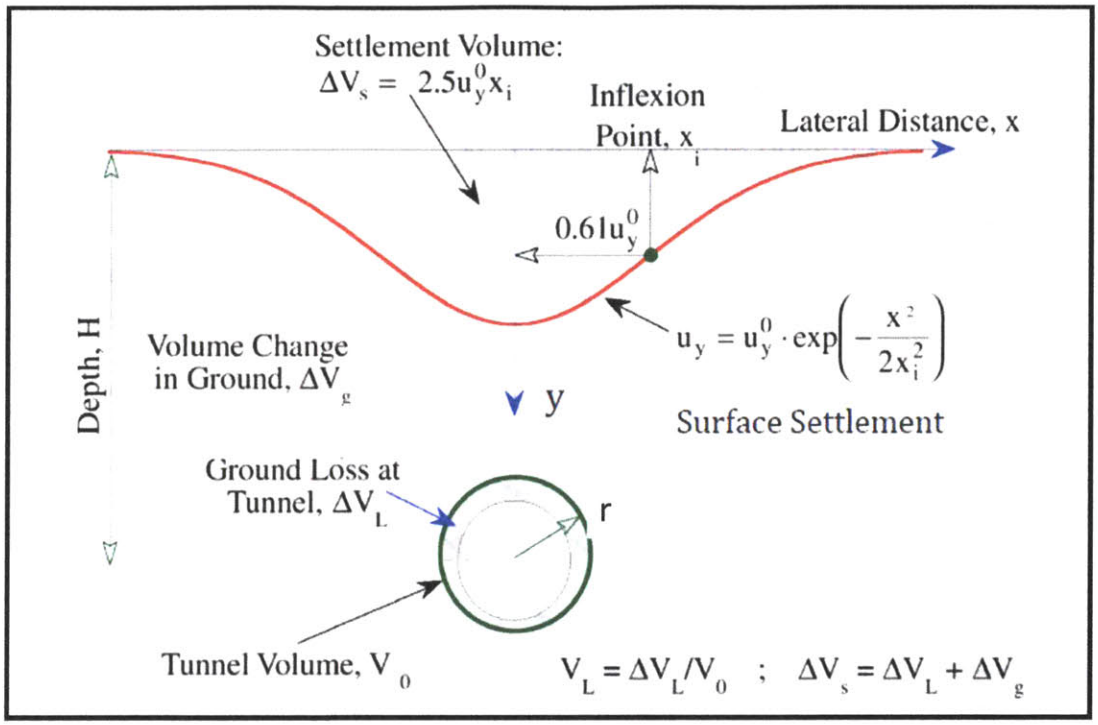

Figure 2-6: Empirical function for transversal surface settlement trough (Whittle & Sagaseta, 2003)

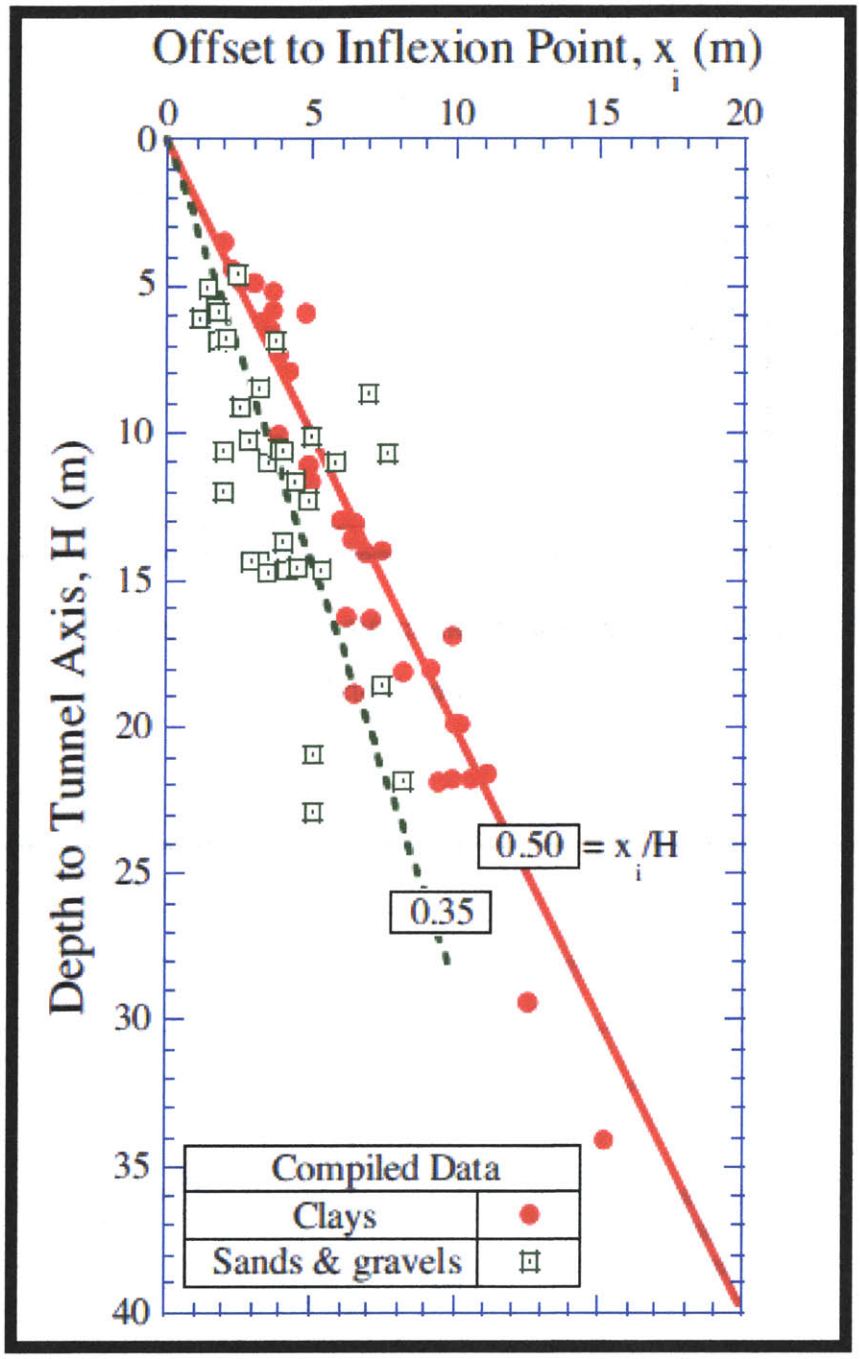

Figure 2-7: Variation in surface settlement trough width parameter x_i with tunnel depth for soft ground tunneling (after Mair & Taylor, 1997)

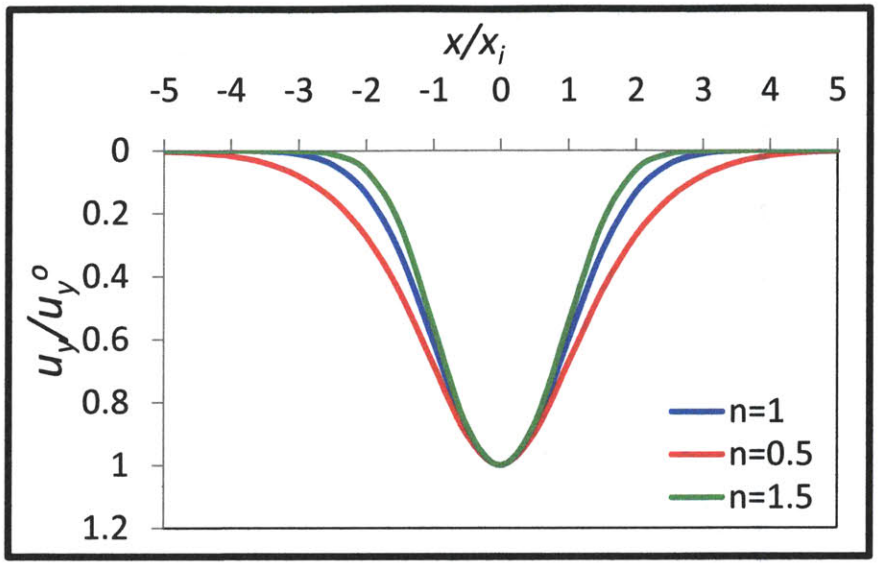

Figure 2-8: Modified Gaussian curve describing the settlement distribution (after Vorster, 2005)

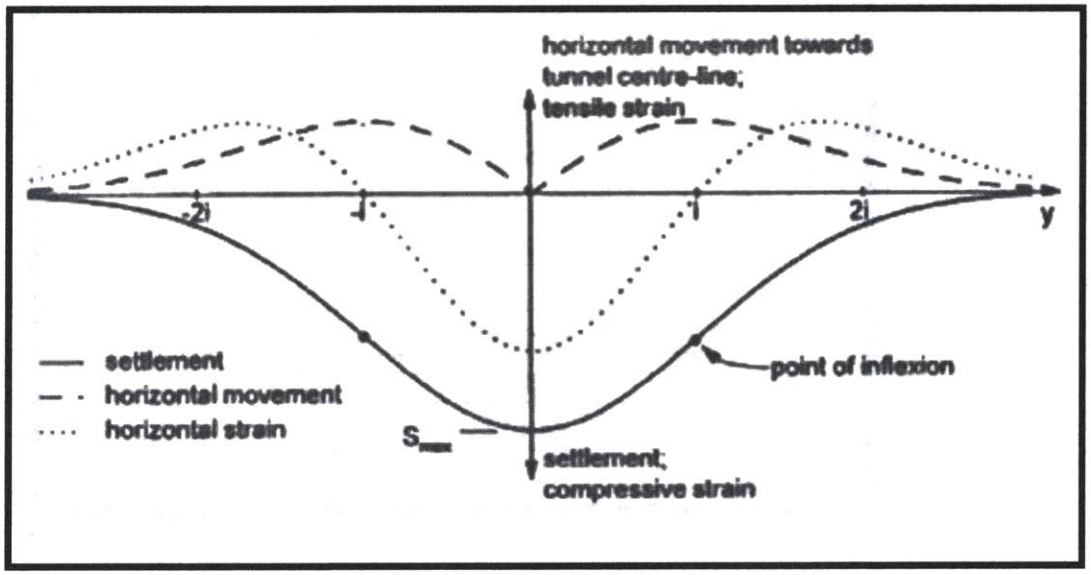

Figure 2-9: Horizontal ground movement and strain (Mair et al., 1996)

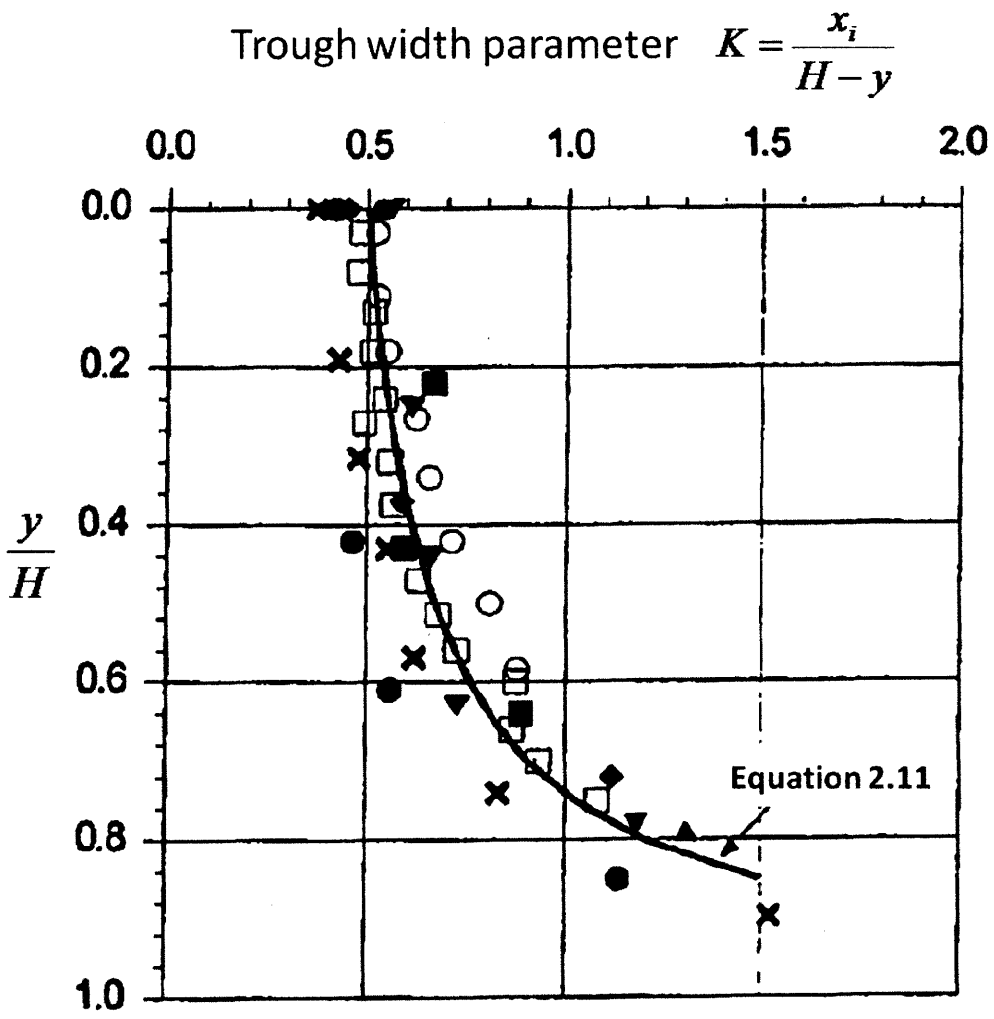

Figure 2-10: Variation of Trough width parameter K with normalized depth (y/H) for tunnels in clay (Mair et al, 1993)

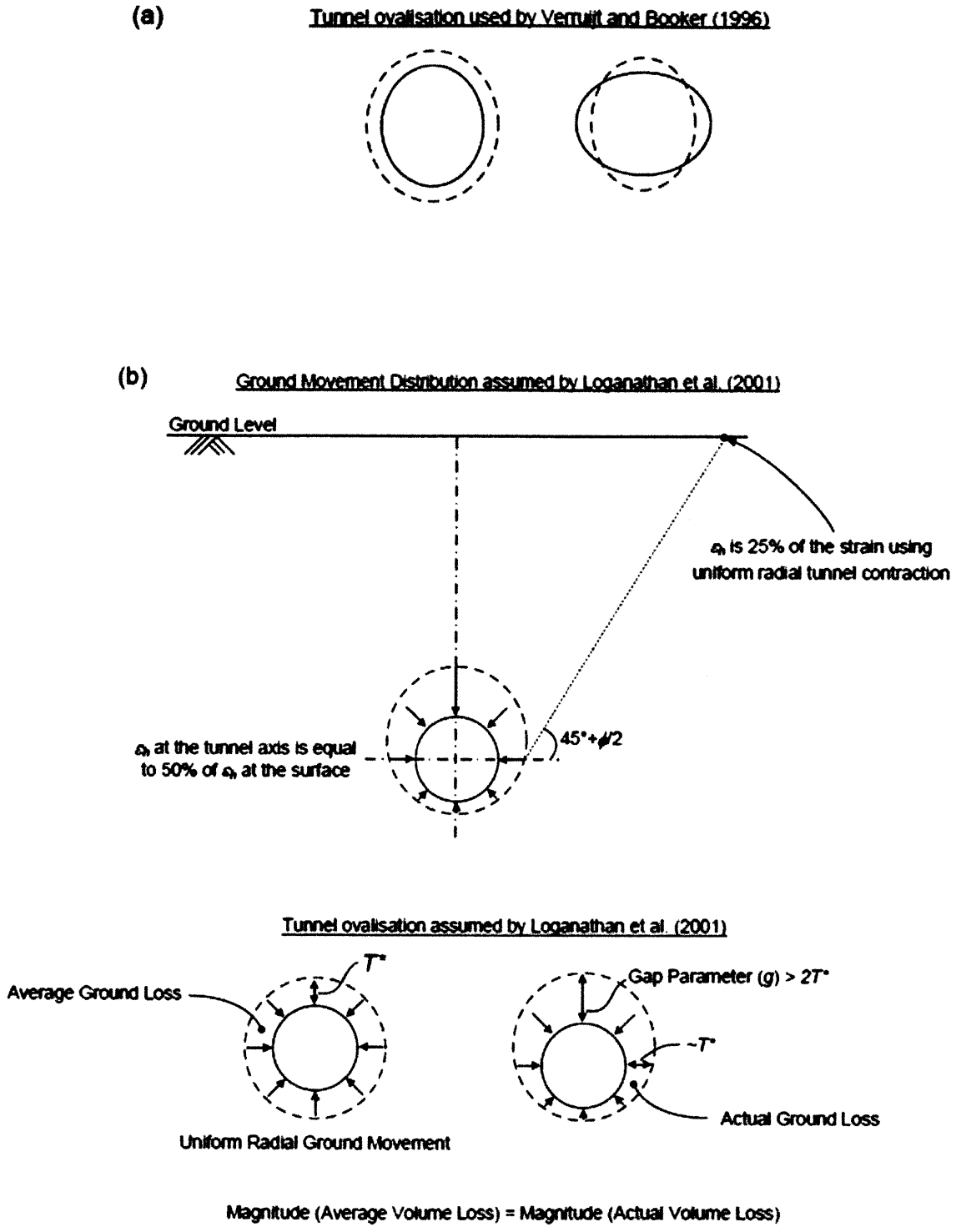

Figure 2-11: Assumption of ovalization and distribution of ground movement

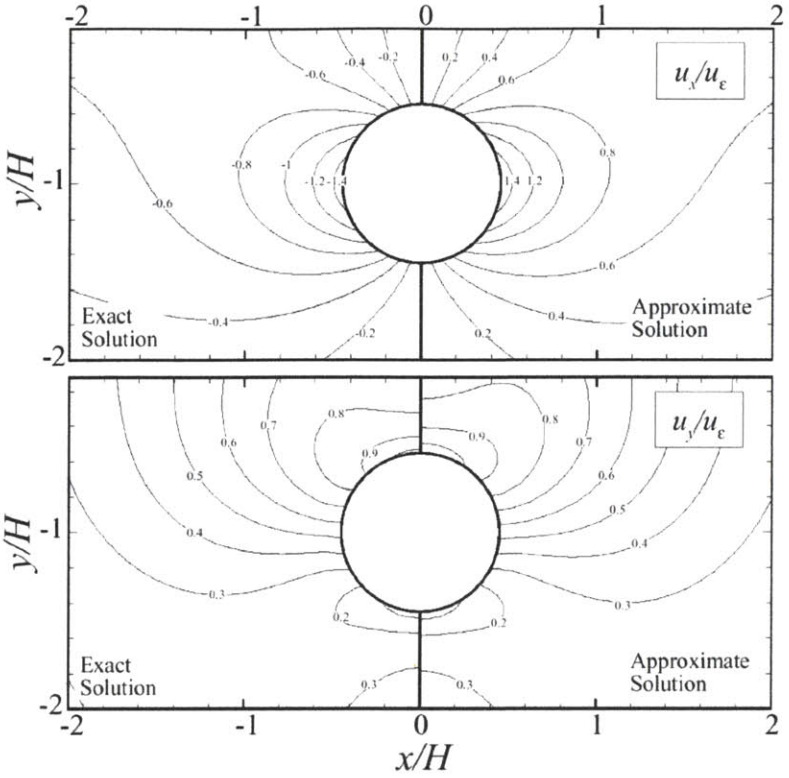

Figure 2-12: Comparison of elastic solutions for shallow tunnels (Pinto, 1999)

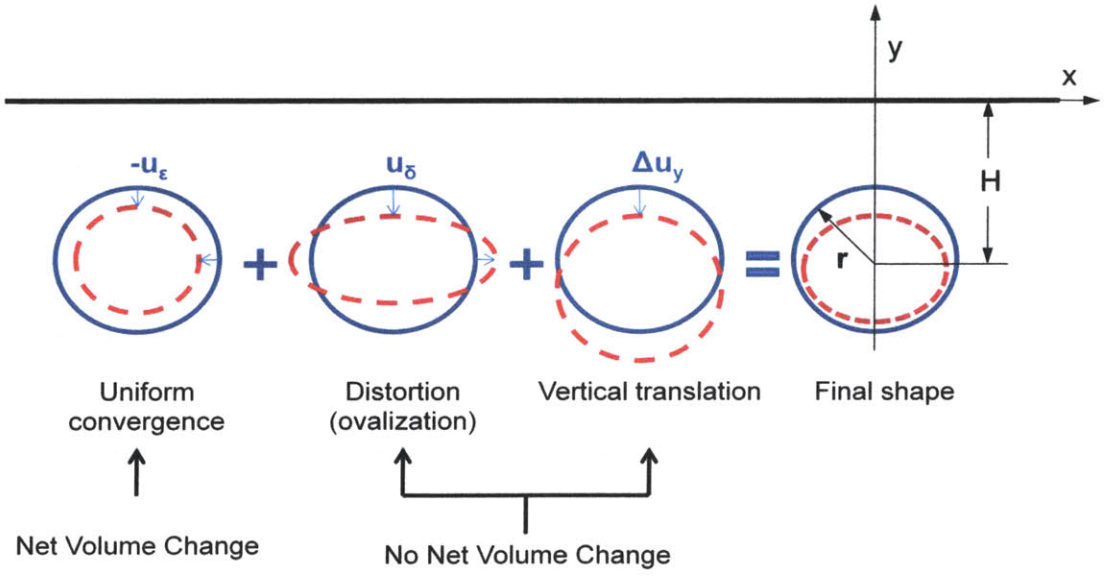

Figure 2-13: Deformation modes around tunnel cavity
(after Whittle and Sagaseta, 2003)

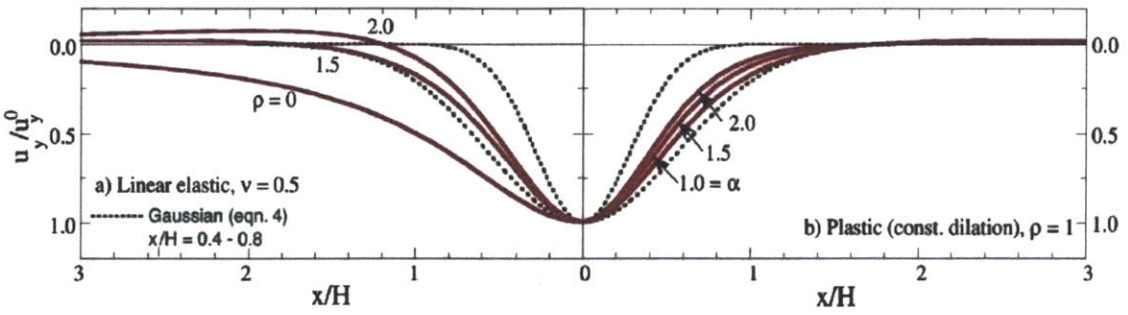

Figure 2-14: Effect of input parameters on surface settlement distribution (Whittle and Sagaseta, 2003)

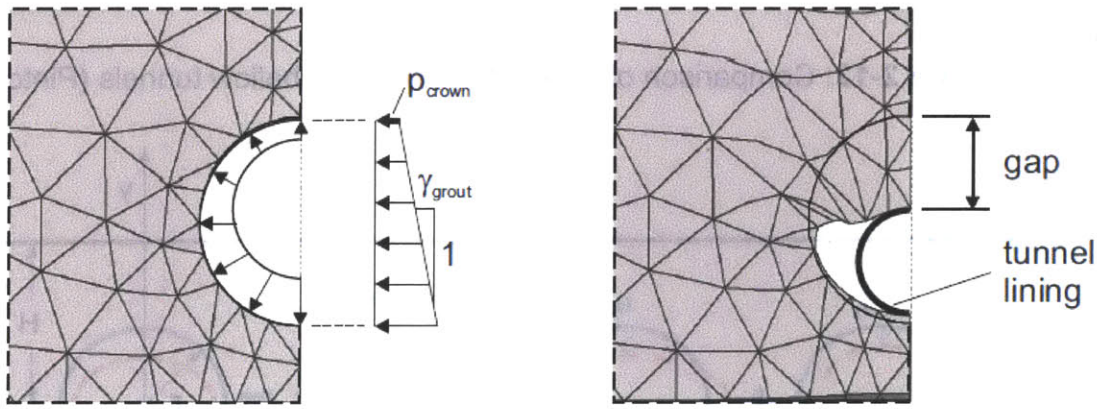

Figure 2-15: Display of the grout pressure method (Moeller, 2006)

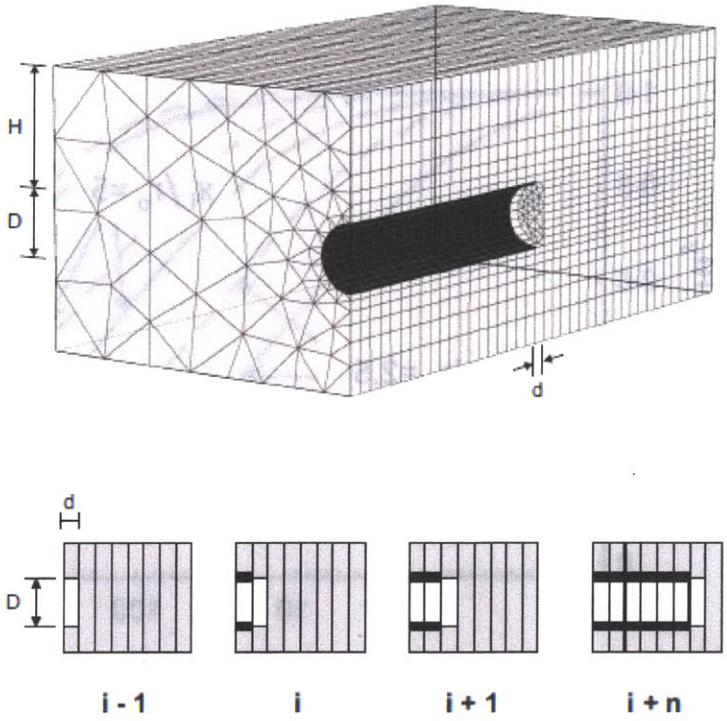

Figure 2-16: Simulation of open-face, NATM tunneling (Moeller, 2006)

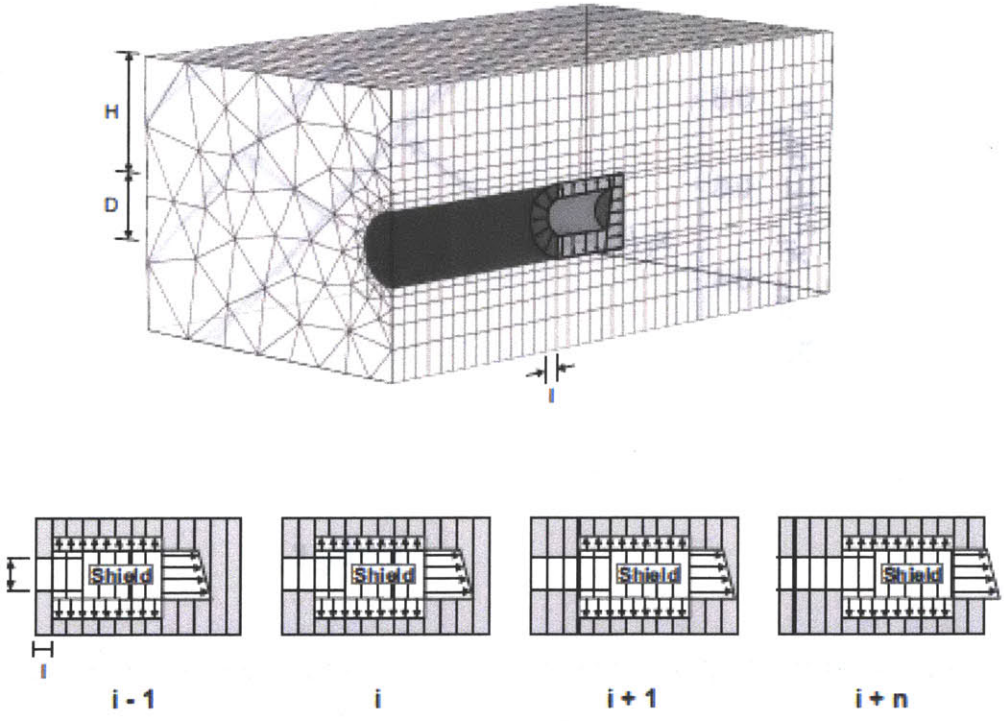

Figure 2-17: Simulation of closed-face, shield tunneling (Moeller, 2006)

a)

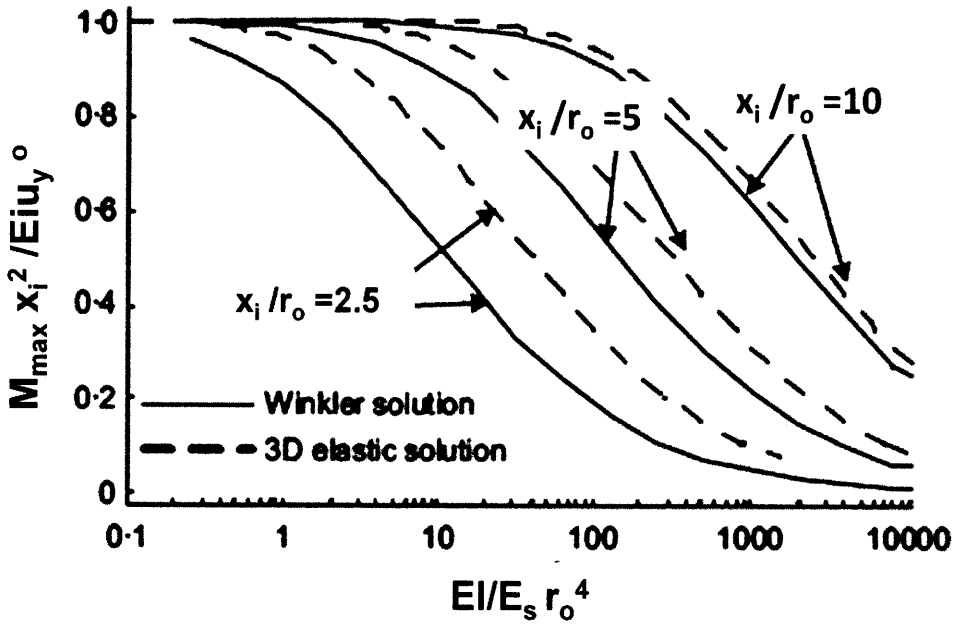

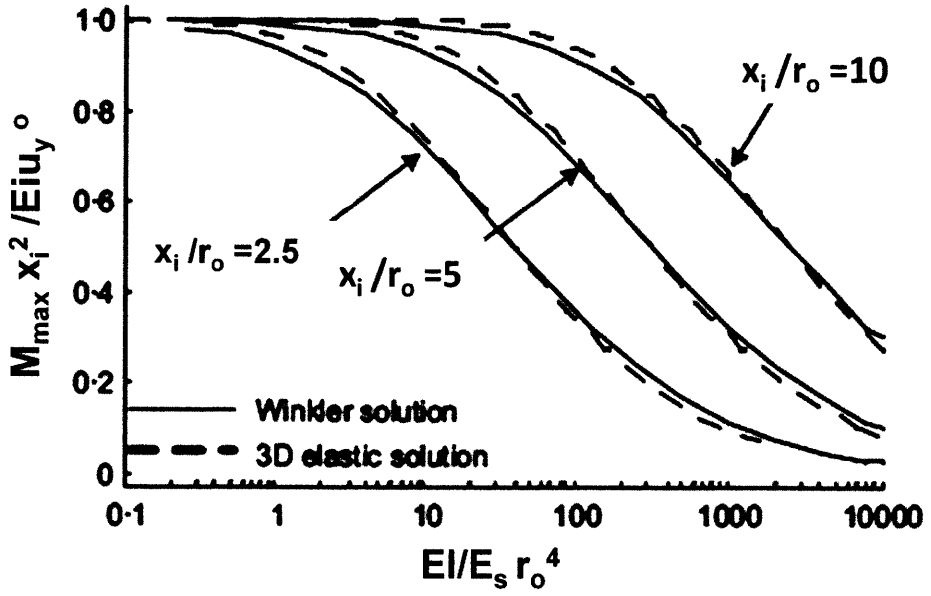

b)

Figure 2-18: Comparison between continuum solution and Winkler model using a)Vesic analog and b) new proposed analog (Klar et al., 2005)

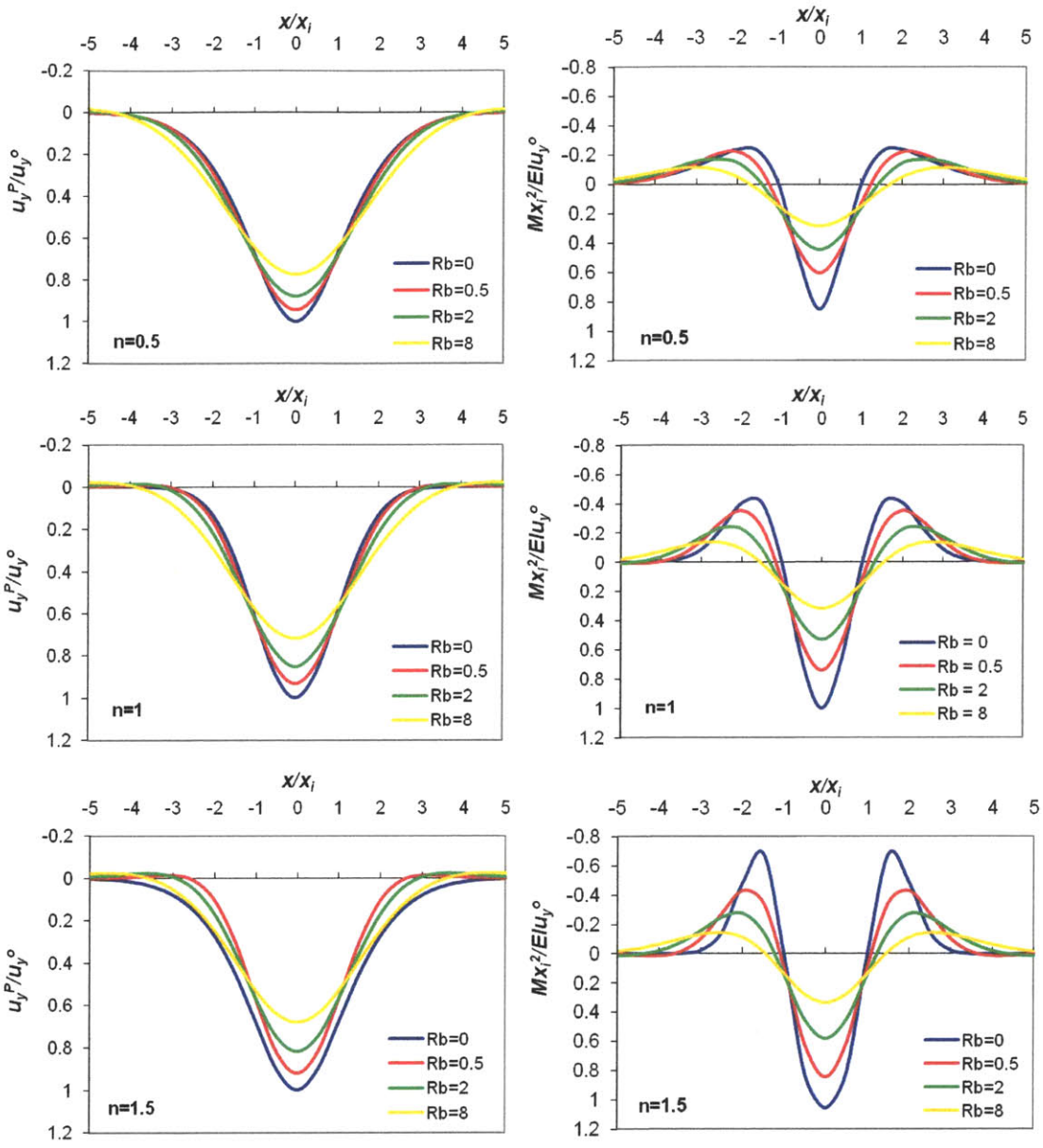

Figure 2-19: Normalized bending stiffness and settlements of a pipe relative to the relative pipe-soil bending rigidity factor R_b (after Vorster et al., 2005)

CHAPTER 3

BENDING RESPONSE OF CONTINUOUS PIPELINES TO TUNNELING

3.0 INTRODUCTION

This chapter describes the model used to simulate the response of continuous pipelines to tunnel-induced ground deformations, assuming that the latter are described either by a modified Gaussian curve distribution or by the analytical solutions proposed by Pinto & Whittle (2001). Interactions between the pipe and the soil are described using a beam-on-elastic-foundation model. The approximations in this model are then validated using numerical finite element analyses.

3.1 FREE-FIELD SETTLEMENTS

Bending moments and settlements of continuous pipelines occur due to external forces associated with tunnel-induced ground displacements. Vertical components of ground displacements have been described by Vorster (2005) using empirical modified Gaussian functions, while Pinto & Whittle (2001) proposed analytical solutions for assumed modes of tunnel cavity deformations (Equations 2.13 and 2.14). Differences in the two solutions give rise to different sets of loads on the pipelines and hence, in predictions of critical stress conditions.

3.1.1 Empirical Solutions (Vorster, 2005)

As it is described in Chapter 2, Vorster (2005) suggested the use of a modified Gaussian function to describe free field settlements observed in a series of centrifuge tests.

$$u_y = u_y^o \frac{n}{(n-1) + e^{A\left(\frac{x}{x_i}\right)^2}} \qquad (3.1a)$$

$$n = \frac{e^A(2A-1)}{(2A+1)} + 1 \qquad (3.1b)$$

where:

x_i = horizontal distance between the tunnel centerline and the inflection point

n = shape function parameter controlling the width of the profile

A = parameter that ensure x_i remains a fixed distance to the inflection point

It has to be noted that α parameter is a number chosen by the user, such that it ensures that x_i remains the distance to the inflection point.

Figure 3-1 illustrates a flow chart shows which shows what the required input parameters are, and what the procedure is in order to obtain the final solution which describes the free field settlements at any depth, by using Vorster's method.

3.1.2 Analytical Solutions (Pinto & Whittle, 2001)

Pinto and Whittle (2001) proposed closed-form analytical solutions for describing the vertical and horizontal tunnel induced free-field displacements. They related the ground displacements to three prescribed displacements

happening at the tunnel cavity: a) uniform convergence u_ε, b) ovalization u_δ and c) uniform vertical translation Δu_y (Figure 2-13). The values of Δu_y are functions of the input parameters u_ε and u_δ as shown in Equations 2.14c and 2.15c. The simplified closed form solutions are given by Equations 2.14 and 2.15. Figure 3-2 summarizes the required input parameters and the procedure in order to obtain the final solution which describes the free field settlements at any depth.

Comparing the two methods, it can be observed that both require the same four parameters; the tunnel depth (H), the tunnel radius (r), the pipe depth (y) and the volume loss (ΔV_L), with $\frac{\Delta V_L}{V_o} = -\frac{2u_\varepsilon}{r}$. In addition, Vorster (2005) method requires the trough shape parameter (A) which best fits the free field settlement data, while Pinto & Whittle (2001) requires the relative distortion $\rho = -u_\delta/u_\varepsilon$ and the Poisson's ratio (v) of the soil.

Figure 3-3 shows a comparison of the Vorster (2005) and Pinto & Whittle (2001) surface settlement troughs for a circular tunnel with $r/H=0.2$ and soil Poisson's ratio $v=0.5$. These examples show that Pinto & Whittle (2001) solutions with relative distortion $\rho=1$, are comparable to surface settlements obtained by Vorster (2005) (modified Gaussian curve) with $n=0.5$, while results for relative distortion $\rho=2$, are in close agreement with the simple Gaussian curve (n=1).

The subsurface free field-settlements for the same case at a depth ratio $y_p/H=0.2$, are shown in Figure 3-4. It can also be observed that P&W solutions can actually give similar results with simple or modified Gaussian curves. More specifically, for this case, P&W with a relative distortion $\rho=1$ fit a simple Gaussian curve and for $\rho=0.5$, fit a modified Gaussian curve with $n=0.5$.

3.2 PIPELINE BENDING RESPONSE

One of the goals of this research is to derive analytical solutions describing the bending response of an existing continuous pipeline due to tunnel-induced ground deformations. For this reason, the mathematical model must be first described.

3.2.1 General Solutions Using a Winkler's Model

Figure 3-5, shows a pipeline of radius r_o, Young's modulus E_p and wall thickness t, buried at a depth y_p in a soil with Young's modulus E_s and Poisson's ratio v. By using a Winkler's model, we assume that the pipeline is connected with the soil with vertical and horizontal spring coefficients, K_v and K_h, respectively. The basic assumptions made are:

[1] the soil is homogeneous and elastic

[2] the pipe is continuous

[3] the pipe does not affect the tunnel

[4] the pipe is always in contact with the soil

Ignoring the horizontal springs and keeping only the vertical, the mathematical model which describes the bending response of a buried pipeline is the same as the model describing a beam on elastic foundation (after Hetenyi 1946). Figure 3-6 shows the response of a beam pipe (u_y^P) connected to the soil with vertical springs of coefficient K_v, to the vertical displacements of the soil (u_y). The general mathematical equation which describes the problem is:

$$\frac{\partial^4 u_y^P}{\partial x^4} + 4\lambda_v{}^4 \cdot u_y^P = 0 \qquad (3.2a)$$

$$\lambda_v = \sqrt[4]{\frac{K_v}{4EI}} \qquad (3.2b)$$

where:

u_y^P = pipeline vertical displacement

K_v = vertical spring coefficient

EI = bending stiffness of the pipe

The general solution of Equation 3.2 is:

$$u_y^P = E_1 e^{-\lambda_v x}(cos\lambda_v x + isin\lambda_v x) + E_2 e^{-\lambda_v x}(cos\lambda_v x - isin\lambda_v x) + E_3 e^{\lambda_v x}(cos\lambda_v x + isin\lambda_v x) + E_4 e^{\lambda_v x}(cos\lambda_v x - isin\lambda_v x)$$

$$u_y^P = e^{-\lambda_v x}(C_1 cos\lambda_v x + C_2 sin\lambda_v x) + e^{\lambda_v x}(C_3 cos\lambda_v x + C_4 sin\lambda_v x) \qquad (3.3)$$

Where E_1, E_2, E_3 and E_4 are grouped as:

$$C_1 = E_1 + E_2$$

$$C_2 = iE_1 - iE_2$$

$$C_3 = E_3 + E_4$$

$$C_4 = iE_3 - iE_4$$

The following boundary conditions are needed in order to solve the Equation 3.3.

- At $x \to \infty$, $u_y^P = 0$

  Because $e^{-\lambda_v x}(C_1 cos\lambda_v x + C_2 sin\lambda_v x) = 0$ for $x \to \infty$, it suffices that $e^{\lambda_v x}(C_3 cos\lambda_v x + C_4 sin\lambda_v x) = 0$. Therefore, $C_3 = C_4 = 0$

- At $x = 0$, $\frac{\partial u_y^P}{\partial x} = 0$

  Therefore, $-(C_1 - C_2) = 0 \Rightarrow C_1 = C_2 = C$

Finally we end up with:

$$u_y{}^P = Ce^{-\lambda_v x}(cos\lambda_v x + sin\lambda_v x) \tag{3.4}$$

The next step is to define the constant C.

The pipe is subjected to an equivalent distributed load $dP = K_v u_y(x)dx$ (based on the free-field displacements, $u_y(x)$) shown in Figure 3-7, such that:

$$\delta u_y{}^P = \frac{\lambda_v \cdot dP(x)}{2K_v} \cdot e^{-\lambda_v x}(cos\lambda_v x + sin\lambda_v x) \tag{3.5}$$

Thus Equation (3.5), becomes:

$$\delta u_y{}^P = \frac{\lambda_v}{2K_v} \cdot K_v du_y(x) \cdot e^{-\lambda_v x}(cos\lambda_v x + sin\lambda_v x) \Rightarrow$$

$$\delta u_y{}^P = \frac{\lambda_v}{2} du_y(x) \cdot e^{-\lambda_v x}(cos\lambda_v x + sin\lambda_v x) \tag{3.6}$$

The integration of Equation 3.6 gives the total settlement distribution of the pipeline (Figure 3-6).

The bending moments acting on the pipe are given by the following equation:

$$M = -EI\frac{\partial^2 u_y{}^P}{\partial x^2} \tag{3.7}$$

The distribution of the bending moments along the pipeline is given by the integration of the bending moments of all the infinitesimal elements of the pipeline which are described by:

$$\delta M = \frac{dP}{4\lambda_v} \cdot e^{-\lambda_v x}(cos\lambda_v x - sin\lambda_v x) \tag{3.8}$$

As it is shown in Figure 3-6, $dP = K_v u_y(x)dx$, thus Equation 3.8 becomes:

$$\delta M = \frac{K_v \cdot du_y(x)}{4\lambda_v} \cdot e^{-\lambda_v x}(cos\lambda_v x - sin\lambda_v x) \tag{3.9}$$

Equations 3.6 and 3.9 are not analytically soluble but are reliably solved numerically, (using Mathematica 7.0 software). In addition, several sets of pipe settlements and bending moments graphs were drawn, for different parameters of the equation that is chosen each time to describe the soil settlements distribution.

Assuming that the free-field settlements are described by a function *f(x)*, with maximum value at x=0, the pipe settlement at a point C (Figure 3-8), can be obtained by:

$$u_y{}^P = \frac{\lambda_v}{2K_v} \cdot \left(\int_0^b f\left(\frac{a-b}{2} + x\right) \cdot e^{-\lambda_v x}(cos\lambda_v x + sin\lambda_v x)dx \right.$$
$$\left. + \int_0^a f\left(\frac{a-b}{2} - x\right) \cdot e^{-\lambda_v x}(cos\lambda_v x + sin\lambda_v x)dx \right) \tag{3.10}$$

Similarly, the bending moments at point C are given by:

$$M = \frac{K_v}{4\lambda_v} \cdot \left(\int_0^b f\left(\frac{a-b}{2} + x\right) \cdot e^{-\lambda_v x}(cos\lambda_v x - sin\lambda_v x)dx \right.$$
$$\left. + \int_0^a f\left(\frac{a-b}{2} - x\right) \cdot e^{-\lambda_v x}(cos\lambda_v x - sin\lambda_v x)dx \right) \tag{3.11}$$

Following the same procedure for all the infinitesimal points of the pipe (by varying points α and b), we end up with the total settlement distribution of the pipeline.

For example, in the case of *f(x)* being a simple Gaussian curve (Equation 2.3). The pipe settlements and bending moments will be given as follows:

$$u_y{}^P = u_y{}^o \frac{\lambda_v}{2} \cdot \left(\int_0^b e^{-\left(\frac{1}{2}\right)\left(\frac{\frac{a-b}{2}+x}{x_i}\right)^2} e^{-\lambda_v x}(cos\lambda_v x + sin\lambda_v x)dx \right.$$

$$\left. + \int_0^a e^{-\left(\frac{1}{2}\right)\left(\frac{\frac{a-b}{2}-x}{x_i}\right)^2} e^{-\lambda_v x}(cos\lambda_v x + sin\lambda_v x)dx \right) \quad (3.12)$$

$$M = u_y{}^o \frac{K_v}{4\lambda_v} \cdot \left(\int_0^b e^{-\left(\frac{1}{2}\right)\left(\frac{\frac{a-b}{2}+x}{x_i}\right)^2} e^{-\lambda_v x}(cos\lambda_v x - sin\lambda_v x)dx \right.$$

$$\left. + \int_0^a e^{-\left(\frac{1}{2}\right)\left(\frac{\frac{a-b}{2}-x}{x_i}\right)^2} e^{-\lambda_v x}(cos\lambda_v x - sin\lambda_v x)dx \right) (3.13)$$

Application of the modified Gaussian equation and Pinto & Whittle (2001) analytical solutions, are presented in Appendix I.

The above equations are solved numerically and the solutions are presented in Figure 2-19. These graphs reproduce pipe settlements and bending moments of the analyses proposed by Vorster (2005) analyses, estimating using modified Gaussian curves, for different bending rigidity factors R_b.

$$R_b = \frac{EI}{E_s r_o {x_i}^3} \quad (3.14)$$

The factor R_b indicates the relative rigidity of the pipe in bending. For typical water pipes, the range of R_b is $0<R_b\leq 8$.

Pinto & Whittle (2001) free field settlements have been integrated in Equations 3.12 and 3.13 (for details, see Appendix I) and twelve sets of normalized pipe settlements and bending moments are proposed for different values of ρ, y/H,

r/H, v and R_b in Figures 3-9 through 3-16. The pipe settlement are normalized by the maximum free-field settlement at the pipe level (u_y^P/u_y^o), while dimensionless pipe bending moments follow the expression $M_n=Mx_i^2/EIu_y^o$ proposed by Vorster (2005). For the Pinto and Whittle (2001) solutions, the inflection point parameter x_i is found from the second derivative of the equation that describes the free field settlements at the pipe level.

For all the analyses performed, the vertical spring coefficient K_v, is defined by Klar et al. (2005).

$$K_v = \frac{12E_s r_o}{x_i} \tag{3.15}$$

This expression has been verified by matching the analytical solutions with finite element analyses performed using PLAXIS 3D Tunneling as shown in Chapter 5.

From Figures 3-9 through 3-16 the following conclusions are drawn:

- As the ratio r/H increases, the settlement trough becomes wider and the normalized bending moments M_n slightly increase (Figures 3-9 and 3-12).
- As the relative distortion (ρ) increases, the settlement trough becomes narrower, the maximum value of u_y^P/u_y^o decreases and the normalized bending moments (M_n) also increase for any R_b value (Figures 3-10 and 3-14).
- As the pipe depth (y_p/H) increases, the settlement trough becomes narrower and both the ratio u_y^P/u_y^o and the normalized bending moments increase (Figures 3-11 and 3-15).
- Finally, as the Poisson's ratio (v) increases, the settlement trough becomes narrower, the ratio u_y^P/u_y^o decreases, and the normalized bending moments (M_n) increase (Figures 3-12 and 3-16).

3.2.2 Pipe Strains and Stresses

The pipe settlements and bending moments are computed in order to estimate the strains and stresses acting on the pipelines. The axial strain ε_b is the strain in the extreme pipe fiber due to bending.

$$\varepsilon_b = r_o \frac{M(x)}{EI} = r_o \frac{\partial^2 u_y^P}{\partial x^2} \tag{3.16}$$

Figure 3-17 shows the sign of the axial strain ε_b, considering tension as positive and compression as negative.

The axial pipe stresses (σ_x), can be computed using the axial strains by:

$$\sigma_x = E_P \cdot \varepsilon_b \tag{3.17}$$

where E_p is the pipe material Young's modulus. Once again, tensile stresses are considered positive and compressive, negative.

The axial stresses acting on pipes due to bending are computed in order to estimate the possibility of pipe failure in tension or compression. This is achieved by comparing the axial stress acting on the pipe with the maximum allowable stress (tensile and compressive) which depends on the pipe material. It must be noted though that the maximum allowable axial stress decreases as the age of the pipe increases and therefore, the value of the maximum stress at failure of an existing pipeline will not be the one reported in the standards, for new installed pipelines.

Figures 3-13 through 3-16 give the normalized bending moments $M_n = Mx_i^2/EIu_y^o$ acting on a pipeline, and in the mean time they can give the pipe normalized strains and stresses. From Equations 3.7 and 3.16 we get:

$$M = -EI \frac{\partial^2 u_y{}^P}{\partial x^2} \Rightarrow \frac{M}{EI} = \frac{\varepsilon_b}{r_o} \tag{3.18}$$

Also from Equations 3.17 and 3.18 we get:

$$\frac{M}{EI} = \frac{\varepsilon_b}{r_o} = \frac{E_p \cdot \sigma_x}{r_o} \tag{3.19}$$

Therefore, Figures 3.13 through 3.16 also illustrate the normalized axial pipe strains, $\varepsilon_{b_n} = \varepsilon_b x_i^2 / r_o u_y^o$ and stresses $\sigma_{x_n} = \sigma_x x_i^2 / E_p r_o u_y^o$ due to bending. Representatively, Figure 3-18 gives the normalized axial pipe strains and stresses for *r/H=0.25, ρ=0.5, y_p/H=-0.2* and *v=0.5.*

3.3 SUMMARY

This chapter compares free-field settlements computed according to empirical methods used by Vorster (2005) with analytical solutions from Pinto & Whittle (2001). A Winkler model is used, in order to describe the response of an existing continuous pipeline to tunnel-induced ground settlements. The pipeline response (settlements and bending moments) was derived under the assumption that the problem of a pipe on an elastic half-space is equivalent to a Winkler's beam on elastic foundation, where the pipeline is connected to the soil with vertical springs.

Solving the equations which describe the Winkler problem, assuming that the free-field settlements are described analytical closed-form solutions (Pinto & Whittle 2001), a set of graphs is produced for estimating the pipe settlements and bending moments, by varying the pipe depth y_p, the tunnel radius *r,* the tunnel depth *H*, the Poisson's ratio *v* and the relative distortion *ρ* happening at the tunnel cavity. All graphs are drawn for different pipe-soil relative bending rigidity factors R_b, the value of which indicates how rigid is the pipe compared to its surrounding soil.

Finally, from the computed pipe bending moments, pipe axial strains and stresses can be evaluated. In order to estimate the possibility of pipe failure to tension or compression, axial stresses acting on the pipe should be compared with the allowable axial stresses which depend on the pipe material.

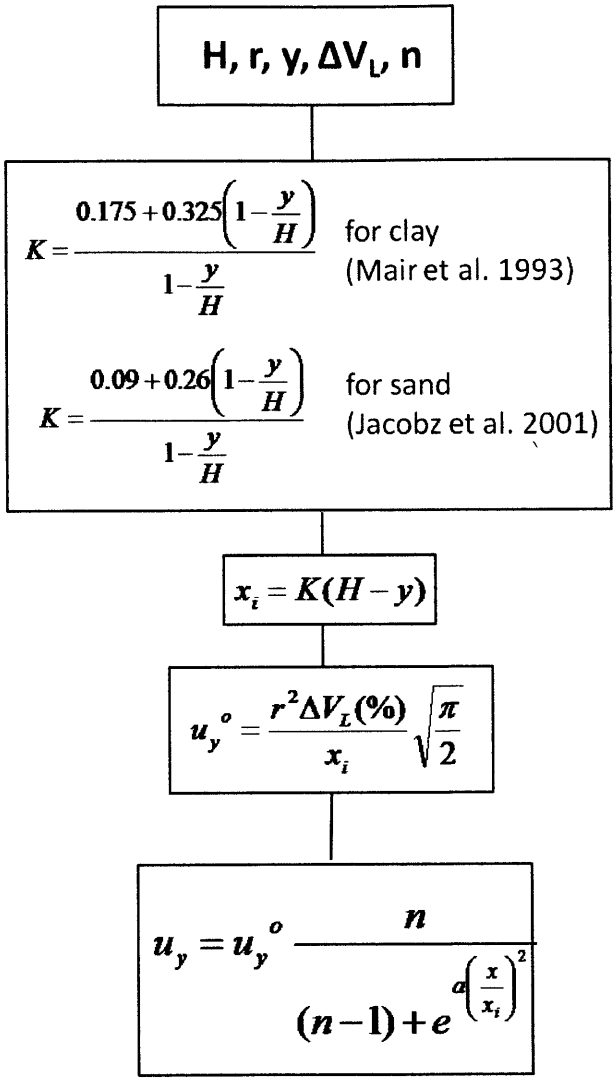

Figure 3-1: Vorster (2005) method to describe the free field settlements

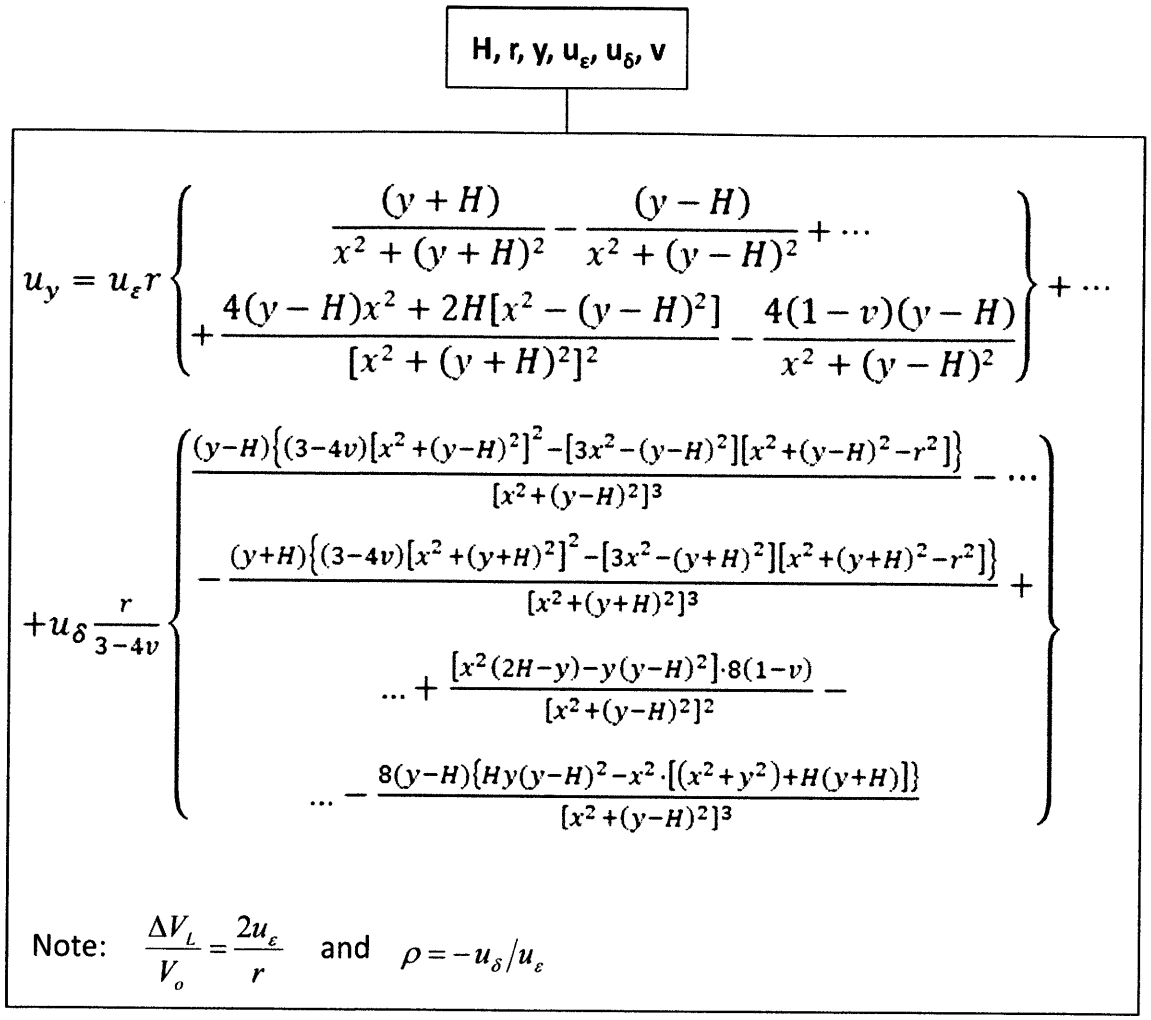

Figure 3-2: Pinto and Whittle (2001) method to describe free field settlements

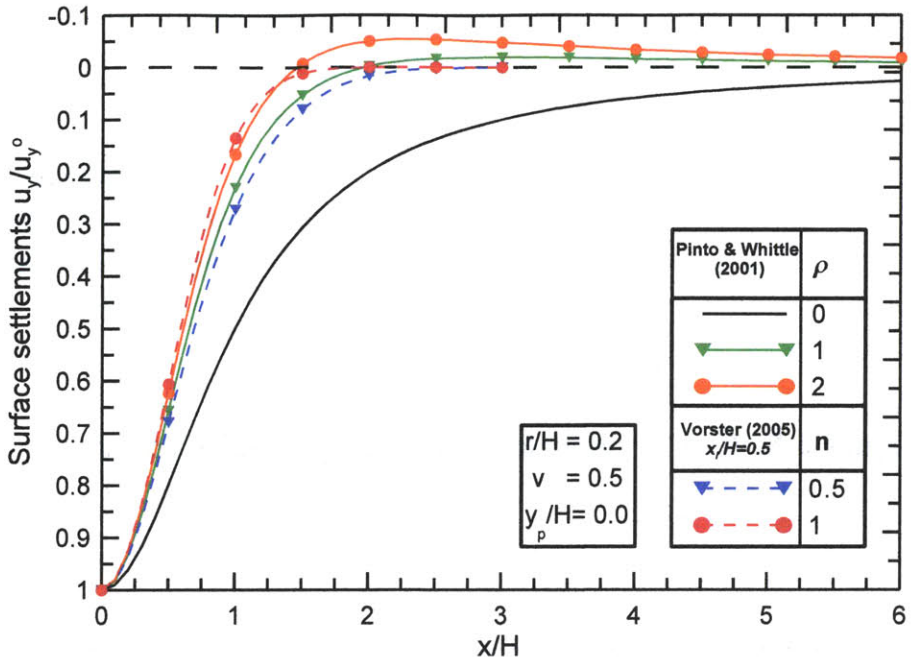

Figure 3-3: Comparison between surface free-field normalized settlements computed by empirical and analytical ground models

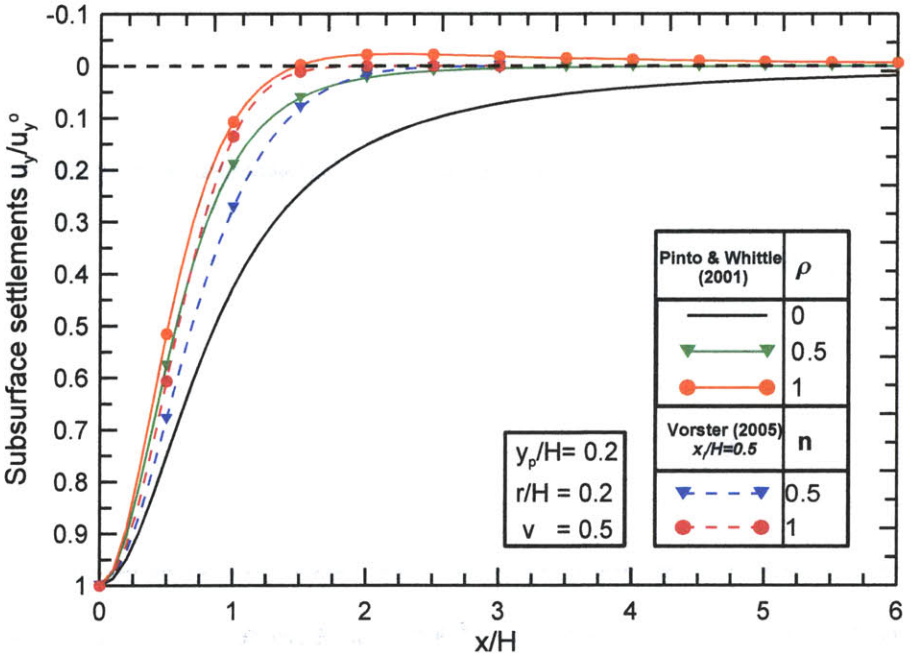

Figure 3-4: Comparison between subsurface free-field normalized settlements computed by empirical and analytical ground models

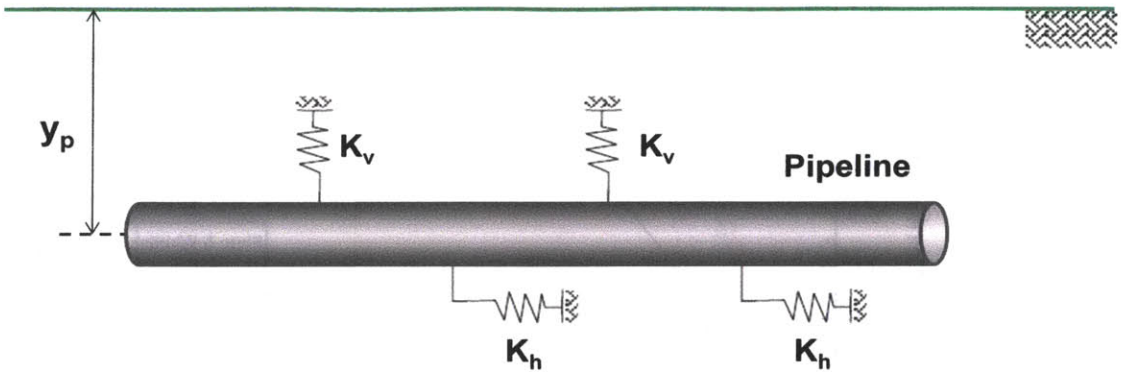

Figure 3-5: Winkler model for representing a buried continuous pipeline in the ground

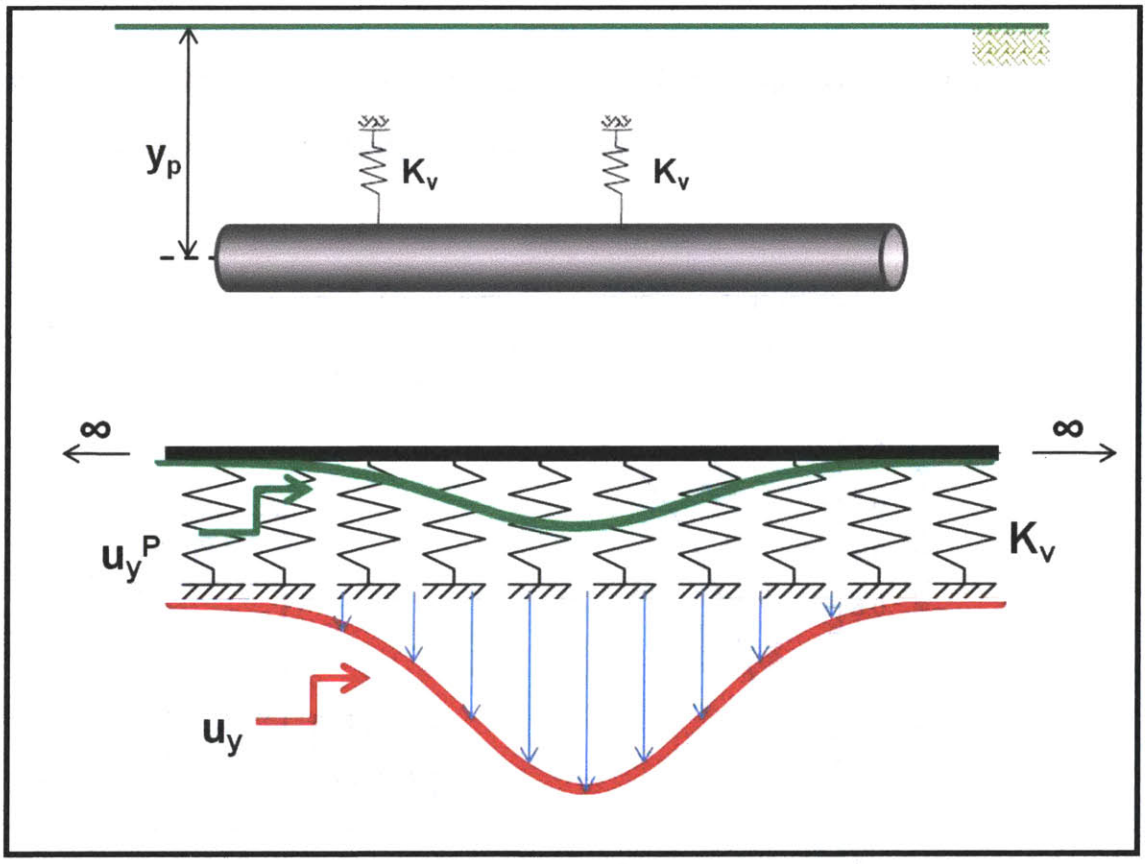

Figure 3-6: Bending response of a pipeline represented by a Winkler analogue of a beam lying on elastic foundation (Hetenyi, 1946)

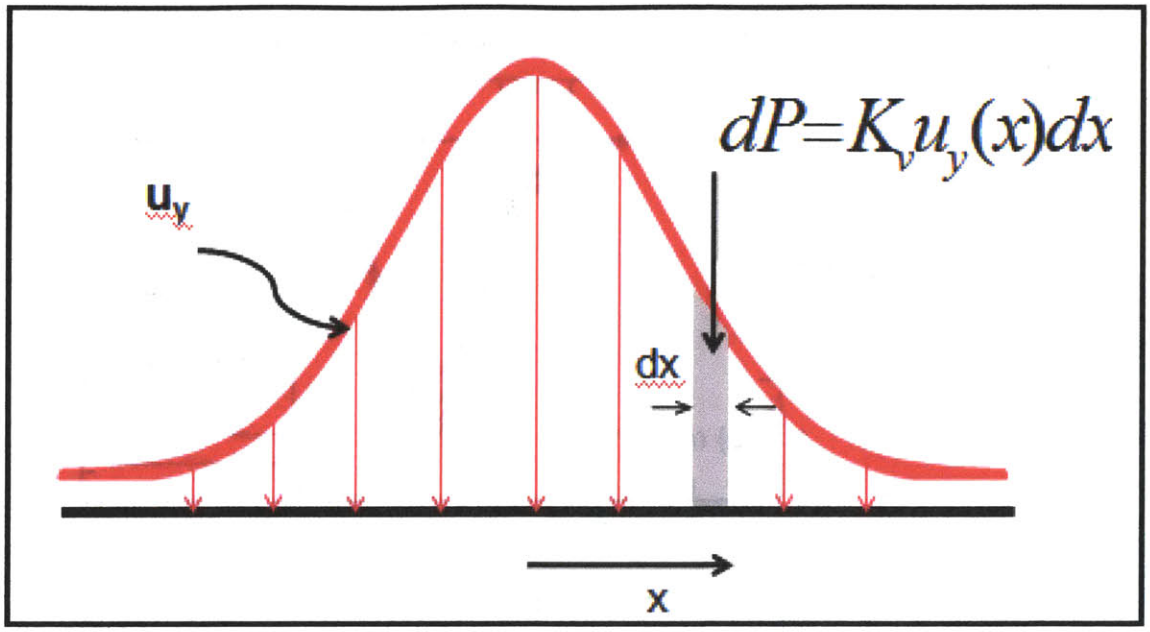

Figure 3-7: Vertical loading of a pipeline with infinite pointed loads dP

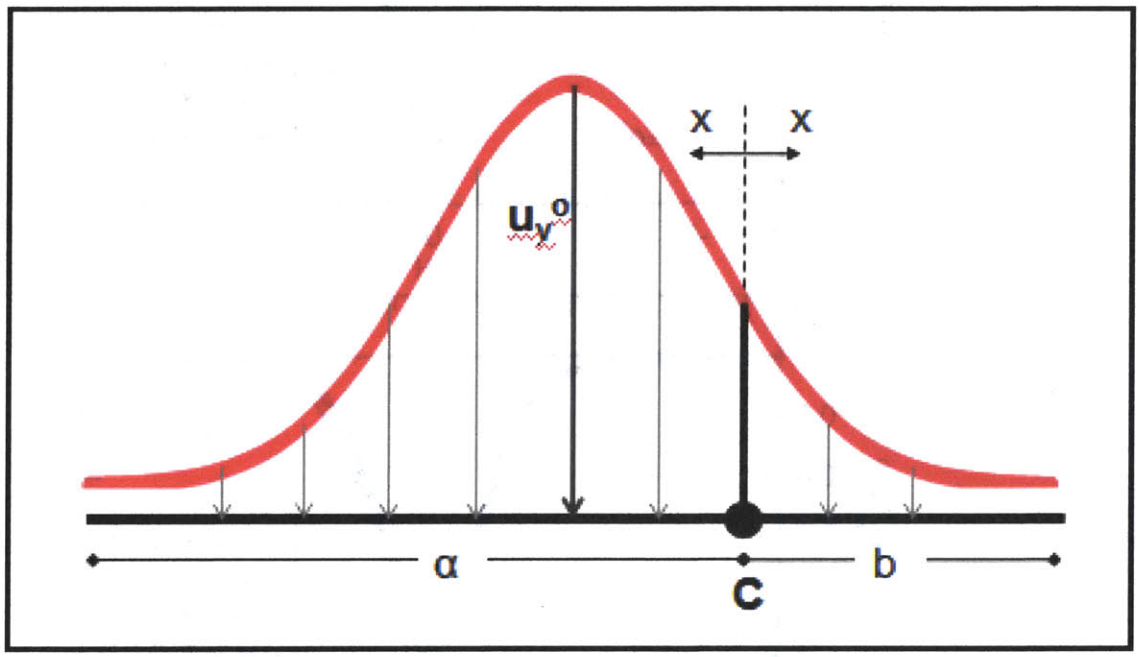

Figure 3-8: Defining the location of an arbitrary point C, where pipe displacements are computed due to vertical loading at parts α and b

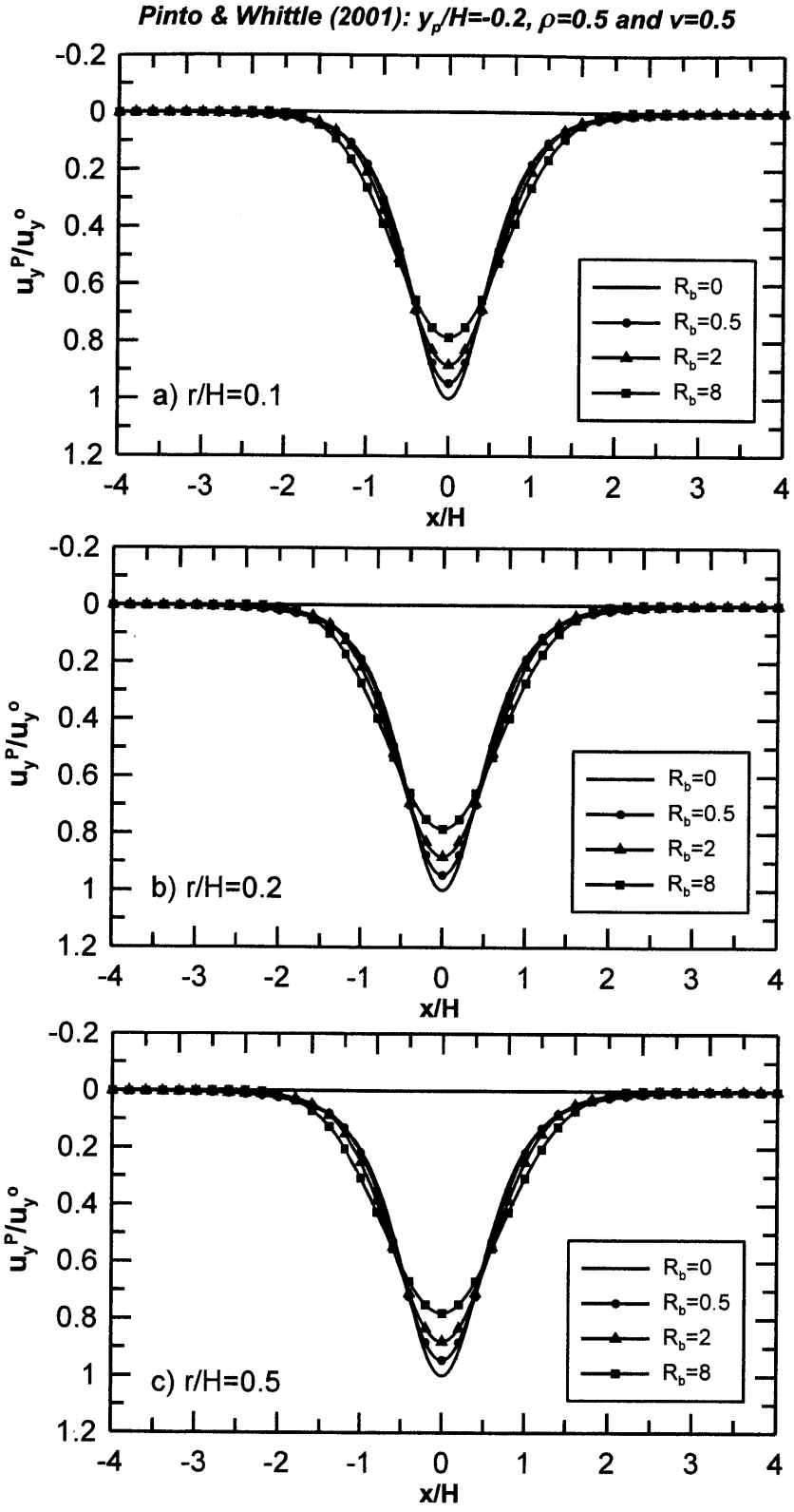

Figure 3-9: Effect of pipe radius and relative pipe-soil bending rigidity factor, $R_b=EI/E_s r_o x_i^3$, on normalized pipe settlements

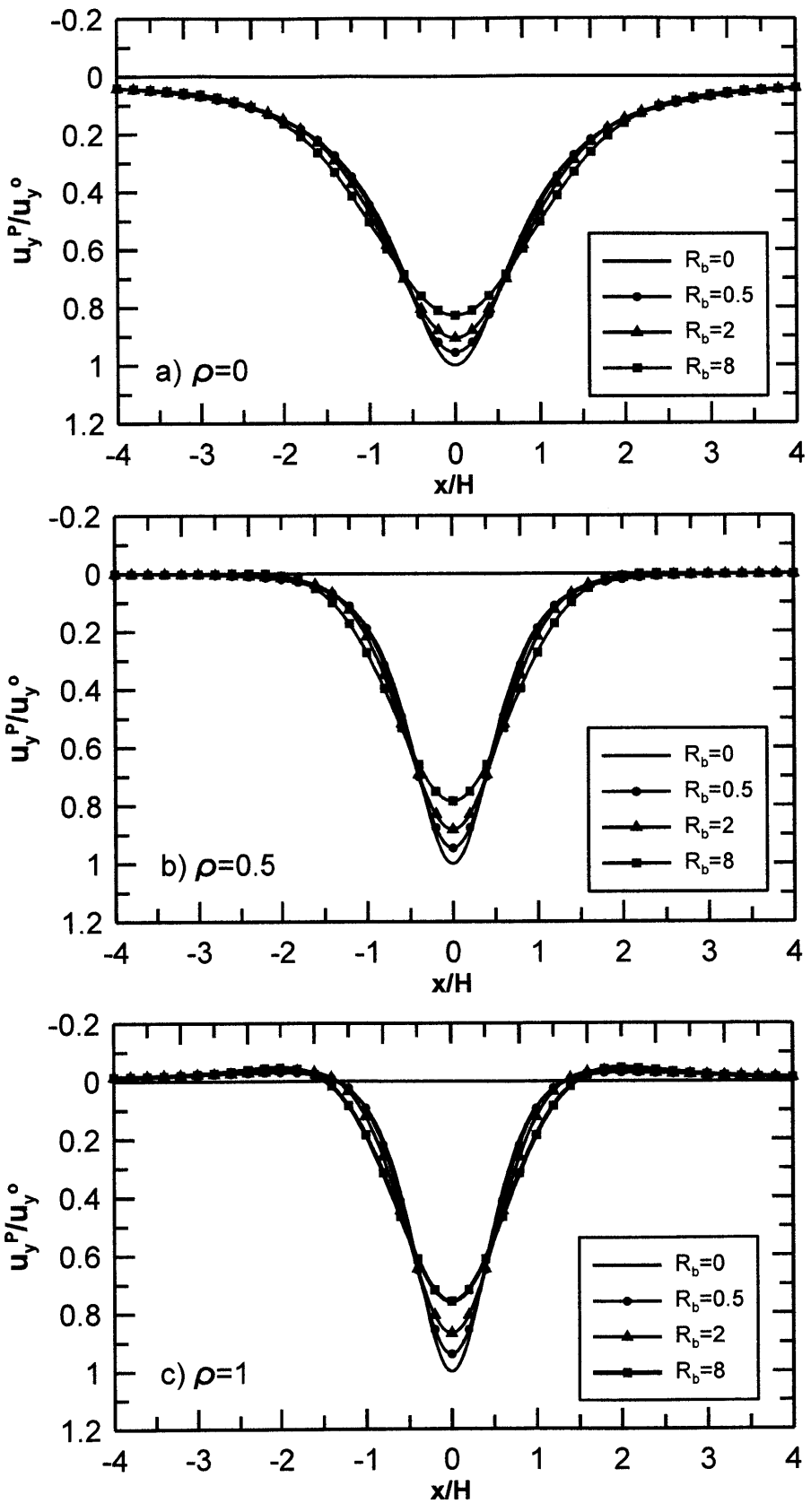
Pinto & Whittle (2001): y_p/H=-0.2, r/H=0.25 and v=0.5
u_y^P/u_y^o
x/H
a) ρ=0
b) ρ=0.5
c) ρ=1
R_b=0
R_b=0.5
R_b=2
R_b=8

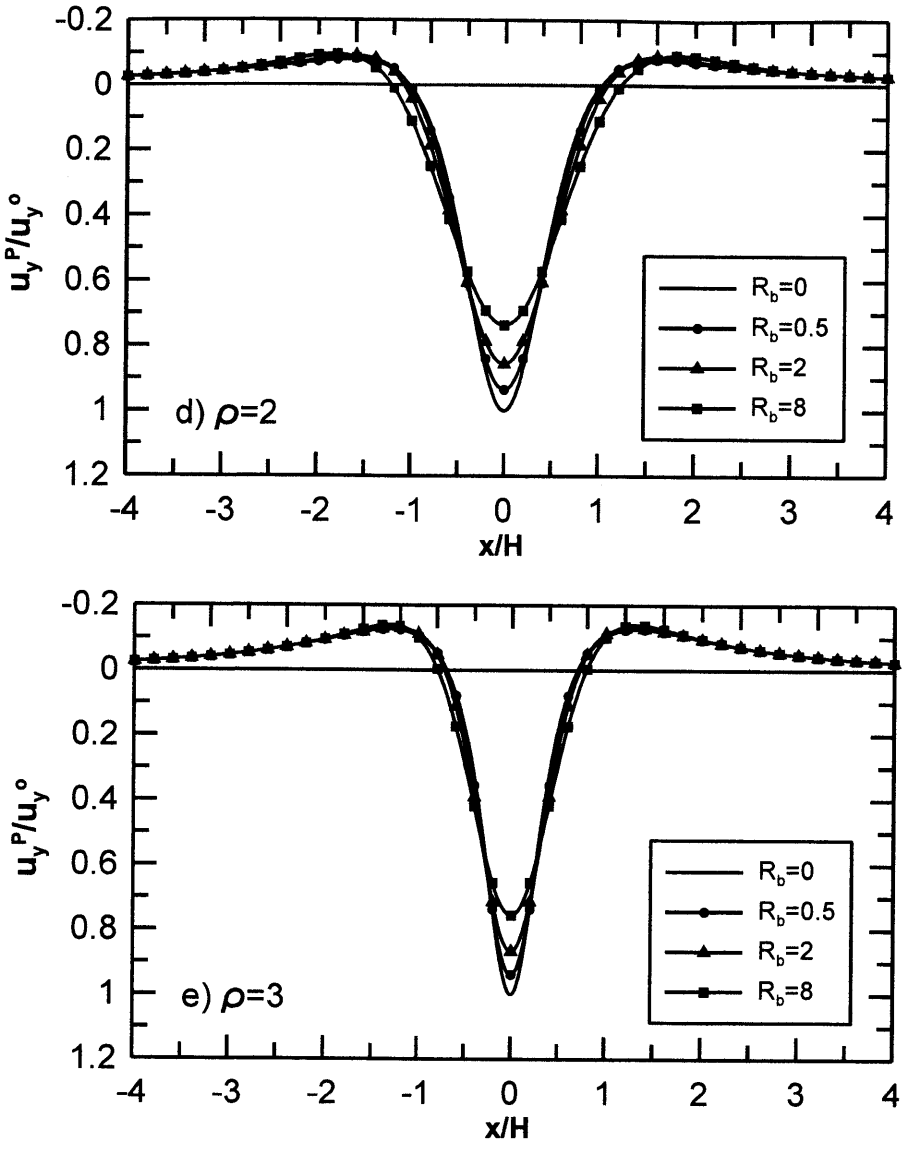

Figure 3-10: Effect of relative distortion, ρ and relative pipe-soil bending rigidity factor, $R_b=EI/E_s r_o x_i^3$, on normalized pipe settlements

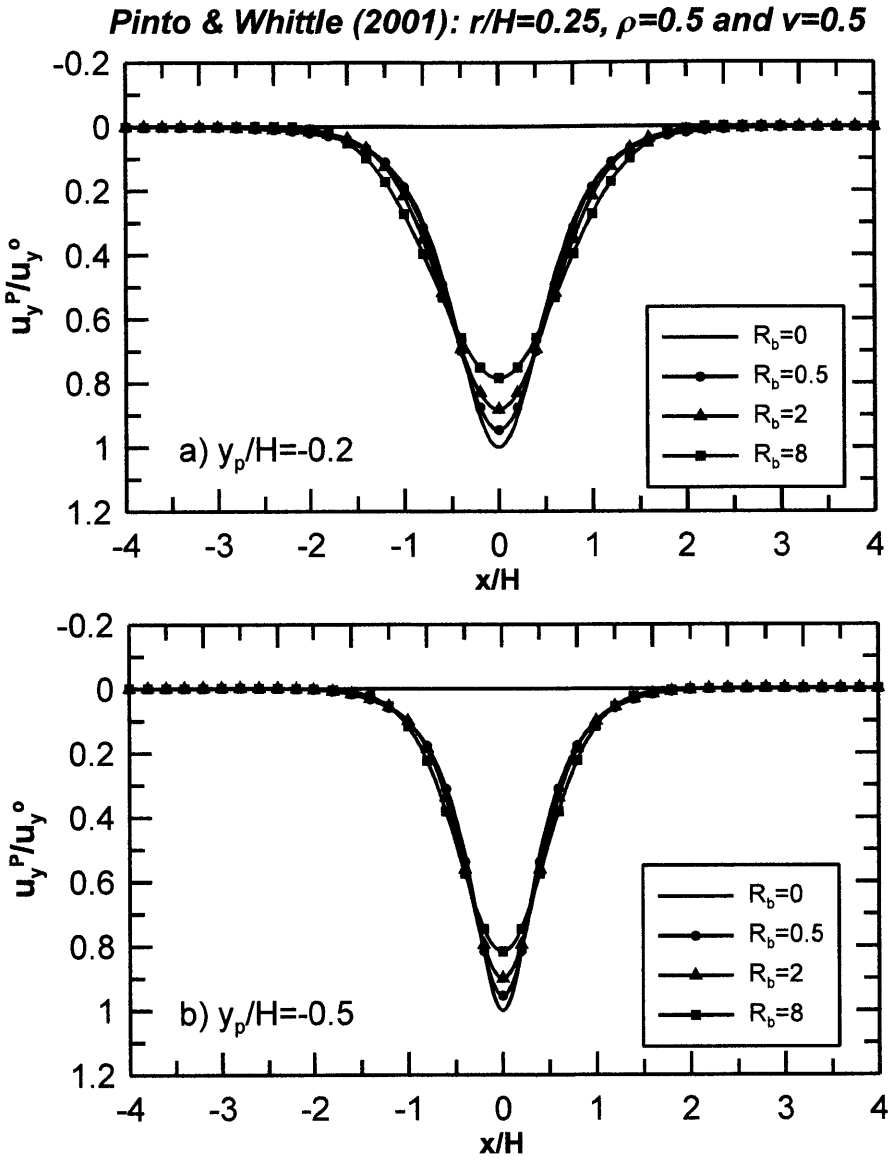

Figure 3-11: Effect of pipe embedment depth, y and relative pipe-soil bending rigidity factor, $R_b=EI/E_s r_o x_i^3$, on normalized pipe settlements

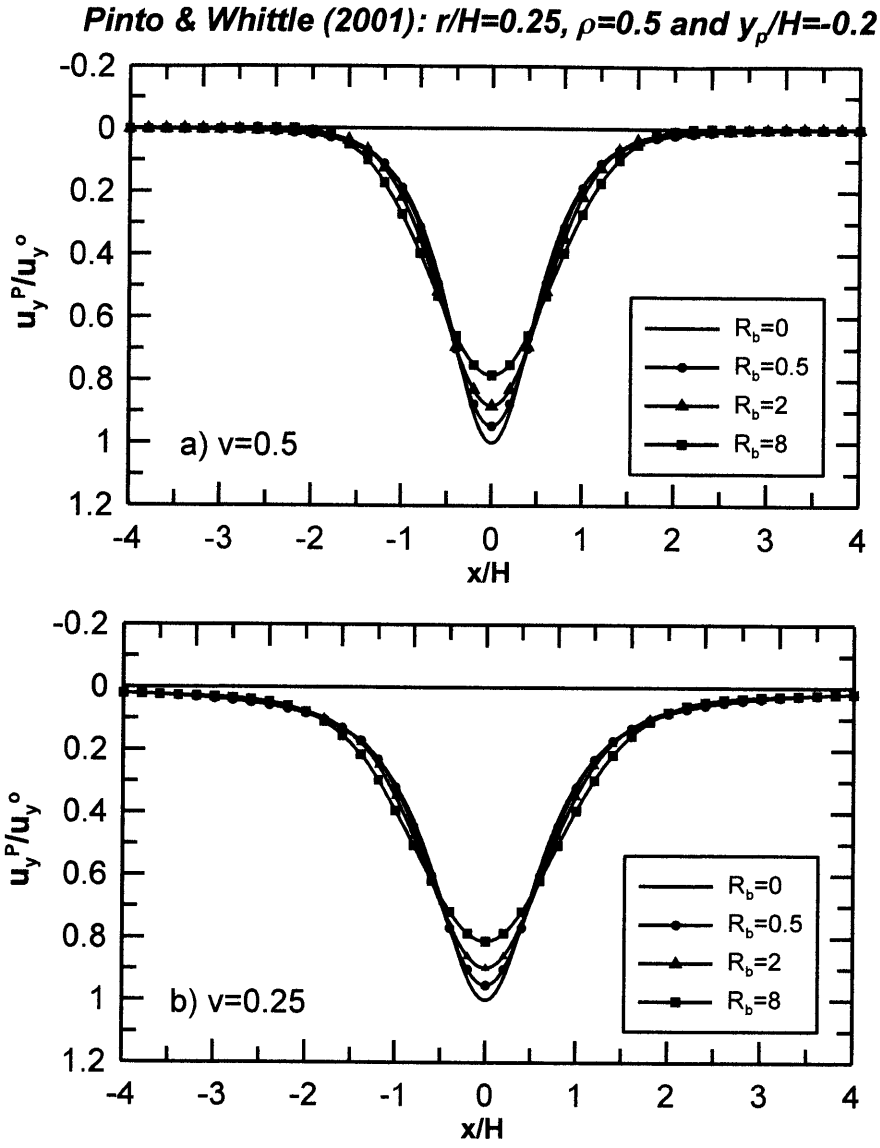

Figure 3-12: Effect of soil Poisson's ratio, v and relative pipe-soil bending rigidity factor, $R_b=EI/E_s r_o x_i^3$, on normalized pipe settlements

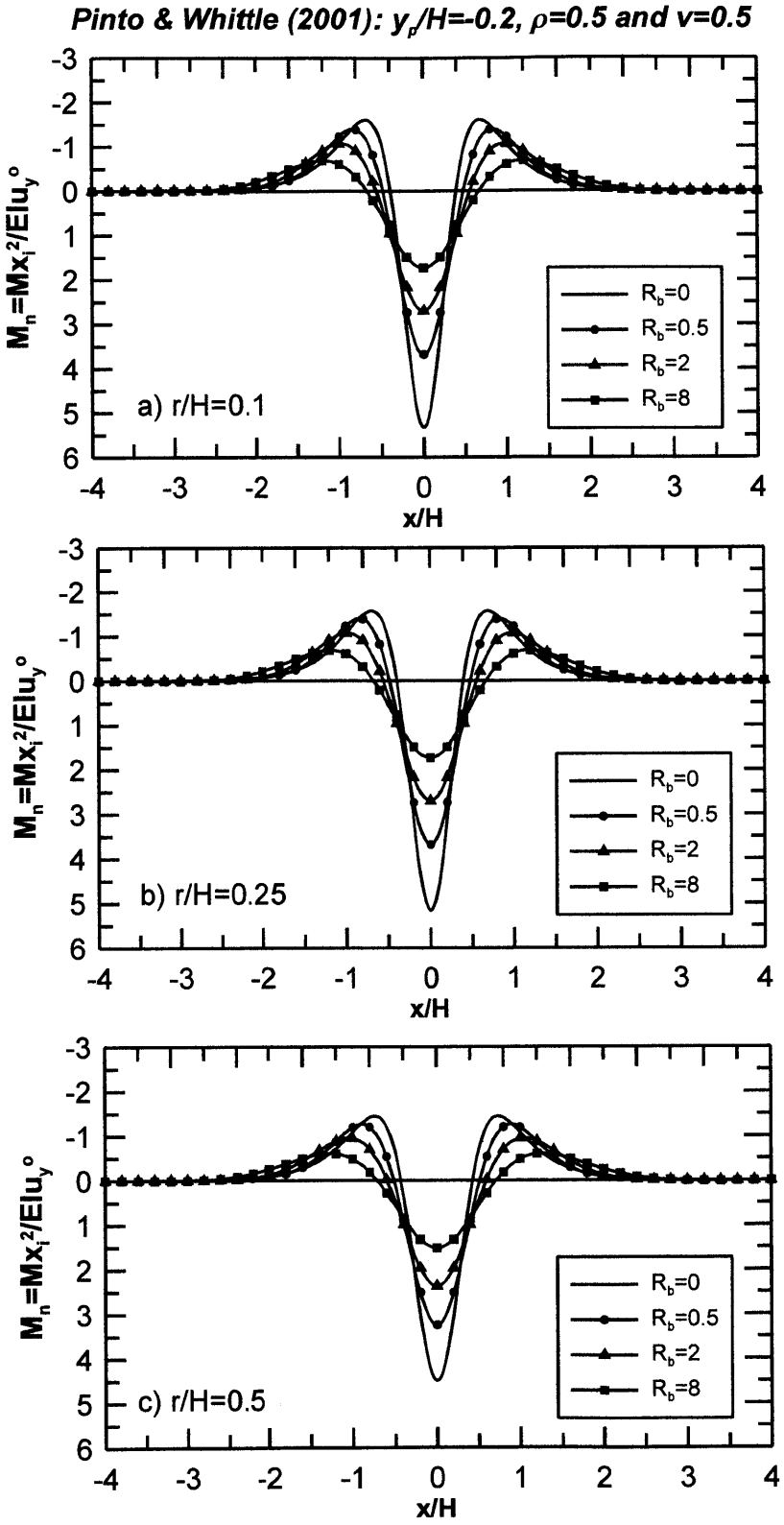

Figure 3-13: Effect of pipe radius and relative pipe-soil bending rigidity factor, $R_b=EI/E_s r_o x_i^3$, on normalized pipe bending moments

Pinto & Whittle (2001): y_p/H=-0.25, r/H=0.25 and v=0.5

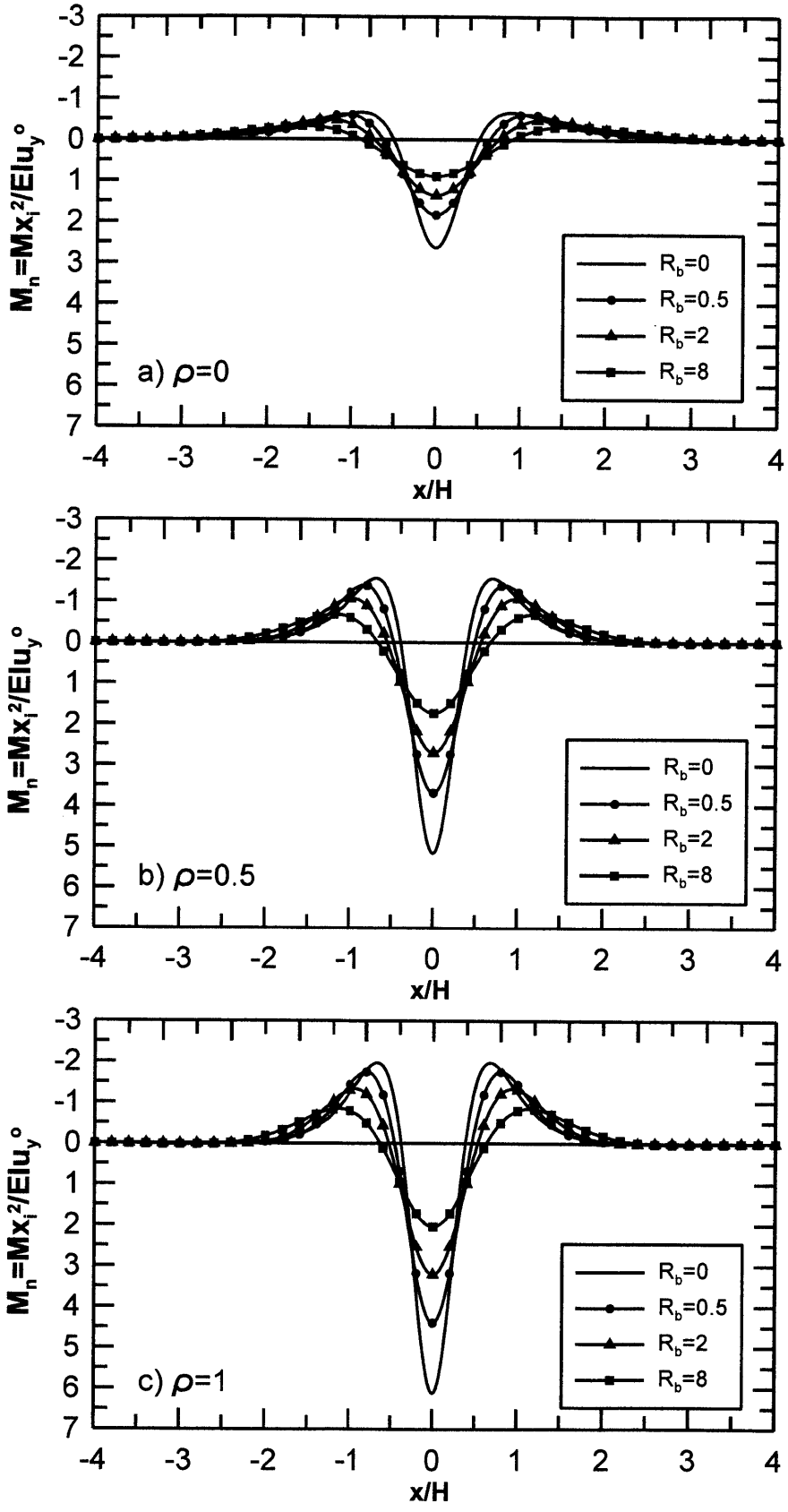

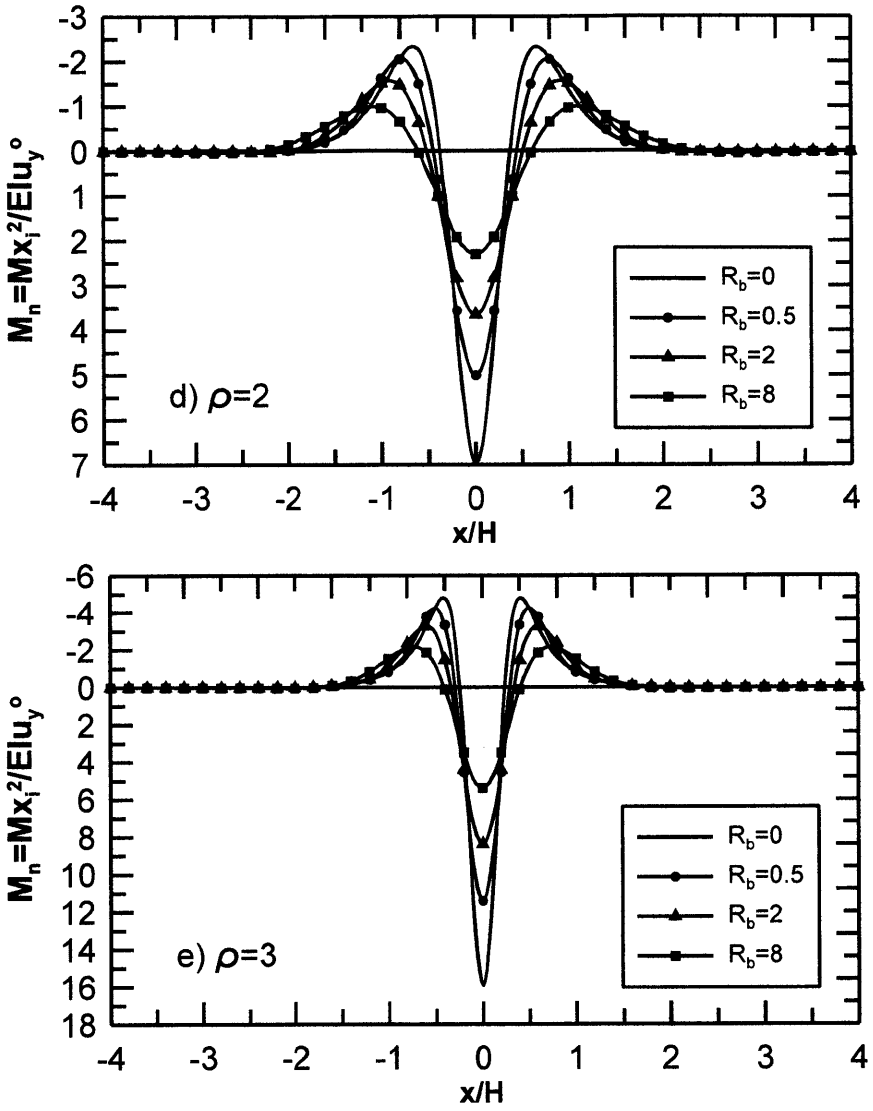

Figure 3-14: Effect of relative distortion, ρ and relative pipe-soil bending rigidity factor, $R_b=EI/E_sr_ox_i^3$, on normalized pipe bending moments

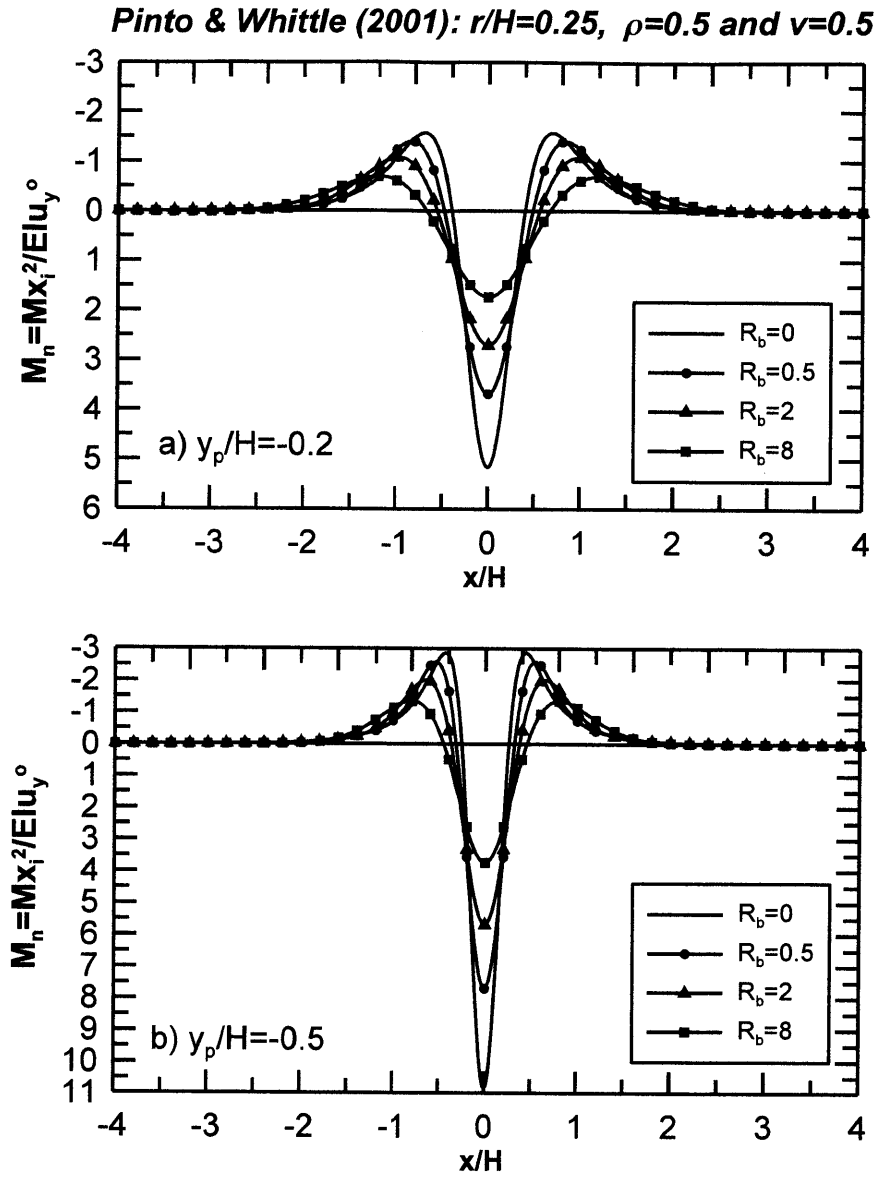

Figure 3-15: Effect of pipe embedment depth, y and relative pipe-soil bending rigidity factor, $R_b=EI/E_s r_o x_i^3$, on normalized bending moments

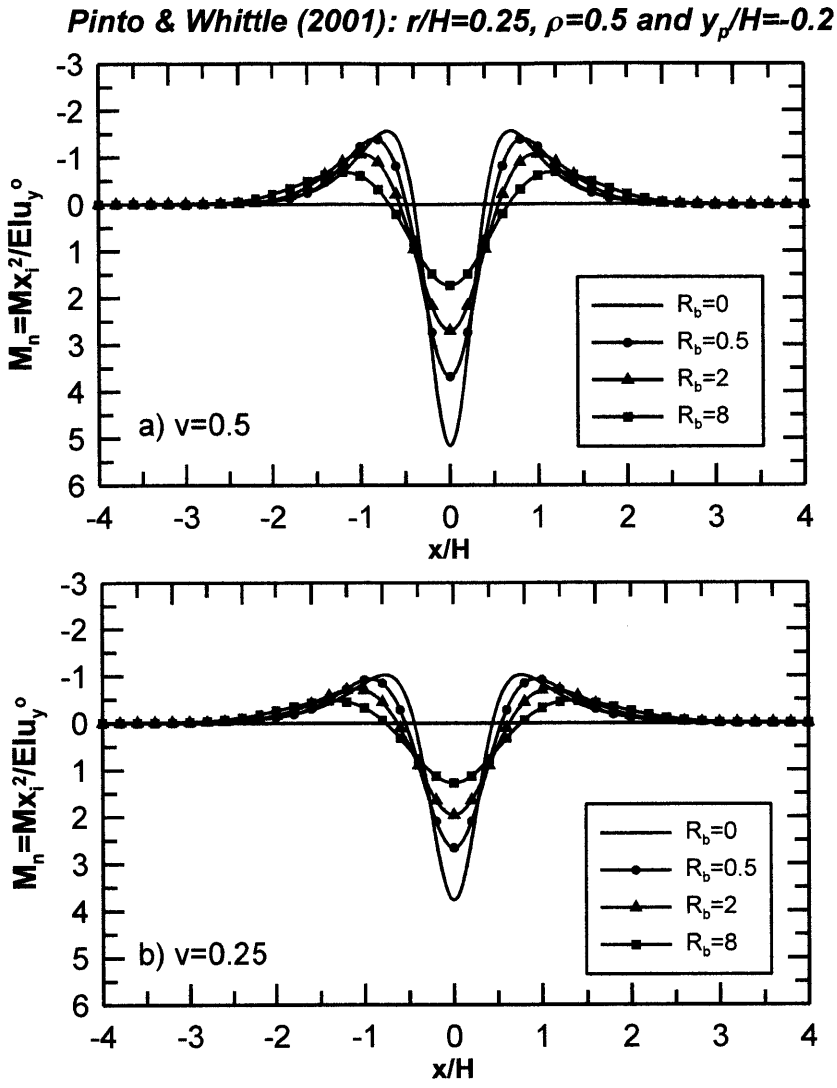

Figure 3-16: Effect of soil Poisson's ratio, v and relative pipe-soil bending rigidity factor, $R_b=EI/E_s r_o x_i^3$, on normalized pipe bending moments

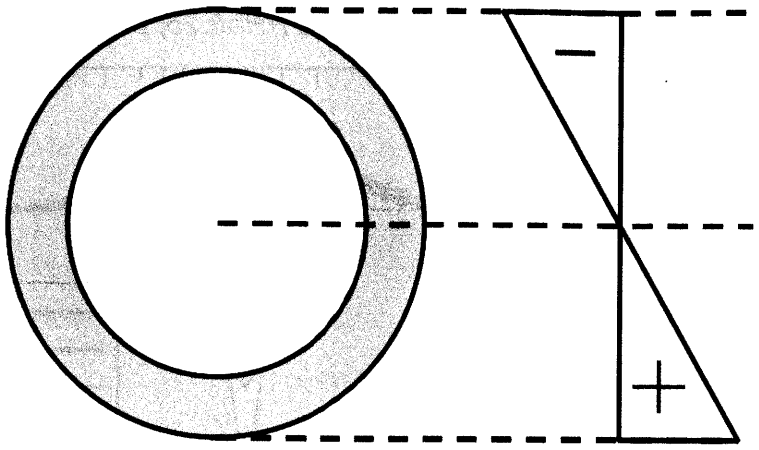

Figure 3-17: Sign notation of pipe strain and stresses due to bending

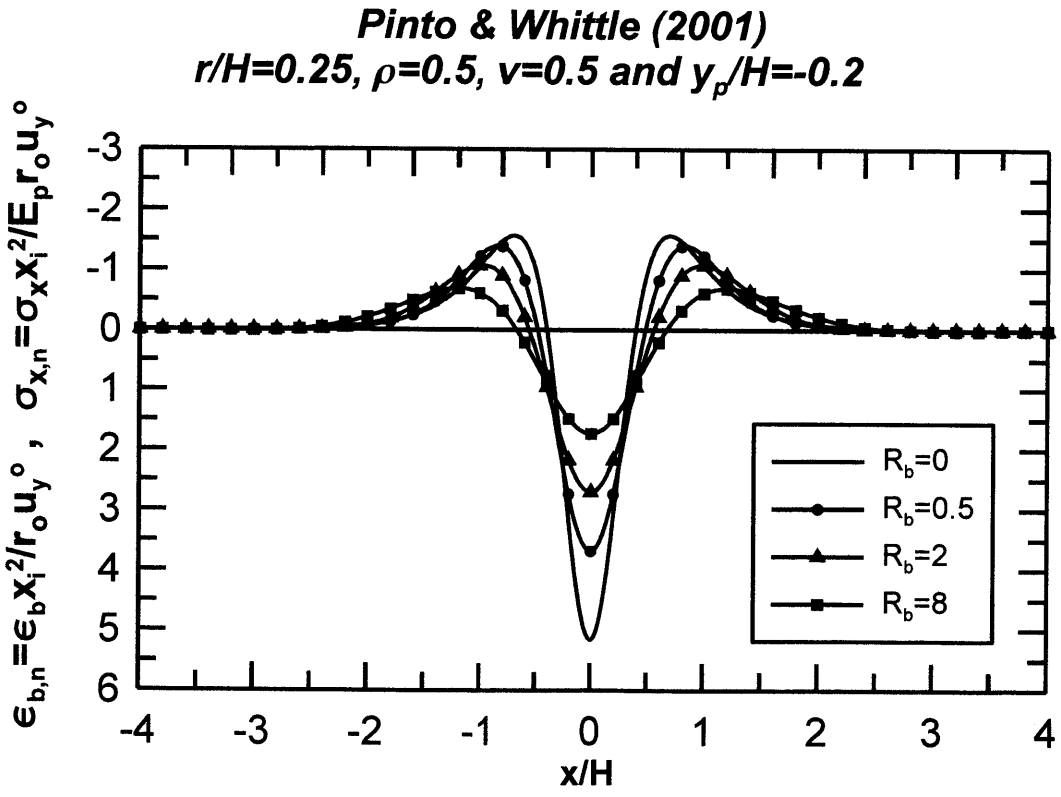

Figure 3-18: Effect of the relative pipe-soil bending rigidity factor, $R_b=EI/E_s r_o x_i^3$, on normalized axial pipe strains and stresses

CHAPTER 4

AXIAL RESPONSE OF CONTINUOUS PIPELINES TO TUNNELING

4.0 INTRODUCTION

This chapter describes the modeling of the axial response of continuous pipelines to horizontal components of ground deformations induced by tunneling. The free-field movements are described by empirical methods or by analytical closed-form solutions proposed by Pinto & Whittle (2001). The pipe-soil interaction is modeled analytically in elasticity, using a Winkler spring approach.

4.1 FREE-FIELD HORIZONTAL DISPLACEMENTS

4.1.1 Empirical Solutions

Prior studies by Attewell (1978), O'Reilly & New (1982) and Taylor (1995) assume that the horizontal vectors of displacements induced by tunneling are directed to the tunnel axis (Figure 4-1) and hence, the displacement component u_x can be related to the vertical component u_y of deformations presented in Chapter 3.

$$u_x = \frac{x}{H} \cdot u_y \tag{4.1}$$

If the vertical settlements are described by a Gaussian curve distribution, the above assumption leads to the following expression.

$$\frac{u_x}{u_x^o} = 1.65\frac{x}{x_i}exp\left(-\frac{x^2}{2x_i{}^2}\right) \tag{4.2a}$$

$$u_x^o = 0.61 \cdot K \cdot u_y^o \tag{4.2b}$$

where the empirical constant K has been discussed in Chapter 2, (Mair et al., 1993 and Jacobsz, 2002).

Vorster (2005) assumes that the subsurface displacement vectors are also directed to the tunnel centerline (Figure 4-1) and suggested the following expression:

$$u_x = \frac{x}{\left(1+\frac{d}{c}\right)H - y}u_y \tag{4.3}$$

where y is the depth of interest, H is the tunnel depth, x is the distance from the tunnel centerline, u_y is the equation which describes the vertical displacements at the depth of interest. The coefficients *d=0.175, c=0.325* are based on correlations proposed by Mair et al. (1993) for clay, and *d=0.09, c=0.26* were proposed by Jacobz (2002) for sand.

4.1.2 Analytical Solutions

Pinto and Whittle (2001) proposed closed-form analytical solutions for describing the horizontal components of the free-field displacements. They related the ground displacements to three boundary displacements happening at the tunnel cavity: a) uniform convergence u_ε, b) ovalization u_δ and c) uniform vertical translation Δu_y (Figure 2-10). These parameters must be interpreted from measured ground movements as described in Chapter 2. The simplified closed form solutions are given by Equations 2.13 and 2.14. Figure 4-2 shows a flow chart which summarizes the required input parameters and the procedure

in order to obtain the final solution which describes the free field horizontal displacements at any depth, by using Pinto & Whittle (2001) method.

The analytical solutions provide a complete prediction of the distribution of ground movements without further assumption. Zymnis et al. (2011) show that the analytical solutions are able to represent ground displacement patterns for a range of soil conditions and methods of tunneling (EPB, NATM etc.)

4.2 AXIAL PIPELINE RESPONSE

4.2.1 Winkler's Model

Figure 4-3, shows a pipeline of radius r_o, Young's modulus E_p and wall thickness t, buried at a depth y_p in a soil with Young's modulus E_s and Poisson's ratio v. Using a Winkler's model, we assume that the pipeline is connected with the soil with vertical and horizontal springs of K_v and K_h coefficients respectively. The basic assumptions made are:

[1] the soil is homogeneous and elastic

[2] the pipe is continuous

[3] the pipe does not affect the tunnel

[4] the pipe is always in contact with the soil

As the model is linear, the system can be superimposed. Hence, this chapter considers only the horizontal springs. The mathematical model which describes the axial response of a buried pipeline is analogous to the model describing a pile loaded vertically in an elastic soil. Figure 4-3 shows the response of a pipe (represented as a pile) connected to the soil with springs along its length, of

coefficient K_h, to the horizontal displacements of the soil (u_x). The general mathematical equation for this problem is:

$$\frac{\partial^2 u_x^P}{\partial x^2} - \lambda_h{}^2 \cdot u_x^P = 0 \qquad (4.4a)$$

$$\lambda_h = \sqrt{\frac{K_h}{EA}} \qquad (4.4b)$$

where:

$u_x{}^P$ = pipeline horizontal displacement
K_h = horizontal spring coefficient
EA = axial stiffness of the pipe

The general solution of Equation 4.4 is:

$$u_x{}^P = C_1 e^{-\lambda_h x} + C_2 e^{\lambda_h x} \qquad (4.5)$$

The following boundary conditions are needed in order to solve the Equation 4.5.

- At $x \to \infty$, $u_x{}^P = 0$

As $e^{-\lambda_h x} = 0$ for $x \to \infty$, it suffices that $C_2 e^{\lambda_h x} = 0$. Therefore, $C_2 = 0$

Therefore we end up with:

$$u_x{}^P = C e^{-\lambda_h x} \qquad (4.6)$$

To define the constant C, we use the general case that the pipe is loaded by a distribution of loads $dP_x(x)$ based on the predicted free-field ground deformations.

The horizontal displacement of an infinitesimal element on the pipe is:

$$\delta u_x{}^P = \frac{dP_x \cdot \lambda_h}{2K_h} \cdot e^{-\lambda_h x} \qquad (4.7)$$

The load P_x is actually equal to $K_h u_x(x)dx$ where $u_x(x)$ is the horizontal displacement of the soil at the pipe level, due to tunneling (Figure 4-4). Thus Equation 4.7 becomes:

$$\delta {u_x}^P = \frac{dK_h u_x(x) \cdot \lambda_h}{2K_h} \cdot e^{-\lambda_h x} \Rightarrow$$

$$\delta {u_x}^P = \frac{\lambda_h}{2} du_x(x) \cdot e^{-\lambda_h x} \tag{4.8}$$

Integrating Equation 4.8 over the total length of the pipe $(-\infty, \infty)$ by applying the appropriate λ_h parameter, the total pipe horizontal displacements distribution is estimated.

Assuming that the free-field lateral displacements are described by a function $g(x)$, which become 0 at x=0 (e.g. empirical Equation 4.3, or Pinto & Whittle (2001) analytical solutions (Figure 4-2)), the horizontal pipe displacements at a specific point on the pipeline, can be obtained by:

$${u_x}^P = \frac{\lambda_h}{2} \cdot \int_0^b g\left(\frac{a-b}{2} + x\right) \cdot e^{-\lambda_h x} dx + \int_0^b g\left(\frac{a-b}{2} - x\right) \cdot e^{-\lambda_h x} dx \tag{4.9}$$

Application of the empirical equation (Equation 4.3) assuming the u_y are described by a modified Gaussian curve (Vorster, 2005), and Pinto & Whittle (2001) analytical solutions in Equation 4.9 are presented in Appendix I.

4.2.2 Estimation of the Horizontal Spring Coefficient K_h

A key parameter for solving Equation 4.11 is the λ_h parameter which includes the horizontal spring coefficient K_h (Equation 4.5b). Scott (1981) proposed that the coefficient of the springs along the length of an axially loaded pile in an elastic soil, is given by:

$$K_s = 2\pi r_o \cdot k_s \tag{4.10}$$

$$k_s = \frac{E_s}{2(1-v^2)r_o} \tag{4.11}$$

From Equations 4.10 and 4.11, we get:

$$K_s = \frac{\pi E_s}{4(1-v^2)} \tag{4.12}$$

where E_s is the soil stiffness and v is the soil Poisson's ratio.

In order to examine the appropriateness of this spring coefficient for the problem of a pipe buried in an elastic soil and loaded axially, 130 finite element analyses were carried out (using PLAXIS^{TM} 3D Tunnel) for various pipe, soil and tunnel characteristics and depths. The purpose was to compare the horizontal displacements of the pipe computed numerically to those acquired analytically from Equation 4.8, using the pipe-soil horizontal spring coefficient defined in Equation 4.12. Details of the numerical analyses are presented in Chapter 5.

Figure 4-5 compares the numerical and analytical horizontal pipe displacements $u_x^P{}_{,max}$, as a function of the relative pipe-soil axial rigidity factor $(EA/E_s\pi r_o^2)$, proposed by Attewell et al. (1986) for various values of the relative distortions, ρ at the tunnel cavity. The numerical solutions (by PLAXIS) are in modest agreement with the analytical solutions, suggesting that a better definition of K_h parameter is required.

4.2.2.1 Proposed horizontal spring coefficient K_h

After a trial and error procedure the following horizontal spring coefficient was found to provide an accurate matching between analytically and numerically computed pipe deformations.

$$K_h = \frac{15E_s r_o}{(1+v)(1+\rho)x_j} \tag{4.13}$$

The parameter x_j is the characteristic length that represents the lateral distance to the point of maximum free-field lateral displacement at the pipe level (Figure 4-6). The value of x_j is controlled by the relative distortion, ρ, associated with a particular ground condition and method of tunneling.

As it can be seen from Equation 4.13, the parameters which were found to affect the horizontal spring coefficient K_h (Equation 4.13) are the pipe radius, r_o, the relative distortion of the tunnel cavity, ρ and the Poisson's ratio of the soil, v. The pipe depth, y_p does not affect the coefficient as it is explained below.

Figure 4-7 compares the normalized maximum horizontal pipe displacements $u_x^P{}_{,max}$ as functions of the relative pipe-soil axial rigidity factor $(EA/E_s\pi r_o^2)$, for selected values of relative distortions values ρ. The results show very good agreement between the analytical solutions and the numerical results of the FE analyses with PLAXIS, for a wide range of pipe and tunnel characteristics. Good agreement is also observed for the full range of soil Poisson's ratios *v=0.1, 0.4 and 0.495* (approximately incompressible soil with v=0.5).

Figure 4-8 shows the good match between the analytical and the finite element solutions for *v=0.1* by using the new proposed horizontal spring coefficient (Equation 4.13). Finally, Figures 4-9 and 4-10 show the case of *v=0.5*, *ρ=0* and *ρ=1.5*, for 3 pipes of different axial stiffness where the analytical solutions also fit PLAXIS solutions. Complete results for the horizontal pipe displacements for all the different pipe stiffness selected *(EA)*, different uniform convergence values (u_ε), relative distortion *(ρ)*, soil Poisson's ratio *(v)* and pipe depths (y_p), are presented in Appendix II.

Figure 4-11 shows the case of v=0.4, ρ=1 and y_p=-2m, where it can be seen that the pipe depth *(y_p)* does not affect the spring coefficient K_h as the analytical solutions are derived with the new proposed K_h of Equation 4.13 which does not take into account the pipe depth.

4.2.3 Relative Pipe-Soil Axial Rigidity Factor R_α

To consider the different pipe and soil characteristics and the relation between them, a relative pipe – soil axial rigidity factor R_α is introduced, analogous to the relative pipe – soil bending rigidity factor R_b for the bending pipe response. Attewell et al. (1986) suggested an axial rigidity factor R_α expresses by the following equation:

$$R_a = \frac{EA}{E_s A_s} \tag{4.14}$$

where *EA* is the axial stiffness of the pipeline, E_s is the soil Young's modulus, *A* is the cross-sectional area of the pipe section and A_s is the full cross-sectional area of the pipe represented as a solid element ($A_s = \pi r_o^2$).

Following the same logic as for the relative pipe-soil bending rigidity factor *(R_b)* proposed by Klar et al. (2005), and taking into consideration that x_j is a characteristic length controlling the horizontal displacements, it is suggested that R_α should be given by:

$$R_a = \frac{EA}{E_s \pi r_o^2}\left(\frac{r_o}{x_j}\right) = \frac{EA}{E_s \pi r_o x_j} \tag{4.15}$$

For R_α=*0*, the pipe is very flexible and follows the free-field movements, while for values of R_α>*100* the pipe is effectively rigid compared to its surrounding soil.

Figures 4-12 through 4-15 show the analytical solutions for the normalized pipe horizontal displacements (u_x^P/u_x^o), for various values of parameters ρ, y/H, r/H, v, and for different pipe-soil axial rigidity factors R_α.

From these figures the following conclusions are drawn:

- The distribution of the horizontal displacements is anti-symmetric with the axis of symmetry at $x=0$ which marks actually the tunnel centerline (Figure 4-12).
- As the ratio r/H increases, there is no effect in the pipe horizontal displacements (Figure 4-12).
- As the relative distortion (ρ) increases (Figure 4-13), the pipe horizontal displacements, as well as their maximum value decreases faster for a specific R_α value. There is a well-defined change in mode shape for relative distortions, $\rho \geq 1$. It has to be mentioned that the change in mode shape is influenced by the value of the soil Poisson's ratio, v. More specifically for $v \leq 0.25$, change in mode shape is observed for $\rho > 1$, while for v>0.25, the change in mode shape can be observed for $0.5 < \rho < 1$.
- As the pipe depth (y/H) increases (Figure 4-14), the horizontal pipe displacements and their maximum value decrease for a specific R_α value.
- Finally, as the Poisson's ratio (v) increases (Figure 4-15), the horizontal pipe displacements and their maximum value also decrease for a specific R_α value.

4.2.4 Axial pipe strains and stresses

The pipe horizontal displacements are computed in order to estimate the produced strains and stresses acting on the pipelines. The axial strain ε_α is the

strain in the extreme pipe fiber due to axial deformation. The equation which gives ε_a is:

$$\varepsilon_a = \frac{\partial u_x^P}{\partial x} \tag{4.16}$$

The axial pipe stresses (σ_x), can be computed using the axial strains by:

$$\sigma_x = E_P \cdot \varepsilon_a \tag{4.17}$$

where E_p is the pipe material Young's modulus. Tensile stresses are considered positive and compressive stresses, negative.

The axial pipe stresses due to axial pipe deformation in addition to the axial stresses due to bending (Chapter 3) are computed in order to estimate the possibility of pipe failure in tension or compression, as illustrated in Chapter 6.

4.3 SUMMARY

The response of continuous pipelines to lateral ground displacements due to tunneling is estimated using a Winkler model, assuming that a pipe loaded axially on an elastic half-space is equivalent to a pile loaded axially. The pipe is connected to the ground with horizontal springs and the ground displacements are described by Pinto and Whittle (2001) closed-form solutions.

A new horizontal spring coefficient K_h is introduced (Equation 4.13) so that the analytical solutions fit numerical solutions derived by finite elements simulations in PLAXIS 3D Tunneling. This coefficient includes a new characteristic length x_j, which is the distance to the maximum free-field horizontal displacements at the depth of the pipe, and it is analogous to the distance to the inflection point x_i for the bending pipe response.

Analytical solutions for the pipe horizontal displacements are given in graphs for various values of the pipe depth y_p, the tunnel radius r, the tunnel depth H, the Poisson's ratio v, the relative distortion ρ at the tunnel cavity and for various relative pipe-soil axial rigidity factor R_α.

Finally, in order to estimate the possibility of pipeline failure due to the free-field lateral ground displacements induced by tunneling, pipe axial strains and stresses must be computed. Axial stresses acting on the pipe due to axial deformation and due to bending are compared with the allowable stresses of the pipe (depending on the pipe material) in order to estimate the possibility of the pipe failure to tension or compression.

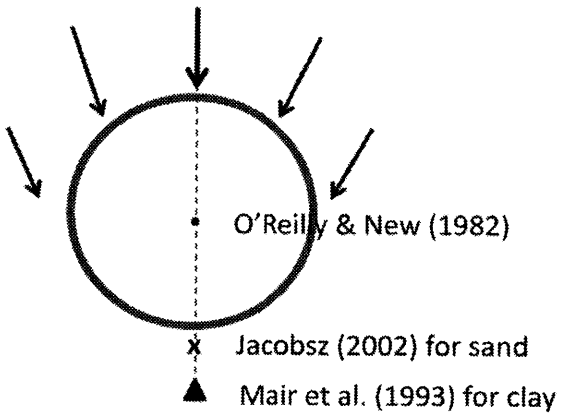

Figure 4-1: Ground displacement vectors pointing at three positions on the tunnel centerline, suggested by O'Reilly & New, 1982, Jacobsz, 2002, and Mair et al., 1993

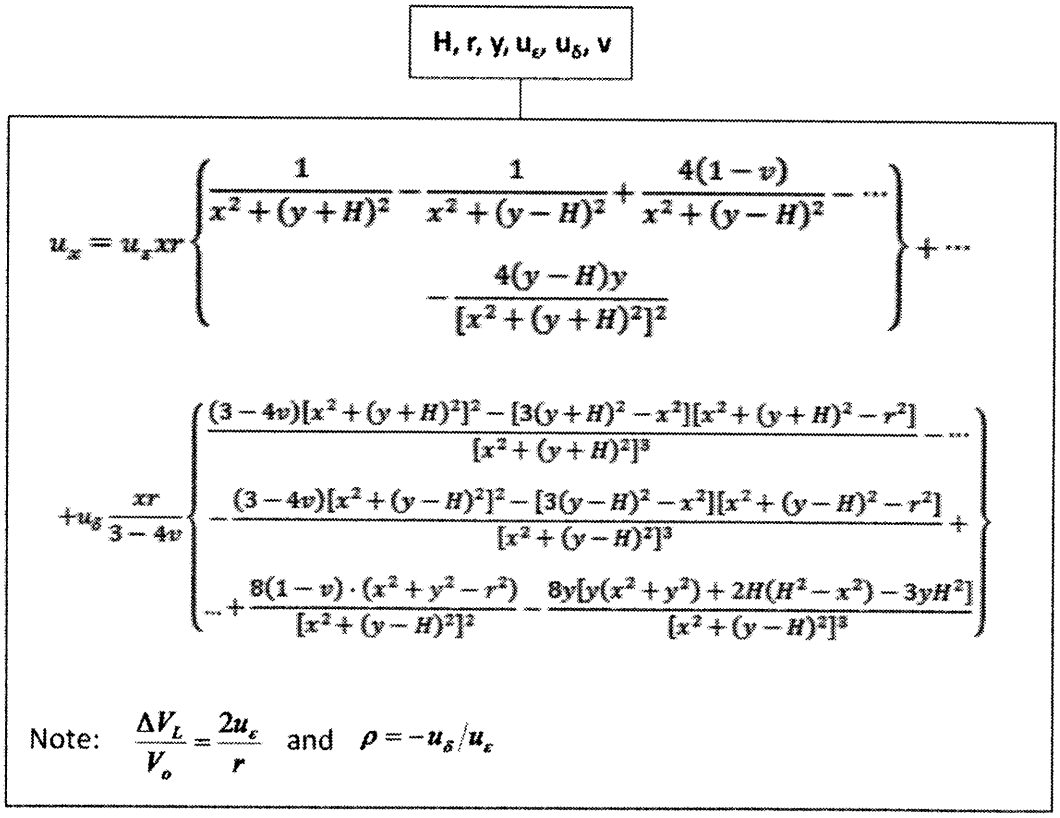

Figure 4-2: Pinto and Whittle (2001) method to describe free-field lateral displacements

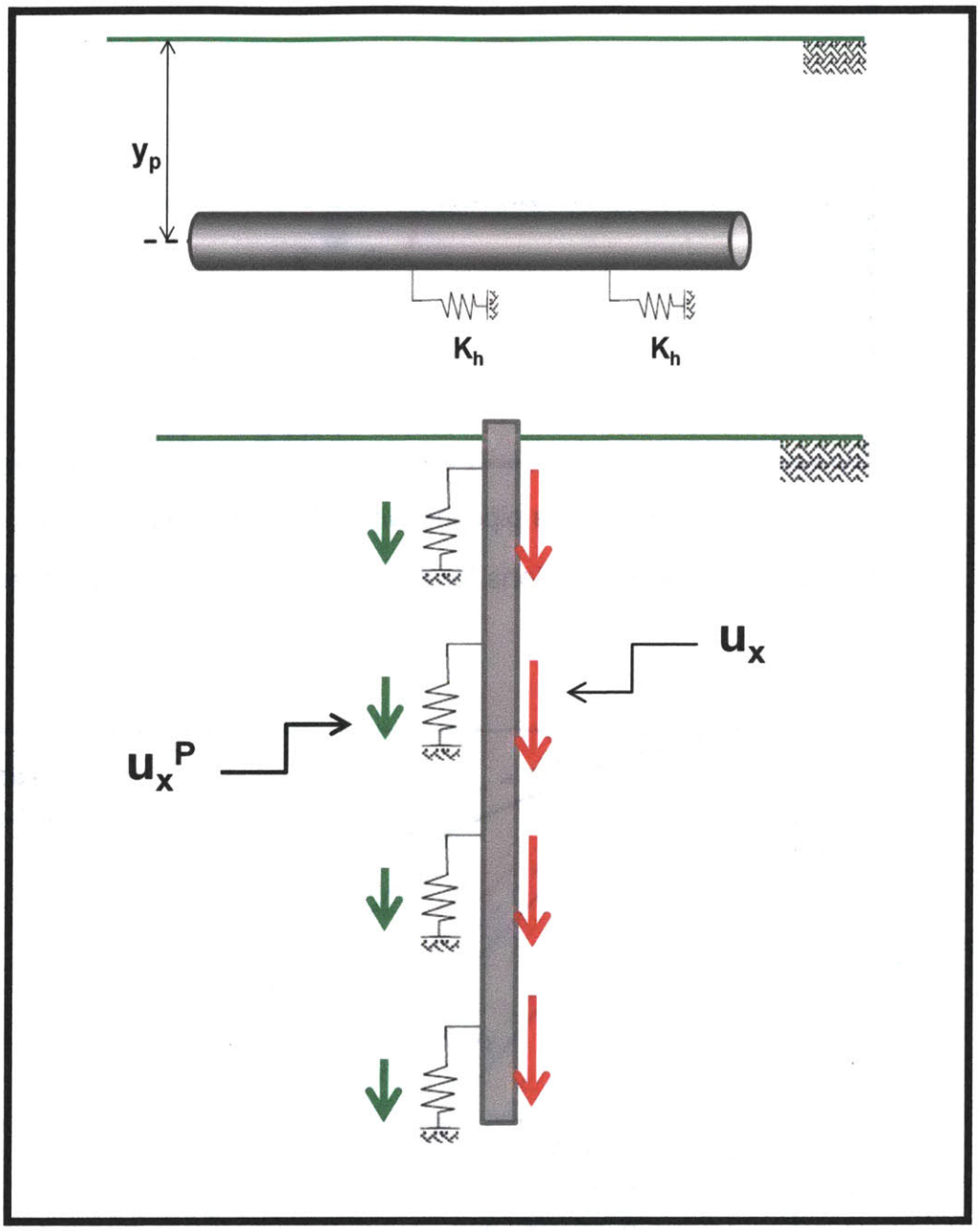

Figure 4-3: Pipeline connected to the soil with horizontal springs and Winkler analog assuming that a pipe loaded axially is equivalent to a pile loaded axially

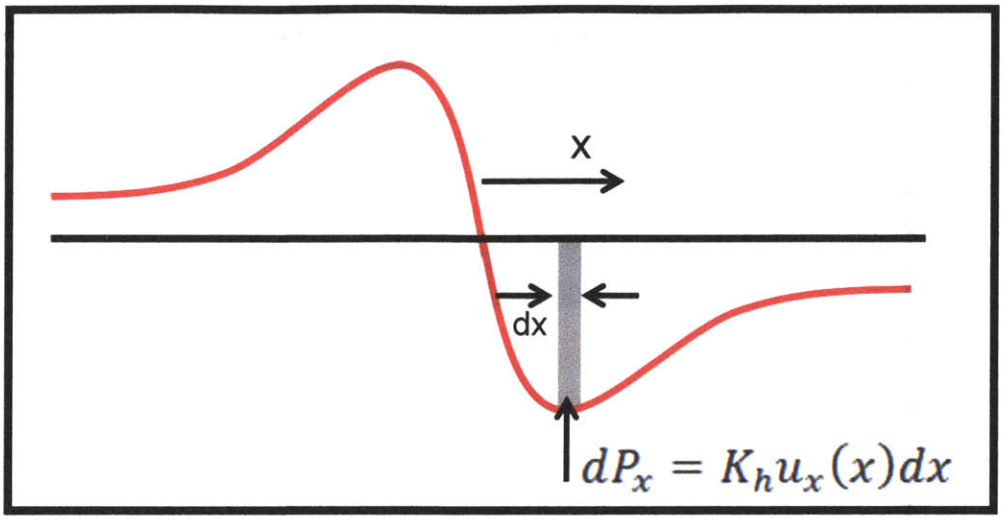

Figure 4-4: Axial loading of a pipeline with infinite pointed loads dP_x assuming P&W (2001) analytical solutions for the free field horizontal displacements u_x

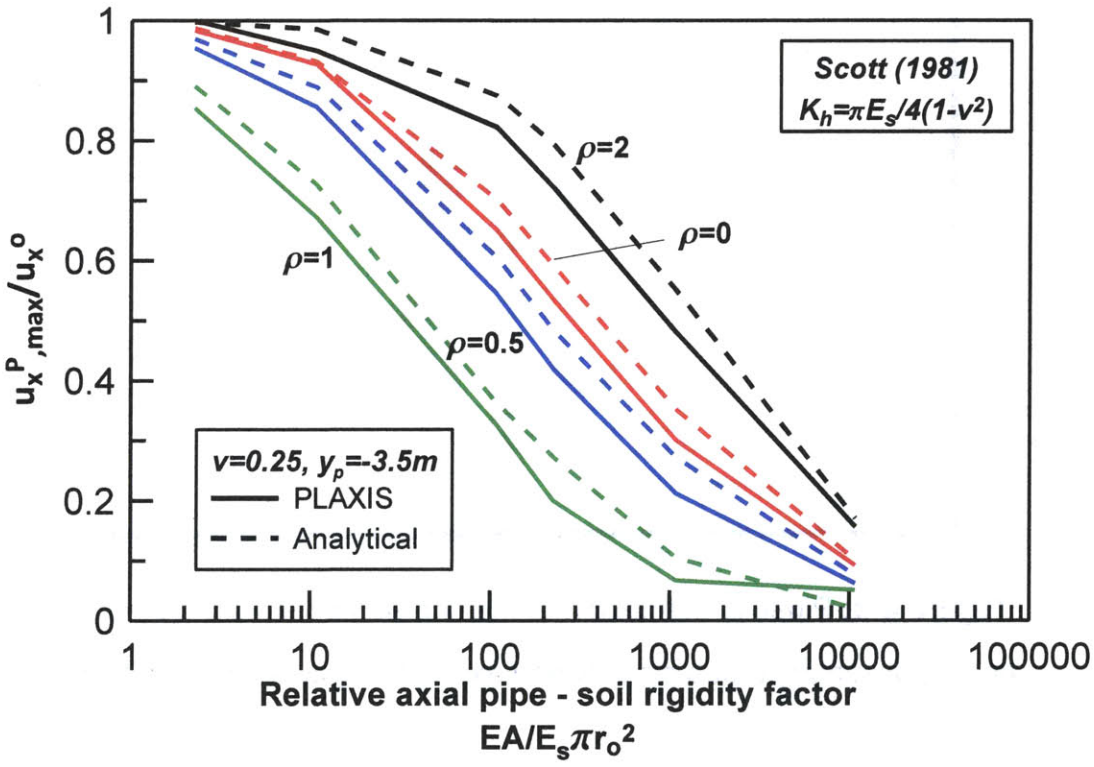

Figure 4-5: Comparison between numerical and analytical solutions for horizontal pipe displacements, using Scott (1981) recommendation for K_h

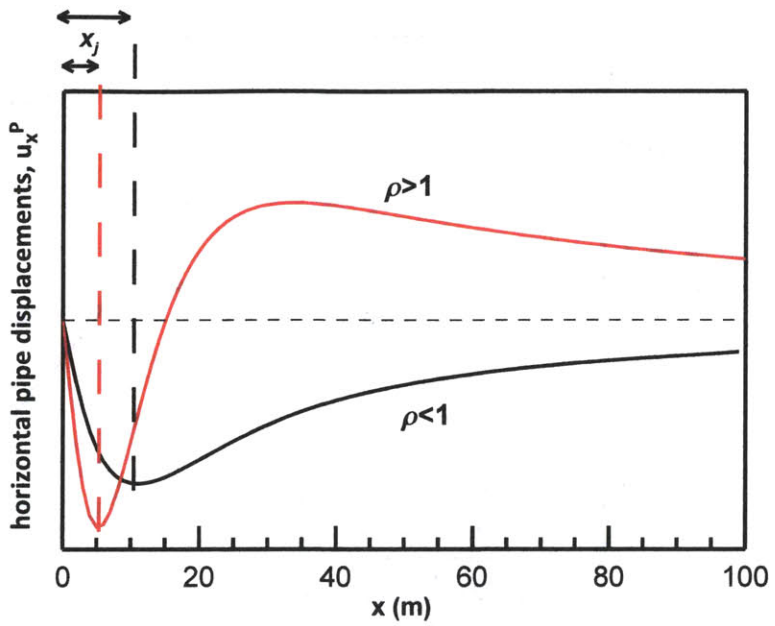

Figure 4-6: Characteristic length x_j for axial pipe deformations distortion of two different relative distortion (ρ) values

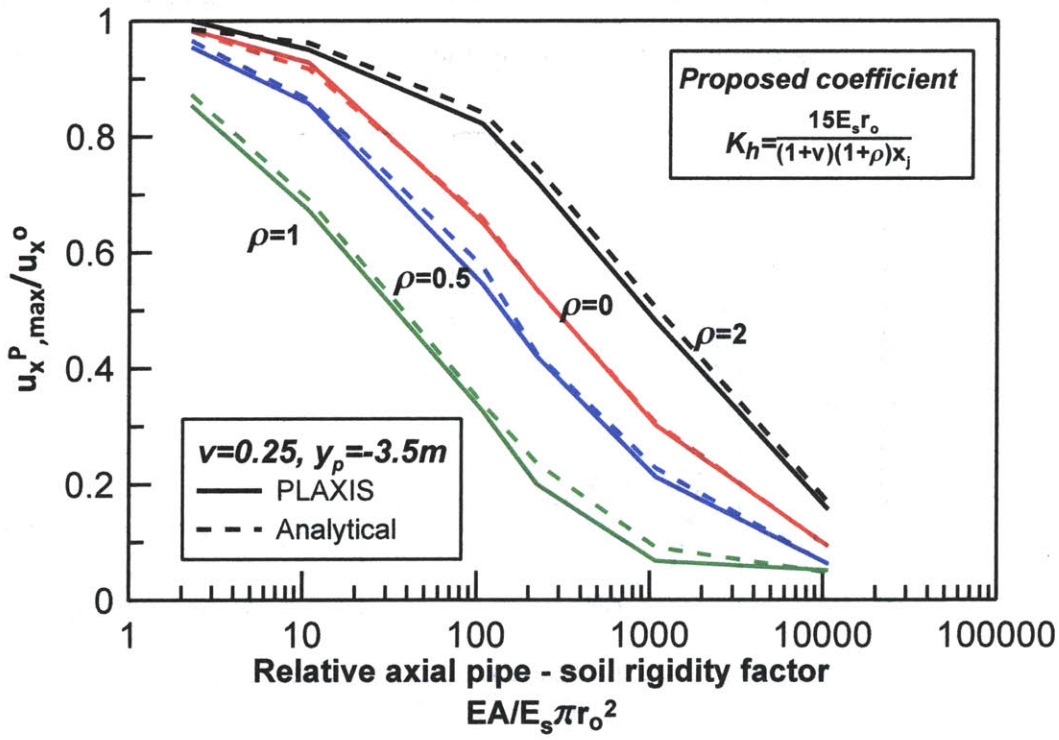

Figure 4-7: Comparison between numerical and analytical solutions for axial pipe displacements, using the proposed pipe-soil coefficient K_h

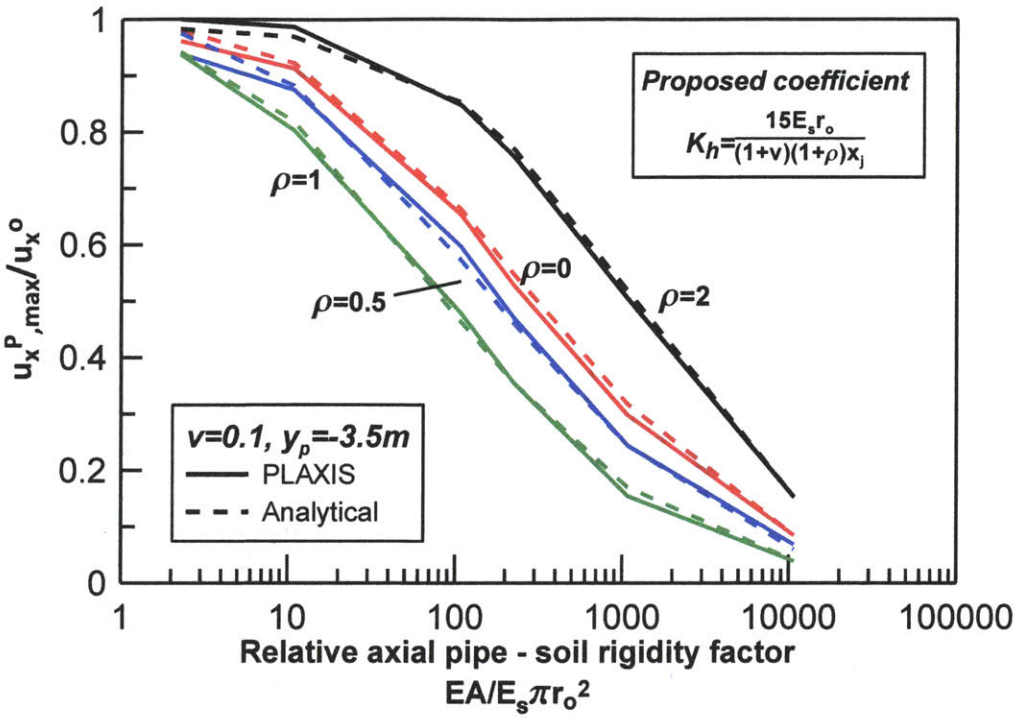

Figure 4-8: Comparison between numerical and analytical solutions for axial pipe displacements, using the proposed pipe-soil coefficient K_h

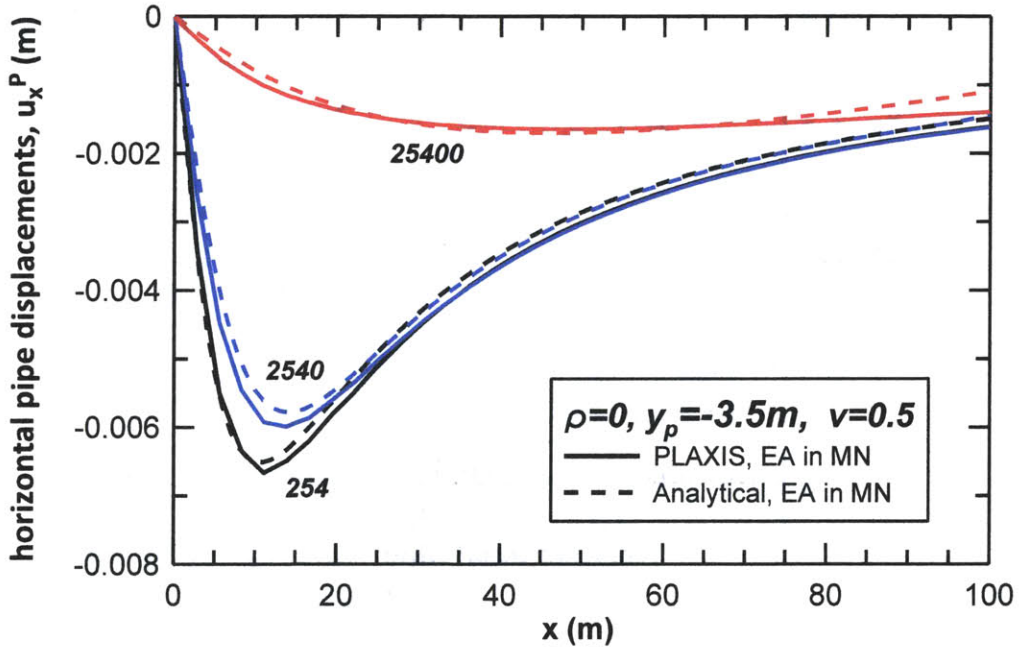

Figure 4-9: Comparison between numerical and analytical solutions for axial pipe displacements for $v=0.5$, $\rho=0$ and $y_p=-3.5m$

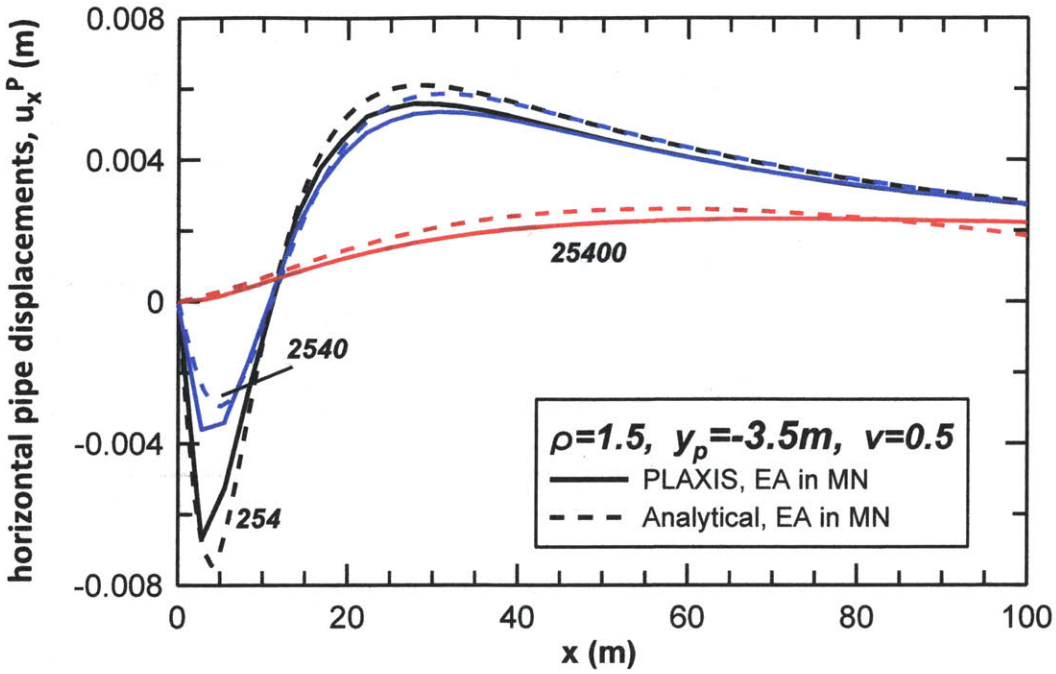

Figure 4-10: Comparison between numerical and analytical solutions for axial pipe displacements for $v=0.5, \rho=1.5$ and $y_p=-3.5m$

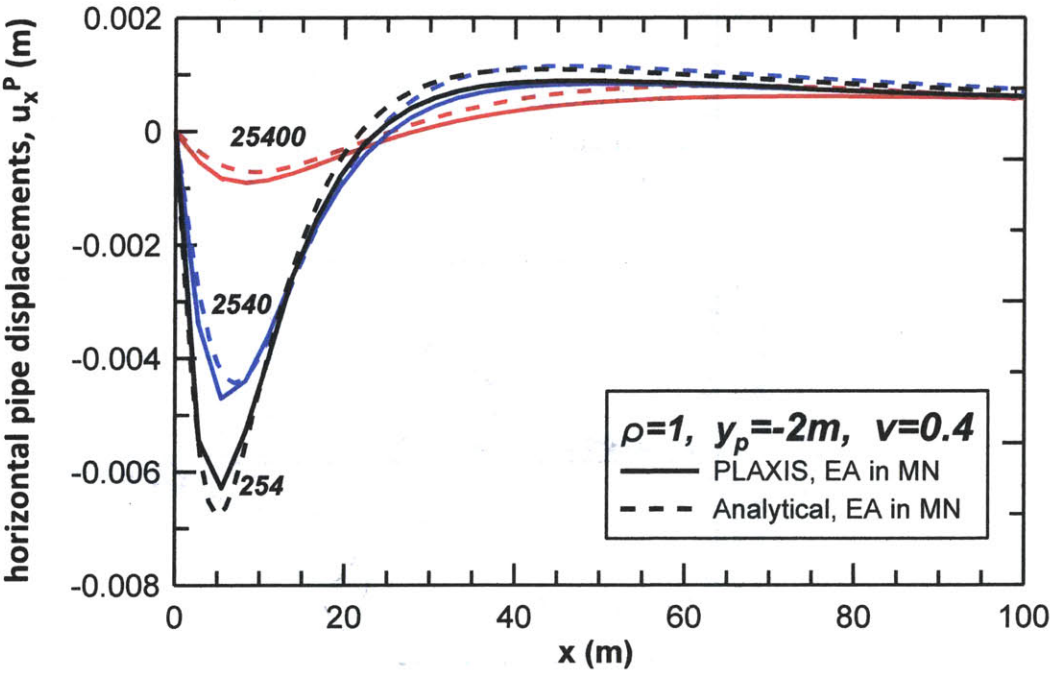

Figure 4-11: Comparison between numerical and analytical solutions for axial pipe displacements for $v=0.4$, $\rho=1$ and $y_p=-2m$

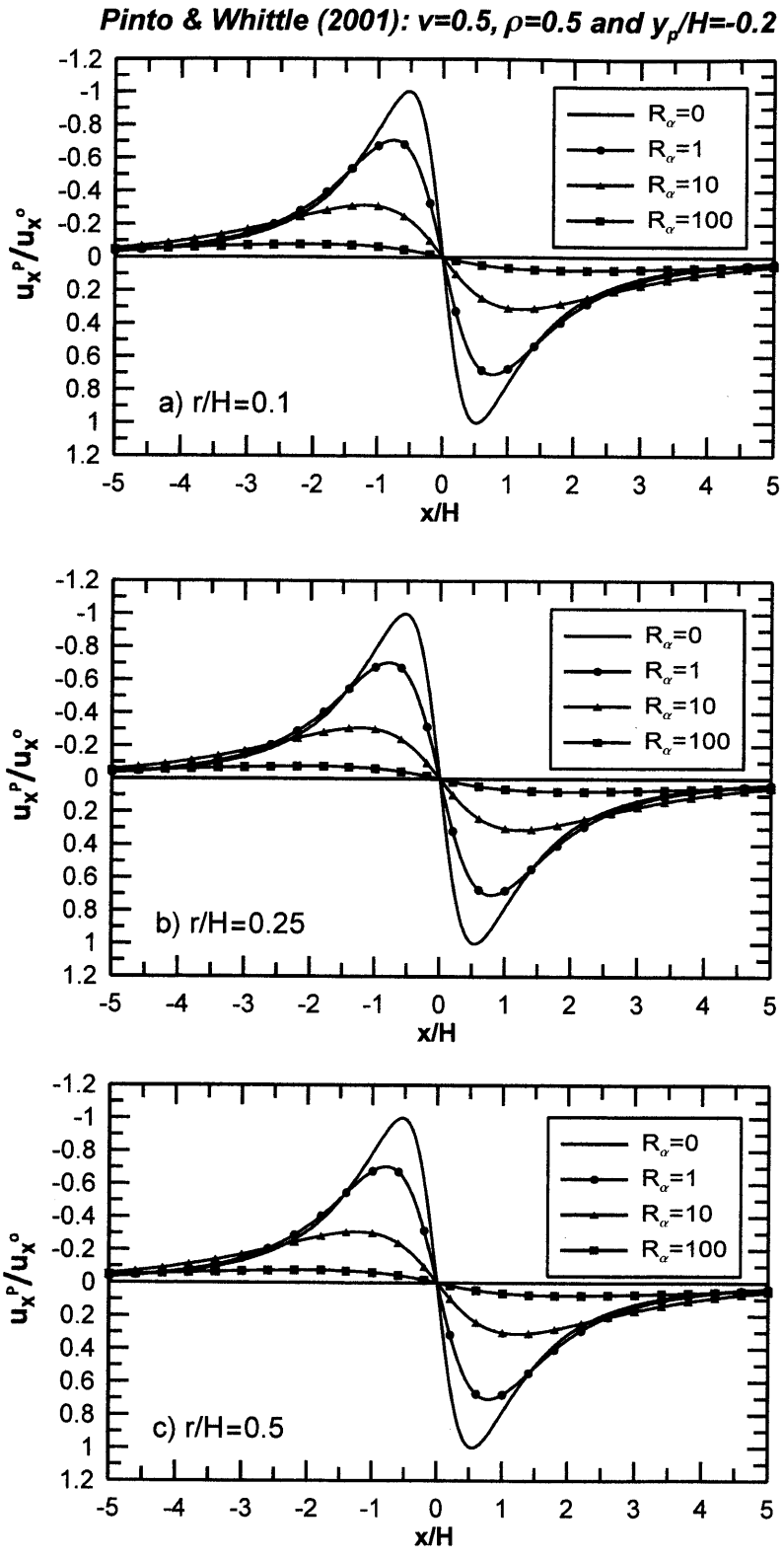

Figure 4-12: Effect of pipe radius and the relative axial pipe-soil rigidity factor $R_a=EA/E_s r_o x_j$ on normalized horizontal pipe displacements

Pinto & Whittle (2001): r/H=0.25, v=0.5 and y_p/H=-0.2

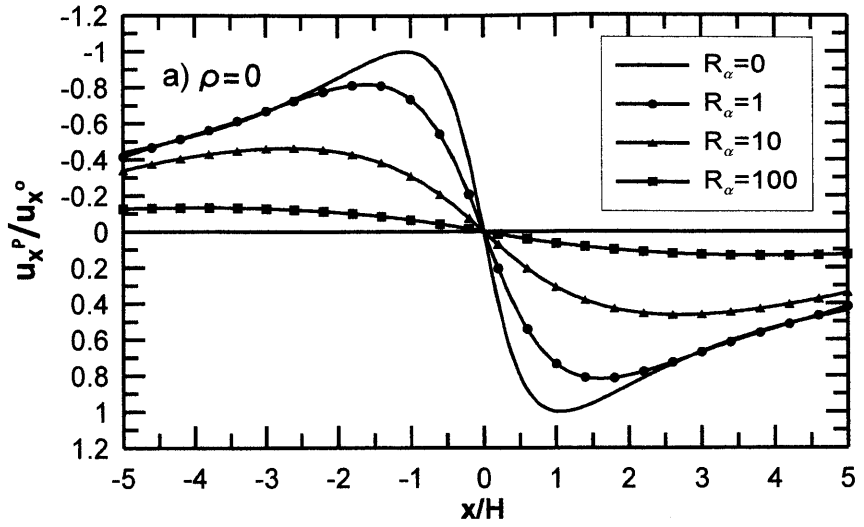

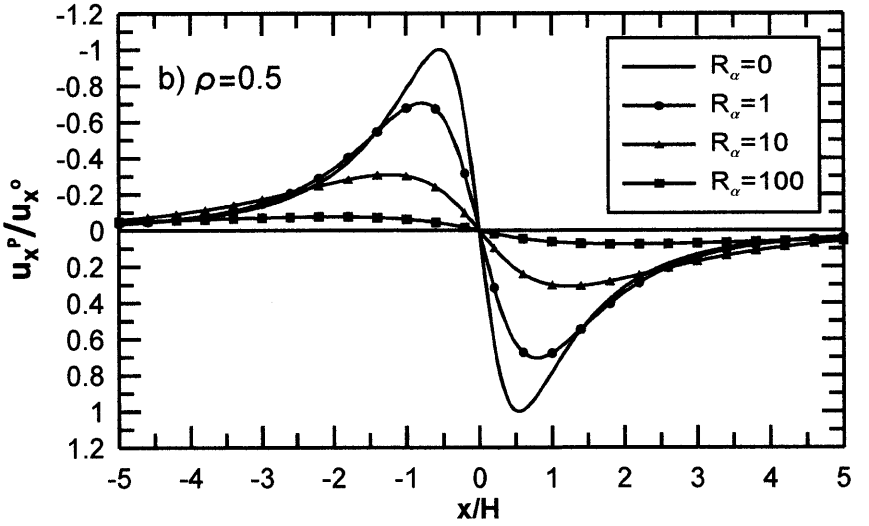

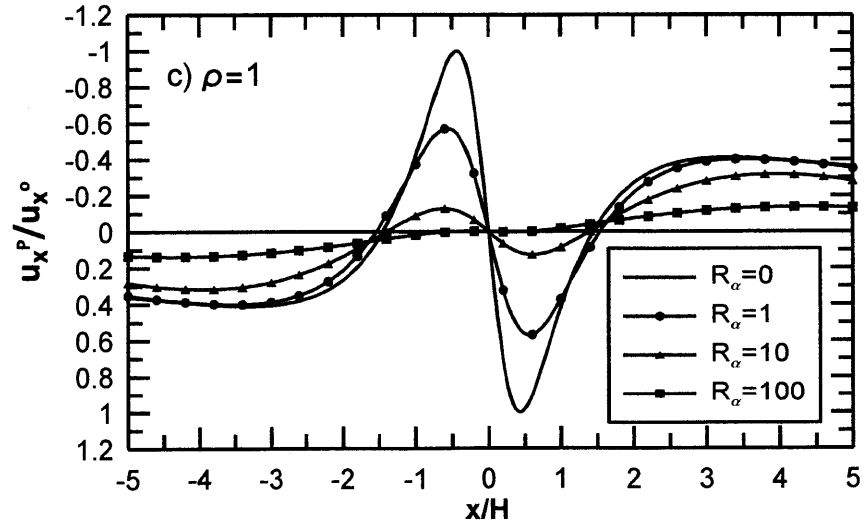

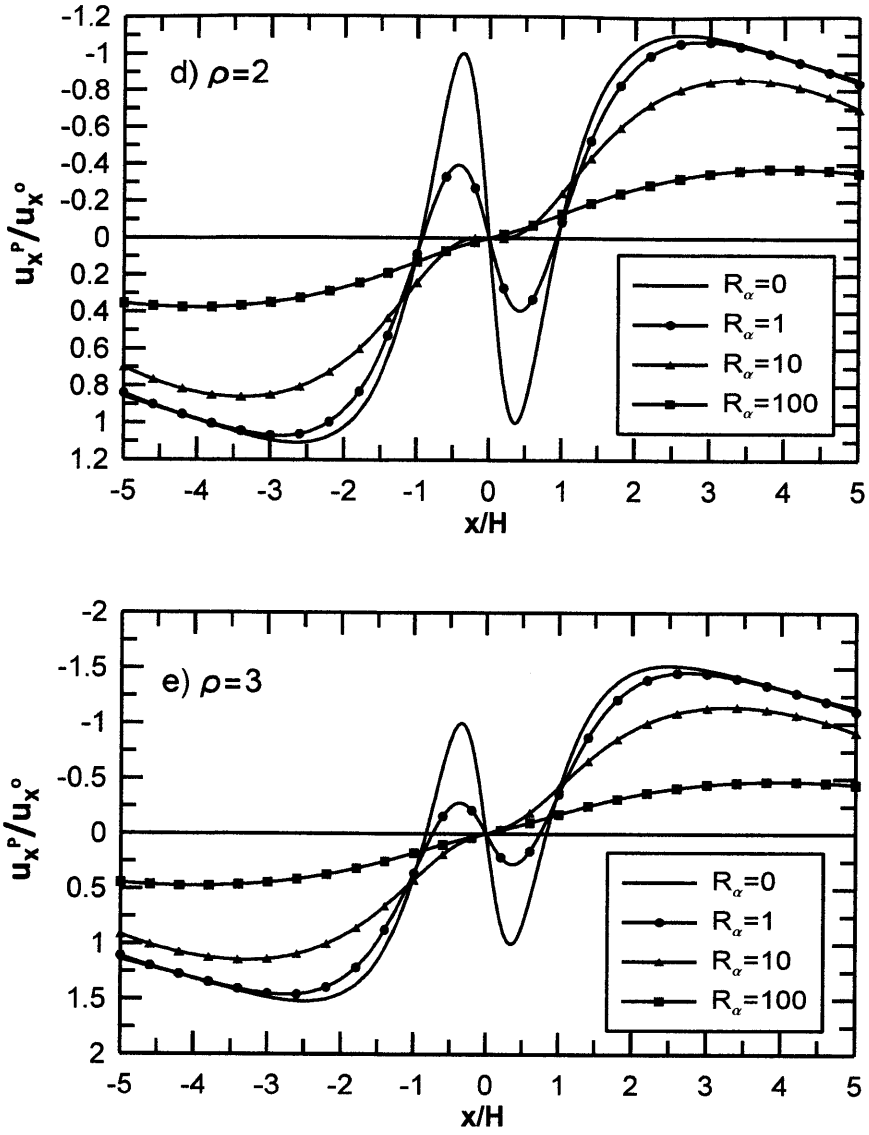

Figure 4-13: Effect of relative distortion, ρ and the relative axial pipe-soil rigidity factor $R_a=EA/E_s r_o x_j$ on normalized horizontal pipe displacements

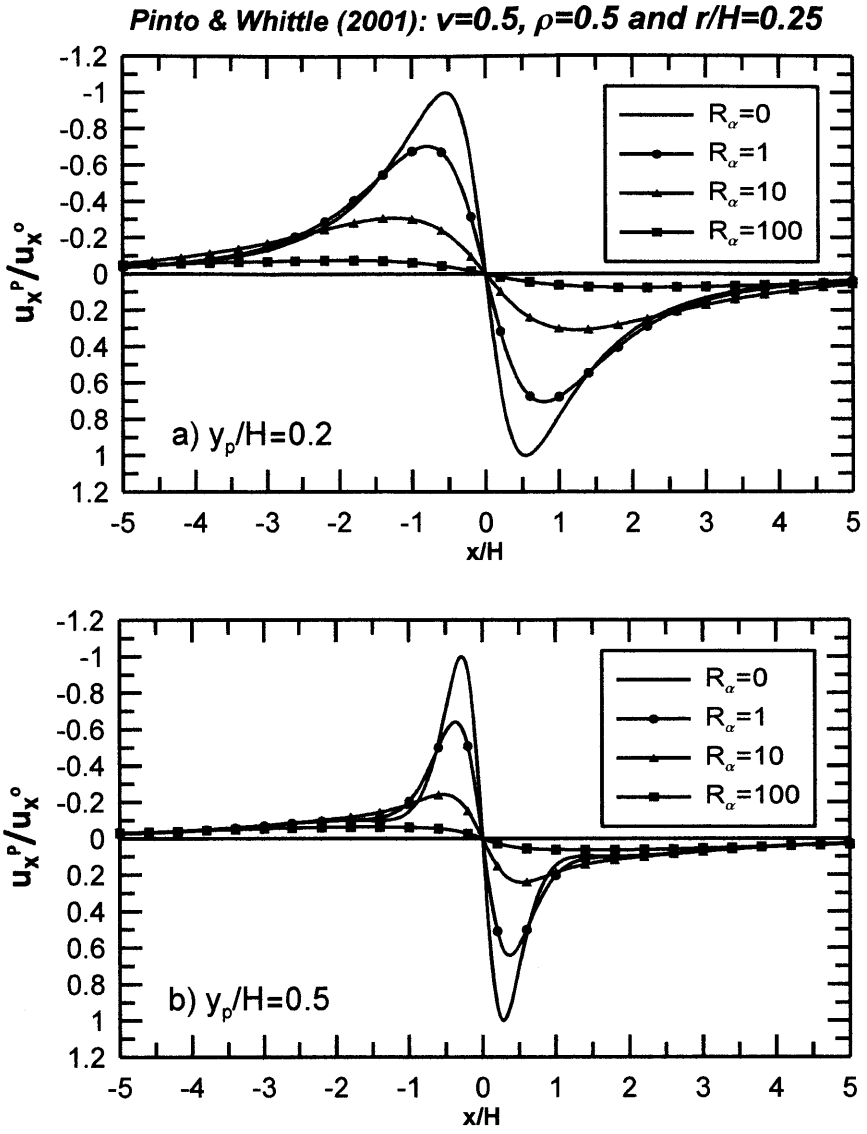

Figure 4-14: Effect of the embedment depth of the pipe, y_p and the relative axial pipe-soil rigidity factor $R_a=EA/E_s r_o x_j$ on normalized horizontal pipe displacements

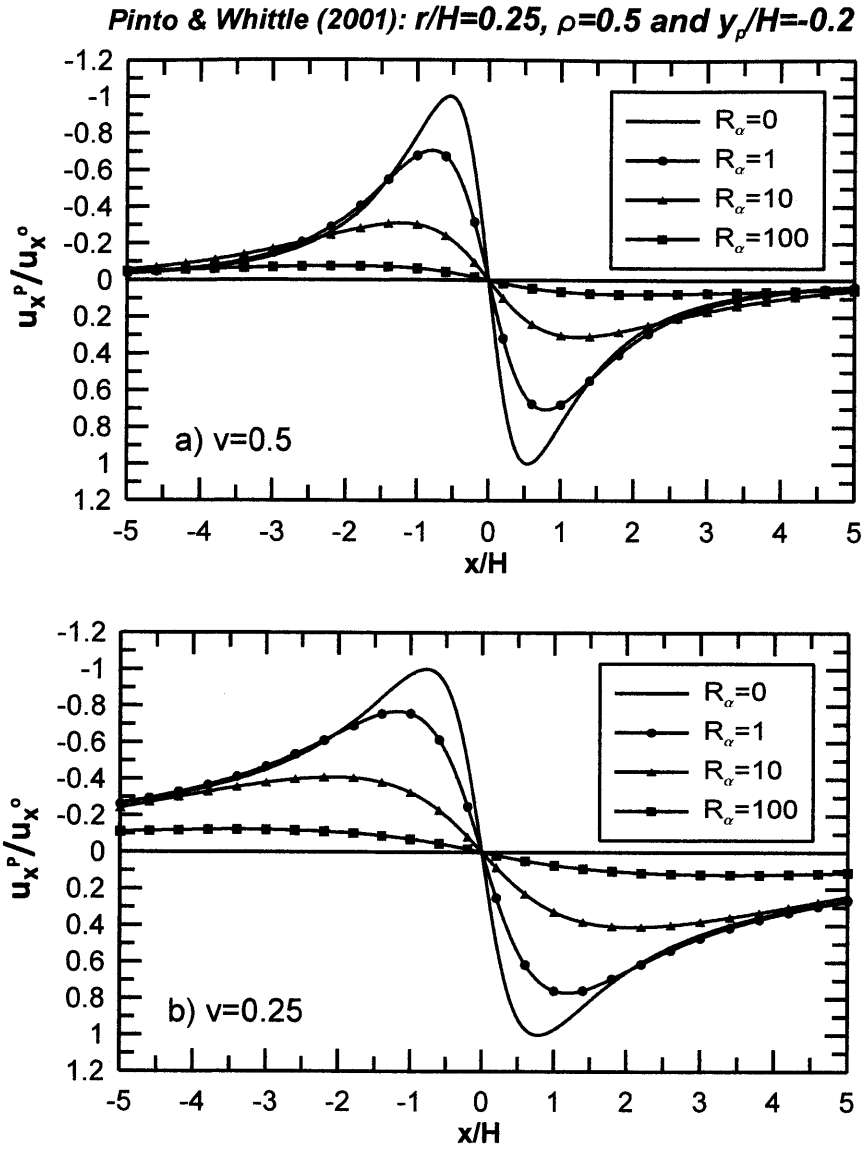

Figure 4-15: Effect of the soil Poisson's ratio, v and the relative axial pipe-soil rigidity factor $R_a=EA/E_s r_o x_j$ on normalized horizontal pipe displacements

CHAPTER 5

FINITE ELEMENT ANALYSES OF PIPE RESPONSE

5.0 INTRODUCTION

A series of numerical elastic finite element solutions have been carried out in order to develop a reliable basis for the analytical models of pipe-soil interactions (i.e. to define spring coefficients K_v and K_h). This chapter presents in details the geometry and the material properties of the model used in the numerical analyses, as well as the limitations of using the specific software for simulating this problem.

5.1 FINITE ELEMENT MODEL

The goal was to model a pipe at a specified embedment depth and its response to a set of ground movements induced by the excavation of a tunnel passing orthogonally beneath the pipeline. The PLAXIS 3D Tunnel software was mainly used (Vortser et al., 2005; Klar et al., 2005) for modeling this problem. However, PLAXIS 2D was also used as a first step for the following two reasons:

a) to specify the appropriate boundaries of the model

b) to ensure that the free-field ground deformations computed in PLAXIS, match the analytical solutions given by Pinto and Whittle (2001).

5.1.1 Model Geometry and Properties

Figure 5-1 shows the problem geometry schematically in a 2D model. The tunnel excavation was modeled as a circular cavity at a constant depth $H=10m$, with a constant radius $r=3m$. The uniform convergence of the tunnel cavity (u_ε) and the relative distortion (ρ) of the tunnel cavity varied as follows: $u_\varepsilon=-0.01m$ and $-0.025m$ and $\rho=0, 0.5, 1, 1.5, 2$ and 3.

The soil was assumed to be massless clay of Young's modulus $E_s=30MPa$, with various Poisson's ratios $v=0.1, 0.25, 0.4$ and 0.5. It has to be mentioned that undrained (incompressible) conditions are approximated using $v=0.495$. Table 5.1 summarizes the combinations of the input parameters for the tunnel wall deflections.

The pipeline was assumed to be continuous hollow cylinder of constant radius $r_o=0.5m$, with wall thickness $t=0.01$ and $0.05m$ and stiffness $E_p=1.7, 17, 170$ and $1700\ GPa$. It should be noted that the values of the pipe Young's modulus (E_p) do not represent real pipe materials (apart from the value 170GPa which corresponds to high quality ductile iron), but were selected to represent a wide range of relative pipe-soil stiffness conditions. The depth of the pipe was also varied with $y_p=-1, -2$ and $-3.5m$. Table 5.2 summarizes the different pipe characteristics used in the model.

Accurate simulation of the free-field ground movements requires careful selections of boundary conditions, mesh, and pipe and tunnel representation.

5.1.1.1 Boundary conditions and mesh

To simplify the model and save computational time, it was chosen to simulate half of the problem with the axis of symmetry at the tunnel centerline (Figure 5-2). Thus, the boundary conditions should be as follows:

- at the bottom of the model, total fixities should are used
- the top part is left free
- the right side of symmetry (tunnel position) has rollers
- and the left side is also free to be able to capture far field displacements

The far-field boundaries are set at *x* axis [0, 300] and *y* axis [-300, 20], for a tunnel with centerline at (0, 0). Regarding the 3D model, it was found that the boundaries in the *z* direction do not affect the solution and therefore $-40 \leq z \leq 40$ with the pipeline located at z=0. It has to be noted that the mesh should be very fine and the planes in *z* direction (3D model) should be sufficiently close to each other so as to form thin slices with adequately small 3D elements. The slices were chosen to be 1m thick.

5.1.1.2 Tunnel cavity deformations and pipeline representation

Uniform convergence of the tunnel cavity is modeled by setting prescribed displacements of the same magnitude at the nodes of the tunnel cavity, pointing to the center of the tunnel. Ovalization, is the change of the circular cavity to an oval shape. This shape cannot be modeled in PLAXIS by using the equation of a random ellipsis. In order to model the exact shape of the cavity resulting from the tunnel ovalization (u_δ), we have to impose the displacements described by the exact solutions (Verruijt, 1997). The exact solution of the tunnel wall displacements at the tunnel cavity due to ovalization is:

$$u_z(\beta) = u_\delta \frac{r}{z(\beta) + iH} \tag{5.1a}$$

where:

$$u_z(\beta) = u_x + iu_y \tag{5.1b}$$

$$z(\beta) = x + iy \qquad (5.1c)$$

with u_δ being the ovalization, r the tunnel radius and H the tunnel depth.

From Equation 5.1b, it can be seen that $u_z(\beta)$ is a complex number with u_x being the wall displacement at the x axis and u_y the wall displacement at the y axis. $z(\beta)$ (from Equation 5.1c) is also a complex number, with x and y the coordinates of the point of interest on the tunnel wall.

Figure 5.3 shows the distortion of a circular tunnel cavity in PLAXIS 2D due to ovalization, assuming: a) an ellipse and b) the correct oval shape (based on the exact solutions). Figures 5.4a) and b) show that PLAXIS 2D solutions fit the analytical solutions for both vertical and horizontal free field displacements by using the exact solutions (Verruijt, 1997) describing the tunnel cavity distortion. It has to be mentioned that uniform translation (Δu_y) (Equation 2.13c) and 2.14c)) has to be added to the tunnel nodes vertical displacements in order to get the correct free field displacements.

The PLAXIS 3D Tunnel software allows the user to create the problem geometry in x-y plane and then extrude it as multiple planes in the z direction, creating a 3D mesh in which slices can be activated or deactivated. Hence, the pipeline is approximated as a beam element of 1m width with bending (EI) and axial (EA) stiffness, corresponding to the actual cylindrical pipe section (Table 5.2). The beam - pipe was only activated in the middle slice of the mesh (z=0) as it is shown in Figure 5-2.

5.2 Comparison Between Analytical and FE Solutions

Having modeled accurately the problem in PLAXIS 3D, the solutions obtained using the FE analyses should fit the analytical solutions for both the vertical and

horizontal pipe and free field displacements. The free field displacements derived numerically fit the analytical solutions, as it is shown in Figures 5.4.

Regarding the vertical pipe displacements, FE analyses were used in order to verify the analytical solutions derived by the assumption of a Winkler's model, using as vertical spring coefficient (K_v), the expression proposed by Klar et al. (2005) (Equation 3.15). Figures 5-5 through 5-9 show PLAXIS and analytically derived pipe displacements for different pipe stiffness and different sets of parameters (v, ρ and u_ε). The analytical solutions have been derived by using K_v from Equation 3.15. From the figures it is observed that PLAXIS fit the analytical solutions with small discrepancies, basically at the region of the maximum pipe settlement. This occurs due to the precision of the mesh. As the mesh becomes finer, the discrepancies diminish while the computational time increases.

On the contrary, for the case of the horizontal pipe displacements, the FE analyses were conducted to define the appropriate horizontal spring coefficient (K_h) used in the analytical solutions presented in Chapter 4. This coefficient was defined through a trial and error procedure, till matching between the FE and analytical solutions. Appendix II summarizes all the graphs showing the comparison of the analytical solutions against FE analyses for different pipe stiffness and different set of parameters (v, ρ, u_ε and y_p).

5.3 SUMMARY

This chapter summarizes the numerical analyses conducted with the finite element codes PLAXIS 2D and 3D Tunnel, to estimate the response of continuous pipelines to tunnel induced ground deformations. The problem geometry, the material properties and the boundary conditions are presented in details.

Using PLAXIS 2D analyses, the vertical and lateral free-field movements estimated by Pinto and Whittle (2001) closed-form analytical solutions were verified, for different combinations of the parameters ρ, v, u_ε, and y_p. Three-dimensional numerical analyses (using PLAXIS 3D Tunnel) were conducted in order to verify the vertical pipe displacements estimated by analytical solutions assuming a Winkler's model, where the vertical spring coefficient K_v is computed by Equation 3.15. The same three-dimensional numerical analyses were also used to estimate the horizontal spring coefficient (K_h) used in the analytical Winkler's model for estimating the axial pipe displacements. The proposed horizontal spring coefficient K_h is presented in Chapter 4 in details.

Table 5.1: Input parameters for the tunnel wall deflections

Soil Poisson's ratio ν	0.25	0.1 0.25 0.4 0.495	0.1 0.25	0.1 0.25 0.495	0.1 0.25 0.495	0.1 0.25	0.1 0.25
Relative distortion ρ	0	0	0.5	1	1.5	2	3
Uniform convergence u_ε (m)	-0.01 -0.05	-0.025	-0.025	-0.025	-0.025	-0.025	-0.025

Table 5.2: Pipe characteristics

	PIPE 1	***PIPE 2***	***PIPE 3***	***PIPE 4***	***PIPE 5***	***PIPE 6***
Wall thickness t(m)	0.01	0.05	0.05	0.01	0.05	0.05
Young's modulus E_p (GPa)	1.7	1.7	17	170	170	1700
EI (MNm^2/m)	6.54	28.7	287	654	2870	28700
EA (MN/m)	53	254	2540	5300	25400	254000

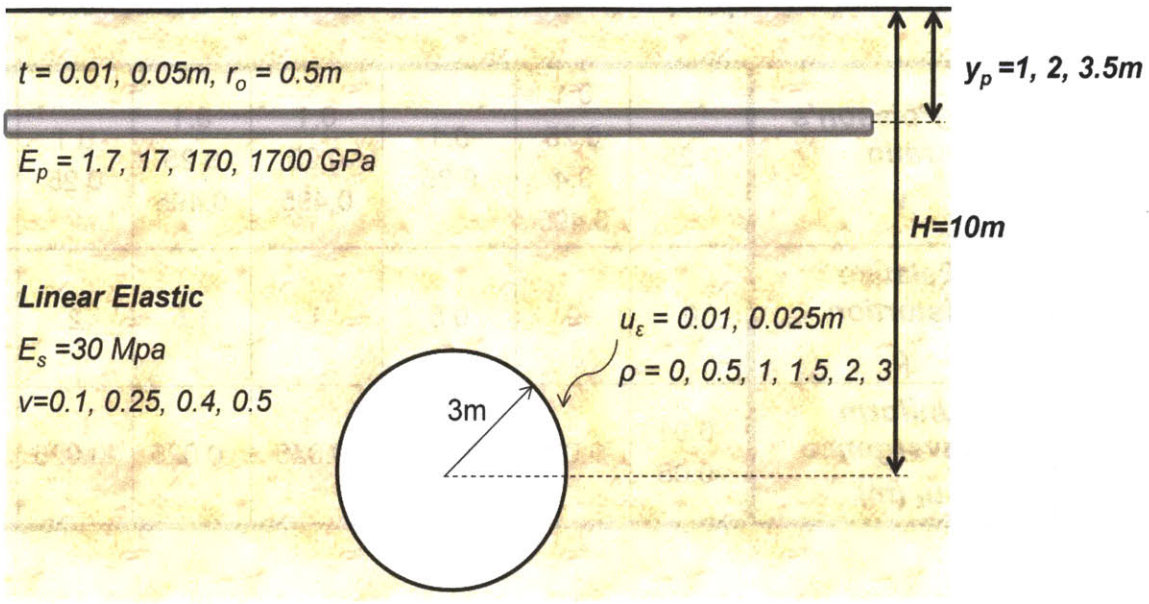

Figure 5-1: Schematic representation of the problem in 2D

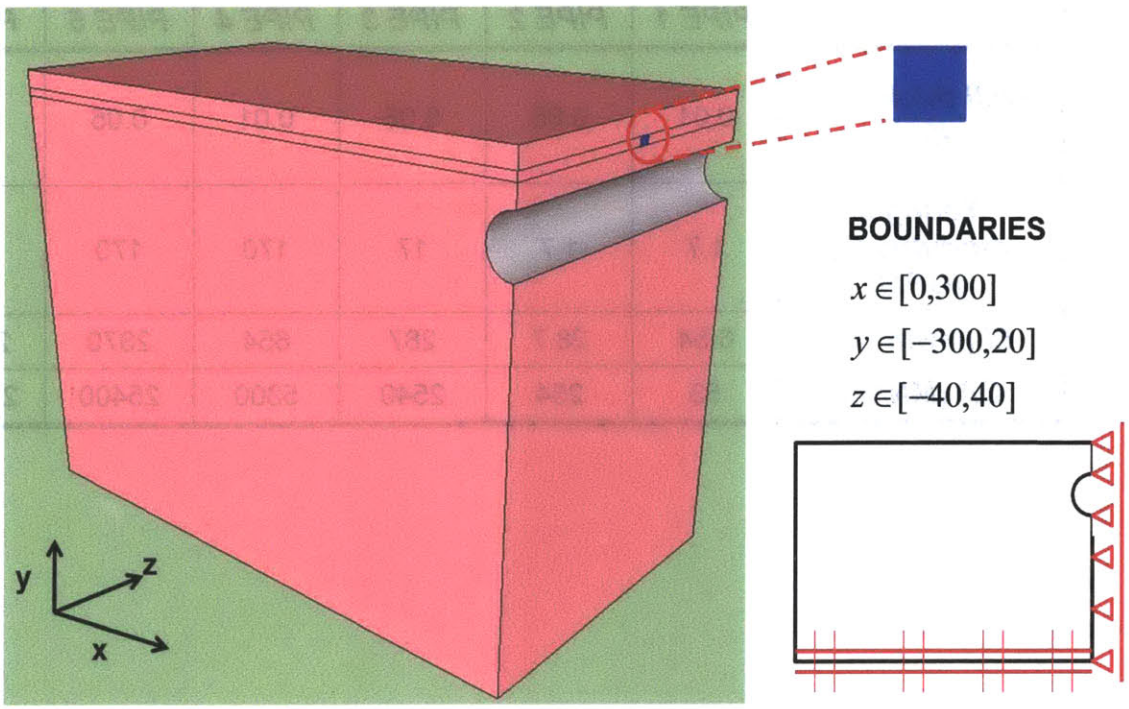

Figure 5-2: Boundary conditions and pipe representation in the 3D model

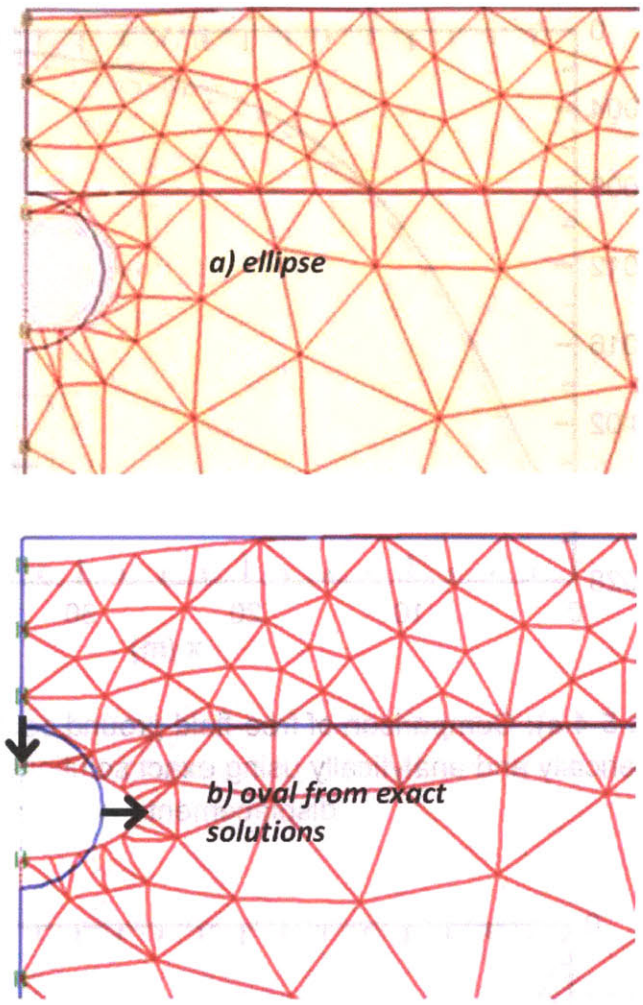

Figure 5-3: Distortion of tunnel cavity assuming a) an ellipse, b) oval shape resulting from the exact solutions

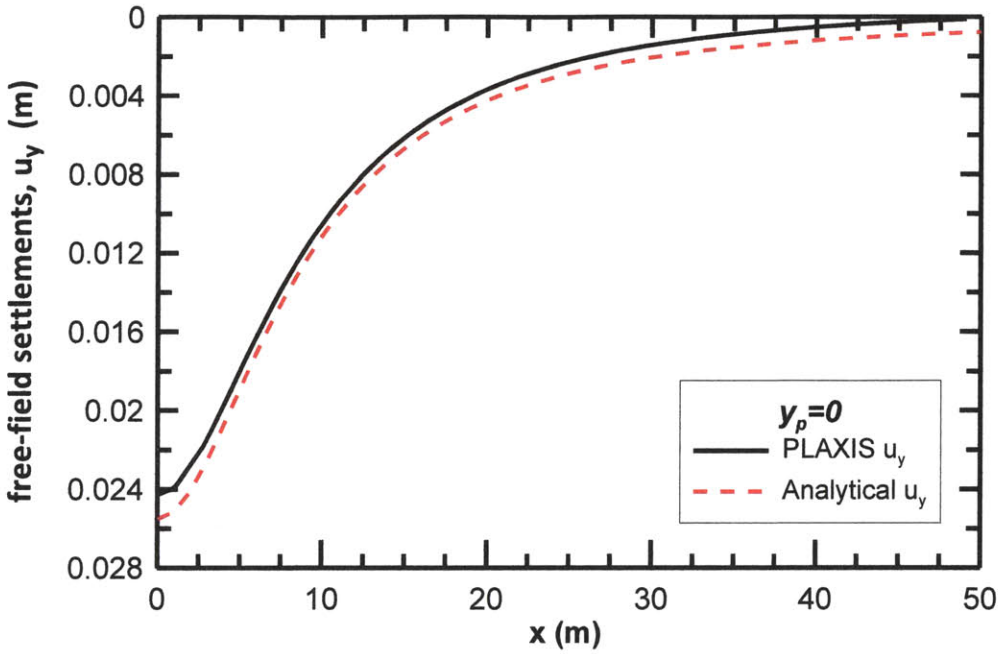

Figure 5-4 a): Comparison of free-field ground settlements computed numerically and analytically using exact solutions for tunnel cavity displacements

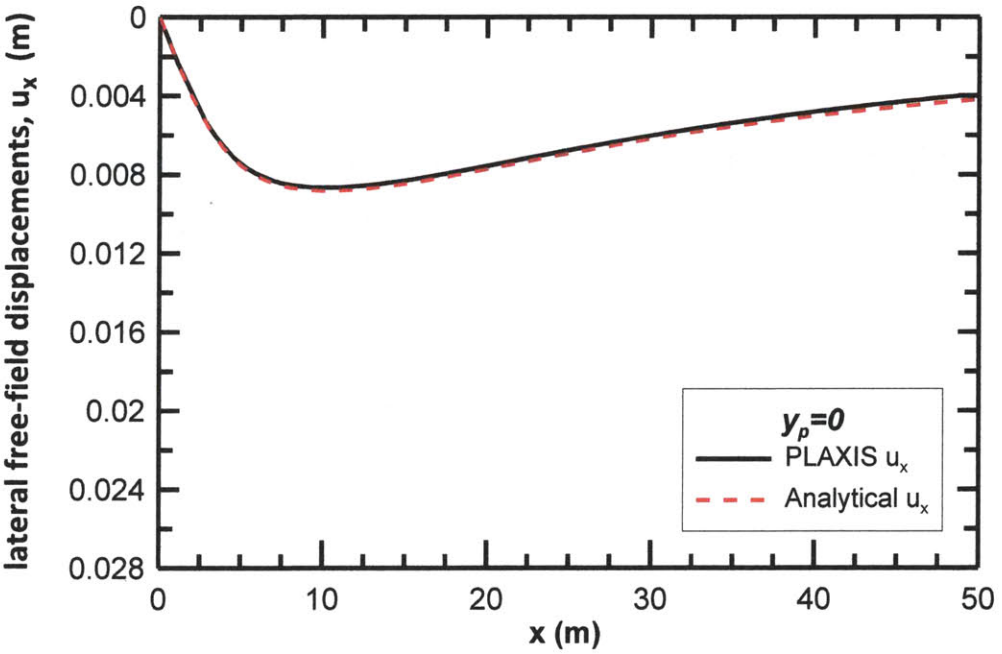

Figure 5-4 b): Comparison of free-field ground lateral displacements computed numerically and analytically using exact solutions for tunnel cavity displacements

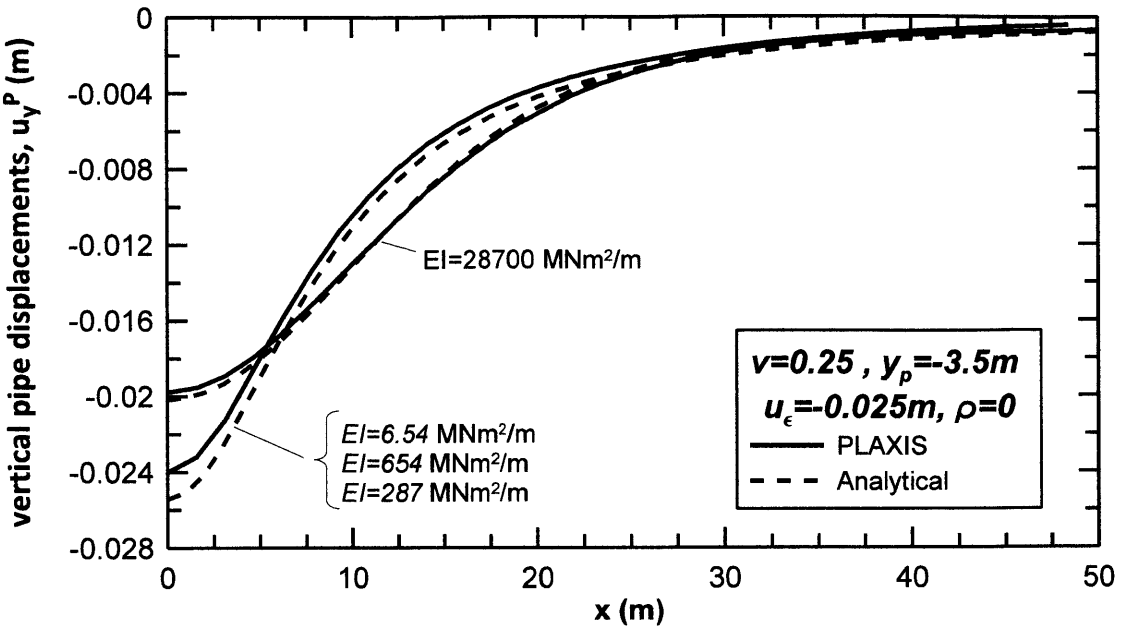

Figure 5-5: Comparison between numerical and analytical solutions of vertical pipe displacements for $v=0.25$, $\rho=0$, $y_p=-3.5m$ and $u_\varepsilon=-0.025m$

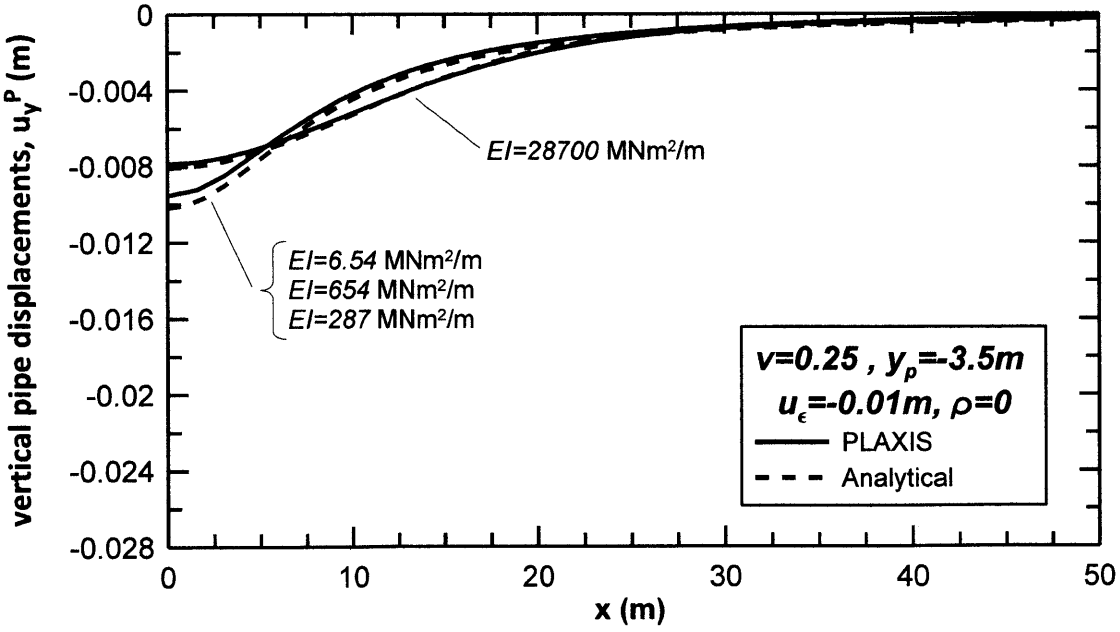

Figure 5-6: Comparison between numerical and analytical solutions of vertical pipe displacements for $v=0.25$, $\rho=0$, $y_p=-3.5m$ and $u_\varepsilon=-0.01m$

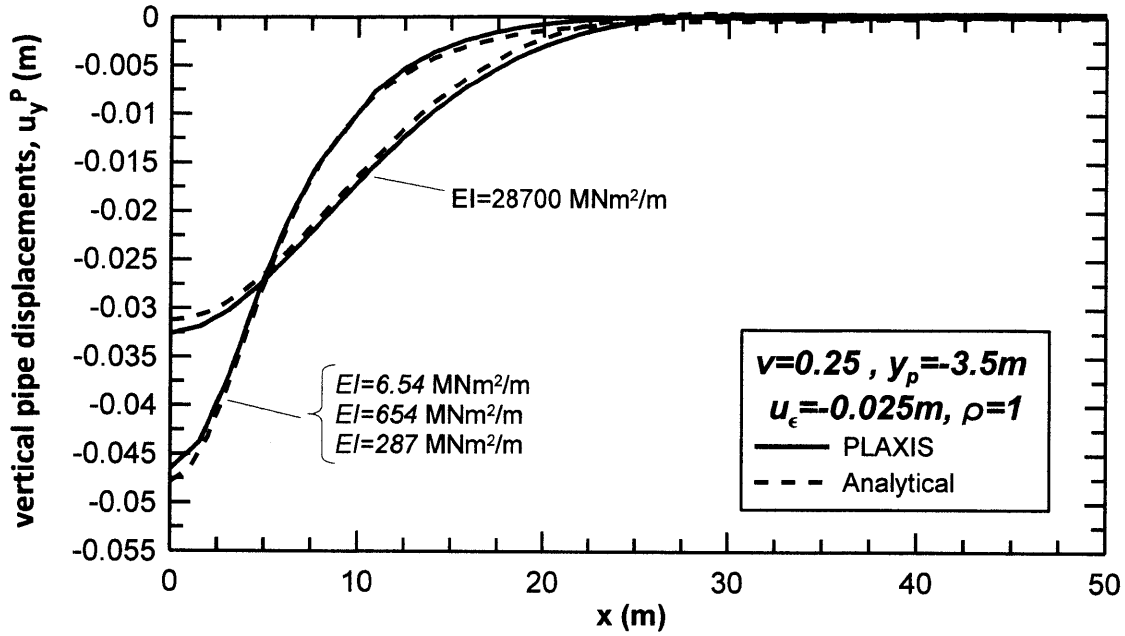

Figure 5-7: Comparison between numerical and analytical solutions of vertical pipe displacements for $v=0.25$, $\rho=1$, $y_p=-3.5m$ and $u_\varepsilon=-0.025m$

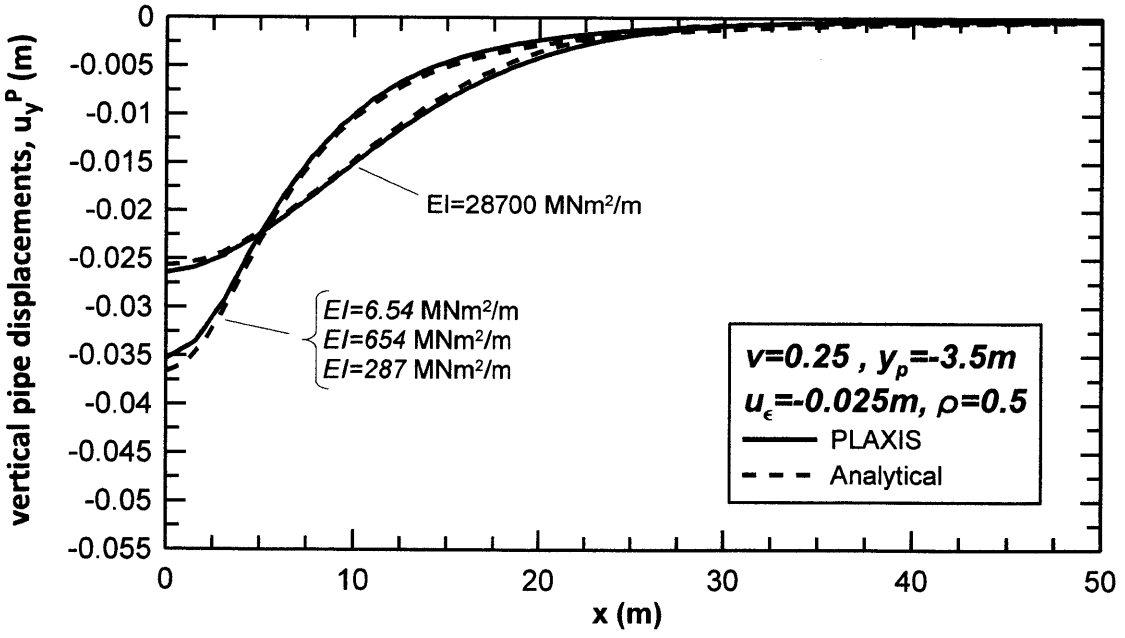

Figure 5-8: Comparison between numerical and analytical solutions of vertical pipe displacements for $v=0.25$, $\rho=0.5$, $y_p=-3.5m$ and $u_\varepsilon=-0.025m$

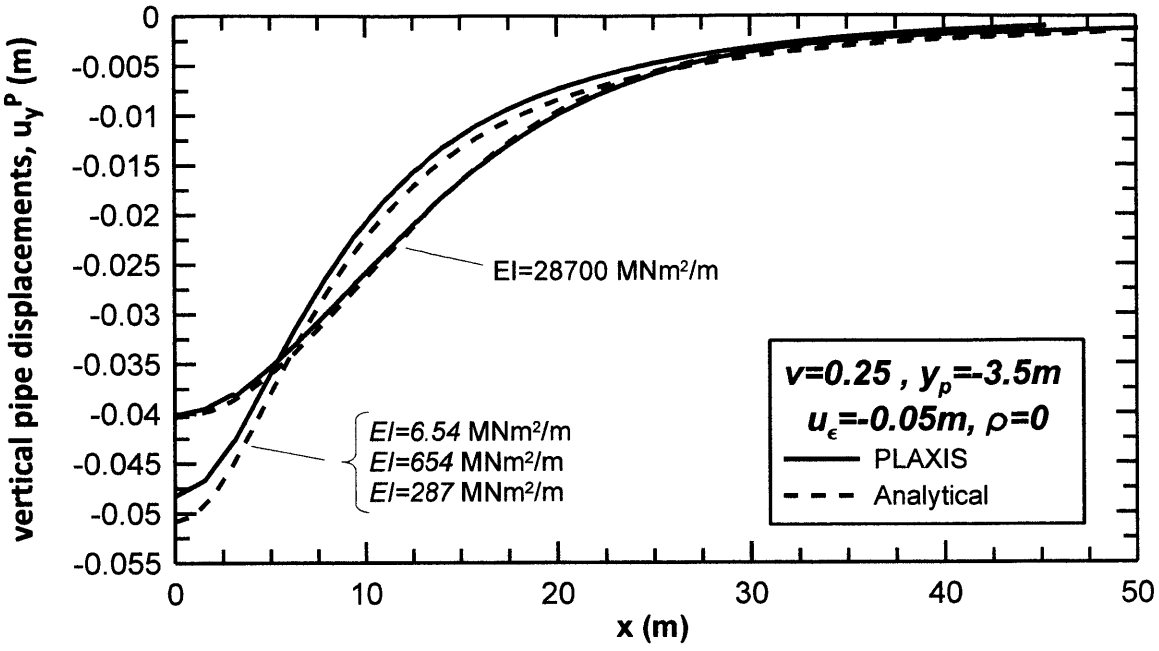

Figure 5-9: Comparison between numerical and analytical solutions of vertical pipe displacements for $v=0.25$, $\rho=0$, $y_p=-3.5m$ and $u_\varepsilon=-0.05m$

CHAPTER 6

APPLICATION OF THE PROPOSED ANALYSES

6.0 INTRODUCTION

This chapter presents the application of the proposed analyses in two cases. The first is the Chingford Pipe Jacking case, where the analyses are used to interpret deformations of an instrumented water main due to the construction of a new tunnel. The second is the N-2 Sewer Tunnel project in San-Francisco, where the analyses are applied to estimate the effects of ground movements caused by the construction of the sewer tunnel, on hypothetical pipelines. In both cases, the free-field ground movements are computed using both empirical and analytical (Pinto & Whittle, 2001) solutions.

6.1 APPLICATION TO CHINGFORD PIPE-JACKING CASE

This section describes the case of a 30" concrete-lined steel cylinder water main which was affected by pipe jacking at a site in Chingford, North London (Vorster, 2005) and how the analytical solutions are applied. As part of the upgrading of the Chingford Water Treatment Works (CWTW), a 2.465m diameter tunnel was constructed at a depth of 11.8m by the method of pipe-jacking. In order to estimate the potential effect of the tunnel construction on the overlying jointed water main, the designers assumed a volume loss of 2% to 3% and it was proposed that the tunnel would cross at a depth of 10.2m approximately below the invert of the water main. During construction, the free-field and the pipeline settlements were monitored.

6.1.1 Site Description and Geology

Figure 6-1 and 6-2 show a cross-section of the stratigraphy and plan view of the instrumentation for monitoring the ground movements due to tunnel construction. The geology of the site comprises 1.1m of made ground, 1.9m River Terrace Gravels, overlying a 10.9m thick layer of London Clay.

The water main comprises a 4.57m long jointed composite concrete-steel pipe with outer diameter 942mm and wall thickness, 90mm. The longitudinal bending stiffness ($E_p I_p$=358 MNm^2) was calculated by taking account of the transformed section of the composite material (concrete-steel). The edge of the entry shaft was located 8.9m from the pipeline centerline, with the jacking route crossing the longitudinal axis of the pipe at 87.5° and at a depth of approximately 10.2m from the invert of the pipe.

The project was monitored with settlement rods installed in 3 lines, one directly on top of the pipe and two others on either sides of it, at offsets of 2m (Line R) and 4m (Line L) respectively from the pipe centerline (Figure 2-6). Ribbon optic fibers were also used on the crown of the pipeline to monitor strain changes. The general objective of monitoring was to capture: a) the free-field response of the soil surrounding the pipeline, b) the pipeline response compared to the free field soil, c) the pipe joint rotation and d) the development of pipe strains, including movements across joints (full details are presented by Vorster, 2005).

6.1.2 Free-Field Soil and Pipe response

Pipe jacking is a technique of installing underground pipelines, ducts etc, by minimizing surface excavation (Vorster, 2005). Pipe sections are jacked from an entry shaft, while the spoil is disposed of by means of a conveyor system. After breaking through the exit shaft, the shield is removed and the remaining annulus

between the jacked pipe and the surrounding soil is grouted up to limit further ground movement due to contraction of the excavated cavity around the pipe. At the Chingford site, hydraulic jacks pushed the bottom half of the 2.43m outer diameter concrete pipe sections in jacking stages along the tunnel. Bentonite was used to lubricate pipe work during jacking in order to minimize friction between the pipe and the surrounding soil (Figure 6-3).

Excess pore pressures can develop in the low permeability clay around the jacks of the shield due to displacement of clay. Behind the shield, a cavity was formed due to overcutting of the shield. This tail void remained unsupported until grouting took place after breaking through the exit shaft. As excavation progressed, the tail void is believed to have acted as a drain, allowing excess pore pressure to dissipate into the cavity, leading to increases in ground movements. Further excess pore pressured are also believed to have been caused by the application of bentonite of pipe sections during jacking (*Immediate response*).

An additional mechanism of ground movements is the stress relief behind the shield due to the lack of support of the tail void. This resulted in a further component of ground movement associated with the swelling into the excavation (*Intermediate response*).

Finally, 2 months after completion of grouting, ground movement continued, possibly because of the dissipation after grouting of the excess pore pressures which were developed during jacking of the shield, resulting in further consolidation (*Post grouting response*). Table 6.1 shows the volume loss associated with the ground movement development. The volume losses are estimated from the curves fitted to the surface settlement trough. Figure 6-4, shows the total duration of the project and the staged of the construction.

Vorster (2005), fitted the modified Gaussian curves (Equation 2.6) to the free field settlement trough (Line L). The parameters used are: pipe bending stiffness $EI=358MNm^2$, pipe radius $r_o=0.471m$, soil stiffness $E_s=40MPa$. The assumed maximum free-field settlement at line L is $u_y^o=7.6mm$, n=0.39 (A=0.16) and distance to the inflection point $x_i=7.5m$. In order to compare the modified Gaussian curve with analytical solutions of Pinto & Whittle (2001), data from Line L were fitted using genetic algorithms, for uniform convergence $u_\varepsilon=23.43mm$ and relative distortion $\rho=0.23$. Figure 6-5 shows the monitored free-field settlements after grouting the tail void (68th day), the modified Gaussian curve suggested by Vorster (2005) in order to fit the data and the analytical solutions proposed by Pinto & Whittle (2001). It can be seen that the analytical solutions predict more accurately the free-field settlements than the modified Gaussian curve.

The basic assumption in order to estimate the water main response is that the pipe behaves as a continuous pipeline. Based on Vorster's predictions, the distance to the inflection point of the free-field settlement trough at the pipe level is $x_i=4.11m$ and the maximum free field settlement is $u_y^o=3.9mm$. Taking into account that $EI=358MNm^2$, $r_o=0.471m$ and $E_s=40MPa$, the relative pipe-soil bending rigidity factor R_b (Equation 3.14) is 0.16. Vorster et al. (2005) reported that pipelines with $R_b<0.5$ behave as very flexible and simply follow the ground movements. Hence, the water main is expected to be very flexible compared to its surrounding soil.

The pipe settlements are estimated by applying the proposed analytical method, assuming that the free-field settlements at the pipe level are described by the analytical solutions of Pinto & Whittle (2001). Figure 6-6 shows the monitored pipe settlements, the free-field settlements at the pipe level and the predicted pipe settlements based on the proposed analytical method. It can be seen that

the pipeline simply follows the ground movements and therefore the Chingford case does not contribute much in verifying of the proposed analytical method.

Vorster (2005) also reported that the horizontal free-field ground displacements should be given by the empirical Equation 4.2 for *d=0.175, c=0.325, H=11.8m* and *y=1.6m.* Taking into account that the free-field settlements are described by a modified Gaussian curve with u_y^o=*7.6mm*, n=0.39 (A=0.16) and x_i=*7.5m,* the lateral free-field displacements are given by:

$$u_x = 0.0076 \cdot \frac{x}{16.55} \cdot \frac{0.39}{(0.39-1) + e^{0.16*\left(\frac{x}{7.5}\right)^2}} \tag{6.1}$$

In order to compare the empirical solutions with analytical solutions of Pinto & Whittle (2001), lateral free-field displacements were computed using uniform convergence u_ε=*23.43mm* and relative distortion ρ=*0.23*. Figure 6-7 shows the empirical and the analytical predictions for the free-field horizontal movements at the pipe level. It can be seen that the two methods converge close to the tunnel, while the empirical solutions underpredict the horizontal free-field movements, as the distance from the tunnel centerline increases.

The pipe axial displacements are estimated by applying the proposed analytical method, assuming that the free-field lateral displacements at the pipe level are described by the analytical solutions of Pinto & Whittle (2001). Figure 6-8 shows the pipe axial displacements for pipe stiffness, E_p=*30600MPa*, pipe radius, r_o= *0.471m*, wall thickness, *t=45mm* (A_p=*0.1266m*^{2}).

The settlements and axial displacements of the water are used to estimate the pipe strains and stresses. Equations 6.2 and 6.3 give the axial component of the bending strains, the axial strains due to horizontal pipe displacements, the total pipe strains and the axial pipe stresses.

$$\varepsilon_b = r_o \frac{\partial^2 u_y^P}{\partial x^2} \tag{6.2a}$$

$$\varepsilon_a = \frac{\partial u_x^P}{\partial x} \tag{6.2b}$$

$$\sigma_x = E_p \cdot (\varepsilon_b + \varepsilon_a) \tag{6.3}$$

where

u_y^P, u_x^P = Vertical and horizontal pipe displacements

Figure 6.9 illustrates the predicted pipe axial, bending and total strains and stresses by using the proposed analytical method.

6.2 APPLICATION TO N-2 SEWER TUNNEL PROJECT

This section considers the effects of ground movements caused by construction of the N-2 sewer tunnel in San Francisco, on hypothetical pipelines. As reported by Clough et al. (1983), the N-2 San Francisco is a 3.7m diameter and 915m sewer tunnel, part of the San Francisco Clean Water Project started at 1981. It is located on the northeastern portion of the Peninsula near San Francisco Bay. The tunneling was a challenge because of the following reasons:

a) the overlying activities could not be disrupted

b) there was an average of only 9.1m cover

c) the tunnel section was in a soft layer of sediments overlain by a rubble fill of indeterminate quality

d) the ground water table was about 4.6m above the crown

e) wooden piles passed through the tunneling section

f) a high pressure water line was located near the surface only 1.5m off the tunnel center line.

The major portion of the subsurface profile consists of an average of 6.1m rubble fill underlain by 9.1m soft sediment (Recent Bay Mud). A stratum of colluvial and residual sandy clay is encountered below the Bay Mud. The tunnel was advanced entirely within the Recent Bay Mud, which consists of silt and lean clay with some beds of fine sand. The soil is essentially normally consolidated except near the top of the stratum, where it has been lightly overconsolidated by desiccation. Triaxial test data suggest that the undrained shear strength of the Recent Bay Mud, $s_u = 24.3\ kN/m^2$ just below the fill and increases approximately at $\Delta s_u/\Delta z = 0.63\ kN/m^2/m$ with depth. An idealized soil profile is shown in Figure 6-10.

6.2.1 EPB Tunneling Method

The tunneling method used is the EPB (Earth Balance Pressure) method. The EPB tunneling machine (Figure 6-11) consists of a rotating cutterhead which excavate the soil and pass it through slots to a spoil retaining area behind the cutterhead. Two rows of teeth are set on the cutterhead between the slots to cut the soil at the face of the shield. The soil is removed via a screw auger, is deposited onto a conveyor belt and is transferred outside the tunnel.

The main idea of the EPB shield is that it allows control of the amount of the soil excavated as the shield advances. If the auger operates too fast, the void created by the soil removal can lead to possible flowing soil conditions. This is avoided by monitoring the amount of soil in the spoil retaining area and the rate of screw auger rotation. For the N2 project, the earth pressure was chosen so that the screw auger would remove soil from the retaining area at a slightly

slower rate than the rate of the soil entering the cutterhead. This practice was designed to initially heave the soil outwards from the shield to some degree and to compensate partially for the subsequent inwards movement caused by the tail void closure (Kimura et al. 1981).

6.2.2 Measured Free-Field Movements

In order to monitor the free field ground displacements, ground instrumentation was installed at four locations along the tunnel alignment as it is shown in Figure 6-10. Lines 2, 3 and 4 were monitored throughout the total tunneling procedure, while Line 1 readings were taken less frequently. Lines 1 and 2 were located at the first third of the project, and Lines 3 and 4 were located at the middle third, close to areas where piles existed.

As reported by Clough et al. (1983), readings from all the Lines showed that initially the ground heaved vertically only a small amount of 0.63cm. After the shield passage, the ground began to settle and continued so for about 40 days. A maximum settlement of 3cm was reached at this time. Readings taken at 150 days showed actually no further settlement. This vertical soil movement occurred due to closure of the tail void.

Regarding the lateral movements, inclinometers at Lines 1 and 2 showed lateral soil movements towards the centerline of the tunnel, while readings from inclinometers at Lines 3 and 4 showed that the soil was actually pushed ahead of and away from the shield as it advanced. However, after shield passage the vectors reflected incremental inwards movements towards the tunnel, caused by the presence of the tail void, but still the net positions were away from the tunnel. Figure 6-12 shows vertical and horizontal movements at Line 4, fifteen days after shield passage.

Figure 6-13 shows the 'long-term' lateral movements measured 15 – 30 days after shield passage at the inclinometers immediately adjacent to the tunnel for all four Lines. Where the net movements were inwards, the earth pressure was low (Lines 1 and 2), while where the net movement was heave, the earth pressure was high. Table 6.2 summarizes the non-dimensional earth pressure of the shield machine and the maximum net lateral movement after shield passage for the four Lines.

6.2.3 Interpreted Free-Field Movements

6.2.3.1 Empirical Solutions

Empirical solutions were used to fit the high earth pressure data (Line 4), assuming the Gaussian curve (n=1) distribution for the free field ground settlements, with maximum settlement of $u_y^o=0.033m$ and distance to the inflection point $x_i=3.13m$.

The ground displacements are assumed to be directed towards the tunnel centerline. Taking into account that at the tunnel is entirely excavated into the Recent Bay Mud, we assume that the fill above it has the same properties and thus the whole soil profile is actually clay with undrained shear strength $s_u=24.3$ kN/m^2. Following Mair et al. (1993), we obtain:

$$u_x = \frac{x}{12.76} e^{-\frac{1}{2}\left(\frac{x}{3.13}\right)^2} \tag{6.4}$$

Equation 6.4 has been derived by Equation 4.3 with $d=0.175$, $c=0.325$, $H=9.6m$ and $y=2m$.

6.2.3.2 Analytical Solutions

Analytical solutions (Pinto & Whittle, 2001) were used to fit high (Line 4) and low (Line 2) face pressure data. Zymnis et al. (2011) report uniform convergence u_ε = *-0.017m* and relative distortion ρ = *2.06* for Line 4, and u_ε= *-0.031m* and ρ = *0.32*, for Line 2 data. Figure 6-14 compares the-free field ground settlements evaluated by the empirical and analytical solutions at an embedment depth y=-2m. The displacements are very similar in a region of x≤6m (20ft) from the tunnel centerline. However for x>6m, the analytical solutions show heave of the soil (negative settlements), that is not described by the empirical functions. The measured data do not extend more than 6m from the tunnel centerline and thus they cannot verify the occurrence of heave described in the analytical solutions.

Regarding the horizontal free-field ground displacements, empirical solutions assume that the displacements point at the tunnel centerline. However, data from Line 4 showed that the soil was actually pushed away from the tunnel centerline after some distance (Figure 6-13), due to high earth pressure. Figure 6-15 shows that analytical solutions are able to capture this mechanism.

For Line 2, analytical solutions are used. Figure 6-16 shows the free-field settlements and horizontal displacements described by P&W (2001) analytical solutions, at a depth of y= -2m. The horizontal free-field displacements indicate horizontal soil movements towards the tunnel centerline. This was expected as the Line 2 data from Figure 6-13 show that soil moved laterally towards the tunnel.

6.2.4 Response of Hypothetical Pipelines

The response of hypothetical pipelines at y=-2m is now considered using the proposed pipe-soil interaction models.

6.2.4.1 Pipeline characteristics

The pipelines of primary interest are continuous cast-iron sections (the majority of old water mains are made of cast-iron). Typical pipeline diameters, range between 0.3m and 1.0m. Figure 6-17 shows the model geometry and properties of this problem with the N2 – San Francisco tunnel at a depth of 9.6m and a continuous pipeline buried at depth y_p=-2m. Table 6.2 summarizes all the characteristics of the pipelines considered in the analyses, with Young's modulus of cast iron E_{CI}=100 GPa. The vertical spring coefficient K_v is defined by equation 3.15 with x_i=*4.88m* and the horizontal spring coefficient K_h is defined by Equation 4.13 with x_j=*3.125m*, where x_i and x_j are defined by the free-field displacements at the depth of interest (e.g. y=-2m).

6.2.4.2 Vorster method (2005)

Due to the fact that empirical solutions were used to evaluate free field displacements produced only by high earth pressure (Line 4), Vorster (2005) method, which uses empirical solutions, was also used for estimating pipeline response to free field movements in Line 4. Figure 6-18 shows a flow chart with the required input parameters and the procedure to obtain the vertical pipe displacements with Vorster's method.

Horizontal pipe displacements are not included in Vorster (2005) method and thus they are not computed in this analysis. The pipe settlements evaluated by Vorster (2005) method for the 8 different pipes selected, are therefore used to compute the bending pipe strains and stresses (Equations 3.13 and 3.14) which are described below in details.

6.2.4.3 Proposed method

The proposed method estimates the pipe response to vertical and horizontal displacements, using the analytical free-field solutions (Pinto & Whittle, 2001). Figure 6-19 shows a flow chart with the required input parameters and the procedure to obtain the vertical and horizontal pipe displacements with the proposed method. The method is used for both cases of low (Line 2) and high (Line 4) face pressure of the EPB machine.

Low face pressure - Line 2

The vertical and horizontal pipe displacements computed by the proposed method are used to evaluate the axial and bending pipe strain and stresses (Equation 6.2, 6.3).

Figures 6-20 shows the axial, bending and total pipe strains and stresses for both the upper and lower fiber of the pipe30 (diameter 0.3m) representatively. The corresponding graphs for the rest of the pipes selected (Pipe40 to Pipe100) are presented in Appendix III. The largest compressive stress (62MPa) was observed in pipe30. Smaller stresses were observed over the larger pipe section (Pipe40 to Pipe100 – Appendix III). This was expected, as the pipes with bigger diameters are stiffer and thus they undergo smaller strains.

High face pressure - Line 4

Figure 6-21 compares the pipe strains and stresses for the 0.3m diameter cast-iron pipe (Pipe30) representatively, using Vorster (2005) and the proposed analyses method. The corresponding graphs for the rest of the pipes selected (Pipe40 to Pipe100) are presented in Appendix III. The method of Vorster

(empirical) tends to overestimate the pipe strains and stresses, as it does not account for axial compression due to lateral displacements in the soil. More specifically, the maximum axial stress observed is 125MPa computed empirically, while with the proposed method the axial stress drops to 115MPa. Smaller differences arose in larger diameter pipes. This happens due to the fact that the pipes are stiffer and thus they get smaller trains and stresses.

6.2.5 Possibility of Pipeline Failure

To estimate the possibility of pipeline failure, comparison between the applied stresses and the allowable stresses on the pipes has to be done. In the previous paragraphs, the applied pipe stresses are computed with empirical and analytical methods due to ground movements at Lines 2 and 4. The following paragraphs present the cast iron allowable stresses and the possibility of failure of the hypothetical pipelines chosen.

6.2.5.1 Cast-Iron strength

In general cast-iron pipelines can be divided in 2 categories: the pit and the spun cast iron pipes. The pit cast-iron pipes are cast vertically, while the spun cast-iron are cast horizontally. Due to the difference of casting direction, the two categories have significant different strengths.

Many researchers have reported results from tests conducted to find the tensile and compressive strength of cast-iron pipelines. Most of the tests were done on coupons cut from old cast-iron pipelines which were excavated from the ground. The coupons were mainly tested in tension as the compressive strength of cast-iron is much higher than its tensile strength. Table 6.4 summarizes the tensile strength of pit and spun cast- iron pipes reported from different researchers.

The most complete research on cast-iron pipe strength is Seica & Packer (2004) who tested 111 old, preexisting and corroded pipes. Four kinds of tests were performed: a) tension, b) compression, c) ring bearing and d) bending. Tension and compression were done on pipe coupons, ring bearing tests on pipe ring sections and four – point bending tests on whole pipes.

The compression strength reported from the tests ranges from *519 MPa* to *1047 MPa* (mean value *783 MPa*), while the tensile strength reported ranges from *47MPa* to 297 *MPa* (mean value 172 MPa) for all pit and spun cast – iron pipes. Regarding the bending tests, the results from the six pipes tested are summarized in Table 6.5. It has to be mentioned that Seica & Packer (2004) reported only the total failure load and not the failure moment. The latter are calculated by the failure loads, assuming a pipe wall thickness t=35mm for a 152mm diameter pipe and, t=9.6mm for a 102mm diameter pipe. Figure 6-22 shows the typical four point pipe bending load configuration with its corresponding [Q] and [M] diagrams.

The bending moments have been derived from diagram [M] of Figure 6-23 and the failure stress is given by Equation 6.5.

$$\sigma_x = \frac{M \cdot r_o}{I} \tag{6.5}$$

From Table 6.5 it can be observed that pipes 2 and 6 have a low total failure load. This happened because ID #2 had a lot of variations on its wall thickness and #6 had a small diameter. For this reason these two pipes are excluded from calculation of the mean value of the failure stress, which is finally *155 MPa*.

6.2.5.2 Estimation of the possibility of pipeline failure

The hypothetical pipelines at N2-San Francisco case act as beams under constrained bending and axial conditions during the excavation of the tunnel. For this reason, the pipe stresses computed empirically and analytically are compared with failure stresses reported from the pipe bending tests by Seica & Packer (2004). In addition the computed stresses are also compared with the material compression and tensile strength.

The maximum compressive stress that is observed on the pipes examined is 125 MPa for Pipe30 at Line 4 case. The minimum cast – iron compression strength reported by Seica & Packer (2004) is 519 MPa. Therefore, there is no possibility of pipe failure in compression,.

Regarding possibility of pipeline failure in tension, Figure 6-21 summarizes the cases where the computed tensile stresses using the proposed method exceed the lowest estimates of tensile strength for cast-iron pipes. The results clearly show that all pipes are more vulnerable to the case where high face pressures were used for the N-2 tunnel (Line 4), while only small diameter pipes (r_o<0.2m) are vulnerable at the lower face pressure (Line 2).

Examining the failure stress in bending, it is observed that even Pipe30, which is the most flexible, under high earth pressure ground movements (Line 4) does not reach the lowest failure stress of 130 MPa (Table 6-5). Therefore, none of the pipes examined is susceptible to bending failure.

6.3 SUMMARY

This chapter illustrates the application of the proposed method in 2 cases. Chingford pipe-jacking tunnel case was used in order to examine whether

analytical solutions (Pinto & Whittle, 2001) can accurately predict the free-field settlements and also whether our mathematical model can accurately predict the pipeline response. In Chingford (London) an existing concrete water main was monitored as it was subjected to ground movements caused by tunneling. Free-field subsoil displacements, as well as pipe settlements data are available in Vorster (2005). Results from this research showed that the analytical solutions can predict more accurately the free-field settlements than a Gaussian or a modified Gaussian curve. Regarding the pipeline response, application of the proposed method did not give a remarkable result as the pipeline was very flexible relative to its surrounding soil and it simply followed the ground movements.

This chapter also illustrates a proposed method for computing stress conditions in a cast-iron water pipe due to ground movements caused by construction of the N-2 San Francisco sewer tunnel. The proposed method considers the effects of face pressure applied by the EPB tunneling method.

Data from the free field ground movements are matched with empirical (Vorster, 2005) and analytical (Pinto & Whittle, 2001) solutions for the lowest and highest face pressure. Comparison between the two solutions shows that the empirical approach does not estimate accurately the lateral free-field ground movements under high face pressure conditions.

The case of hypothetical pipeline response to N-2 tunneling is examined, assuming a pre-existing cast-iron continuous pipeline at 2m depth. The response of the pipeline is estimated empirically using Vorster's method, and analytically using the proposed method taking into account the lateral free-field ground movements that empirical methods ignore. It is observed that in some cases the empirical solutions slightly overestimate the stresses and strains acting on the pipes.

The computed stresses acting on the hypothetical pipes are compared to the allowable stresses reported by several researchers. The allowable stresses are given from tensile and compressive tests done on cast iron coupons cut from old pipelines and also from bending tests done on while old excavated cast-iron pipelines served as water mains. It is observed that comparing the applied stresses with the lowest allowable stresses, there is possibility of pipeline failure in tension for high earth pressure conditions.

Table 6.1: Volume Loss associated with ground movements

End of Ground Movement Development Stage	Volume Loss Line L	Volume Loss Line R
Immediate settlement (3^{rd} day)	0.60 %	1.30%
Intermediate settlement (19^{th} day)	2.70%	3.80%
Post grouting (68^{th} day)	3.80%	5.10%

Table 6.2: Earth Pressure and Net Lateral Movement

Line #	Non-dimensional Earth Pressure	Max. net lateral movement after shield passage (cm)
1	0.4	-1.02 (inward)
2	0.4	-1.27 (inward)
3	1.0	5.84 (heave)
4	0.8	3.05 (heave)

Table 6.3: Cast – iron pipeline characteristics used

PIPE	OUTER DIAMETER (m)	WALL THICK. (m)	EA (kN)	EI (kNm^2)	K_v (kPa)	K_h (kPa)
30	0.3	0.014	$1.26*10^6$	$13*10^3$	$9*10^3$	$2.4*10^3$
40	0.4	0.015	$1.8*10^6$	$34*10^3$	$12*10^3$	$3.3*10^3$
50	0.5	0.016	$2.43*10^6$	$71*10^3$	$15*10^3$	$4.1*10^3$
60	0.6	0.018	$3.3*10^6$	$140*10^3$	$18*10^3$	$5*10^3$
70	0.7	0.019	$4.1*10^6$	$236*10^3$	$21*10^3$	$5.8*10^3$
80	0.8	0.02	$4.9*10^6$	$373*10^3$	$24*10^3$	$6.6*10^3$
90	0.9	0.021	$5.8*10^6$	$560*10^3$	$27*10^3$	$7.7*10^3$
100	1	0.023	$7.06*10^6$	$840*10^3$	$30*10^3$	$8.3*10^3$

Table 6.4: Tensile strength of Cast-Iron pipes

REFERENCE	SPUN CAST IRON	PIT CAST IRON	MEAN VALUE SPUN	MEAN VALUE PIT
Rajani et al. (2000)	135 – 305	33 - 267	*220*	*150*
Makar & Rajani (2000)	157 - 305	68 - 146	*240*	*107*
Conlin & Baker (1991)	137 - 212		*175*	
Yamamoto et al. (1983)	100 - 150	--	*125*	--
Caproco Corrosion (1985)	70 - 217	--	*144*	--
Ma & Yamada (1994)	40 - 320	--	*180*	--

Table 6.5: Tensile strength of Cast – iron pipes (Seica & Packer, 2004)

ID No.	Nominal D(mm)	Tensile strength (MPa)	Total failure load (kN)	Bending moment (MNm)	Moment of inertia (m^4)	Failure stress (MPa)
1	152	130	211	0.047	2.4×10^{-5}	149
2	152	131	75	0.017	2.4×10^{-5}	54
3	152	141	182	0.041	2.4×10^{-5}	130
4	152	159	192	0.043	2.4×10^{-5}	136
5	152	244	286	0.064	2.4×10^{-5}	203
6	102	222	85	0.019	3.06×10^{-6}	322

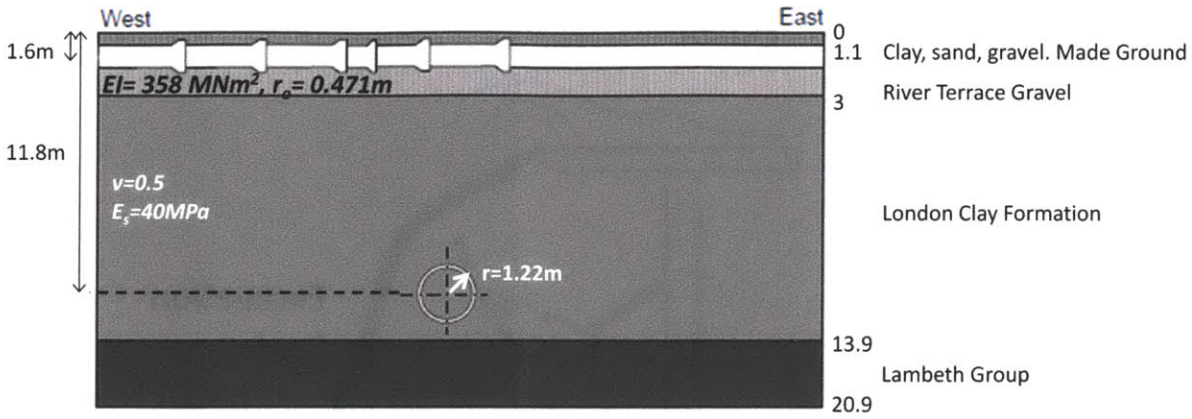

Figure 6-1: Chingford geological profile and geometry

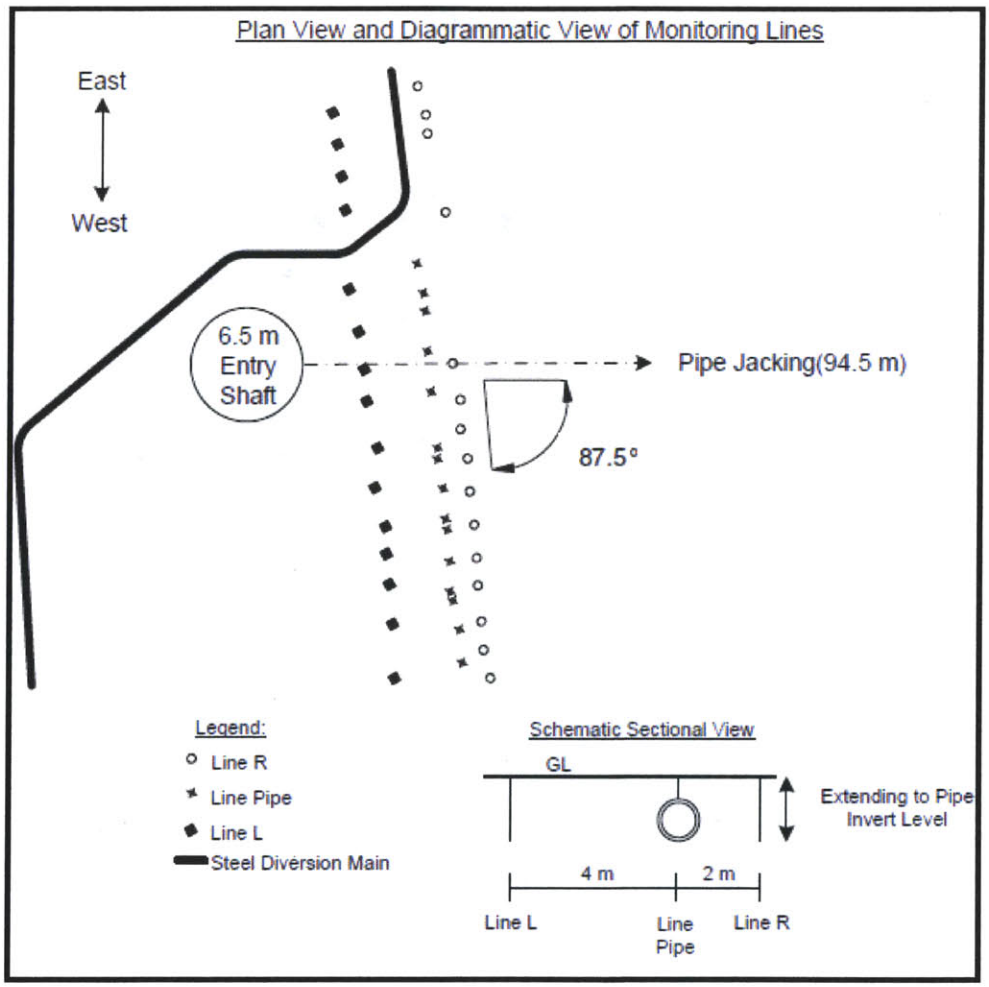

Figure 6-2: Monitoring layout of the Chingford project

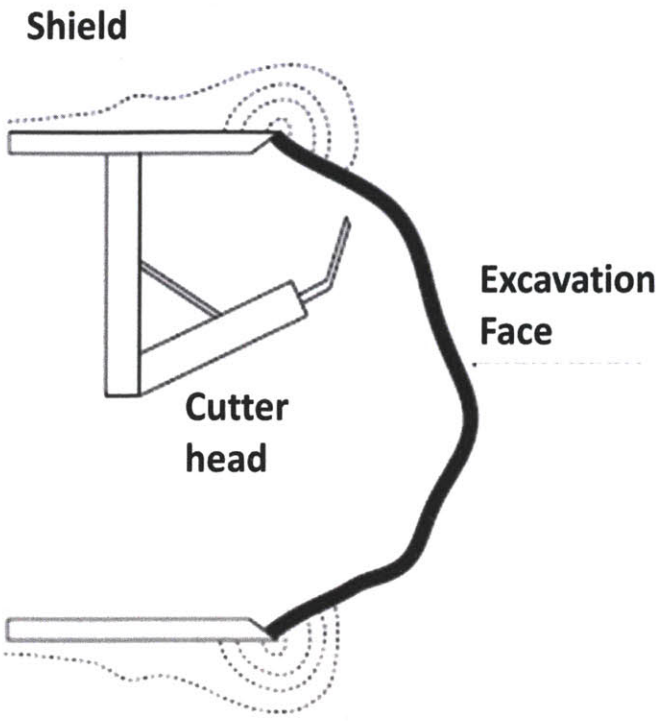

Figure 6-3: Pipe jacking process (Vorster, 2005)

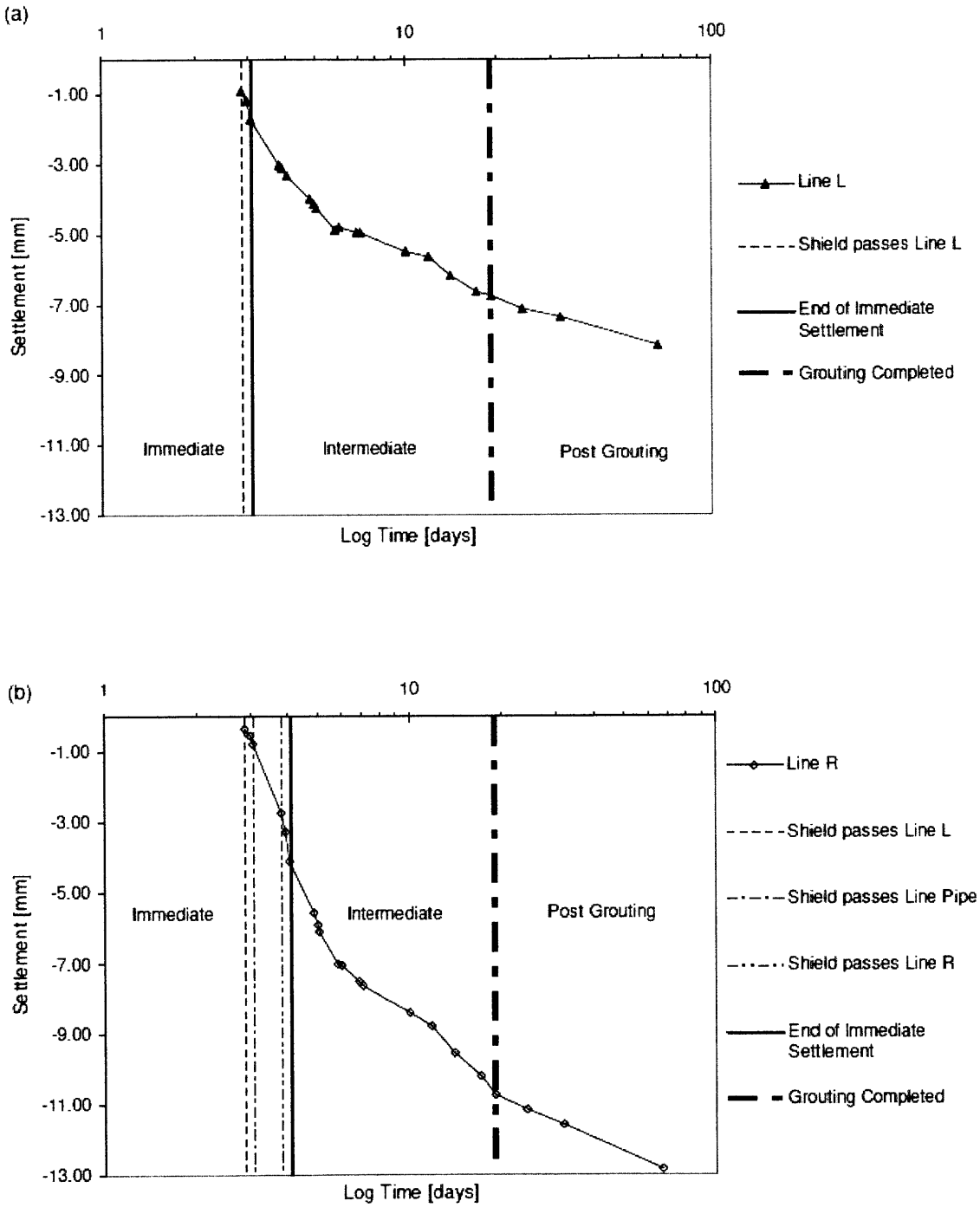

Figure 6-4: Stages and duration of ground movements (a) Line L, (b) Line R

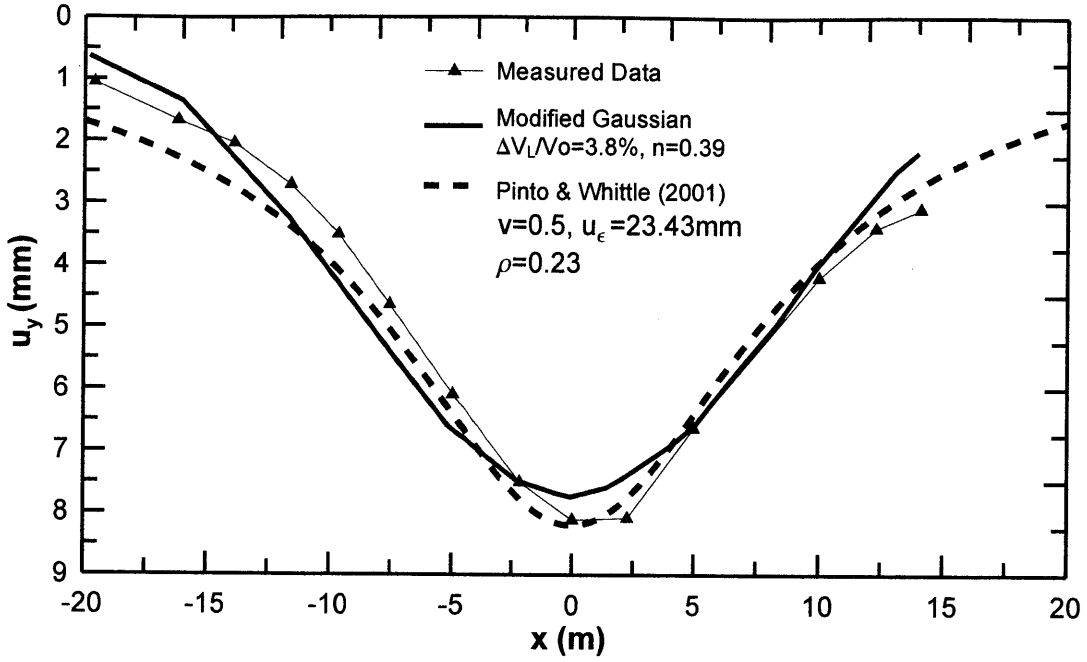

Figure 6-5: Comparison between modified Gaussian and P&W solutions to fit free-field measured data from Line L

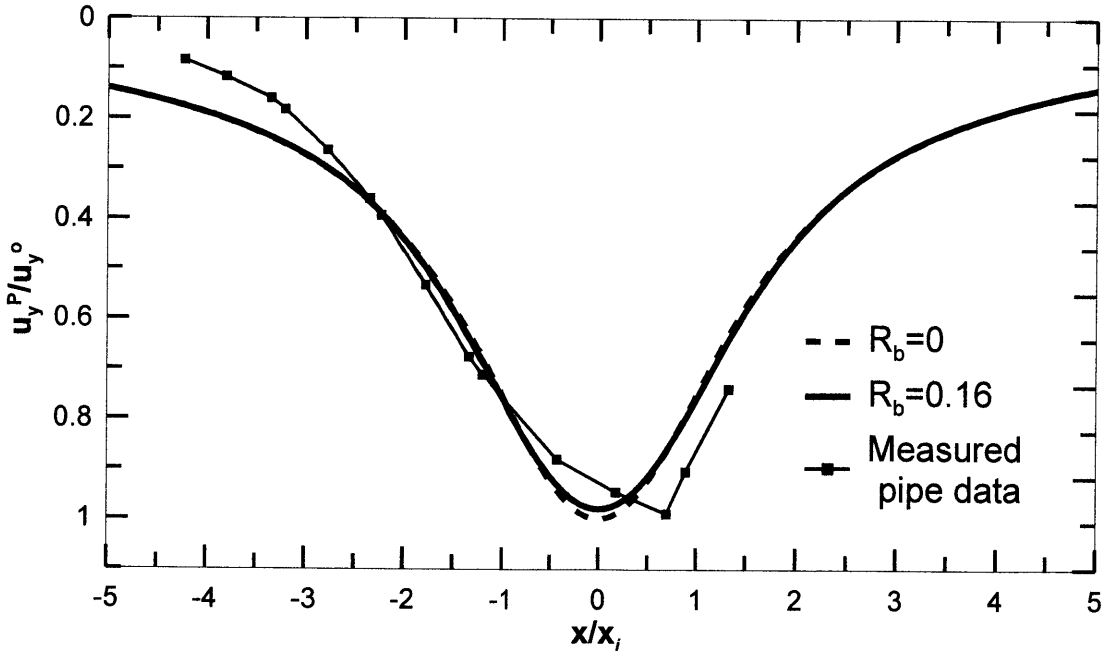

Figure 6-6: Analytically computed free-field settlements and comparison between measured and analytically estimated pipe settlements

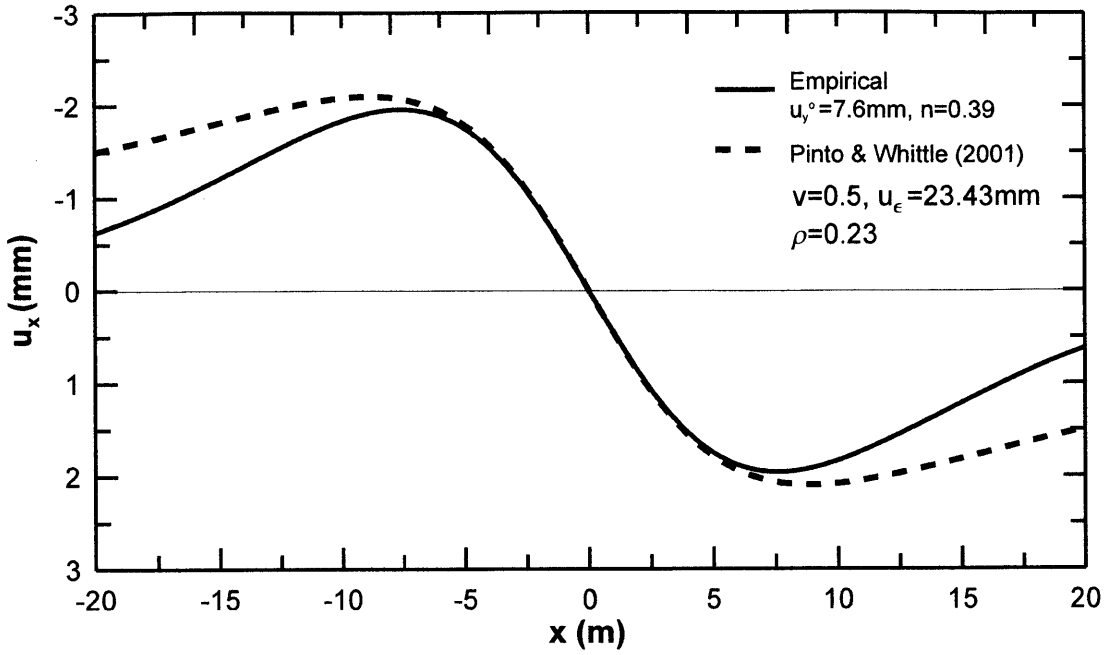

Figure 6-7: Comparison between empirical and analytical solutions for estimating free-field horizontal displacements at Line L

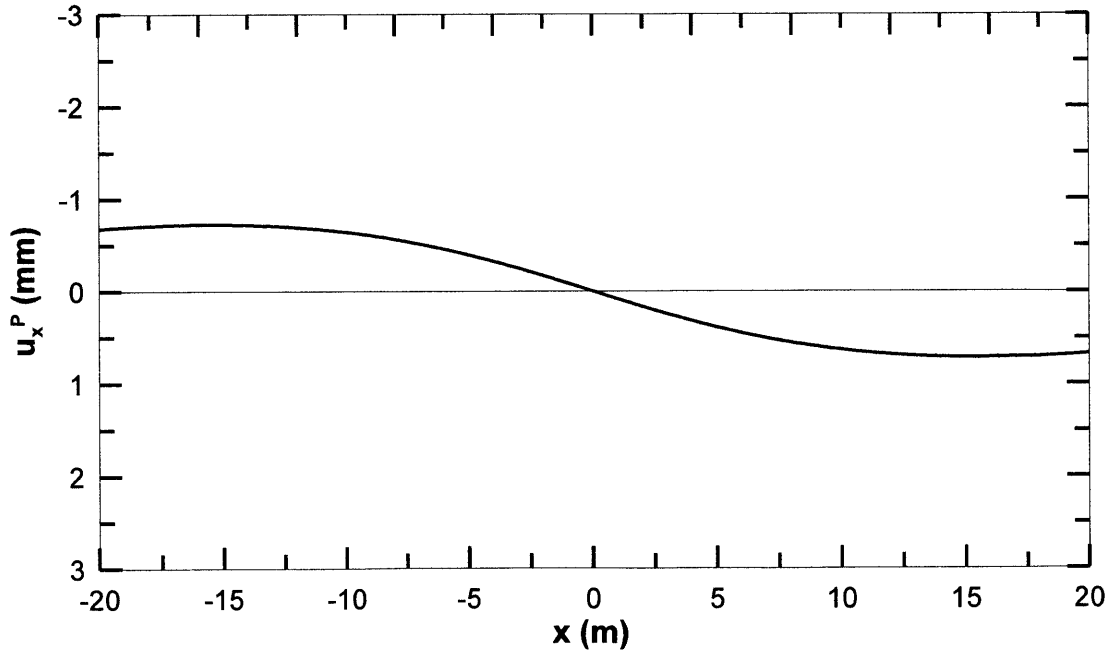

Figure 6-8: Analytically computed pipe axial displacements with the proposed method

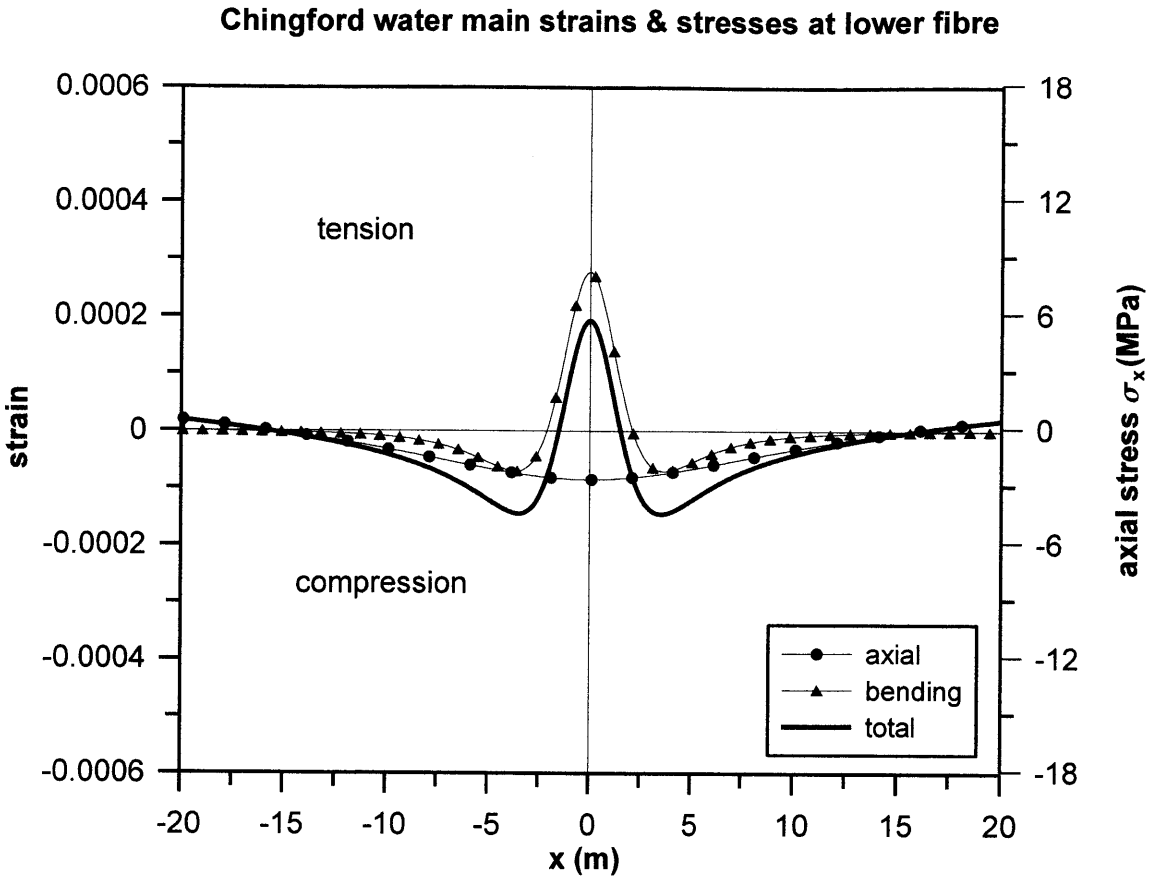

Figure 6-9: Axial and bending strains and stresses at lower fiber of Chingford water main

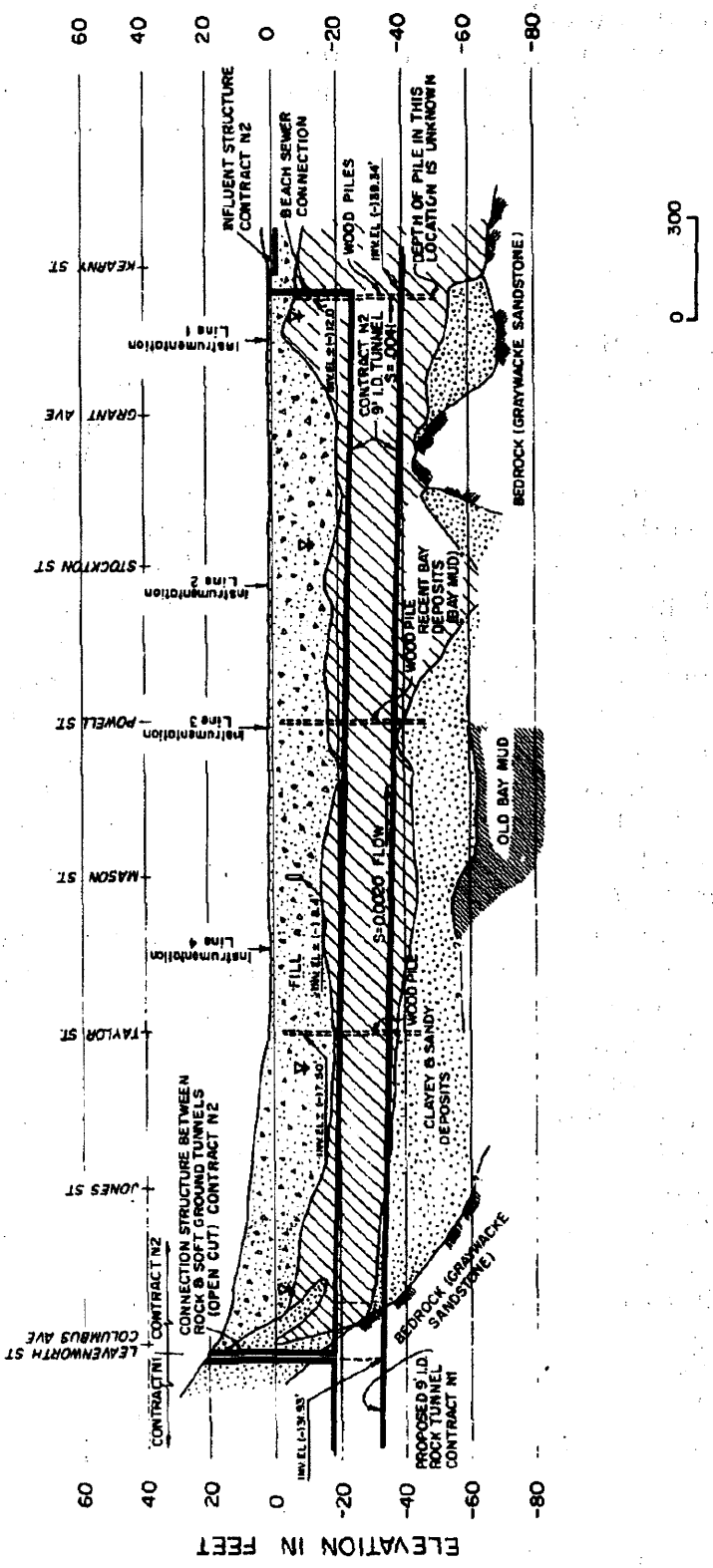

Figure 6-10: Generalized Subsurface Profile (1ft = 0.305 m)

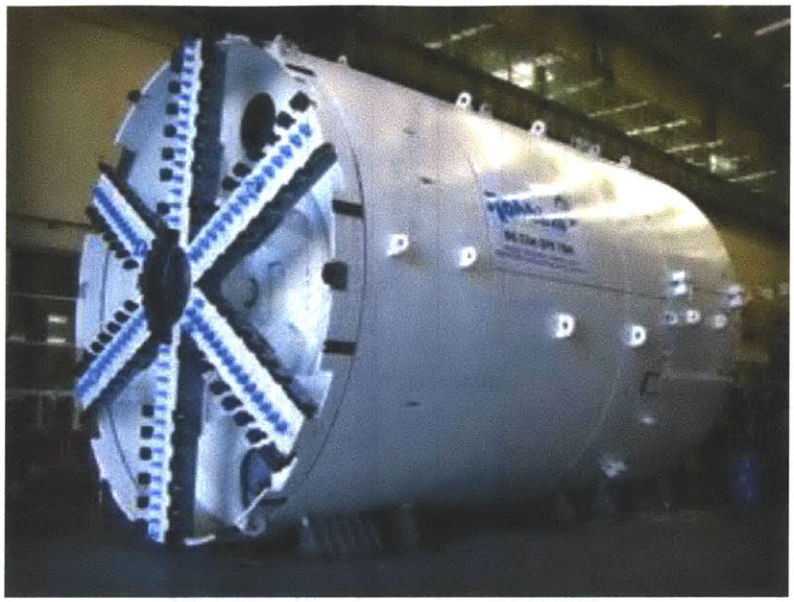

Figure 6-11: Typical front view of EPB shield

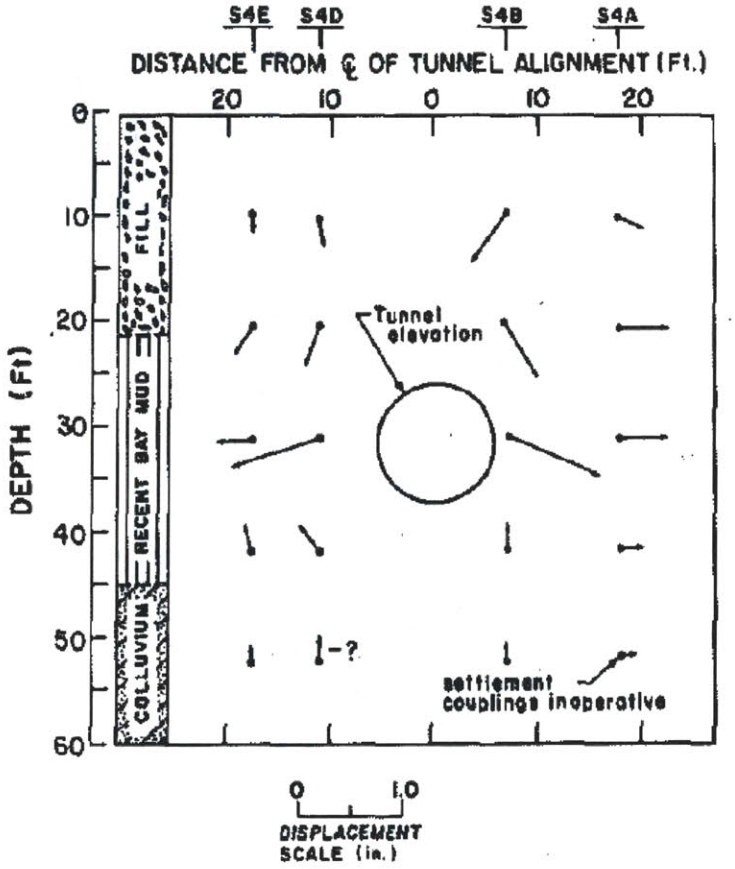

Figure 6-12: Line 4 vertical and lateral movement vectors, 15 days after shield passage

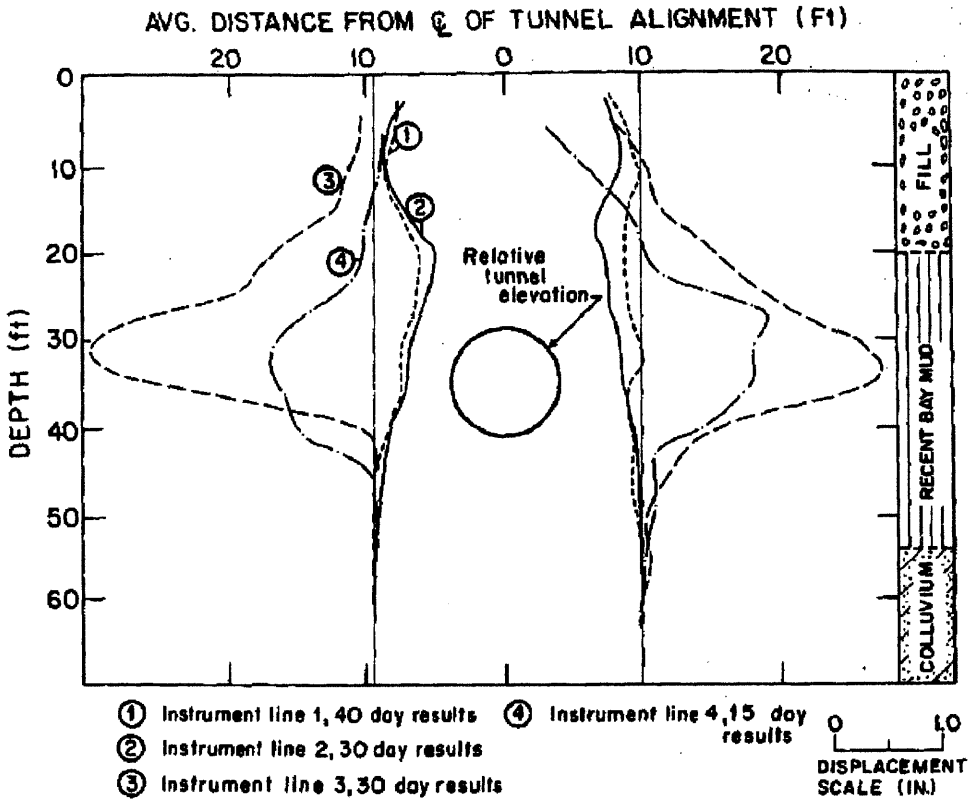

Figure 6-13: Long term lateral deflections at Line 1-4 (1ft = 0.305m and 1in=2.54cm)

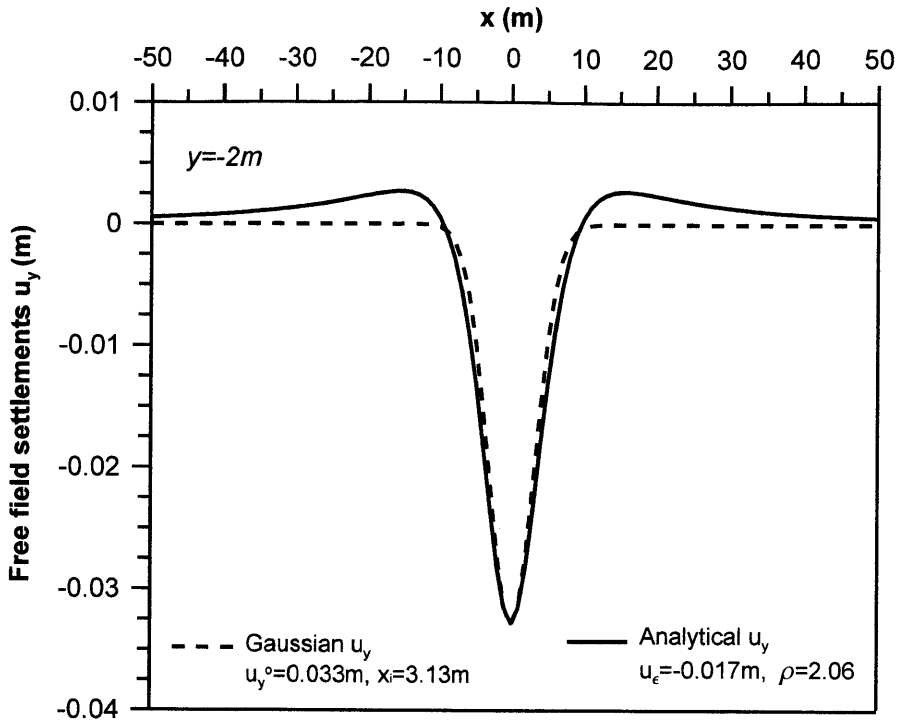

Figure 6-14: Subsurface (y=-2m) free-field settlements at Line 4

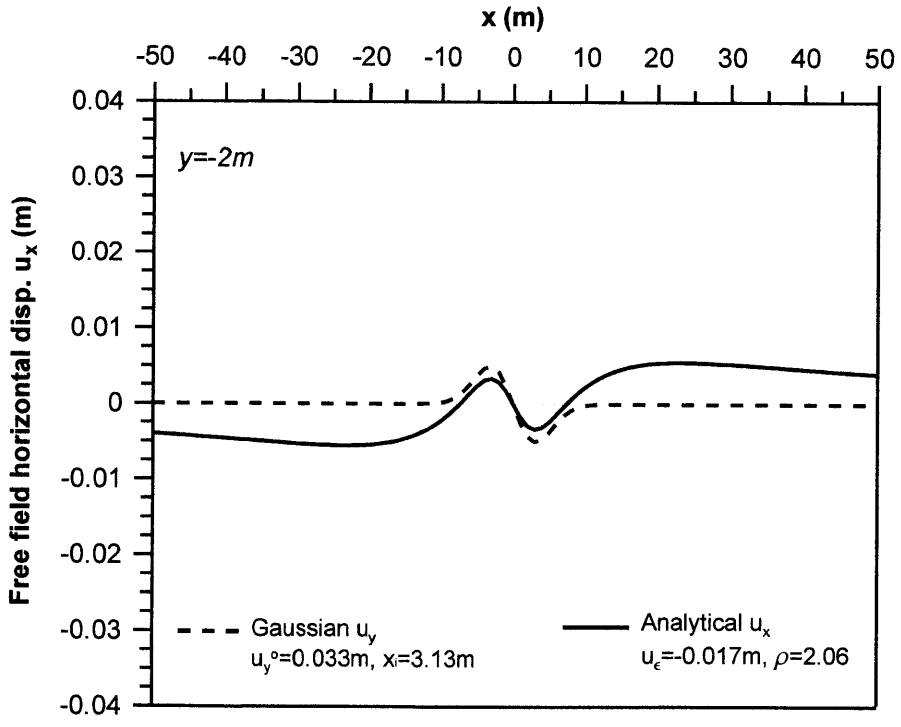

Figure 6-15: Subsurface (y=-2m) free-field horizontal displacements at Line 4

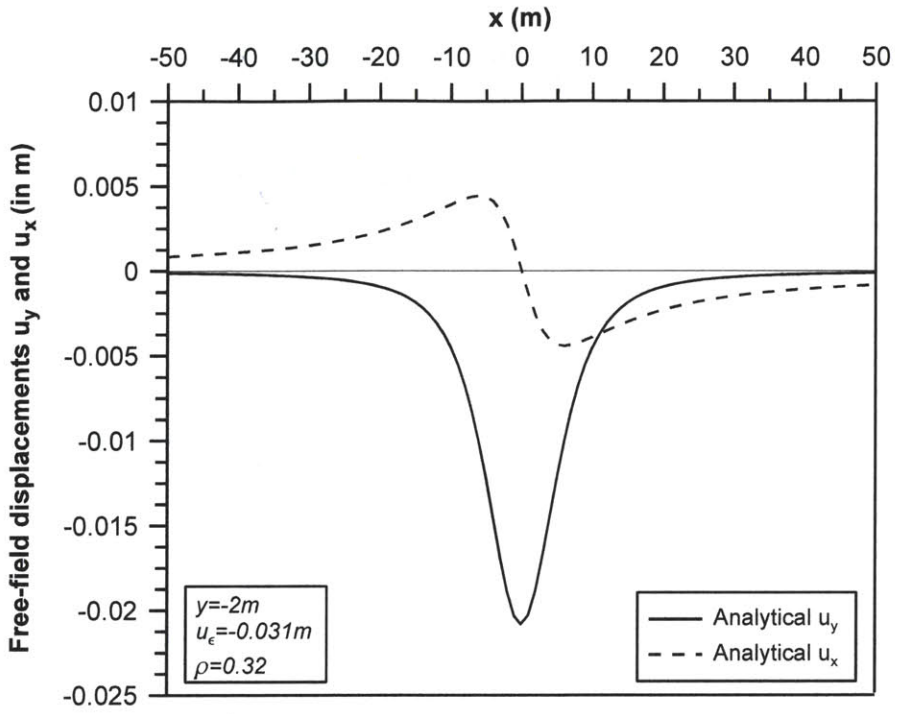

Figure 6-16: Subsurface (y=-2m) free-field horizontal and vertical movements at Line 2

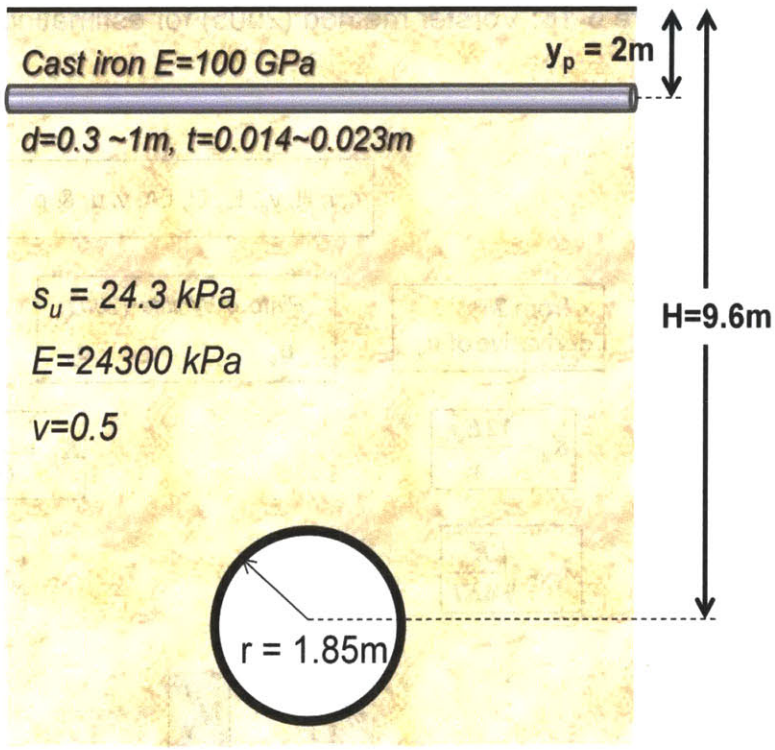

Figure 6-17: Model geometry and properties for N-2 San Francisco tunnel case

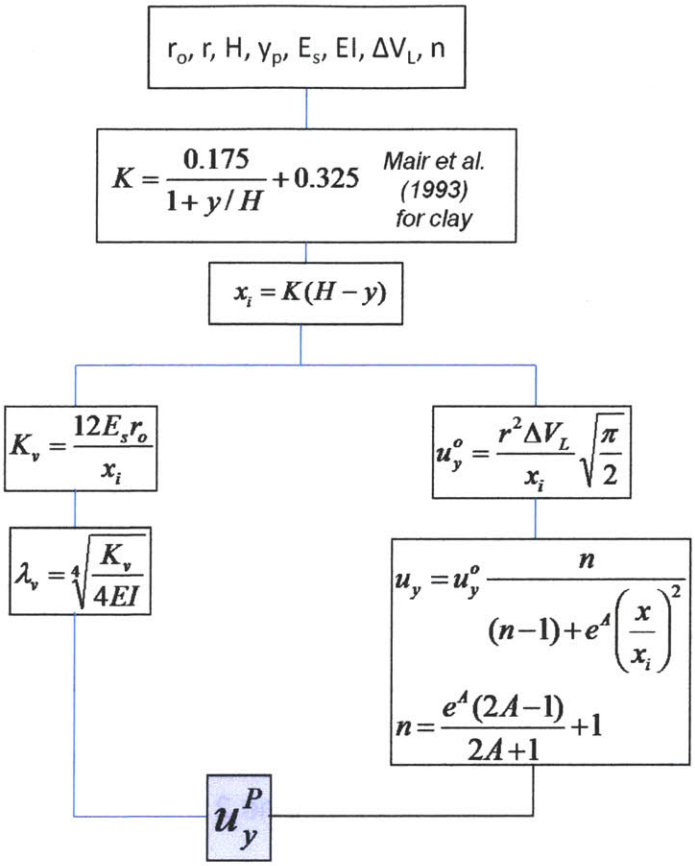

Figure 6-18: Vorster method (2005) for estimating pipe response u_y^P

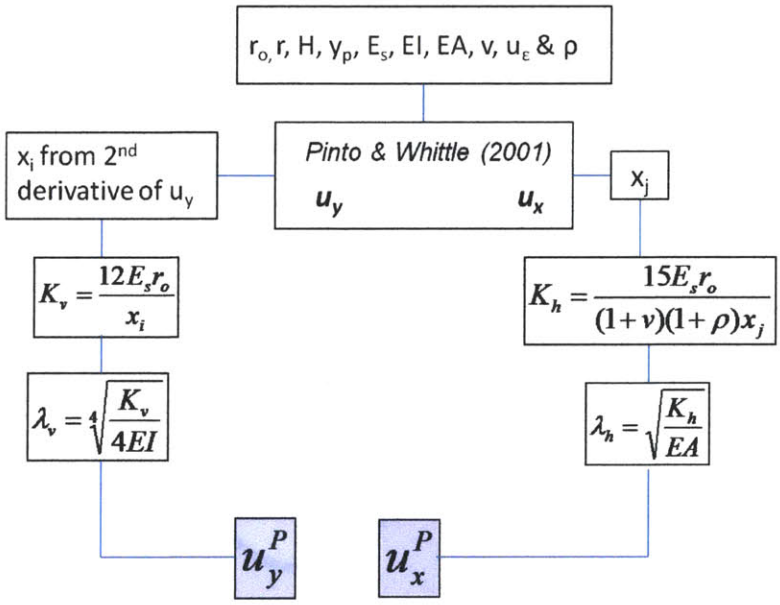

Figure 6-19: Proposed method for estimating pipe response

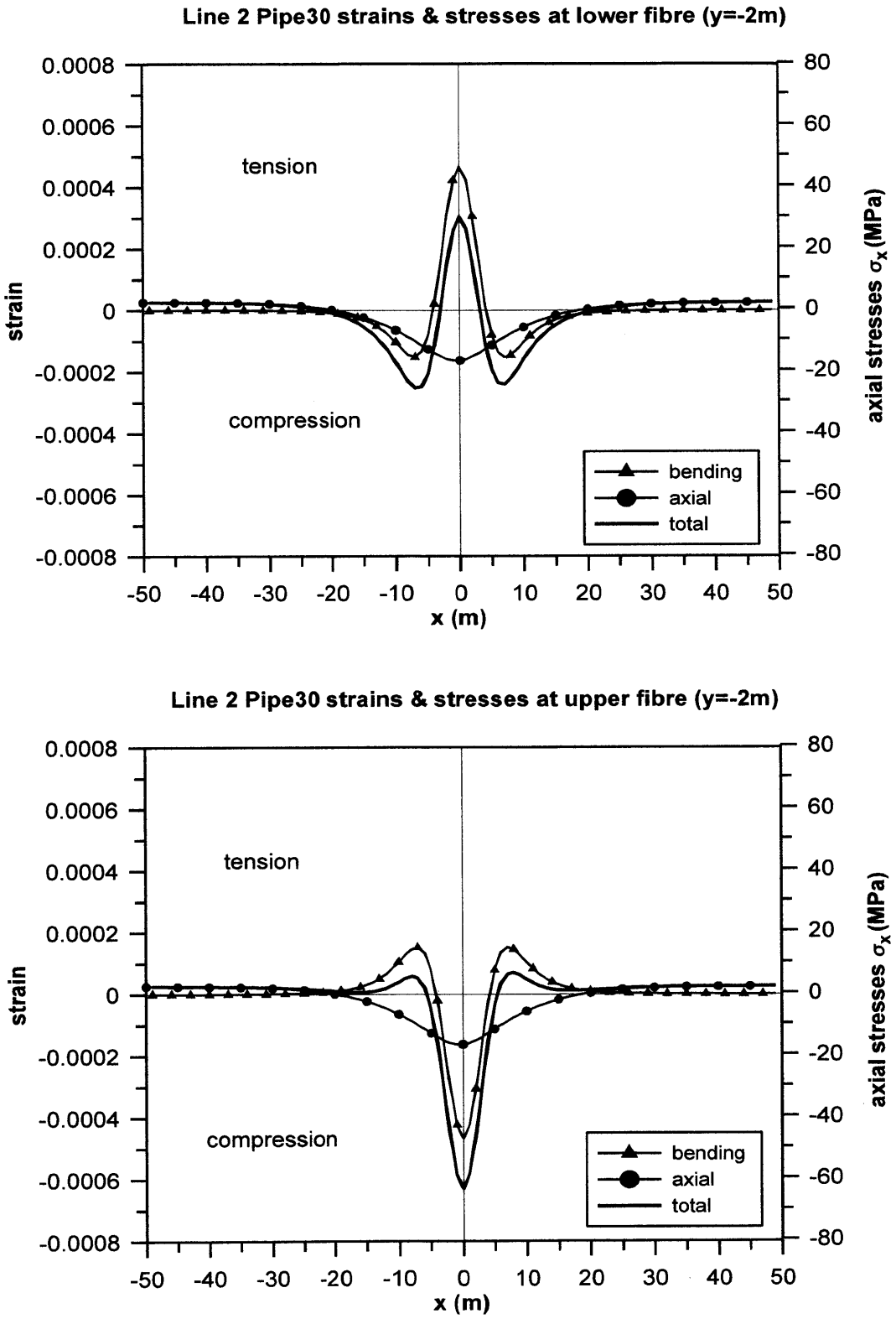

Figure 6-20: Strains and stresses of Pipe30 for soil movements at Line 2

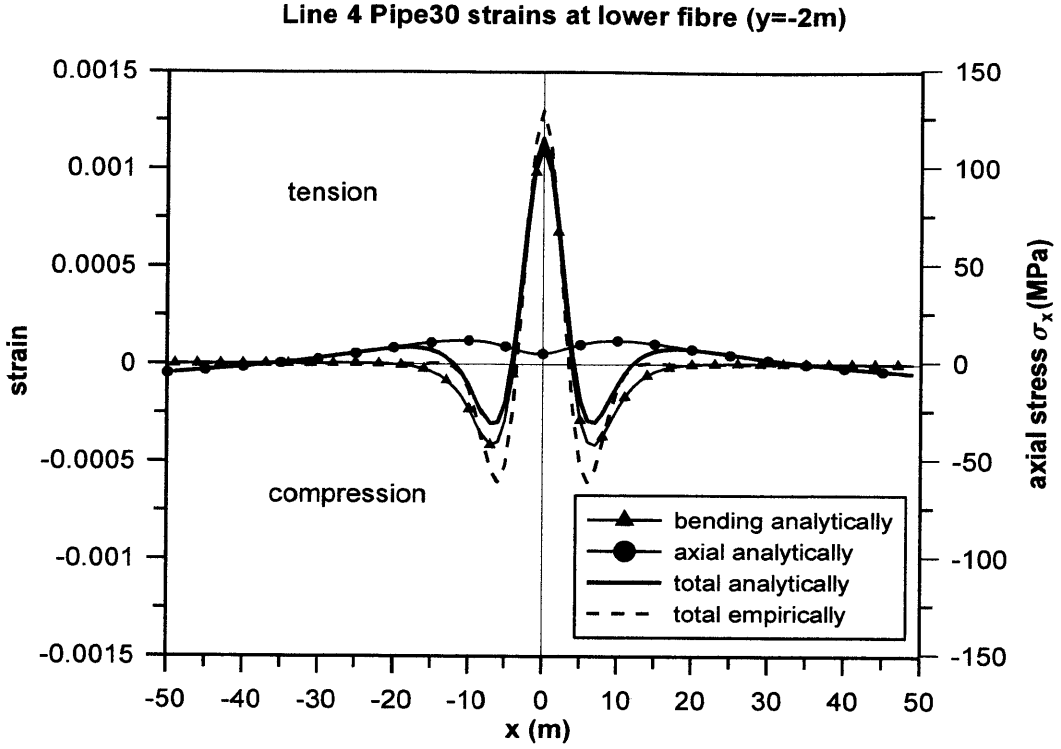

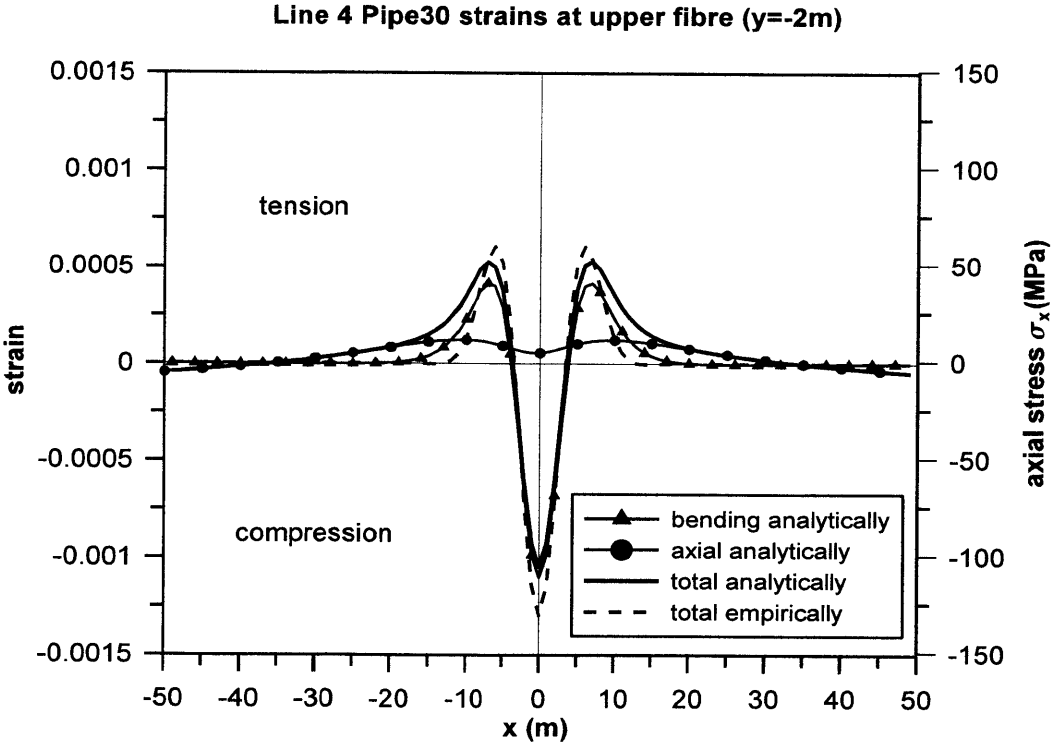

Figure 6-21: Strains and stresses of Pipe30 for soil movements at Line 4

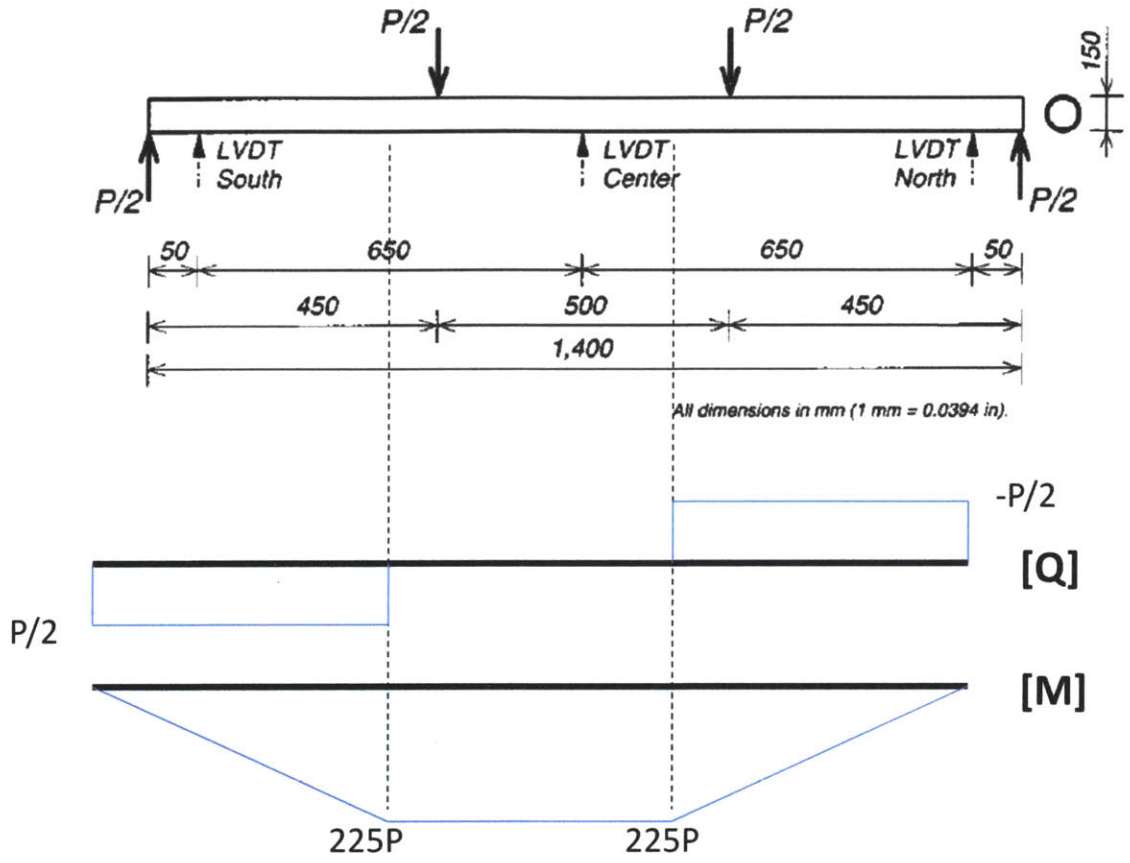

Figure 6-22: Typical four-point pipe bending load configuration with corresponding shear [Q] and moment [M] diagrams.

Face Pressure	Tensile Strength σ_t (MPa)	Pipe diameter (cm)							
		30	40	50	60	70	80	90	100
		Max tensile stress (MPa) analytically							
Low (Line 2)	47 (low)	30	27	26	24	22	20	19	18
	172 (mean)	30	27	26	24	22	20	19	18
High (Line 4)	47 (low)	125	107	100	92	87	70	76	69
	172 (mean)	125	107	100	92	87	70	76	69

Figure 6-23: Possibility of pipe tensile failure depending on the lowest or mean tensile strength value

CHAPTER 7

SUMMARY, CONCLUSIONS AND RECOMMENDATIONS

7.1 SUMMARY & CONCLUSIONS

The goal of the present research was to develop an analytical method for estimating the response of an existing continuous pipeline to ground deformations induced by tunnel construction. The pipeline is assumed to be aligned transverse to the direction of the tunnel, and is fully in contact with its surrounding homogeneous soil. The closed-from solutions for the free-field ground deformations are given from prior work of Pinto & Whittle (2001).

The method uses a conventional Winkler model to explain effects of ground deformations on bending and axial loading of pipelines. The Winkler spring coefficients are derived from matching the analytical results with results of linear elastic finite element analyses. The vertical spring coefficient K_v follows the results presented by Klar et al. (2005).

$$K_v = \frac{12E_s r_o}{x_i} \tag{7.1}$$

where x_i is the distance to the inflection point in the free-field settlement trough at the elevation of the pipe.

A new expression has been derived for the horizontal spring coefficient K_h.

$$K_h = \frac{15E_s r_o}{(1+v)(1+\rho)x_j} \tag{7.2}$$

where x_j is the lateral location of maximum free-field horizontal movements and ρ is the relative distortion that characterizes the field of ground movements.

The pipe deformations are solved numerically with Mathematica 7.0 and their results are presented in graphs for various input parameters and for different relative pipe – soil bending and axial rigidity factors R_b and R_a. The later are ratios of the pipe bending and axial stiffness respectively, over the soil stiffness and they show the rigidity or flexibility of the pipeline compared to its surrounding soil.

Following Vorster et al.(2005), the relative pipe-soil bending rigidity factor R_b is given by:

$$R_b = \frac{EI}{E_s r_o {x_i}^3} \tag{7.3}$$

The relative pipe-soil axial rigidity factor R_a is then obtained as follows:

$$R_a = \frac{EA}{E_s \pi r_o x_j} \tag{7.4}$$

Finite element simulations were conducted (using PLAIXS 2D) to verify the closed-form free-field ground displacements reported by Pinto and Whittle (2001). Simulations using PLAXIS 3D Tunnel were used to validate the suggested expressions for the vertical and horizontal spring coefficients K_v and K_h respectively.

Vertical and horizontal pipe displacements, bending moments and axial stresses and stresses are evaluated in order to predict whether a pipeline can fail due to tunnel- induced ground deformations.

The proposed method is illustrated for 2 cases: a) Chingford pipe-jacking case and b) N-2 San Francisco sewer tunnel case. In Chingford pipe-jacking tunnel case it is observed that the analytical solutions (Pinto & Whittle, 2001) can predict more accurately the free field settlements than empirical solutions. Regarding the pipeline response, application of the proposed method did not

give a remarkable result as the pipeline was very flexible relative to its surrounding soil and it simply followed the ground movements. In N-2 San Francisco sewer tunnel case the proposed method is applied on hypothetical continuous cast-iron pipelines that are buried at a depth of 2m. The specific case was selected because the EPB method was used for this tunnel project with a range of face pressures in the soft Bay Mud. The free-field ground movements were estimated for cases of low and high face pressure using the closed-form solutions of Pinto and Whittle (2001).

The results show that cast-iron pipelines are vulnerable to tensile failures due to EPB tunnel construction, especially for cases of high face pressure and for smaller diameter pipes.

7.2 RECOMMENDATIONS FOR FUTURE RESEARCH

The proposed methodology presented in the current study needs to be validated through well documented case studies. There are very limited data available in the current literature and from laboratory physical model tests. Further development of these analyses should include:

- Possible slippage between the pipe and the soil and possible separation (through finite element simulations).
- Investigation of the effects on jointed pipelines.
- Investigation of other sources of stress, including surcharge loads (vehicle loads), foundation excavations, changes of temperature, earthquakes and others.

REFERENCES

Attewell, P. B. (1978) "Ground movements caused by tunneling in soil", *Proc. International Conference on Lange Movements and Structures*, J.D. Geddes (Ed), Pentech Press, London, 812-948

Attewell, P. B. and Woodman, J. P. (1982) "Predicting the dynamics of ground settlement and its derivatives caused by tunneling in soil", *Ground Engineering*, 15(8), November 1982, 13-22, 36

Attewell, P. B., Yeates, J. and Selby, A. R. (1986) "Soil movements induced by tunneling and their effects on pipelines and structures", *Blackie and Son Ltd*, United Kingdom

Broms, B. B. and Brennermark, H. (1967) "Stability of clay at vertical openings", *Journal of the Soil Mechanics and Foundation Engineering Division*, ASCE, SM1 (93), 71-94

Caproco Corrosion Prevention Ltd. (1985) "Underground corrosion of water pipes in Canadian cities; Case: the city of Calgary"", *Report prepared for CANMET*, Ottawa

Celestino, T. B., Gomes, R. A. M., and Bortolucci, A. A. (2000) "Errors in ground distortions due to settlement trough adjustment", *Tunneling and Underground Space Technology*, 15(1), 97-100

Chatzigiannelis, Y. and Whittle, A. J. (2001) "Analysis of ground deformations caused by shallow tunneling in cross-anisotropic soil", *submitted for publication*

Clough, G. W., Sweeny, B. P. and Finno, R. J. (1983) "Measured soil response to EPB shield tunneling", *J. of Geotechnical Engineering*, ASCE 109(2), February, 131-149

Clough, G. W. and Leca, E. (1989) "With focus on use of finite-element methods for soft ground tunneling", *Review Paper in Tunnels et Micro-Tunnes en Terrain Meuble-du Chantier a la Theorie*, Presse de l'Ecole National des Ponts et Chaussees, Paris, 531-573

Conlin, R. M. and Baker, T. J. (1991) "Application of fracture mechanics to the failure behavior of buried cast-iron mains", *Contract Report No. 266*, Transport and Road Research Laboratory, London

Cording, E. J. and Hansmire, W. H. (1975) "Displacement around soft ground tunnels – General report", *Proc. 5th Pan-American Conference on Soil Mechanics and Foundation Engineering*, Buenos Aires, Session IV, 571-632

Fujita, K. (1994) "Soft ground tunneling and buried structures", *Proc. 13th International Conference on Soil Mechanics and Foundation Engineering*, New Dehli, India, 89-108

Hetenyi, M. (1946) "Beams on Elastic Foundation", University of Michigan Press, Ann Arbor

Jacobsz, S. W. (2002) "The effects of tunneling on piled foundation", *PhD Thesis*, Cambridge University

Kimura, T. and Mair, R. J. (1981) "Centrifugal testing of model tunnels in clay", *Proc. 10th International Conference on Soil Mechanics and Foundation Engineering*, Stockholm, Balkema, Vol 1, 319-322

Klar, A., Vorster, T. E. B., Soga, K. and Mair, R. J. (2005) "Soil-pipe interactiondue to tunneling: comparison between Winkler and elastic continuum solutions", *Geotechnique*, 55 (6), 461-466

Lee, K. M. and Rowe, R. K. (1989) "Deformations caused by surface loading and tunneling: the role of elastic anisotropy", *Geotechnique*, 39 (1), 125-140

Loganathan, N. and Poulos, H. G. (1998) "Analytical predictions for tunneling induced ground movements in clays", *J. of Geotechnical and Geo-Environmental Engineering*, ASCE, 124 (9), 846-856

Lueprasert, P., Suwansawat, S. and Jongpradist, P. (2009) "3D FEA of NATM excavation for Bangkok MRT Blue Line South extension" *review for publication*

Ma, Z. and Yamada, K. (1994) "Durability evaluation of cast-iron water supply pipes by sampling tests", *Proc. Structural Engineering*, Japan, Society of Civil Engineers, Tokyo, 40A

Macklin, S. R. (1999) "The prediction of volume loss due to tunneling in overconsolidated clay based on heading geometry and stability number", *Ground Engineering,* April UK

Mair, R. J. (1979) "Centrifuge modeling of tunnel construction in soft clay", *PhD Thesis*, Cambridge University

Mair, R. J., Taylor, R. N. and Bracegirdle, A. (1993) "Subsurface settlement profiles above tunnels in clay", *Geotechnique*, 43 (2), 315-320

Mair, R. J. and Taylor, R. N. (1997) "Theme Lecture: Board tunneling in the urban environment", *Proc. 14th International Conference on Soil Mechanics and Foundation Engineering*, Hamburg, Balkema, 2353-2385

Mair, R. J., Gunn, M. J. and O'Reilly, M.P. (1981) "Centrifuge testing of model tunnels in soft clay", *Proc. 10th International Conference on Soil Mechanics and Foundation Engineering*, Stockholm, Balkema, Vol 1, 323-328

Makar, M. and Rajani, B. (2000) "Gray cast-iron water pipe metallurgy", *J. of Material in Civil Engineering*, ASCE, 12 (3), 245-253

Marinos, P. G. (1998) "TBM excavation in weak and heterogeneous rock masses for the Athens metro", *Proc. 8th International Congress of IAEG,* Balkema publ., 3513-3522, Vancouver, Canada

Moeller, S. (2006) "Tunnel induce settlements and structural forces in linings", *PhD Thesis,* Institute fur Geotechnik der Universitat Stuttgard

New, B. M., and O'Reilly, M. P. (1991) "Tunneling induced ground movements: predicting their magnitudes and effects", *Proc. 4th International Conference on Ground Movements and Structures*, Cardiff, Pentech Press, 671-697

O'Reilly, M. P. and New, B. M. (1982) "Settlement above tunnels in the United Kingdom – their magnitude and prediction", *Tunneling '82*, London IMM, 173-181

O'Reilly, M. P. and Trautmann, C.H. (1982) "Buried pipeline response to tunnel ground movements", *Europipe '82 Conference*, Basel, Switzerland, 9-15

Peck, R. B. (1969) "Deep excavations and tunneling in soft ground", *Proc. 7th International Conference on Soil Mechanics and Foundation Engineering*, Mexico City, State of the Art Volume, 225-290

Pinto, F. (1999) "Analytical methods to interpret ground deformations due to soft ground tunneling", *SM Thesis*, Dept. of Civil & Environmental Engineering, MIT, Cambridge, MA

Pinto, F. and Whittle, A. J. (2001) "Ground movements due to shallow tunnels in soft ground: 1. Analytical solutions", *submitted for publication*

Pinto, F., Zymnis, D. M. and Whittle, A. J. (2011) "Ground movements due to shallow tunnels in soft ground: 2. Analytical interpretations and predictions", *submitted for publication*

Rajani, B. et al. (2000) "Investigation of gray cast-iron water mains to develop a methodology for estimating service life", *Report No. 280,* American Water Works Association Research Foundation, Denver

Rowe, R. K. and Kach, G. J. (1983) "A theoretical examination of the settlements induced by tunneling: Four case histories", *Canadian Geotechnical Journal,* 20, 299-314

Rumsey, P. B. and Cooper, I. (1982) "Ground movements associated with trench excavation and their effect on adjacent services", *Ground Engineering,* 15 (2), 28-30

Sagaseta, C. (1987) "Analysis of undrained soil deformation due to ground loss", *Geotechnique*, 37 (3), 301-320

Scarpelli, G., Sakellariadi, E. and Furlani, G. (2003) "Evaluation of soil-pipeline longitudinal interaction forces", *Rivista Italiana Di Geotecnica*, 4, Patron Editore, Italy, 24-41

Schmidt, B. (1969) "Settlement and ground movement associated with tunneling in soils", *PhD Thesis*, University of Illinois, Urbana

Scott, M. V. and Packer, J. A. (2004) "Settlement and ground movement associated with tunneling in soils", *J. of Material in Civil Engineering*, ASCE, 16 (1), 69-77

Seica, R. F. (1981) "Foundation analysis", New Jersey, Prentice-Hall

Tagaki, N., Sgimamura, K. and Nishio, N. (1984) "Buried pipe response to adjacent ground movements associated with tunneling and excavations", *Proc. 3th International Conference on Ground Movements and Structures*, University of Wales, Institute of Science and Technology, Cardiff, 97-112

Taylor, R. N. (1995) "Tunneling in soft ground in the UK", *Underground Construction in Soft Ground*, K. Fujita and O. Kusakabe (eds.), Balkema, 123-126

Verruijt, A. and Booker, J. R. (1996) "Surface settlement due to deformation of a tunnel in an elastic half-space", *Geotechnique*, 36 (4), 753-756

Verruijt, A. (1997) "A complex variation solution for a deforming tunnel in an elastic half-plane", *International Journal for Numerical and Analytical Methods in Geomechanics*, 21, 77-79

Vesic, A. B. (1961) "Bending of beams resting on isotropic elastic solids", *J. of Engineering Mechanics Division*, ASCE, 87, 35-53

Vorster, T. E. B. (2005) "The effects of tunneling on buried pipes", *PhD Thesis*, University of Cambridge

Vorster, T. E. B., Klar, A., Soga, K. and Mair, R. J. (2005) "Estimating the effects of tunneling on existing pipelines", *J. of Geotechnical and Geo-Environmental Engineering*, ASCE, 131 (11)

Whittle, A. J. and Sagaseta, C. (2003) "Analyzing the effects of gaining and losing ground", *Soil Behavior and Soft Ground Construction*, ASCE, 119, 255-291

Yamamoto, K., Mizoguti, S., and Yoshimitsu, K. (1983) "Relation between graphitic corrosion and strength degradation of cast-iron pipe", *Corrosion Engineering*, 32 (2), 157

Yeates, J. (1984) "The response of buried pipeline to ground movements caused by tunneling in soil", *Proc. 3th International Conference on Ground Movements and Structures*, University of Wales, Institute of Science and Technology, Cardiff, 129-144

Zymnis, D. M. (2009) "Evaluation of analytical methods to interpret ground deformations due to soft ground tunneling", *SM Thesis*, Dept. of Civil & Environmental Engineering, MIT, Cambridge, MA

APPENDIX I

- Settlement and bending moment at a certain point on the pipe, assuming that the free-field settlements are described by:
  a) A modified Gaussian curve (Vorster et al., 2005)
  b) Pinto & Whittle (2001) analytical closed-form solutions

- Horizontal displacements at a certain point on the pipe, assuming that the free-field lateral displacements are described by:
  a) Empirical method using modified Gaussian curve for describing u_y (Vortser, 2005)
  b) Pinto & Whittle (2001) analytical closed-form solutions

- Mathematica scripts for normalized pipe settlements, bending moments and axial displacements using Pinto & Whittle (2001) for the free-field movements

- Relationship between x_i and x_j with relative distortion,ρ and embedment depth ratio, y/H

- **Settlements and bending moments**

Application of Modified Gaussian Curve (Vorster et al., 2005)

$$u_y{}^P = u_y{}^o \frac{\lambda_v}{2} \cdot \left\{ \int_0^b \left(\frac{n}{(n-1) + \mathrm{e}^{A\left(\frac{\frac{a-b}{2}+x}{x_i}\right)^2}} \cdot e^{-\lambda_v x}(cos\lambda_v x + sin\lambda_v x) \right) dx \right.$$

$$\left. + \int_0^a \left(\frac{n}{(n-1) + \mathrm{e}^{A\left(\frac{\frac{a-b}{2}-x}{x_i}\right)^2}} \cdot e^{-\lambda_v x}(cos\lambda_v x + sin\lambda_v x) \right) dx \right\}$$

$$M = u_y{}^o \frac{K_v}{4\lambda_v} \cdot \left\{ \int_0^b \left(\frac{n}{(n-1) + \mathrm{e}^{A\left(\frac{\frac{a-b}{2}+x}{x_i}\right)^2}} \cdot e^{-\lambda_v x}(cos\lambda_v x + sin\lambda_v x) \right) dx \right.$$

$$\left. + \int_0^a \left(\frac{n}{(n-1) + \mathrm{e}^{A\left(\frac{\frac{a-b}{2}-x}{x_i}\right)^2}} \cdot e^{-\lambda_v x}(cos\lambda_v x + sin\lambda_v x) \right) dx \right\}$$

Application of Pinto & Whittle (2001) Closed-Form Solutions

$$u_y{}^P = \frac{\lambda_v}{2} \cdot \left[\int_0^b \left(f\left(\frac{a-b}{2} + x\right) \cdot e^{-\lambda_v x} (cos\lambda_v x + sin\lambda_v x) \right) dx \right.$$

$$\left. + \int_0^a \left(f\left(\frac{a-b}{2} - x\right) \cdot e^{-\lambda_v x} (cos\lambda_v x + sin\lambda_v x) \right) dx \right]$$

$$M = \frac{K_v}{4\lambda_v} \cdot \left[\int_0^b \left(f\left(\frac{a-b}{2} + x\right) \cdot e^{-\lambda_v x} (cos\lambda_v x + sin\lambda_v x) \right) dx \right.$$

$$\left. + \int_0^a \left(f\left(\frac{a-b}{2} - x\right) \cdot e^{-\lambda_v x} (cos\lambda_v x + sin\lambda_v x) \right) dx \right]$$

with:

$$f(x) = u_\varepsilon r \left\{ \begin{array}{c} \frac{(y+H)}{(\mathrm{x})^2 + (y+H)^2} - \frac{(y-H)}{(\mathrm{x})^2 + (y-H)^2} + \cdots \\ + \frac{4(y-H)(\mathrm{x})^2 + 2H[(\mathrm{x})^2 - (y-H)^2]}{[(\mathrm{x})^2 + (y+H)^2]^2} - \frac{4(1-v)(y-H)}{(\mathrm{x})^2 + (y-H)^2} \end{array} \right\} + \cdots$$

$$+u_\delta \frac{r}{3-4v} \left\{ \begin{array}{c} \frac{(y-H)\left\{(3-4v)\left[(\mathrm{x})^2+(y-H)^2\right]^2 - \left[3(\mathrm{x})^2-(y-H)^2\right]\left[(\mathrm{x})^2+(y-H)^2-r^2\right]\right\}}{\left[(\mathrm{x})^2+(y-H)^2\right]^3} - \cdots \\ - \frac{(y+H)\left\{(3-4v)\left[(\mathrm{x})^2+(y+H)^2\right]^2 - \left[3(\mathrm{x})^2-(y+H)^2\right]\left[(\mathrm{x})^2+(y+H)^2-r^2\right]\right\}}{\left[(\mathrm{x})^2+(y+H)^2\right]^3} + \\ \cdots + \frac{8(1-v)\cdot\left\{(\mathrm{x})^2(2H-y) - y(y-H)^2\right\}}{\left[(\mathrm{x})^2+(y-H)^2\right]^2} - \\ \cdots - \frac{8(y-H)\left\{Hy(y-H)^2 - (\mathrm{x})^2\cdot\left[\left((\mathrm{x})^2+y^2\right)+H(y+H)\right]\right\}}{\left[(\mathrm{x})^2+(y-H)^2\right]^3} \end{array} \right\}$$

- **Horizontal displacements**

Application of Empirical Method Using Modified Gaussian Curve for Describing u_y (Vorster, 2005)

$$u_x{}^P = u_y{}^o \frac{\lambda_h}{2} \cdot \left\{ \int_0^b \frac{\frac{a-b}{2} + \mathrm{x}}{\left(1+\frac{d}{c}\right)H - y} \cdot \frac{n}{(n-1) + \mathrm{e}^{\mathrm{A}\left(\frac{\frac{a-b}{2}+\mathrm{x}}{\mathrm{x_i}}\right)^2}} \cdot e^{-\lambda_h x} dx + \int_0^a \frac{\frac{a-b}{2} - \mathrm{x}}{\left(1+\frac{d}{c}\right)H - y} \cdot \frac{n}{(n-1) + \mathrm{e}^{\mathrm{A}\left(\frac{\frac{a-b}{2}-\mathrm{x}}{\mathrm{x_i}}\right)^2}} \cdot e^{-\lambda_h x} dx \right\}$$

Application of Pinto & Whittle (2001) Closed-Form Solutions

$$u_x{}^P = \frac{\lambda_h}{2} \cdot \left[\int_0^b \left(g\left(\frac{a-b}{2} + x\right) \cdot e^{-\lambda_h x} \right) dx + \int_0^a \left(g\left(\frac{a-b}{2} - x\right) \cdot e^{-\lambda_h x} \right) dx \right]$$

with:

$$g(x) = u_\varepsilon xr \left\{ \frac{1}{x^2 + (y+H)^2} - \frac{1}{x^2 + (y-H)^2} + \frac{4(1-v)}{x^2 + (y-H)^2} - \cdots - \frac{4(y-H)y}{[x^2 + (y+H)^2]^2} \right\} + \cdots$$

$$+u_\delta \frac{xr}{3-4v} \left\{ \frac{(3-4v)[x^2 + (y+H)^2]^2 - [3(y+H)^2 - x^2][x^2 + (y+H)^2 - r^2]}{[x^2 + (y+H)^2]^3} - \cdots - \frac{(3-4v)[x^2 + (y-H)^2]^2 - [3(y-H)^2 - x^2][x^2 + (y-H)^2 - r^2]}{[x^2 + (y-H)^2]^3} + \cdots + \frac{8(1-v)\cdot(x^2 + y^2 - r^2)}{[x^2 + (y-H)^2]^2} - \frac{8y[y(x^2+y^2) + 2H(H^2 - x^2) - 3yH^2]}{[x^2 + (y-H)^2]^3} \right\}$$

- **Mathematica scripts**

```
(* Normalized free-field and pipe settlements and bending moments *)

(* General Parameters *)
r=0.25
y=-0.5
v=0.5
p=3
H=10

(* Free-field solution *)
Sv[x_]:=((((y+1)*r/((x^2+(y+1)^2)))+p*(r/(3-4*v))*(y+1)*((3-4*v)*((x^2+(y+1)^2)^2)-
((3*x^2-(y+1)^2)*(x^2+(y+1)^2-r^2)))/((x^2+(y+1)^2)^3))-(((y-1)*r/((x^2+(y-
1)^2)))+p*(r/(3-4*v))*(y-1)*((3-4*v)*((x^2+(y-1)^2)^2)-((3*x^2-(y-1)^2)*(x^2+(y-1)^2-
r^2)))/((x^2+(y-1)^2)^3))+2*r*(((2*(y-1)*(x^2)+1*(x^2-(y-1)^2))/((x^2+(y-1)^2)^2))-(2*(1-
v)*(y-1)/(x^2+(y-1)^2)))-(8*p*r/(3-4*v))*((((1-v)*x^2*(2*1-y)-y*(y-1)^2)/((x^2+(y-1)^2)^2))-
(((y-1)*(1*y*(y-1)^2-(x^2)*((x^2+y^2)+1*(y+1))))/((x^2+(y-1)^2)^3))))

Plot [Sv[x],{x,-5,5}]
FindMaximum[Sv[x],x]
{3.94444,{x->1.01425*10^-14}}
Export ["name.dat", Table[Sv[x],{x,-5,5,0.02}]]

(*Find the inflection point It=xi/H*)
Solve[D[D[(((y+1)*r/((x^2+(y+1)^2)))+p*(r/(3-4*v))*(y+1)*((3-4*v)*((x^2+(y+1)^2)^2)-
((3*x^2-(y+1)^2)*(x^2+(y+1)^2-r^2)))/((x^2+(y+1)^2)^3))-(((y-1)*r/((x^2+(y-
1)^2)))+p*(r/(3-4*v))*(y-1)*((3-4*v)*((x^2+(y-1)^2)^2)-((3*x^2-(y-1)^2)*(x^2+(y-1)^2-
r^2)))/((x^2+(y-1)^2)^3))+2*r*(((2*(y-1)*(x^2)+1*(x^2-(y-1)^2))/((x^2+(y-1)^2)^2))-(2*(1-
v)*(y-1)/(x^2+(y-1)^2)))-(8*p*r/(3-4*v))*((((1-v)*x^2*(2*1-y)-y*(y-1)^2)/((x^2+(y-1)^2)^2))-
(((y-1)*(1*y*(y-1)^2-(x^2)*((x^2+y^2)+1*(y+1))))/((x^2+(y-1)^2)^3))),x],x]==0,x]
```

```
(* For Rb=EI/Es*ro*xi^3 *)
R=8
It=0.24047319446299206  (*It=xi/H*)
L=(1/It)*((3/R)^(1/4))

(* Vertical normalized pipe displacements uyp/uyo, x is normalised vs H*)
Do[Export["uyp_R_8.dat",Table[(((L/2)*(NIntegrate[((((y+1)*r/(((a-
6+x)^2+(y+1)^2)))+p*(r/(3-4*v))*(y+1)*((3-4*v)*(((a-6+x)^2+(y+1)^2)^2)-((3*(a-6+x)^2-
(y+1)^2)*((a-6+x)^2+(y+1)^2-r^2)))/(((a-6+x)^2+(y+1)^2)^3))-(((y-1)*r/(((a-6+x)^2+(y-
1)^2)))+p*(r/(3-4*v))*(y-1)*((3-4*v)*(((a-6+x)^2+(y-1)^2)^2)-((3*(a-6+x)^2-(y-1)^2)*((a-
6+x)^2+(y-1)^2-r^2)))/(((a-6+x)^2+(y-1)^2)^3))+2*r*(((2*(y-1)*((a-6+x)^2)+1*((a-6+x)^2-
(y-1)^2))/(((a-6+x)^2+(y-1)^2)^2))-(2*(1-v)*(y-1)/((a-6+x)^2+(y-1)^2)))-(8*p*r/(3-
4*v))*((((1-v)*(a-6+x)^2*(2*1-y)-y*(y-1)^2)/(((a-6+x)^2+(y-1)^2)^2))-(((y-1)*(1*y*(y-1)^2-
((a-6+x)^2)*(((a-6+x)^2+y^2)+1*(y+1))))/(((a-6+x)^2+(y-1)^2)^3))))
*Exp[-L*x]*(Cos[L*x]+Sin[L*x]),{x,0,12-a}]+NIntegrate[((((y+1)*r/(((a-6-
x)^2+(y+1)^2)))+p*(r/(3-4*v))*(y+1)*((3-4*v)*(((a-6-x)^2+(y+1)^2)^2)-((3*(a-6-x)^2-
(y+1)^2)*((a-6-x)^2+(y+1)^2-r^2)))/(((a-6-x)^2+(y+1)^2)^3))-(((y-1)*r/(((a-6-x)^2+(y-
1)^2)))+p*(r/(3-4*v))*(y-1)*((3-4*v)*(((a-6-x)^2+(y-1)^2)^2)-((3*(a-6-x)^2-(y-1)^2)*((a-6-
x)^2+(y-1)^2-r^2)))/(((a-6-x)^2+(y-1)^2)^3))+2*r*(((2*(y-1)*((a-6-x)^2)+1*((a-6-x)^2-(y-
1)^2))/(((a-6-x)^2+(y-1)^2)^2))-(2*(1-v)*(y-1)/((a-6-x)^2+(y-1)^2)))-(8*p*r/(3-4*v))*((((1-
v)*(a-6-x)^2*(2*1-y)-y*(y-1)^2)/(((a-6-x)^2+(y-1)^2)^2))-(((y-1)*(1*y*(y-1)^2-((a-6-
x)^2)*(((a-6-x)^2+y^2)+1*(y+1))))/(((a-6-x)^2+(y-1)^2)^3))))*Exp[-
L*x]*(Cos[L*x]+Sin[L*x]),{x,0,a}])))/3.944444444444444,{a,0,6,0.02}]],{a,0,6,0.02}]


(* Free-field moments Mn (Mn=M*H^2/EI*uyo), x is normalised vs H*)
D[D[(((y+1)*r/((x^2+(y+1)^2)))+p*(r/(3-4*v))*(y+1)*((3-4*v)*((x^2+(y+1)^2)^2)-((3*x^2-
(y+1)^2)*(x^2+(y+1)^2-r^2)))/((x^2+(y+1)^2)^3))-(((y-1)*r/((x^2+(y-1)^2)))+p*(r/(3-
4*v))*(y-1)*((3-4*v)*((x^2+(y-1)^2)^2)-((3*x^2-(y-1)^2)*(x^2+(y-1)^2-r^2)))/((x^2+(y-
1)^2)^3))+2*r*(((2*(y-1)*(x^2)+1*(x^2-(y-1)^2))/((x^2+(y-1)^2)^2))-(2*(1-v)*(y-1)/(x^2+(y-
1)^2)))-(8*p*r/(3-4*v))*((((1-v)*x^2*(2*1-y)-y*(y-1)^2)/((x^2+(y-1)^2)^2))-(((y-1)*(1*y*(y-
1)^2-(x^2)*((x^2+y^2)+1*(y+1))))/((x^2+(y-1)^2)^3))),x],x]
Mn[x_]:=-((1.`  x^2)/(0.25`+x^2)^3-0.25`/(0.25`+x^2)^2+(3.`  x^2)/(2.25`+x^2)^3-
0.75`/(2.25`+x^2)^2+0.5`  ((24  x^2  (-2.25`-2.`  x^2))/(2.25`+x^2)^4+(44.`
```

```
x^2)/(2.25`+x^2)^3-(4 (-2.25`-2.` x^2))/(2.25`+x^2)^3-7.`/(2.25`+x^2)^2)+(1.125` (-16.`
x^2-6 (2.1875`+x^2)+4.` (2.25`+x^2)-2 (-2.25`+3 x^2)))/(2.25`+x^2)^3-(13.5` x (-6 x
(2.1875`+x^2)+4.` x (2.25`+x^2)-2 x (-2.25`+3 x^2)))/(2.25`+x^2)^4+(54.` x^2 (1.`
(2.25`+x^2)^2-(2.1875`+x^2) (-2.25`+3 x^2)))/(2.25`+x^2)^5-(6.75` (1.` (2.25`+x^2)^2-
(2.1875`+x^2) (-2.25`+3 x^2)))/(2.25`+x^2)^4+(0.375` (-16.` x^2-6 (0.1875`+x^2)+4.`
(0.25`+x^2)-2 (-0.25`+3 x^2)))/(0.25`+x^2)^3-(4.5` x (-6 x (0.1875`+x^2)+4.` x
(0.25`+x^2)-2 x (-0.25`+3 x^2)))/(0.25`+x^2)^4+(18.` x^2 (1.` (0.25`+x^2)^2-
(0.1875`+x^2) (-0.25`+3 x^2)))/(0.25`+x^2)^5-(2.25` (1.` (0.25`+x^2)^2-(0.1875`+x^2) (-
0.25`+3 x^2)))/(0.25`+x^2)^4-6.` (-((20.` x^2)/(2.25`+x^2)^3)+2.5`/(2.25`+x^2)^2+(24 x^2
(1.125`+1.25` x^2))/(2.25`+x^2)^4-(4 (1.125`+1.25` x^2))/(2.25`+x^2)^3+(1.5` (-10 x^2-2
(0.75`+x^2)))/(2.25`+x^2)^3-(18.` x (-2 x^3-2 x (0.75`+x^2)))/(2.25`+x^2)^4+(72.` x^2 (-
1.125`-x^2(0.75`+x^2)))/(2.25`+x^2)^5-(9.(-1.125`-x^2
(0.75`+x^2)))/(2.25`+x^2)^4))/3.944444444444444

Plot [Mn[x],{x,-5,5}]

Export ["*.dat", Table[Mn[x],{x,-5,5,0.02}]]

(* Normalized pipe moments Mpn (Mpn=Mp*H^2/EI*uyo), x is normalised vs H*)
Do[Export["Mnp_R_8.dat",Table[(((L^3)*(NIntegrate[((((y+1)*r/(((a-
6+x)^2+(y+1)^2)))+p*(r/(3-4*v))*(y+1)*((3-4*v)*(((a-6+x)^2+(y+1)^2)^2)-((3*(a-6+x)^2-
(y+1)^2)*((a-6+x)^2+(y+1)^2-r^2)))/(((a-6+x)^2+(y+1)^2)^3))-(((y-1)*r/(((a-6+x)^2+(y-
1)^2)))+p*(r/(3-4*v))*(y-1)*((3-4*v)*(((a-6+x)^2+(y-1)^2)^2)-((3*(a-6+x)^2-(y-1)^2)*((a-
6+x)^2+(y-1)^2-r^2)))/(((a-6+x)^2+(y-1)^2)^3))+2*r*(((2*(y-1)*((a-6+x)^2)+1*((a-6+x)^2-
(y-1)^2))/(((a-6+x)^2+(y-1)^2)^2))-(2*(1-v)*(y-1)/((a-6+x)^2+(y-1)^2)))-(8*p*r/(3-
4*v))*((((1-v)*(a-6+x)^2*(2*1-y)-y*(y-1)^2)/(((a-6+x)^2+(y-1)^2)^2))-(((y-1)*(1*y*(y-1)^2-
((a-6+x)^2)*(((a-6+x)^2+y^2)+1*(y+1))))/(((a-6+x)^2+(y-1)^2)^3))))
*Exp[-L*x]*(Cos[L*x]-Sin[L*x]),{x,0,12-a}]+NIntegrate[((((y+1)*r/(((a-6-
x)^2+(y+1)^2)))+p*(r/(3-4*v))*(y+1)*((3-4*v)*(((a-6-x)^2+(y+1)^2)^2)-((3*(a-6-x)^2-
(y+1)^2)*((a-6-x)^2+(y+1)^2-r^2)))/(((a-6-x)^2+(y+1)^2)^3))-(((y-1)*r/(((a-6-x)^2+(y-
1)^2)))+p*(r/(3-4*v))*(y-1)*((3-4*v)*(((a-6-x)^2+(y-1)^2)^2)-((3*(a-6-x)^2-(y-1)^2)*((a-6-
x)^2+(y-1)^2-r^2)))/(((a-6-x)^2+(y-1)^2)^3))+2*r*(((2*(y-1)*((a-6-x)^2)+1*((a-6-x)^2-(y-
1)^2))/(((a-6-x)^2+(y-1)^2)^2))-(2*(1-v)*(y-1)/((a-6-x)^2+(y-1)^2)))-(8*p*r/(3-4*v))*((((1-
v)*(a-6-x)^2*(2*1-y)-y*(y-1)^2)/(((a-6-x)^2+(y-1)^2)^2))-(((y-1)*(1*y*(y-1)^2-((a-6-
```

```
x)^2)*(((a-6-x)^2+y^2)+1*(y+1))))/(((a-6-x)^2+(y-1)^2)^3))))*Exp[-L*x]*(Cos[L*x]-
Sin[L*x]),{x,0,a}])))/3.944444444444444,{a,0,6,0.02}]],{a,0,6,0.02}]



(* Normalized free-field and pipe axial displacements *)
r=0.25(*r=r/H*)
H=10
y=-0.5  (*y=y/H*)
v=0.5
p=0.5
(* Free-field solution*)
ux[x_]:=(((x*r/((x^2+(y+1)^2))))-p*((r/(3-4*v))*(x)*((3-4*v)*((x^2+(y+1)^2)^2)-((3*(y+1)^2-
x^2)*(x^2+(y+1)^2-r^2)))/((x^2+(y+1)^2)^3))-((x*r/((x^2+(y-1)^2))))+p*((r/(3-4*v))*(x)*((3-
4*v)*((x^2+(y-1)^2)^2)-((3*(y-1)^2-x^2)*(x^2+(y-1)^2-r^2)))/((x^2+(y-1)^2)^3))+4*r*((x*(1-
v))/(x^2+(y-1)^2)-((y-1)*x*y/((x^2+(y-1)^2)^2)))-(8*p*r/(3-4*v))*((((1-v)*x*(x^2+y^2-
1^2))/((x^2+(y-1)^2)^2))-(x*y*(y*(x^2+y^2)+2*1*(1^2-x^2)-3*y*(1^2))/((x^2+(y-1)^2)^3))))
Plot[ux[x],{x,-5,5}]
FindMaximum[ux[x],x]
{0.229595,{x->0.281912}}
Export ["ux_.dat", Table[ux[x],{x,-5,5,0.02}]]



(* For Ra=EA/Es*ro*\[Pi]*xj *)
Ra=10
J=0.2819117474991075(*J=xj/H*)
\[Lambda]=(1/J)*((15/(3.1415*Ra*(1+v)*(1+p)))^(1/2))

(* Normalized axial pipe displacements uxp/uxo *)
Do[Export["uxp_Ra_10.dat",Table[(\[Lambda]/(2*0.22959456037561465))*((NIntegrate[
((((a-6-x)*r/(((a-6-x)^2+(y+1)^2)))-p*(r/(3-4*v))*(a-6-x)*((3-4*v)*(((a-6-x)^2+(y+1)^2)^2)-
((3*(y+1)^2-(a-6-x)^2)*((a-6-x)^2+(y+1)^2-r^2)))/(((a-6-x)^2+(y+1)^2)^3))-(((a-6-x)*r/(((a-
6-x)^2+(y-1)^2)))-p*(r/(3-4*v))*(a-6-x)*((3-4*v)*(((a-6-x)^2+(y-1)^2)^2)-((3*(y-1)^2-(a-6-
x)^2)*((a-6-x)^2+(y-1)^2-r^2)))/(((a-6-x)^2+(y-1)^2)^3))+4*r*(((a-6-x)*(1-v))/((a-6-x)^2+(y-
```

```
1)^2)-((y-1)*(a-6-x)*y/(((a-6-x)^2+(y-1)^2)^2)))-(8*p*r/(3-4*v))*((((1-v)*(a-6-x)*((a-6-
x)^2+y^2-1^2))/(((a-6-x)^2+(y-1)^2)^2))-((a-6-x)*y*(y*((a-6-x)^2+y^2)+2*1*(1^2-(a-6-
x)^2)-3*y*(1^2))/(((a-6-x)^2+(y-1)^2)^3))))*(Exp[-\[Lambda]*x]),{x,0,a}]+NIntegrate[((((a-
6+x)*r/(((a-6+x)^2+(y+1)^2)))-p*(r/(3-4*v))*(a-6+x)*((3-4*v)*(((a-6+x)^2+(y+1)^2)^2)-
((3*(y+1)^2-(a-6+x)^2)*((a-6+x)^2+(y+1)^2-r^2)))/(((a-6+x)^2+(y+1)^2)^3))-(((a-
6+x)*r/(((a-6+x)^2+(y-1)^2)))-p*(r/(3-4*v))*(a-6+x)*((3-4*v)*(((a-6+x)^2+(y-1)^2)^2)-
((3*(y-1)^2-(a-6+x)^2)*((a-6+x)^2+(y-1)^2-r^2)))/(((a-6+x)^2+(y-1)^2)^3))+4*r*(((a-
6+x)*(1-v))/((a-6+x)^2+(y-1)^2)-((y-1)*(a-6+x)*y/(((a-6+x)^2+(y-1)^2)^2)))-(8*p*r/(3-
4*v))*((((1-v)*(a-6+x)*((a-6+x)^2+y^2-1^2))/(((a-6+x)^2+(y-1)^2)^2))-((a-6+x)*y*(y*((a-
6+x)^2+y^2)+2*1*(1^2-(a-6+x)^2)-3*y*(1^2))/(((a-6+x)^2+(y-1)^2)^3))))*(Exp[-
\[Lambda]*x]),{x,0,12-a}])),{a,0,6,0.02}]],{a,0,6,0.02}]
```

- **Relationship between x_i and x_j with relative distortion,ρ and embedment depth ratio, y/H**

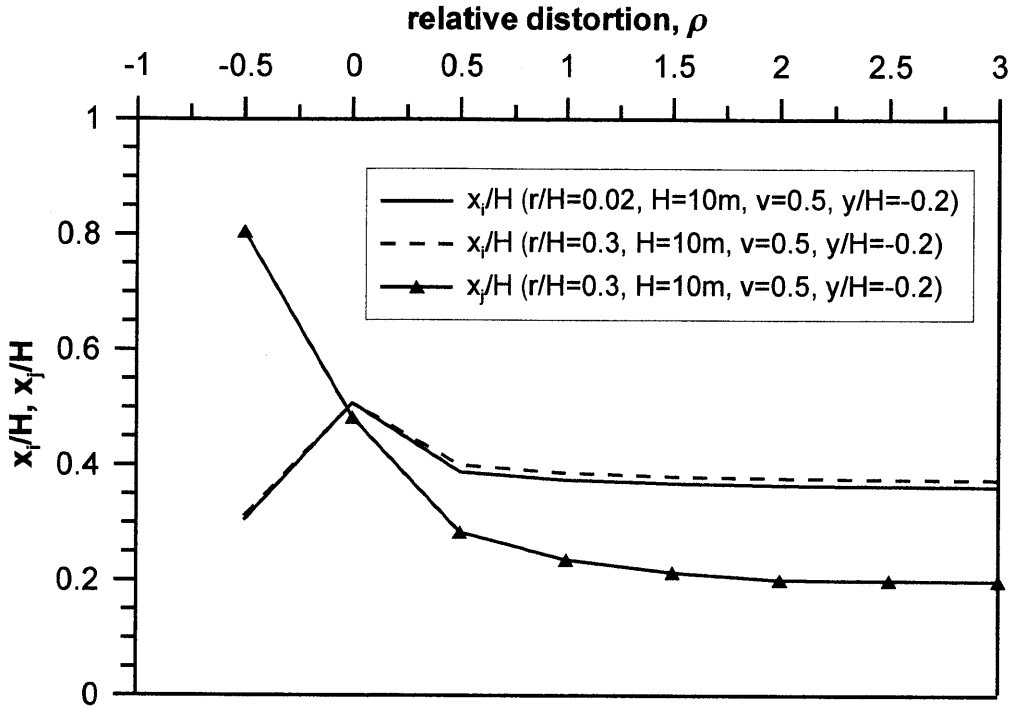

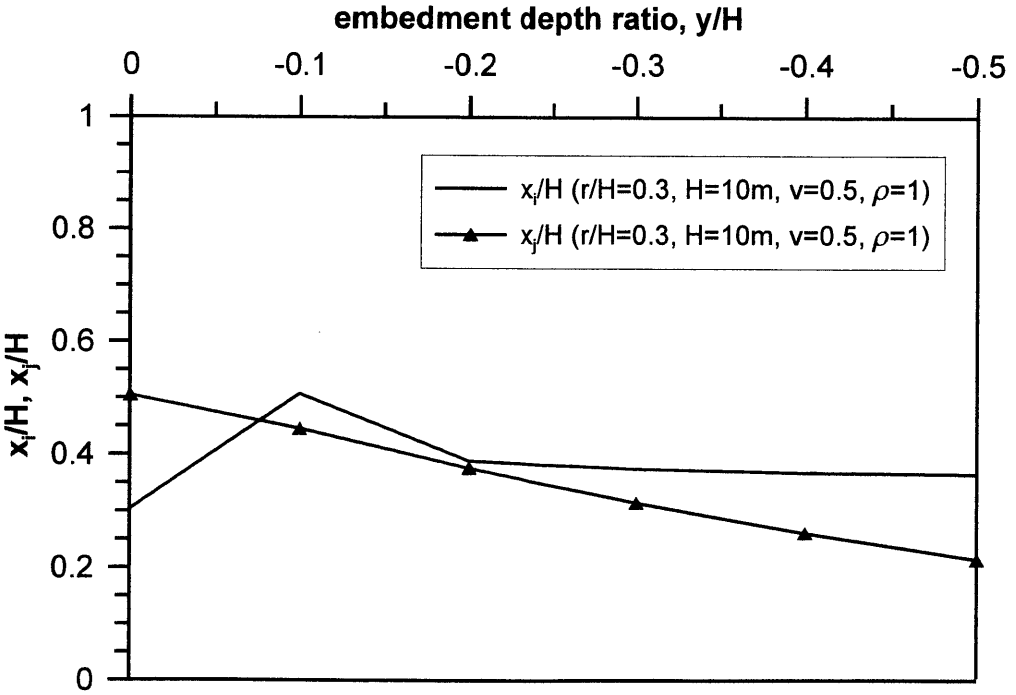

APPENDIX II

Evaluation of horizontal displacements of several pipelines with different axial stiffness, using two methods:

a) finite element (PLAXIS 3D)

b) analytical solutions computed by using the new horizontal spring coefficient $K_h=15E_s r_o/(1+v)(1+\rho)j$.

The following graphs summarize the comparison between the two methods for different sets of the following parameters:

- relative distortion of the tunnel walls (ρ)
- pipe depth (y_p)
- uniform convergence of the tunnel walls (u_ε)
- soil Poisson's ratio (v)

The constant parameters are:

- tunnel depth H=10m
- tunnel radius r=3m
- soil stiffness E_s=30 MPa

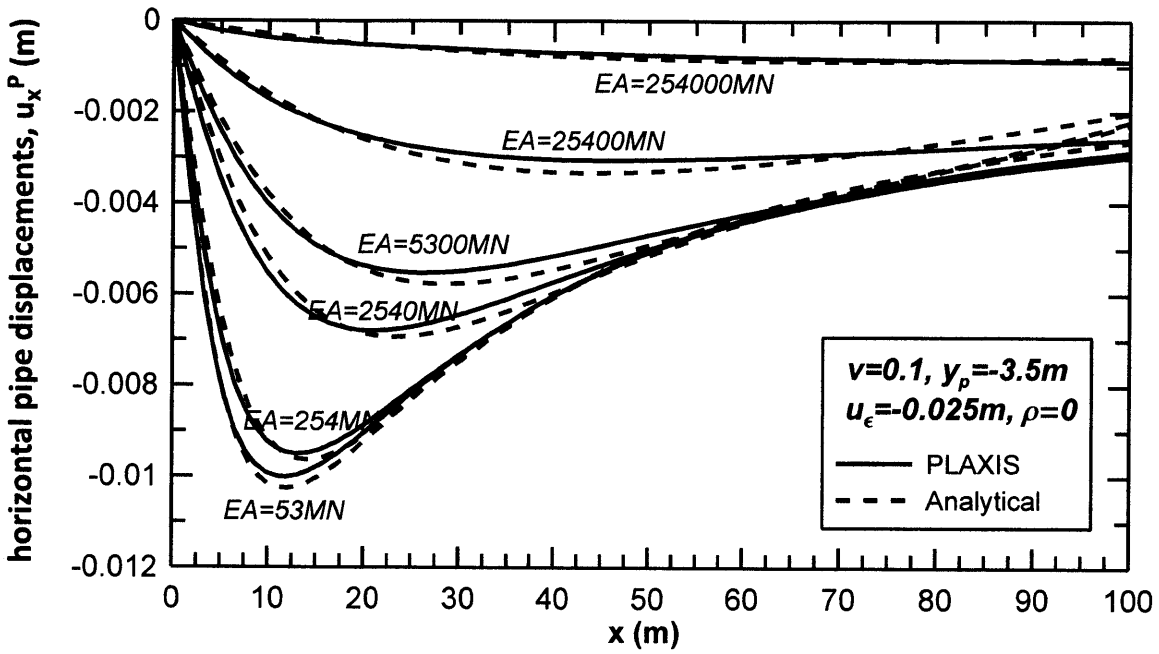
horizontal pipe displacements, u_x^P (m)
0
-0.002
-0.004
-0.006
-0.008
-0.01
-0.012
0
10
20
30
40
50
60
70
80
90
100
x (m)
EA=254000MN
EA=25400MN
EA=5300MN
EA=2540MN
EA=254MN
EA=53MN
v=0.1, y_p=-3.5m
u_ϵ=-0.025m, ρ=0
PLAXIS
Analytical

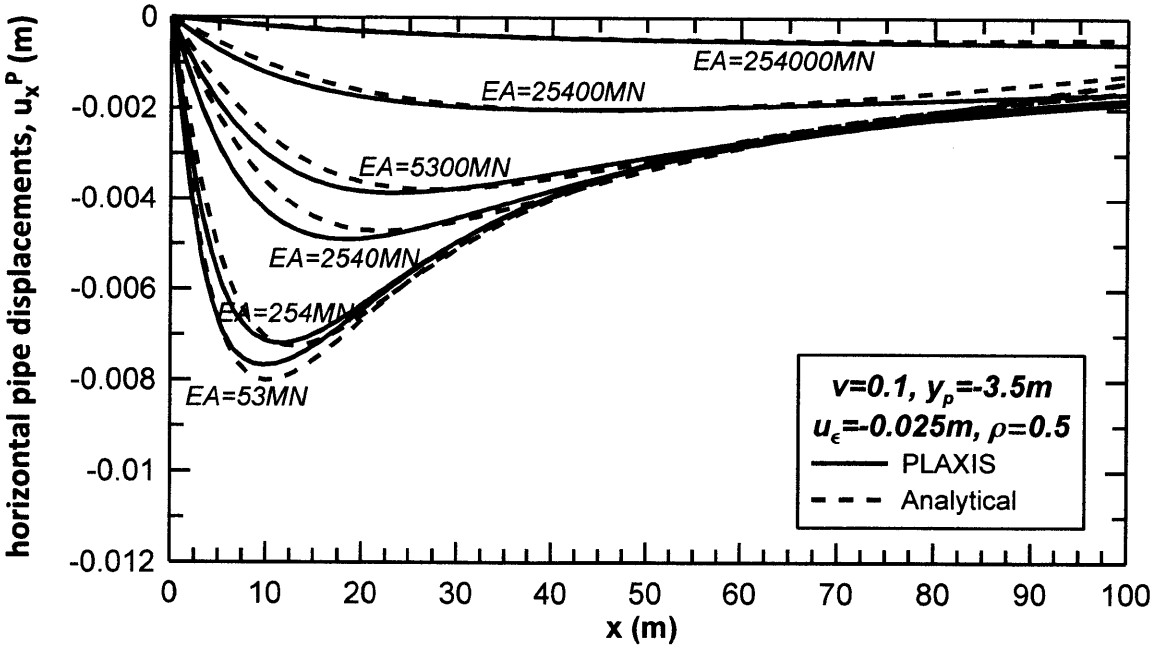
horizontal pipe displacements, u_x^P (m)
0
-0.002
-0.004
-0.006
-0.008
-0.01
-0.012
0
10
20
30
40
50
60
70
80
90
100
x (m)
EA=254000MN
EA=25400MN
EA=5300MN
EA=2540MN
EA=254MN
EA=53MN
v=0.1, y_p=-3.5m
u_ϵ=-0.025m, ρ=0.5
PLAXIS
Analytical

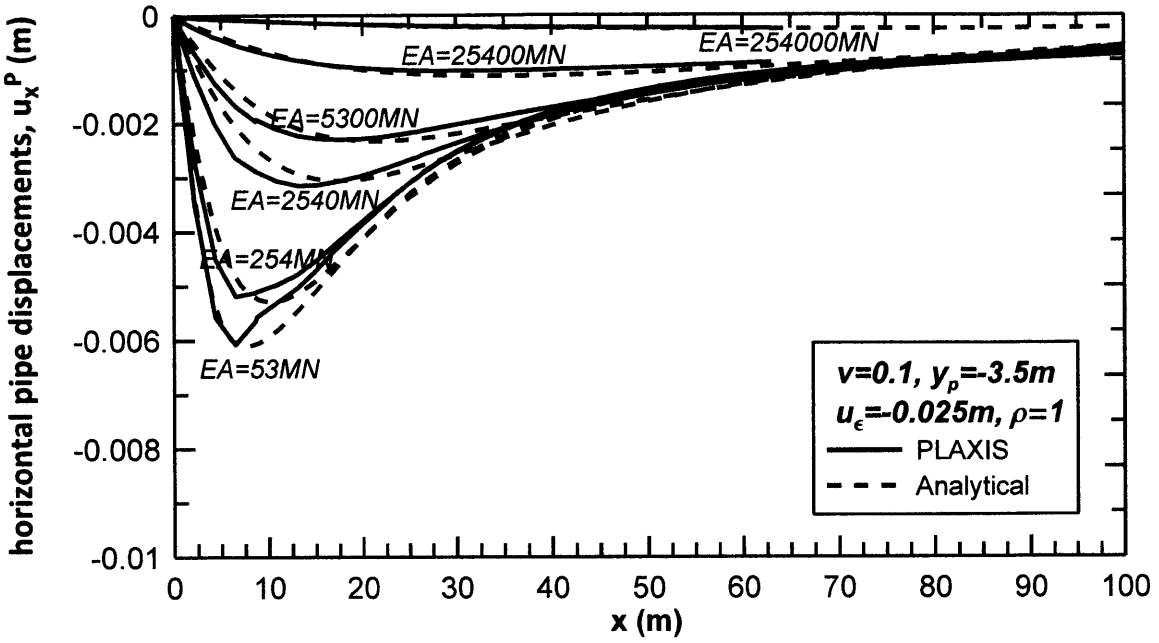
horizontal pipe displacements, u_x^P (m)
0
-0.002
-0.004
-0.006
-0.008
-0.01
EA=25400MN
EA=254000MN
EA=5300MN
EA=2540MN
EA=254MN
EA=53MN
v=0.1, y_p=-3.5m
u_ϵ=-0.025m, ρ=1
PLAXIS
Analytical
0
10
20
30
40
50
60
70
80
90
100
x (m)

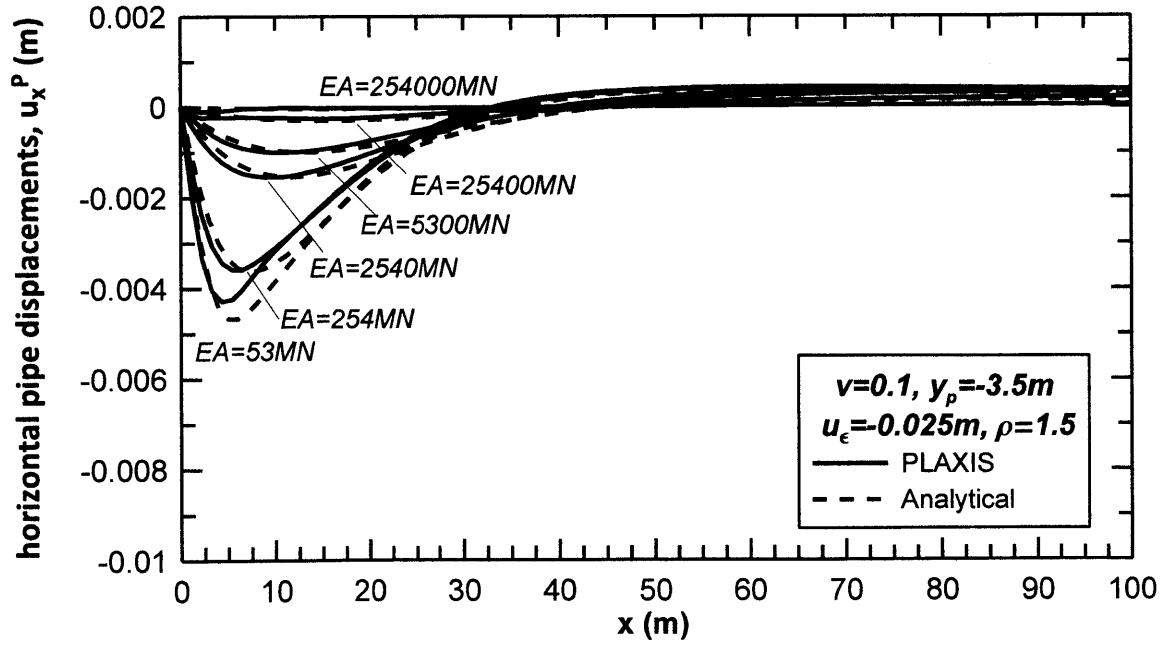
horizontal pipe displacements, u_x^P (m)
0.002
0
-0.002
-0.004
-0.006
-0.008
-0.01
EA=254000MN
EA=25400MN
EA=5300MN
EA=2540MN
EA=254MN
EA=53MN
v=0.1, y_p=-3.5m
u_ϵ=-0.025m, ρ=1.5
PLAXIS
Analytical
0
10
20
30
40
50
60
70
80
90
100
x (m)

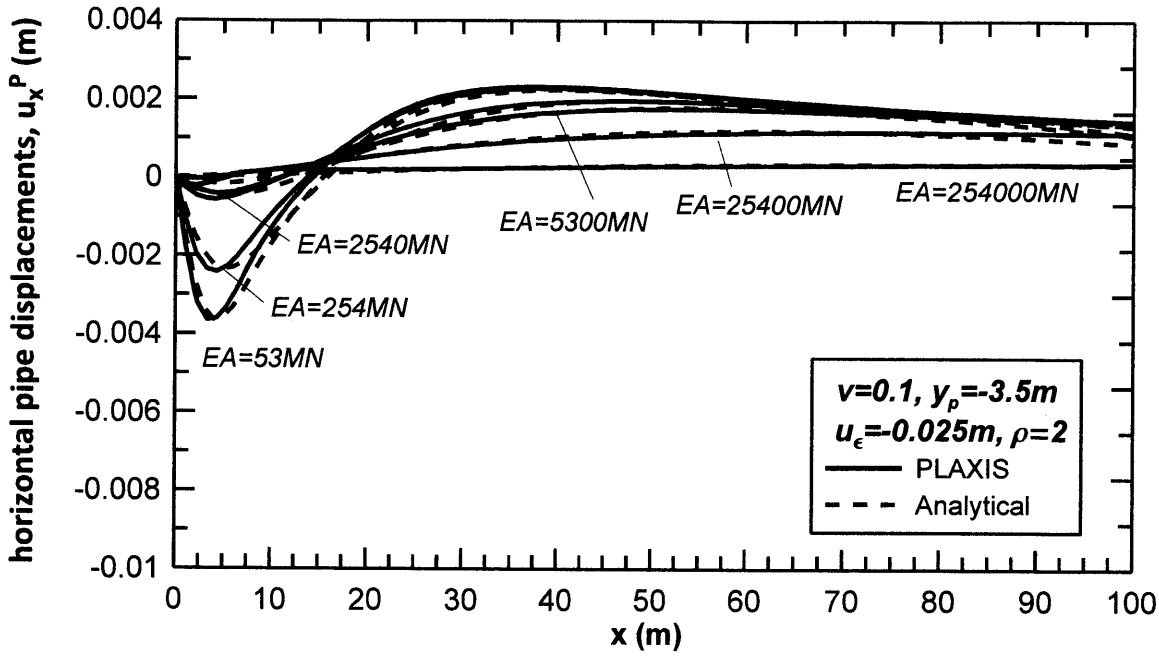
horizontal pipe displacements, u_x^P (m)
0.004
0.002
0
-0.002
-0.004
-0.006
-0.008
-0.01
0
10
20
30
40
50
60
70
80
90
100
x (m)
EA=254000MN
EA=25400MN
EA=5300MN
EA=2540MN
EA=254MN
EA=53MN
v=0.1, y_p=-3.5m
u_ϵ=-0.025m, ρ=2
PLAXIS
Analytical

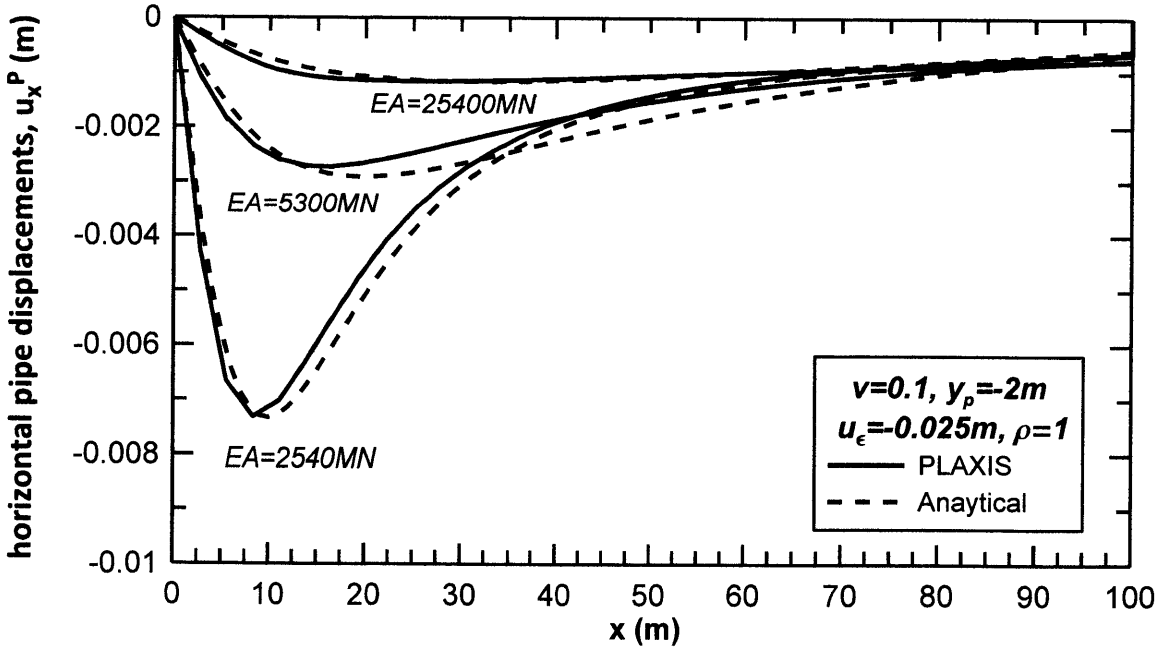
horizontal pipe displacements, u_x^P (m)
0
-0.002
-0.004
-0.006
-0.008
-0.01
0
10
20
30
40
50
60
70
80
90
100
x (m)
EA=25400MN
EA=5300MN
EA=2540MN
v=0.1, y_p=-2m
u_ϵ=-0.025m, ρ=1
PLAXIS
Anaytical

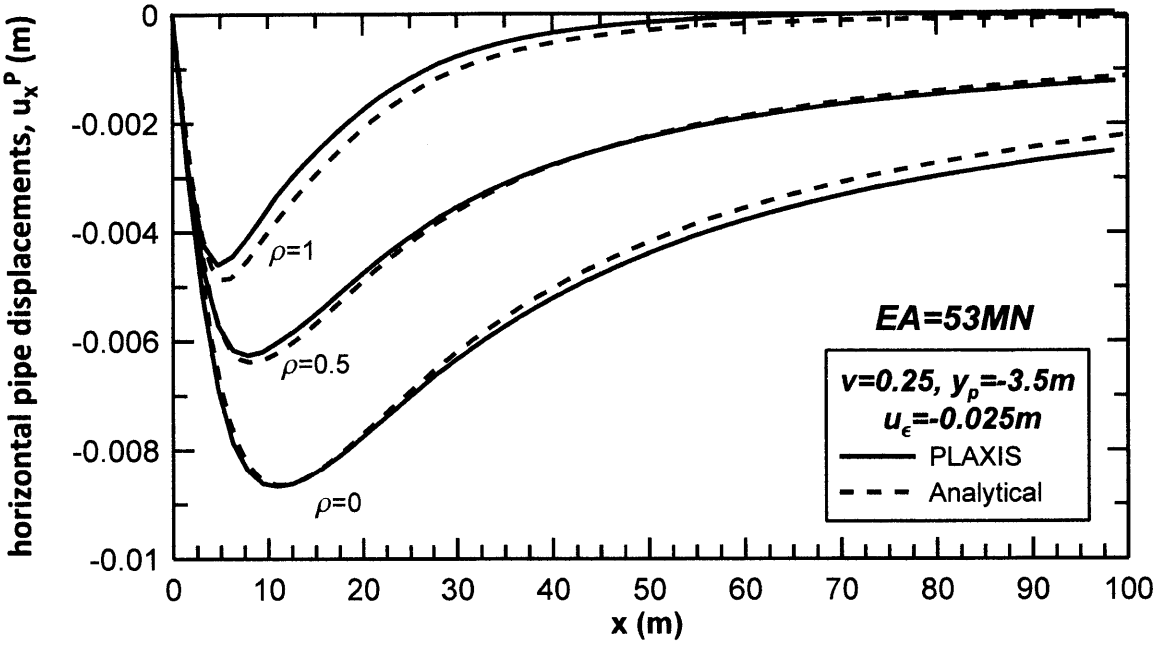
horizontal pipe displacements, u_x^P (m)
0
-0.002
-0.004
-0.006
-0.008
-0.01
0
10
20
30
40
50
60
70
80
90
100
x (m)
ρ=1
ρ=0.5
ρ=0
EA=53MN
v=0.25, y_p=-3.5m
u_ϵ=-0.025m
PLAXIS
Analytical

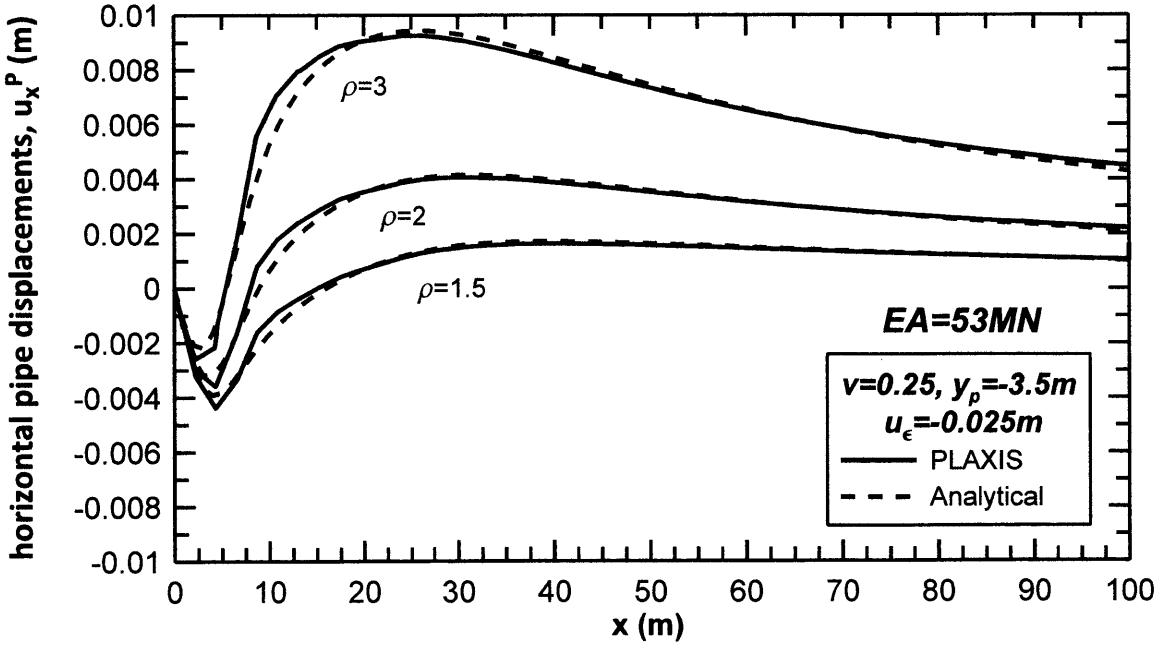
horizontal pipe displacements, u_x^P (m)
0.01
0.008
0.006
0.004
0.002
0
-0.002
-0.004
-0.006
-0.008
-0.01
0
10
20
30
40
50
60
70
80
90
100
x (m)
ρ=3
ρ=2
ρ=1.5
EA=53MN
v=0.25, y_p=-3.5m
u_ϵ=-0.025m
PLAXIS
Analytical

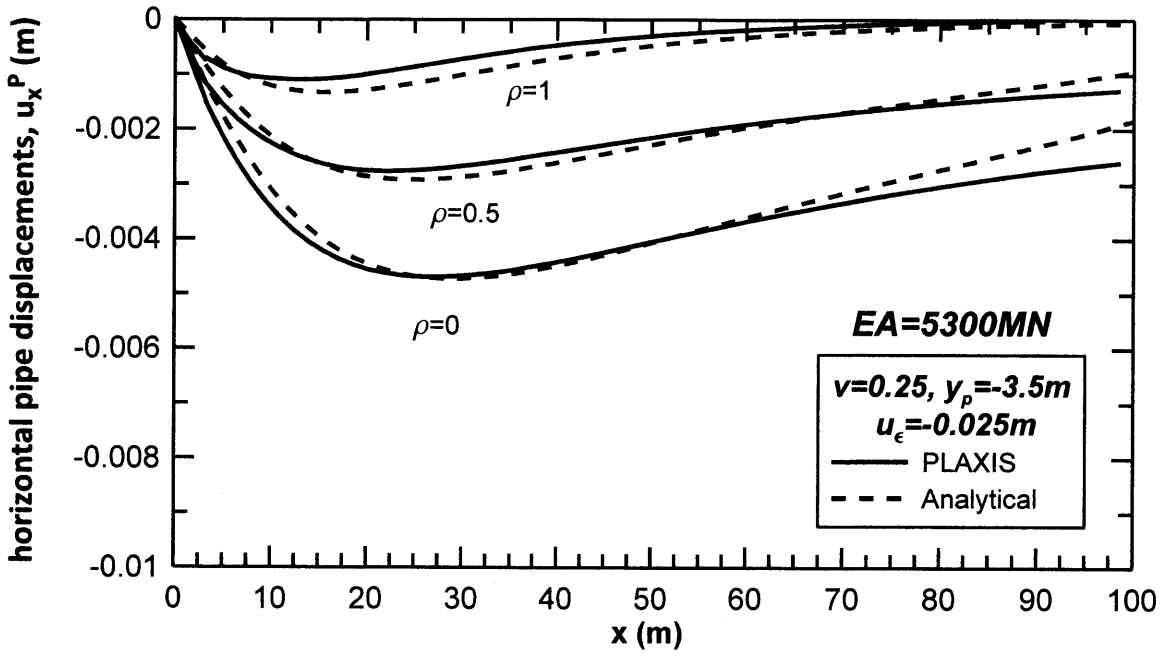
horizontal pipe displacements, u_x^P (m)
0
-0.002
-0.004
-0.006
-0.008
-0.01
0
10
20
30
40
50
60
70
80
90
100
x (m)
ρ=1
ρ=0.5
ρ=0
EA=5300MN
v=0.25, y_p=-3.5m
u_ϵ=-0.025m
PLAXIS
Analytical

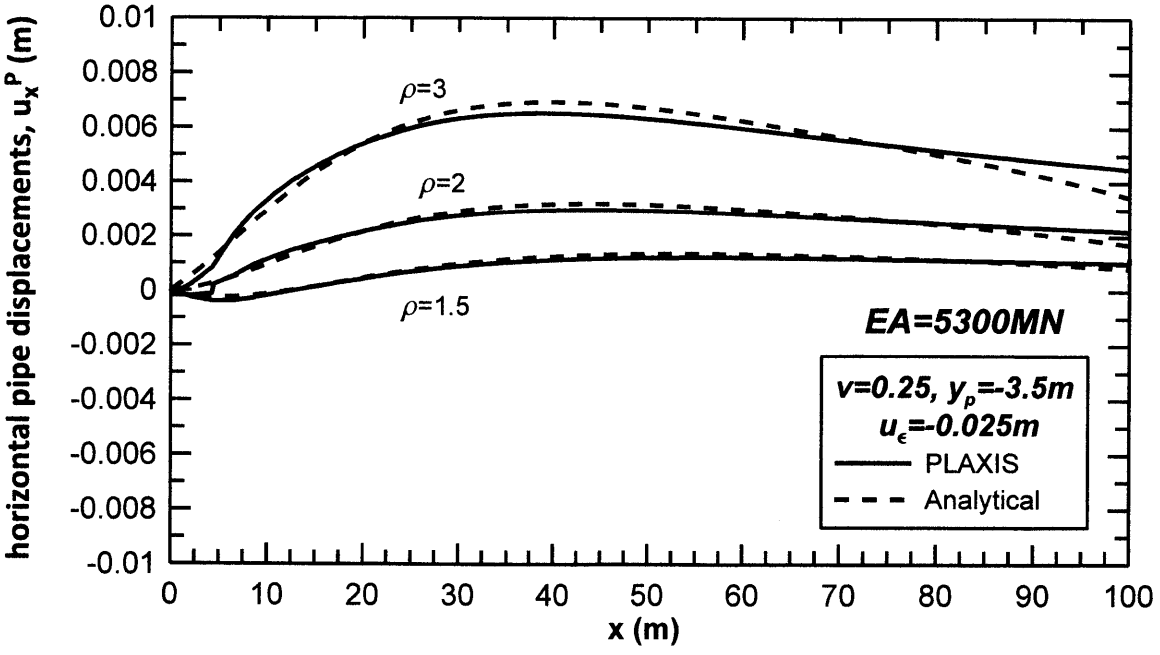
horizontal pipe displacements, u_x^P (m)
0.01
0.008
0.006
0.004
0.002
0
-0.002
-0.004
-0.006
-0.008
-0.01
0
10
20
30
40
50
60
70
80
90
100
x (m)
ρ=3
ρ=2
ρ=1.5
EA=5300MN
v=0.25, y_p=-3.5m
u_ϵ=-0.025m
PLAXIS
Analytical

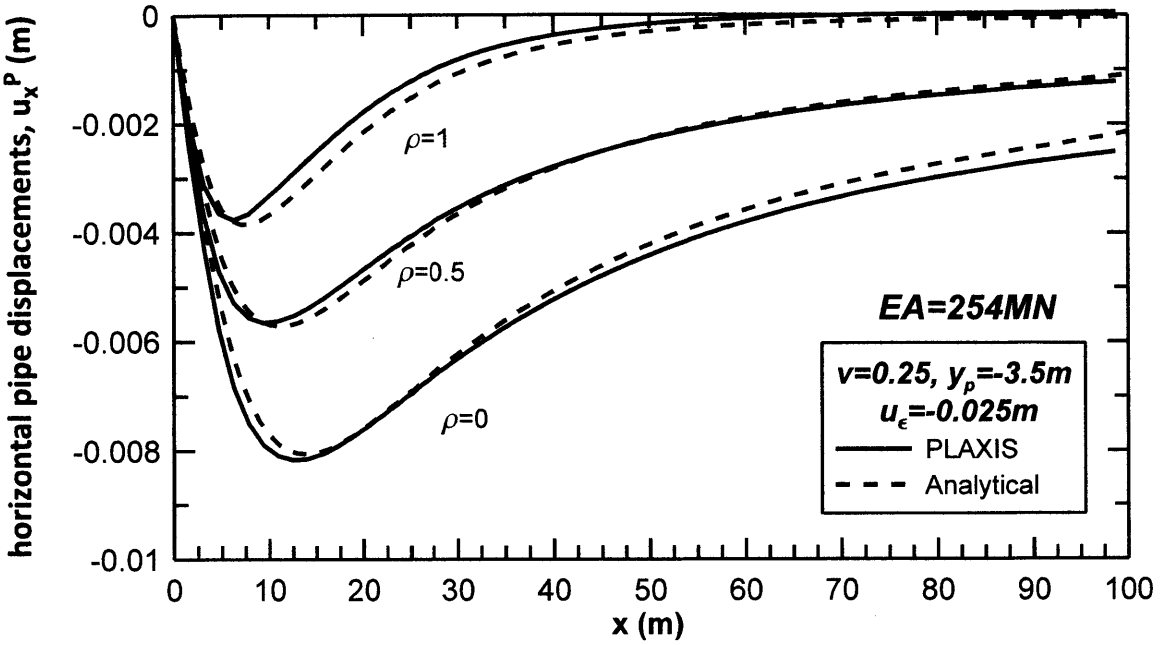
horizontal pipe displacements, u_x^P (m)
0
-0.002
-0.004
-0.006
-0.008
-0.01
0
10
20
30
40
50
60
70
80
90
100
x (m)
ρ=1
ρ=0.5
ρ=0
EA=254MN
v=0.25, y_p=-3.5m
u_ϵ=-0.025m
PLAXIS
Analytical

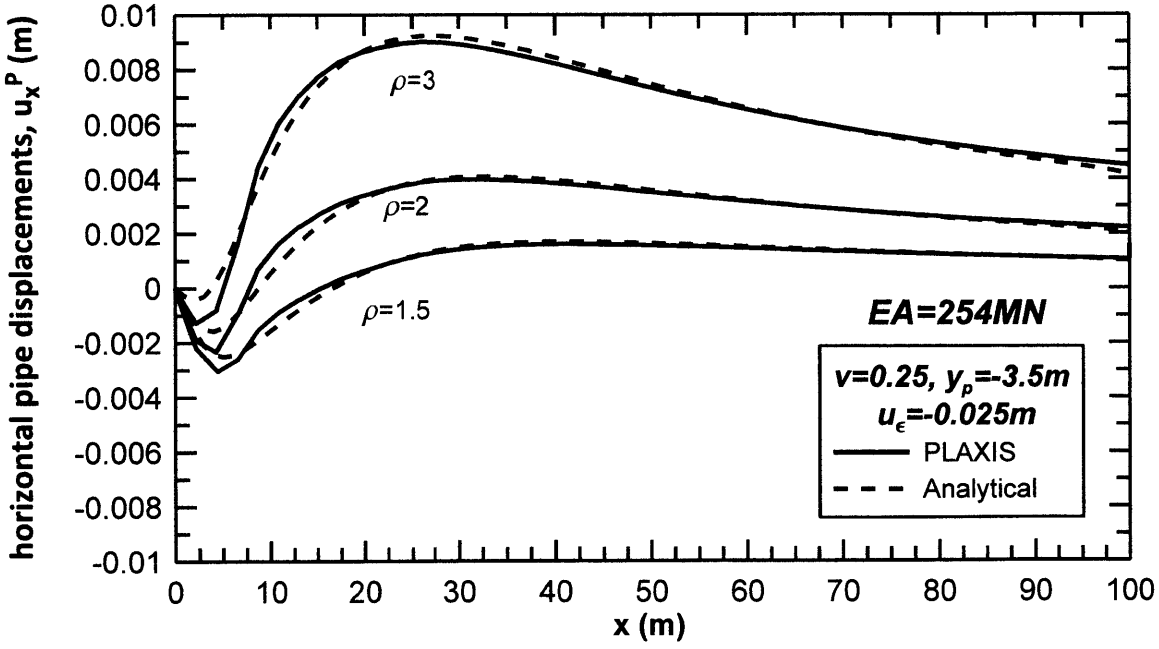
horizontal pipe displacements, u_x^P (m)
0.01
0.008
0.006
0.004
0.002
0
-0.002
-0.004
-0.006
-0.008
-0.01
0
10
20
30
40
50
60
70
80
90
100
x (m)
ρ=3
ρ=2
ρ=1.5
EA=254MN
v=0.25, y_p=-3.5m
u_ϵ=-0.025m
PLAXIS
Analytical

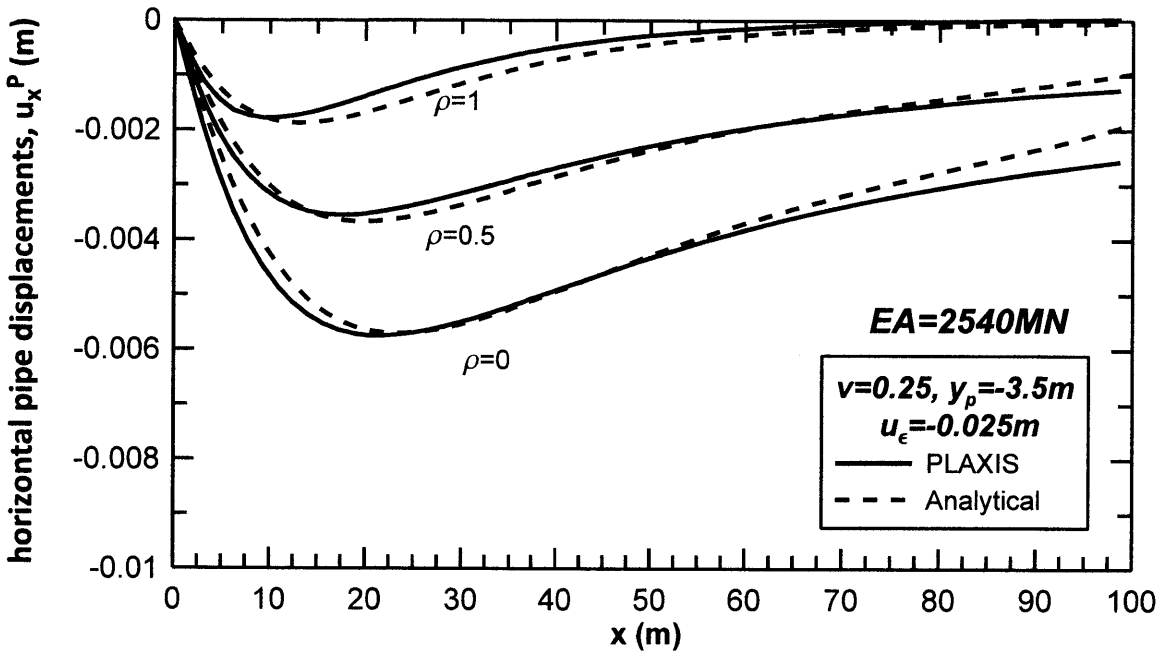
horizontal pipe displacements, u_x^P (m)
0
-0.002
-0.004
-0.006
-0.008
-0.01
0
10
20
30
40
50
60
70
80
90
100
x (m)
ρ=1
ρ=0.5
ρ=0
EA=2540MN
v=0.25, y_p=-3.5m
u_ϵ=-0.025m
PLAXIS
Analytical

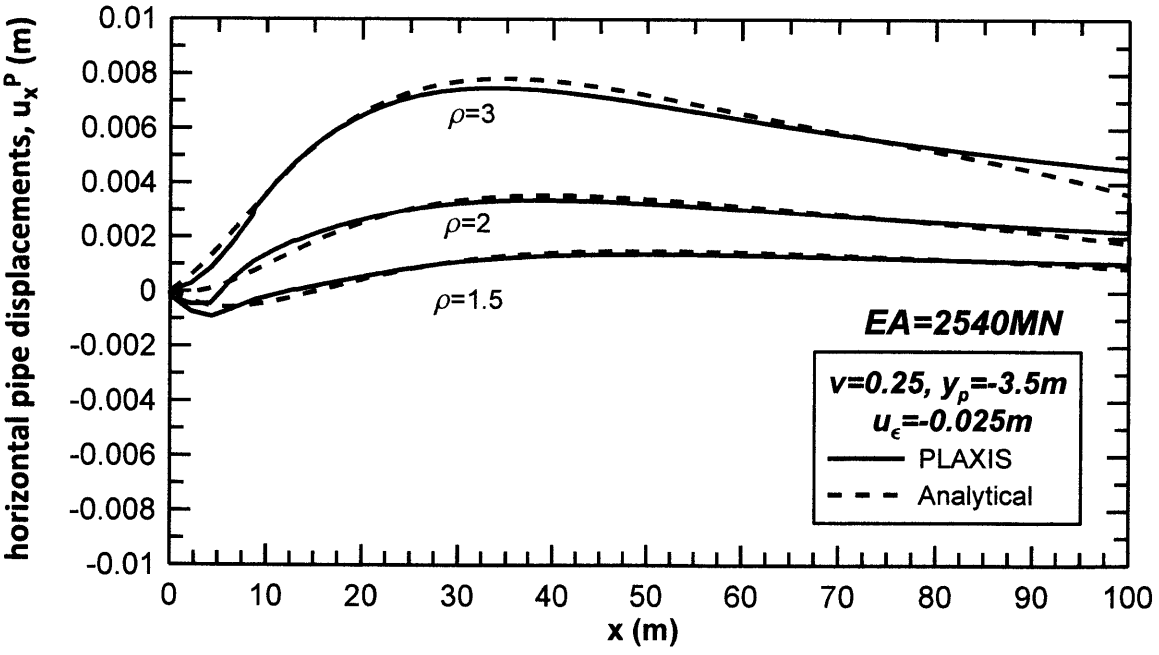
horizontal pipe displacements, u_x^P (m)
0.01
0.008
0.006
0.004
0.002
0
-0.002
-0.004
-0.006
-0.008
-0.01
0
10
20
30
40
50
60
70
80
90
100
x (m)
ρ=3
ρ=2
ρ=1.5
EA=2540MN
v=0.25, y_p=-3.5m
u_ϵ=-0.025m
PLAXIS
Analytical

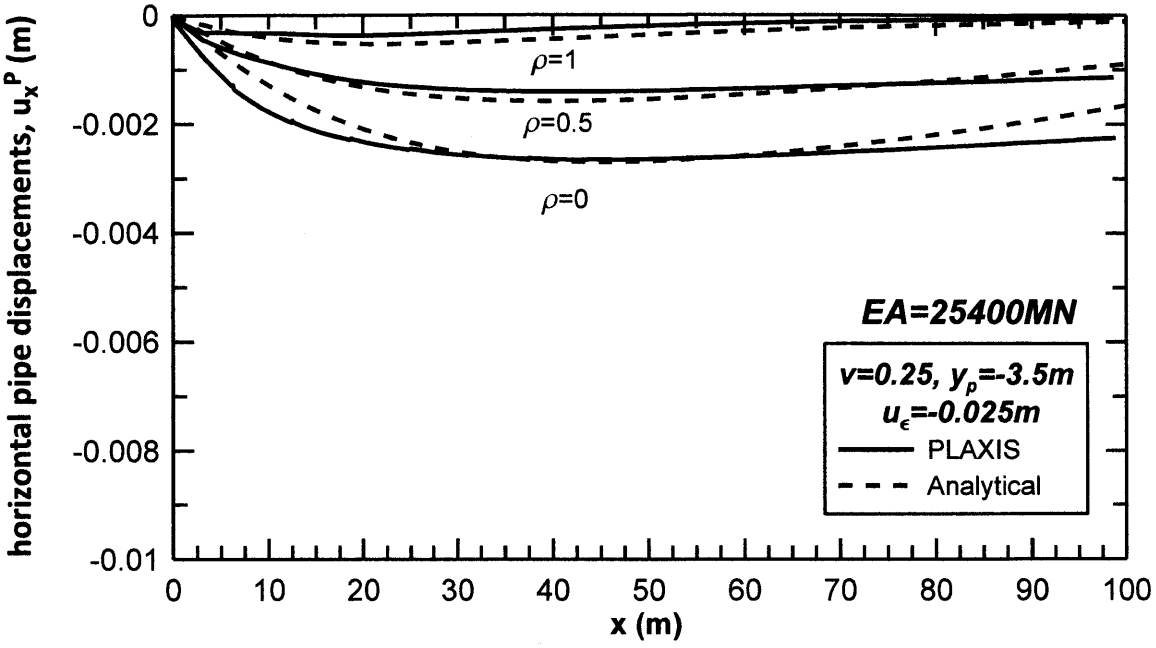
horizontal pipe displacements, u_x^P (m)
0
-0.002
-0.004
-0.006
-0.008
-0.01
0
10
20
30
40
50
60
70
80
90
100
x (m)
ρ=1
ρ=0.5
ρ=0
EA=25400MN
v=0.25, y_p=-3.5m
u_ϵ=-0.025m
PLAXIS
Analytical

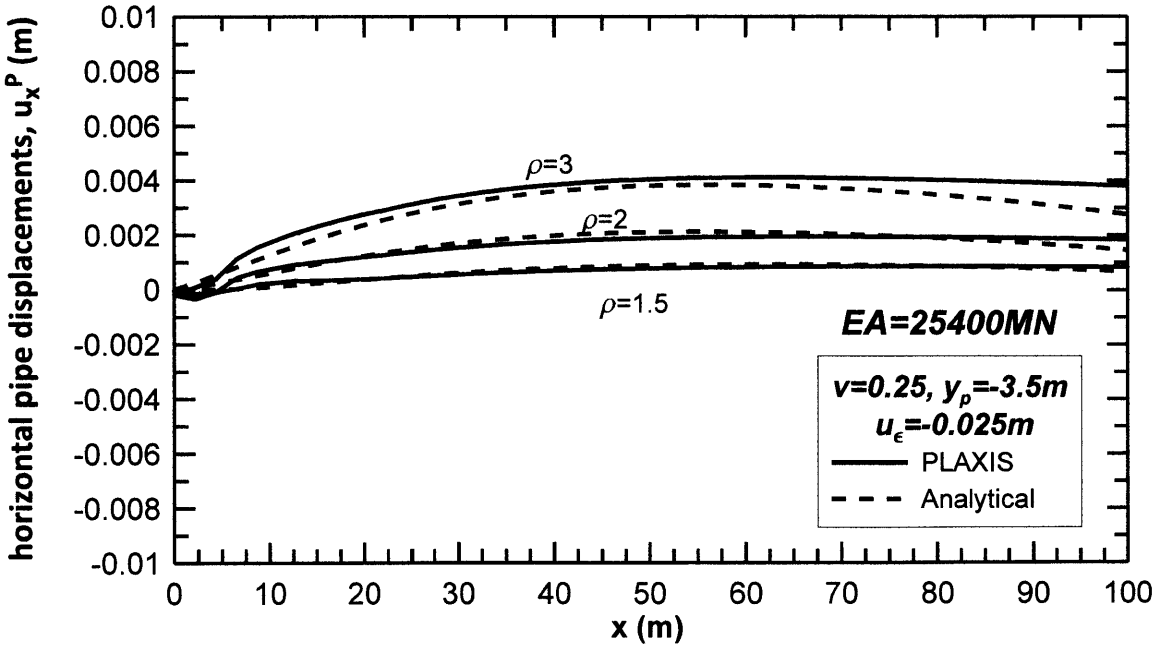
horizontal pipe displacements, u_x^P (m)
0.01
0.008
0.006
0.004
0.002
0
-0.002
-0.004
-0.006
-0.008
-0.01
0
10
20
30
40
50
60
70
80
90
100
x (m)
ρ=3
ρ=2
ρ=1.5
EA=25400MN
v=0.25, y_p=-3.5m
u_ϵ=-0.025m
PLAXIS
Analytical

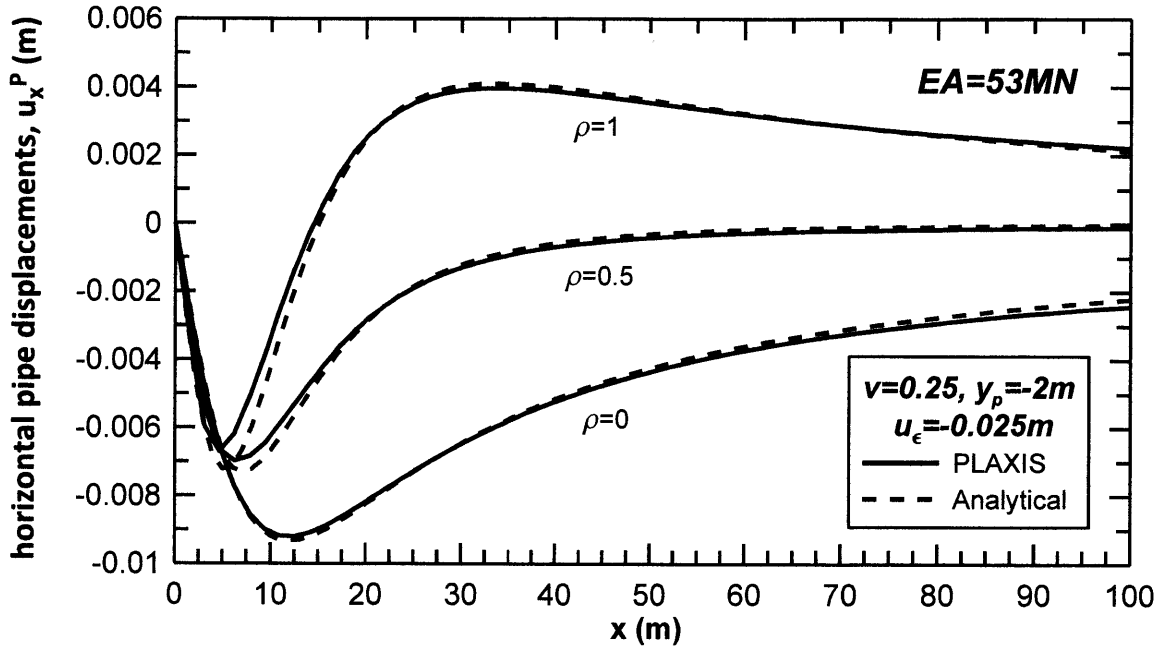
EA=53MN
ρ=1
ρ=0.5
ρ=0
v=0.25, y_p=-2m
u_ϵ=-0.025m
PLAXIS
Analytical
horizontal pipe displacements, u_x^P (m)
x (m)
0.006
0.004
0.002
0
-0.002
-0.004
-0.006
-0.008
-0.01
0
10
20
30
40
50
60
70
80
90
100

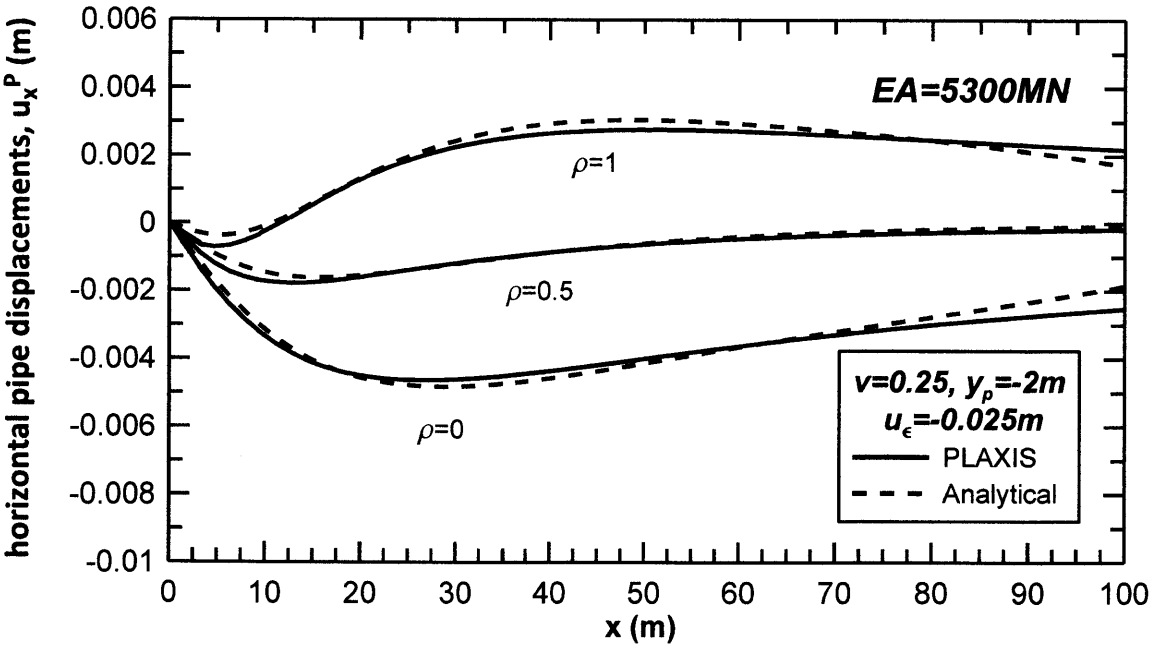
EA=5300MN
ρ=1
ρ=0.5
ρ=0
v=0.25, y_p=-2m
u_ϵ=-0.025m
PLAXIS
Analytical
horizontal pipe displacements, u_x^P (m)
x (m)
0.006
0.004
0.002
0
-0.002
-0.004
-0.006
-0.008
-0.01
0
10
20
30
40
50
60
70
80
90
100

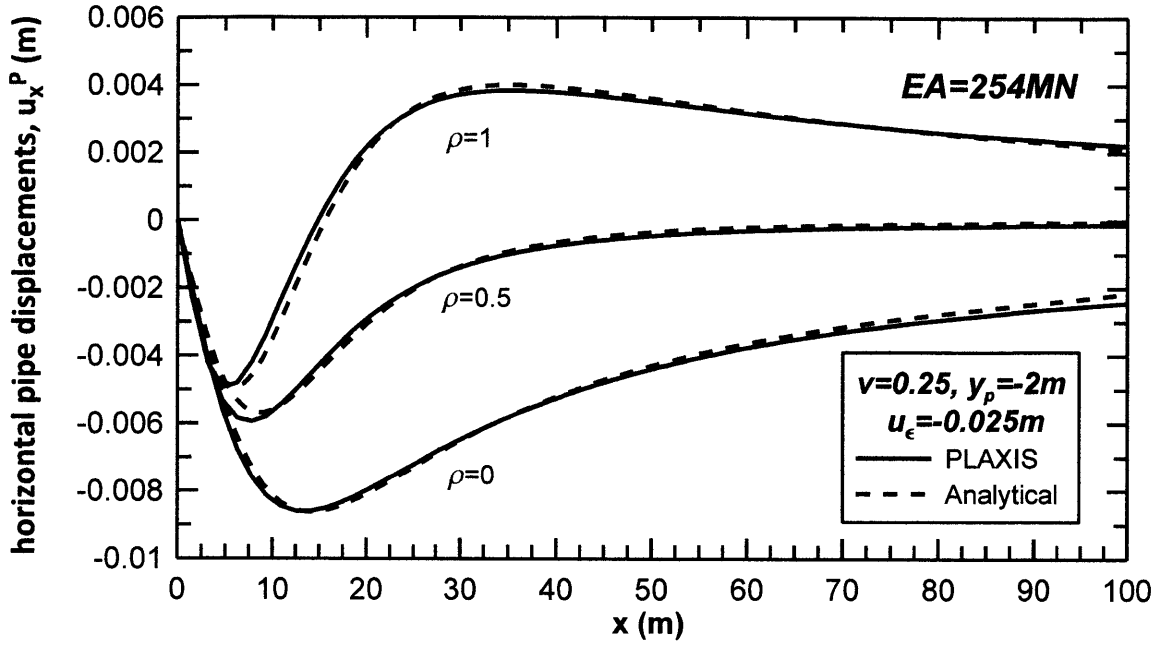
EA=254MN
ρ=1
ρ=0.5
ρ=0
v=0.25, y_p=-2m
u_ε=-0.025m
PLAXIS
Analytical
horizontal pipe displacements, u_x^P (m)
x (m)
0.006
0.004
0.002
0
-0.002
-0.004
-0.006
-0.008
-0.01
0
10
20
30
40
50
60
70
80
90
100

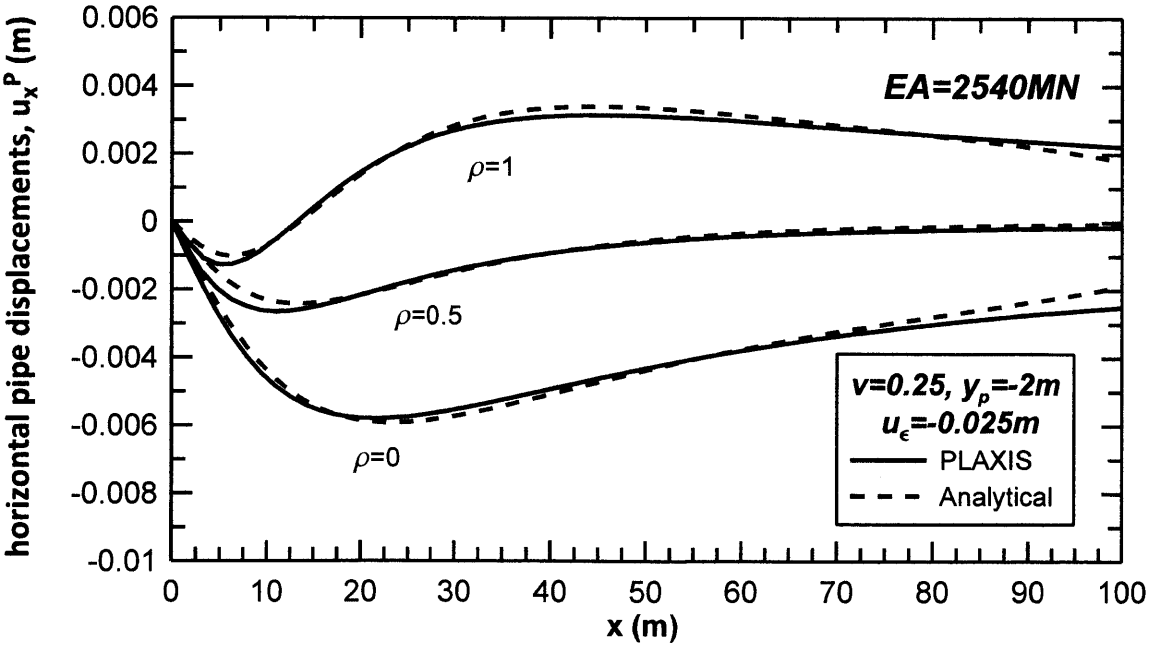
EA=2540MN
ρ=1
ρ=0.5
ρ=0
v=0.25, y_p=-2m
u_ε=-0.025m
PLAXIS
Analytical
horizontal pipe displacements, u_x^P (m)
x (m)
0.006
0.004
0.002
0
-0.002
-0.004
-0.006
-0.008
-0.01
0
10
20
30
40
50
60
70
80
90
100

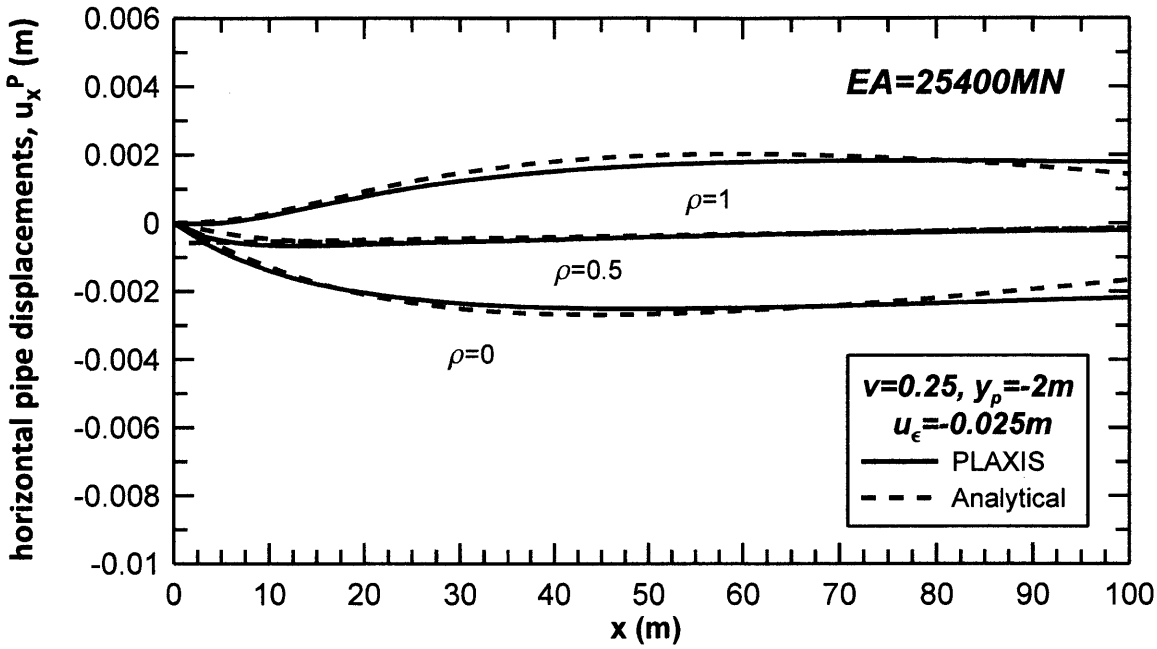
horizontal pipe displacements, u_x^P (m)
0.006
0.004
0.002
0
-0.002
-0.004
-0.006
-0.008
-0.01
0
10
20
30
40
50
60
70
80
90
100
x (m)
EA=25400MN
ρ=1
ρ=0.5
ρ=0
v=0.25, y_p=-2m
u_ϵ=-0.025m
PLAXIS
Analytical

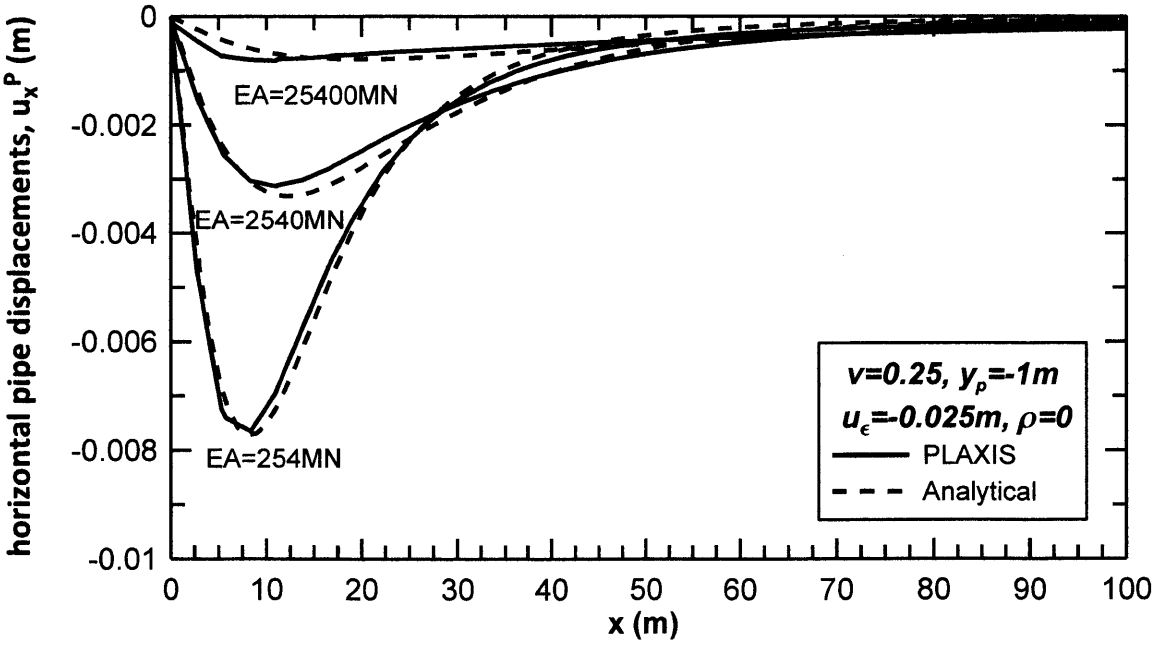
horizontal pipe displacements, u_x^P (m)
0
-0.002
-0.004
-0.006
-0.008
-0.01
0
10
20
30
40
50
60
70
80
90
100
x (m)
EA=25400MN
EA=2540MN
EA=254MN
v=0.25, y_p=-1m
u_ϵ=-0.025m, ρ=0
PLAXIS
Analytical

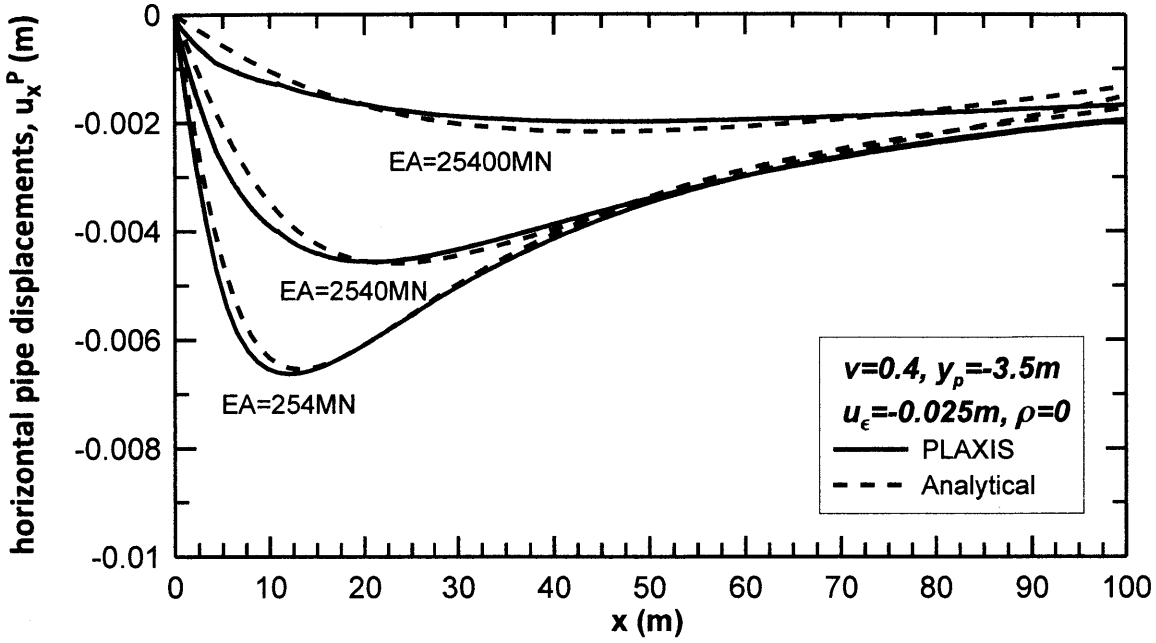
horizontal pipe displacements, u_x^P (m)
0
-0.002
-0.004
-0.006
-0.008
-0.01
0
10
20
30
40
50
60
70
80
90
100
x (m)
EA=25400MN
EA=2540MN
EA=254MN
v=0.4, y_p=-3.5m
u_ϵ=-0.025m, ρ=0
PLAXIS
Analytical

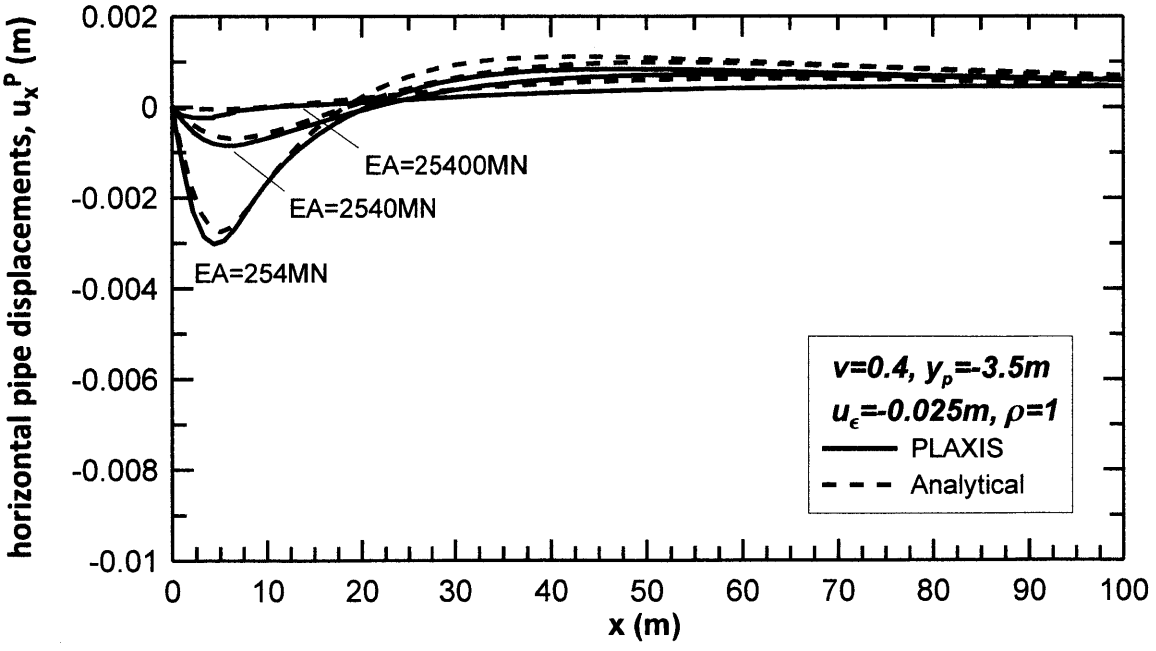
horizontal pipe displacements, u_x^P (m)
0.002
0
-0.002
-0.004
-0.006
-0.008
-0.01
0
10
20
30
40
50
60
70
80
90
100
x (m)
EA=25400MN
EA=2540MN
EA=254MN
v=0.4, y_p=-3.5m
u_ϵ=-0.025m, ρ=1
PLAXIS
Analytical

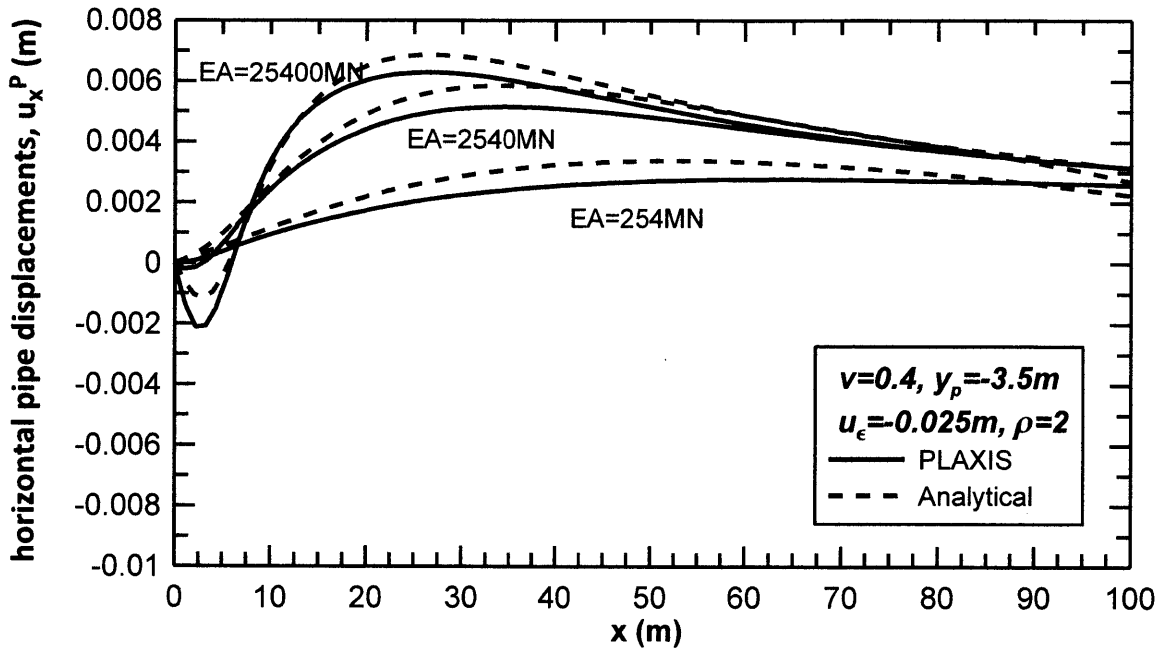
0.008
0.006
0.004
0.002
0
-0.002
-0.004
-0.006
-0.008
-0.01
horizontal pipe displacements, u_x^P (m)
EA=25400MN
EA=2540MN
EA=254MN
v=0.4, y_p=-3.5m
u_ϵ=-0.025m, ρ=2
PLAXIS
Analytical
0
10
20
30
40
50
60
70
80
90
100
x (m)

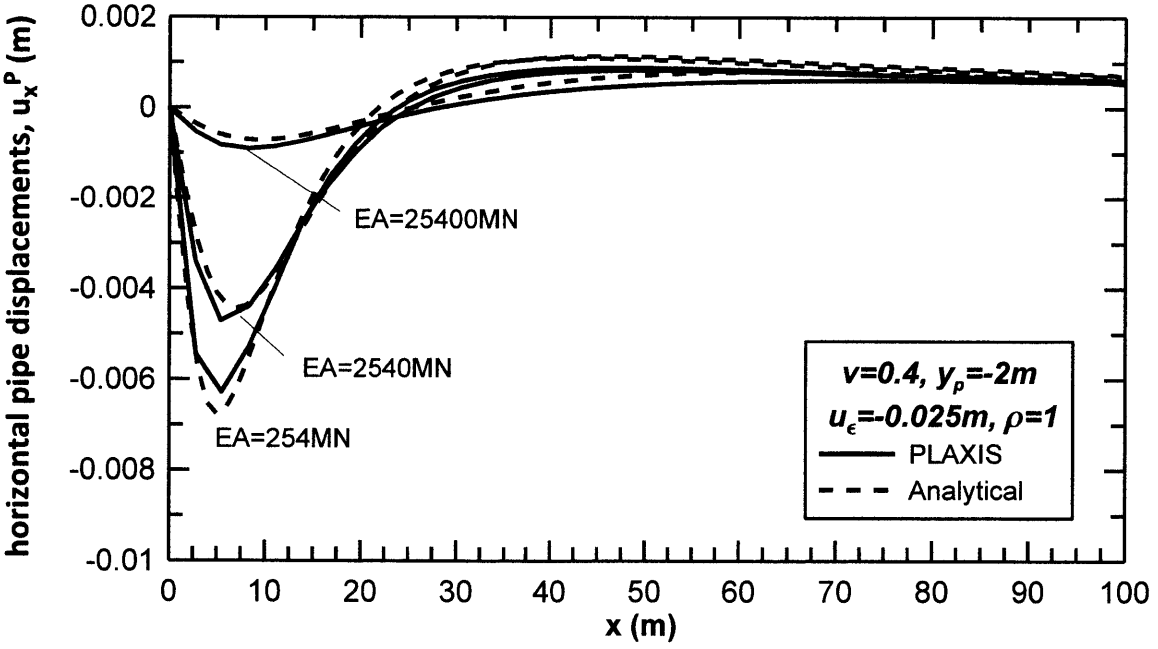
0.002
0
-0.002
-0.004
-0.006
-0.008
-0.01
horizontal pipe displacements, u_x^P (m)
EA=25400MN
EA=2540MN
EA=254MN
v=0.4, y_p=-2m
u_ϵ=-0.025m, ρ=1
PLAXIS
Analytical
0
10
20
30
40
50
60
70
80
90
100
x (m)

APPENDIX III

Axial, bending and total pipe strains and stresses acting on the hypothetical pipelines 40, 50, 60, 70, 80, 90 and 100, for low (Line 2) and high (Line 4) face pressure at N-2 San Francisco sewer tunnel case.

Note: Pipe number corresponds to the pipe diameter in cm

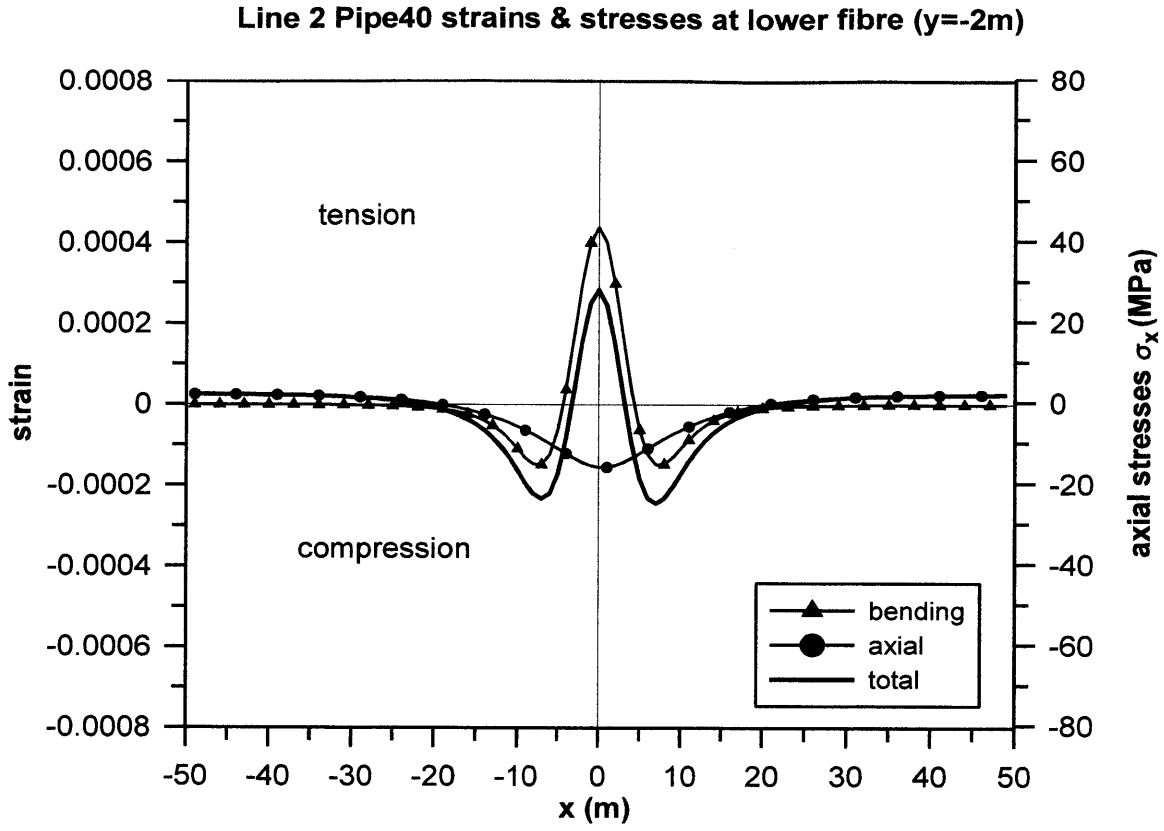
Line 2 Pipe40 strains & stresses at lower fibre (y=-2m)
strain
axial stresses σ_x (MPa)
x (m)
tension
compression
bending
axial
total
0.0008
0.0006
0.0004
0.0002
0
-0.0002
-0.0004
-0.0006
-0.0008
80
60
40
20
0
-20
-40
-60
-80
-50
-40
-30
-20
-10
0
10
20
30
40
50

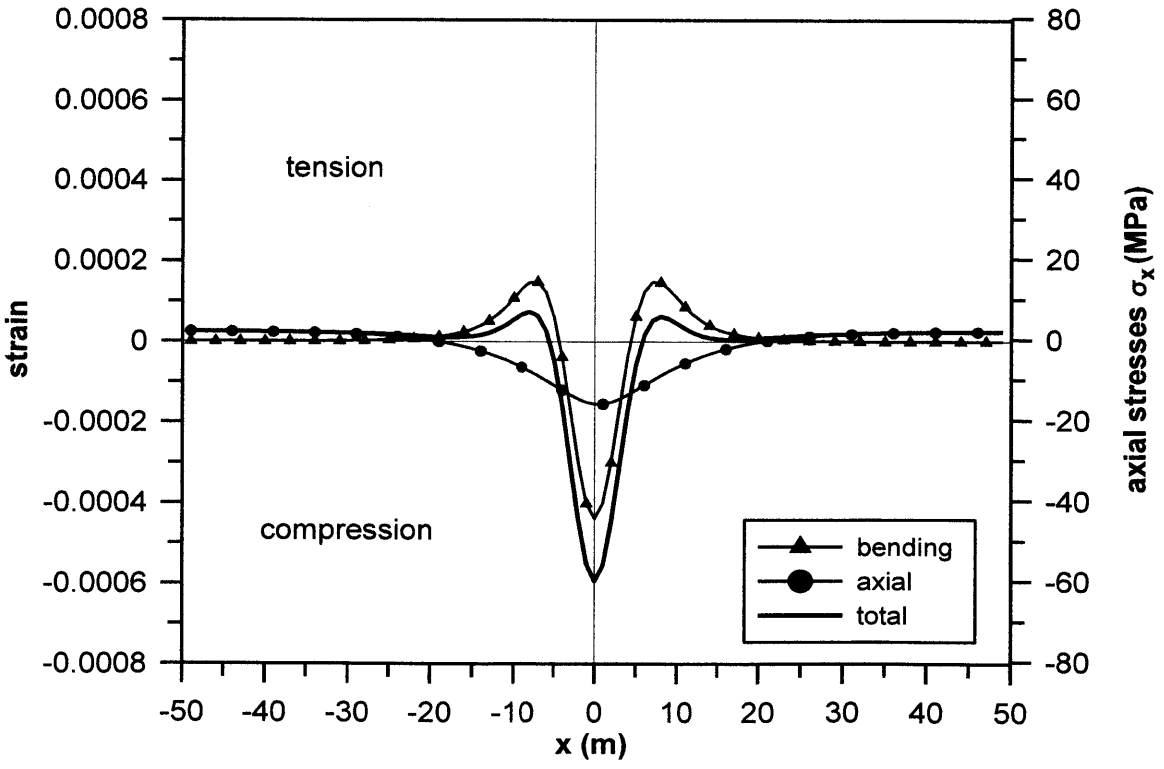
Line 2 Pipe40 strains & stresses at upper fibre (y=-2m)
strain
axial stresses σ_x (MPa)
x (m)
tension
compression
bending
axial
total
0.0008
0.0006
0.0004
0.0002
0
-0.0002
-0.0004
-0.0006
-0.0008
80
60
40
20
0
-20
-40
-60
-80
-50
-40
-30
-20
-10
0
10
20
30
40
50

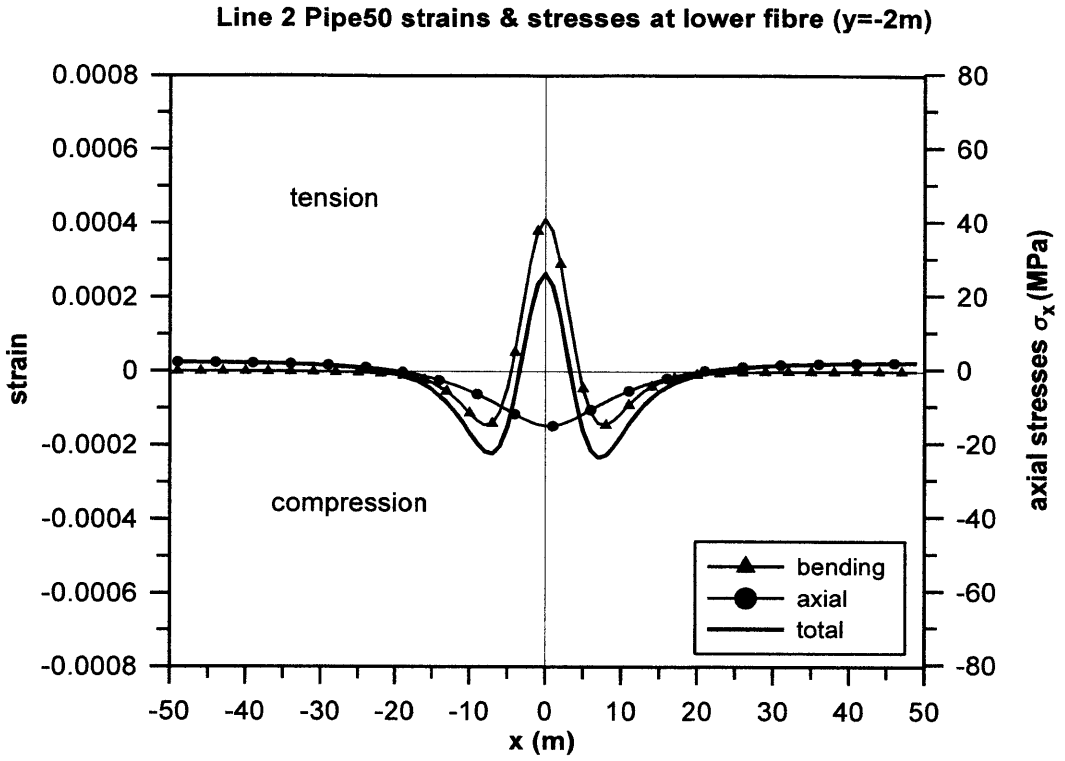
Line 2 Pipe50 strains & stresses at lower fibre (y=-2m)
strain
axial stresses σ_x (MPa)
x (m)
tension
compression
bending
axial
total
0.0008
0.0006
0.0004
0.0002
0
-0.0002
-0.0004
-0.0006
-0.0008
80
60
40
20
0
-20
-40
-60
-80
-50 -40 -30 -20 -10 0 10 20 30 40 50

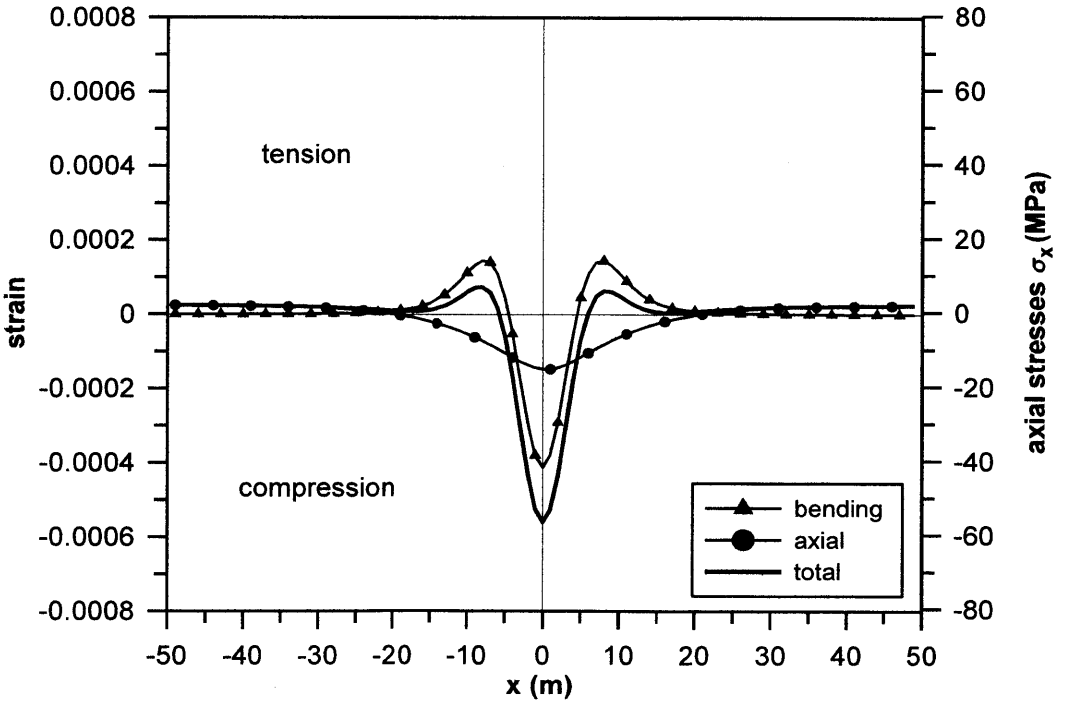
Line 2 Pipe50 strains & stresses at upper fibre (y=-2m)
strain
axial stresses σ_x (MPa)
x (m)
tension
compression
bending
axial
total
0.0008
0.0006
0.0004
0.0002
0
-0.0002
-0.0004
-0.0006
-0.0008
80
60
40
20
0
-20
-40
-60
-80
-50 -40 -30 -20 -10 0 10 20 30 40 50

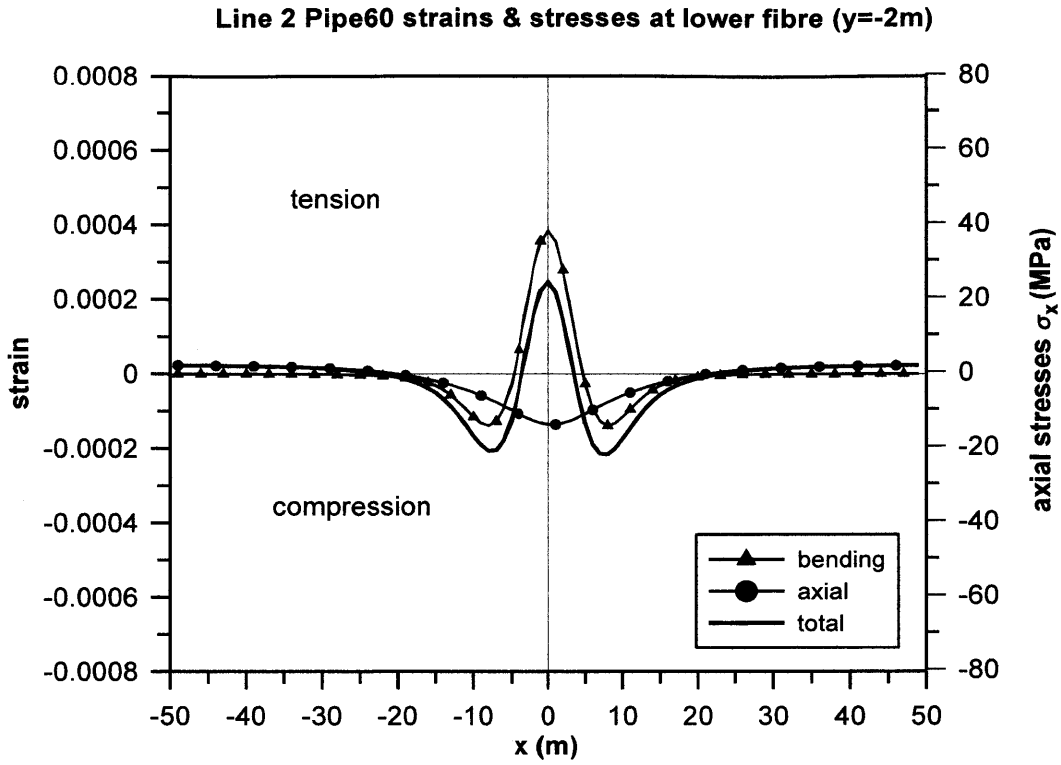
Line 2 Pipe60 strains & stresses at lower fibre (y=-2m)
strain
axial stresses σ_x(MPa)
x (m)
tension
compression
bending
axial
total
0.0008
0.0006
0.0004
0.0002
0
-0.0002
-0.0004
-0.0006
-0.0008
80
60
40
20
0
-20
-40
-60
-80
-50 -40 -30 -20 -10 0 10 20 30 40 50

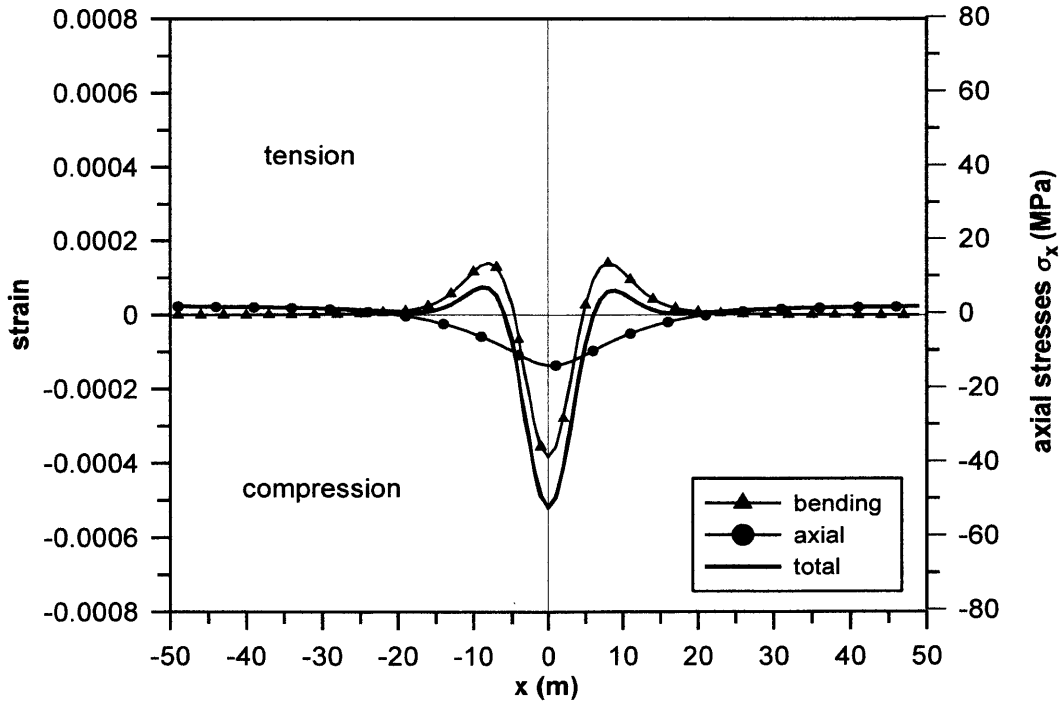
Line 2 Pipe60 strains & stresses at upper fibre (y=-2m)
strain
axial stresses σ_x(MPa)
x (m)
tension
compression
bending
axial
total
0.0008
0.0006
0.0004
0.0002
0
-0.0002
-0.0004
-0.0006
-0.0008
80
60
40
20
0
-20
-40
-60
-80
-50 -40 -30 -20 -10 0 10 20 30 40 50

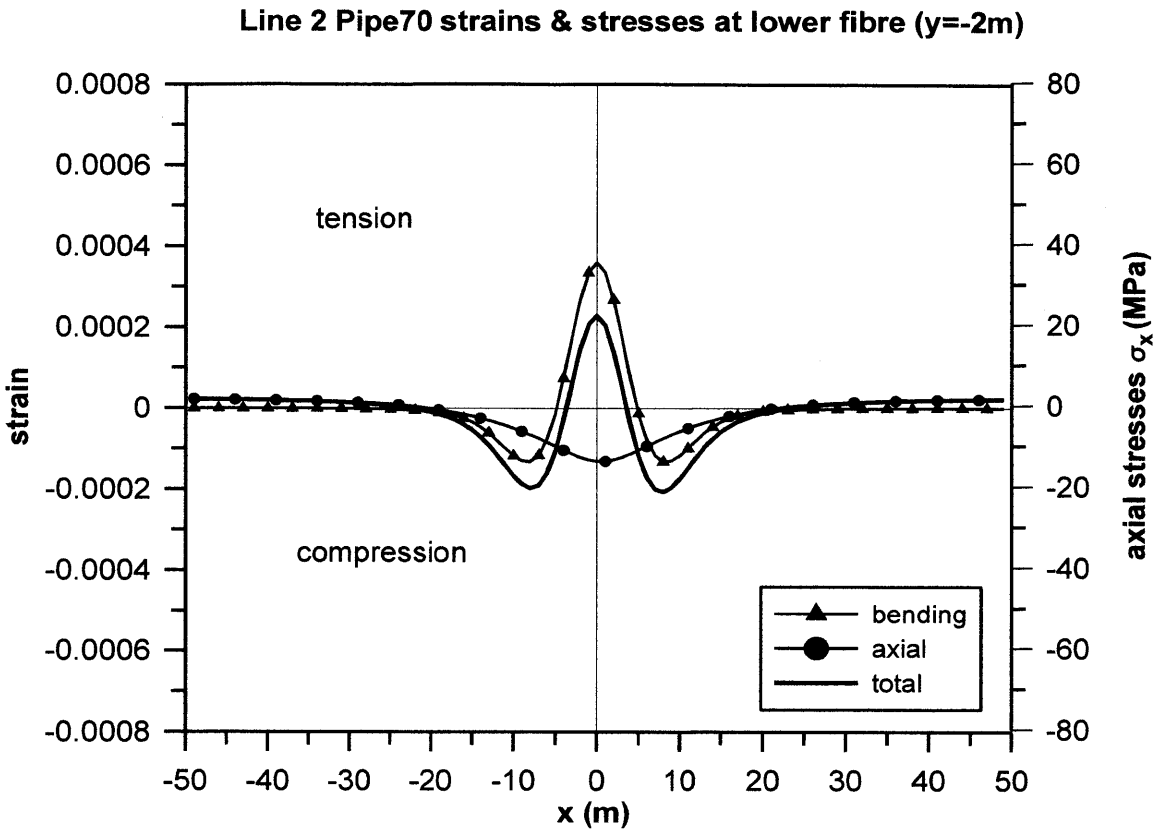
Line 2 Pipe70 strains & stresses at lower fibre (y=-2m)
strain
axial stresses σ_x (MPa)
x (m)
tension
compression
bending
axial
total
0.0008
0.0006
0.0004
0.0002
0
-0.0002
-0.0004
-0.0006
-0.0008
80
60
40
20
0
-20
-40
-60
-80
-50
-40
-30
-20
-10
0
10
20
30
40
50

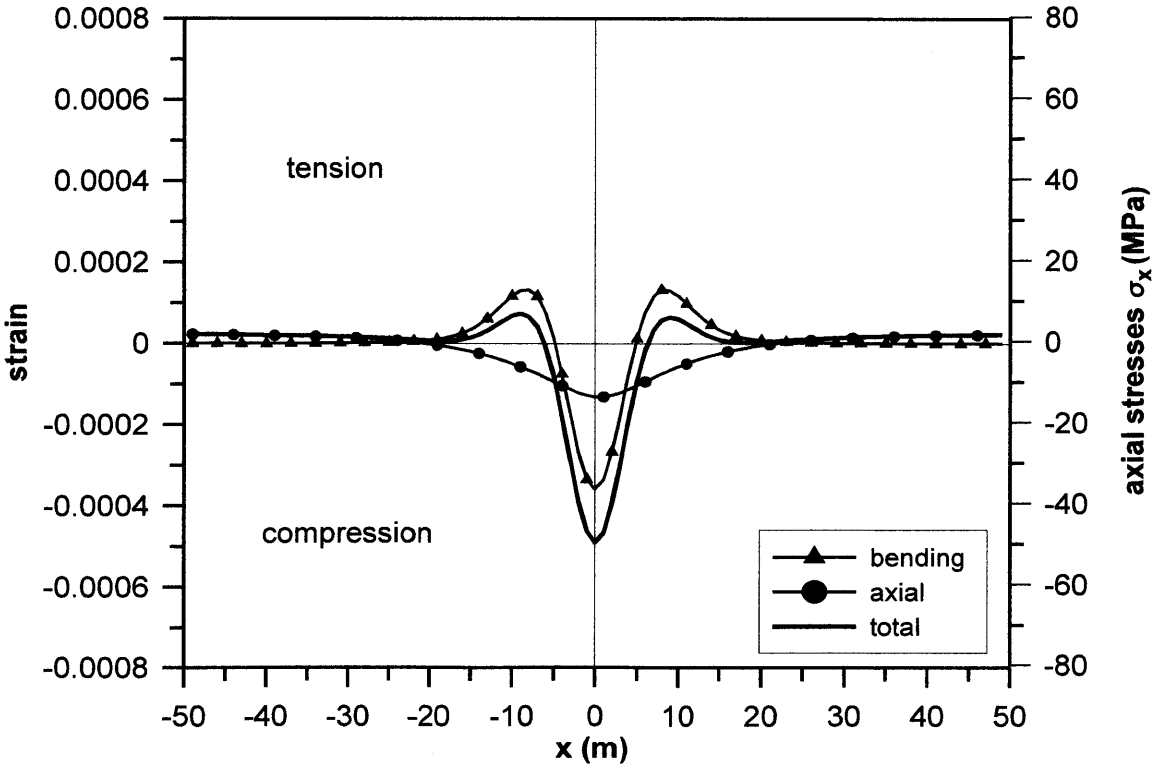
Line 2 Pipe70 strains & stresses at upper fibre (y=-2m)
strain
axial stresses σ_x (MPa)
x (m)
tension
compression
bending
axial
total
0.0008
0.0006
0.0004
0.0002
0
-0.0002
-0.0004
-0.0006
-0.0008
80
60
40
20
0
-20
-40
-60
-80
-50
-40
-30
-20
-10
0
10
20
30
40
50

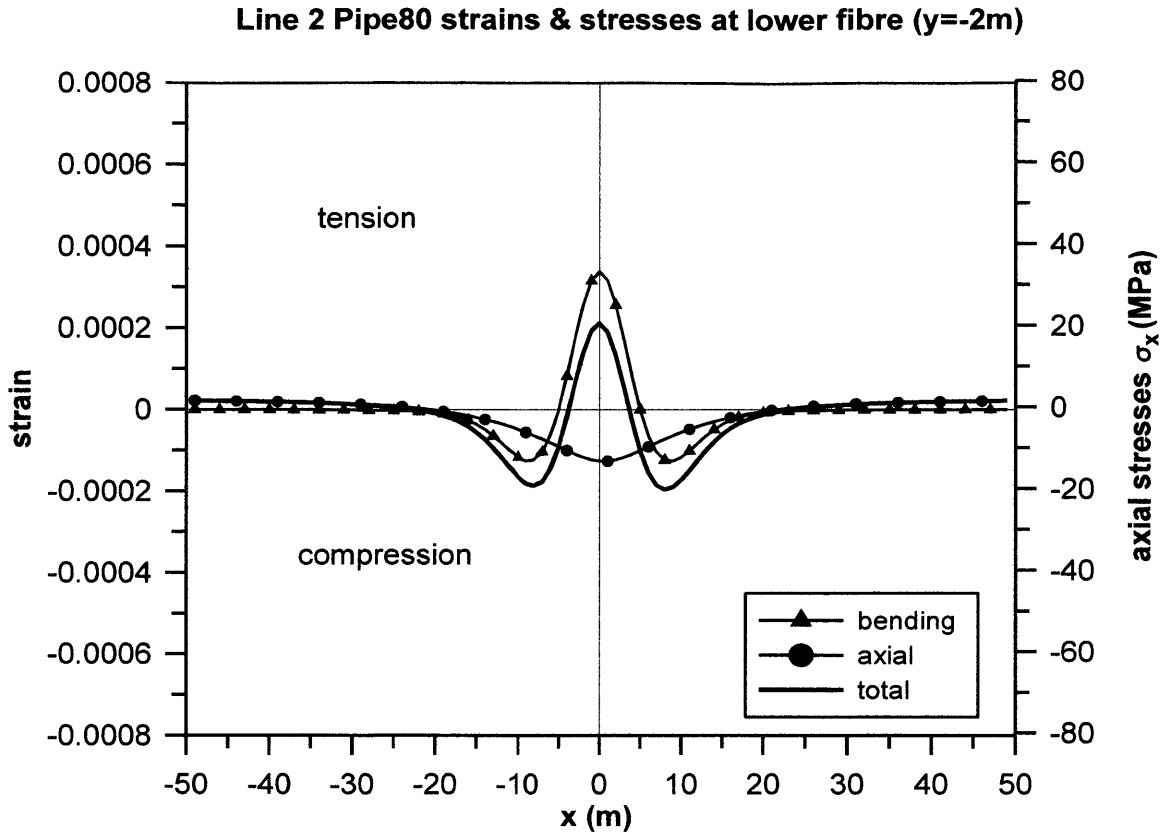
Line 2 Pipe80 strains & stresses at lower fibre (y=-2m)
strain
axial stresses σ_x (MPa)
x (m)
tension
compression
bending
axial
total
0.0008
0.0006
0.0004
0.0002
0
-0.0002
-0.0004
-0.0006
-0.0008
80
60
40
20
0
-20
-40
-60
-80
-50
-40
-30
-20
-10
0
10
20
30
40
50

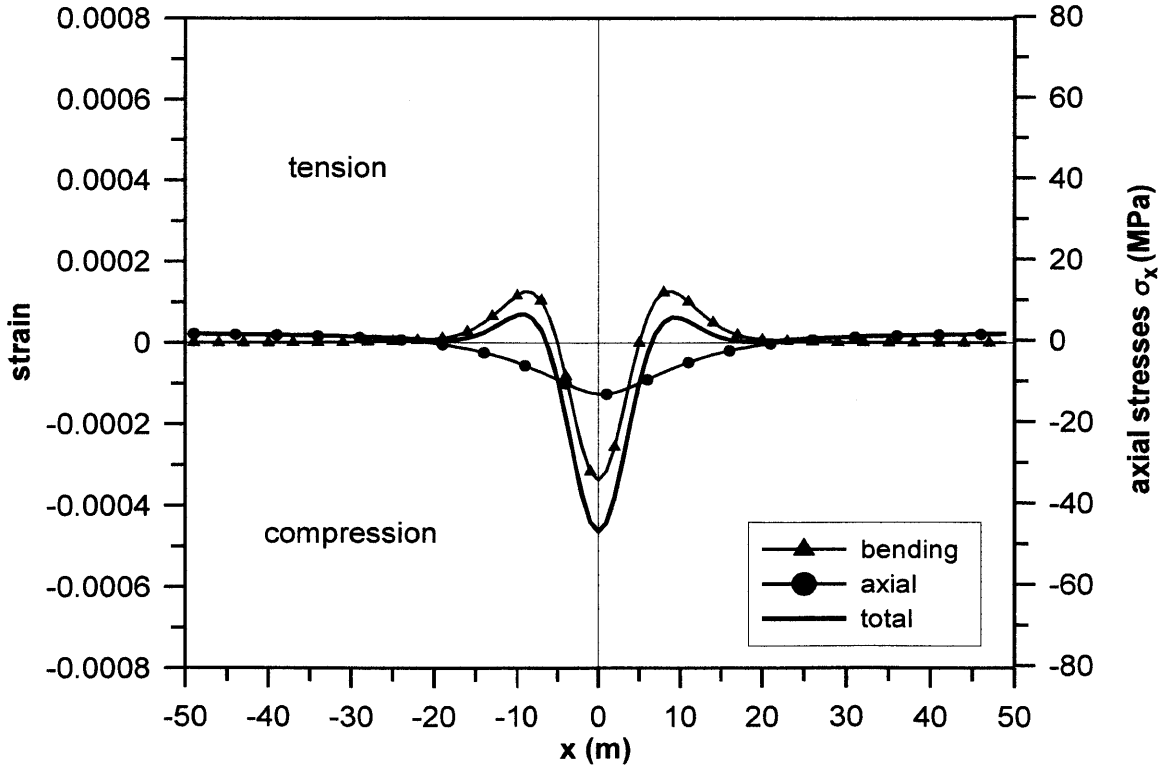
Line 2 Pipe80 strains & stresses at upper fibre (y=-2m)
strain
axial stresses σ_x (MPa)
x (m)
tension
compression
bending
axial
total
0.0008
0.0006
0.0004
0.0002
0
-0.0002
-0.0004
-0.0006
-0.0008
80
60
40
20
0
-20
-40
-60
-80
-50
-40
-30
-20
-10
0
10
20
30
40
50

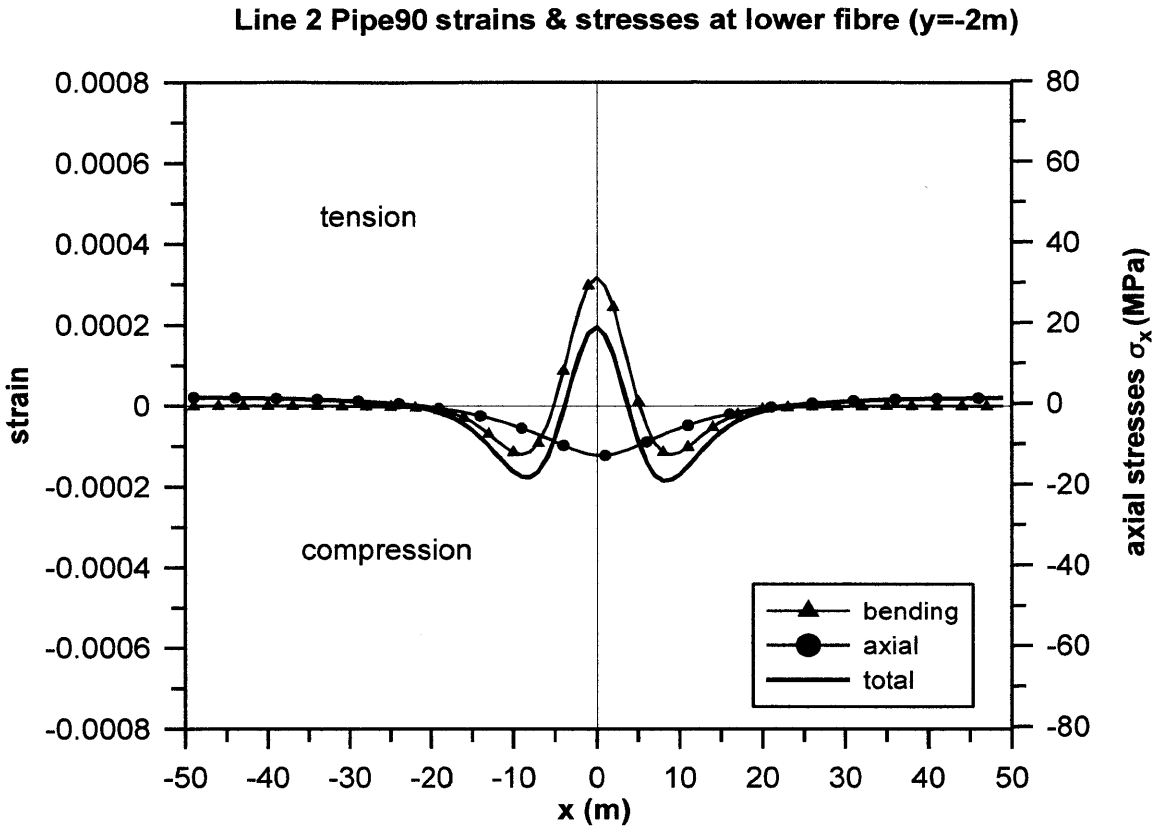
Line 2 Pipe90 strains & stresses at lower fibre (y=-2m)
strain
axial stresses σ_x (MPa)
x (m)
tension
compression
bending
axial
total
0.0008
0.0006
0.0004
0.0002
0
-0.0002
-0.0004
-0.0006
-0.0008
80
60
40
20
0
-20
-40
-60
-80
-50
-40
-30
-20
-10
0
10
20
30
40
50

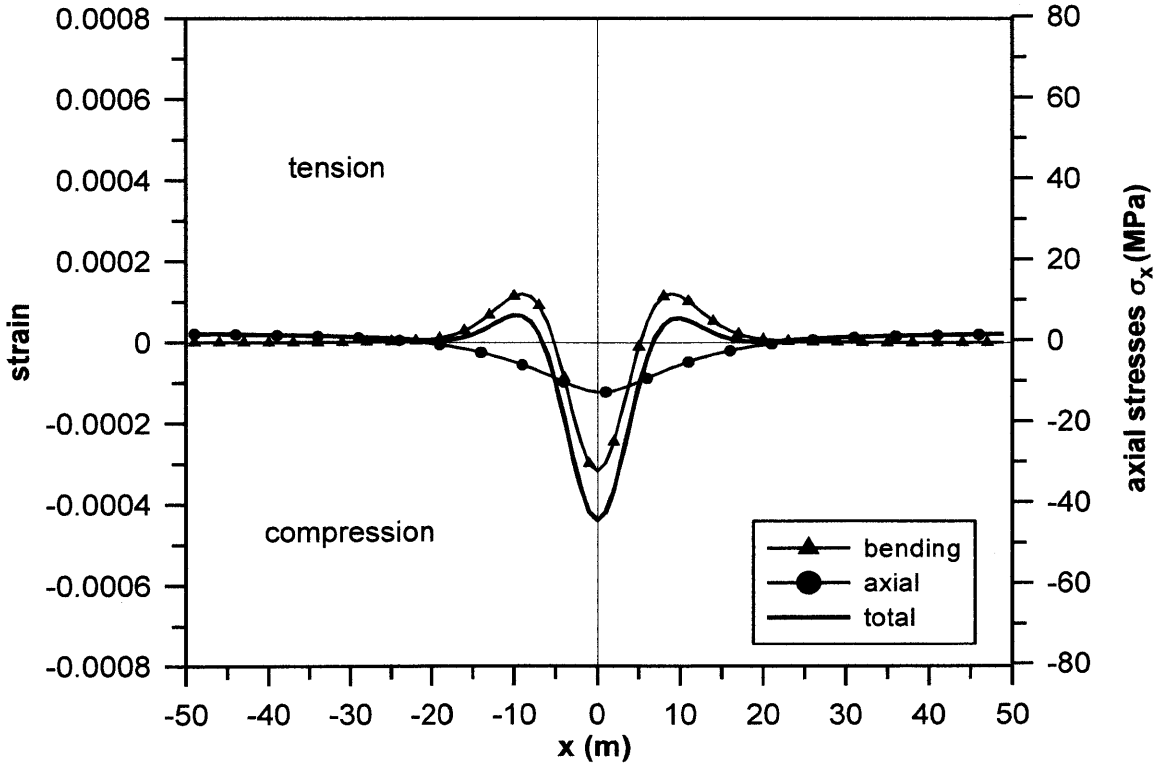
Line 2 Pipe90 strains & stresses at upper fibre (y=-2m)
strain
axial stresses σ_x (MPa)
x (m)
tension
compression
bending
axial
total
0.0008
0.0006
0.0004
0.0002
0
-0.0002
-0.0004
-0.0006
-0.0008
80
60
40
20
0
-20
-40
-60
-80
-50
-40
-30
-20
-10
0
10
20
30
40
50

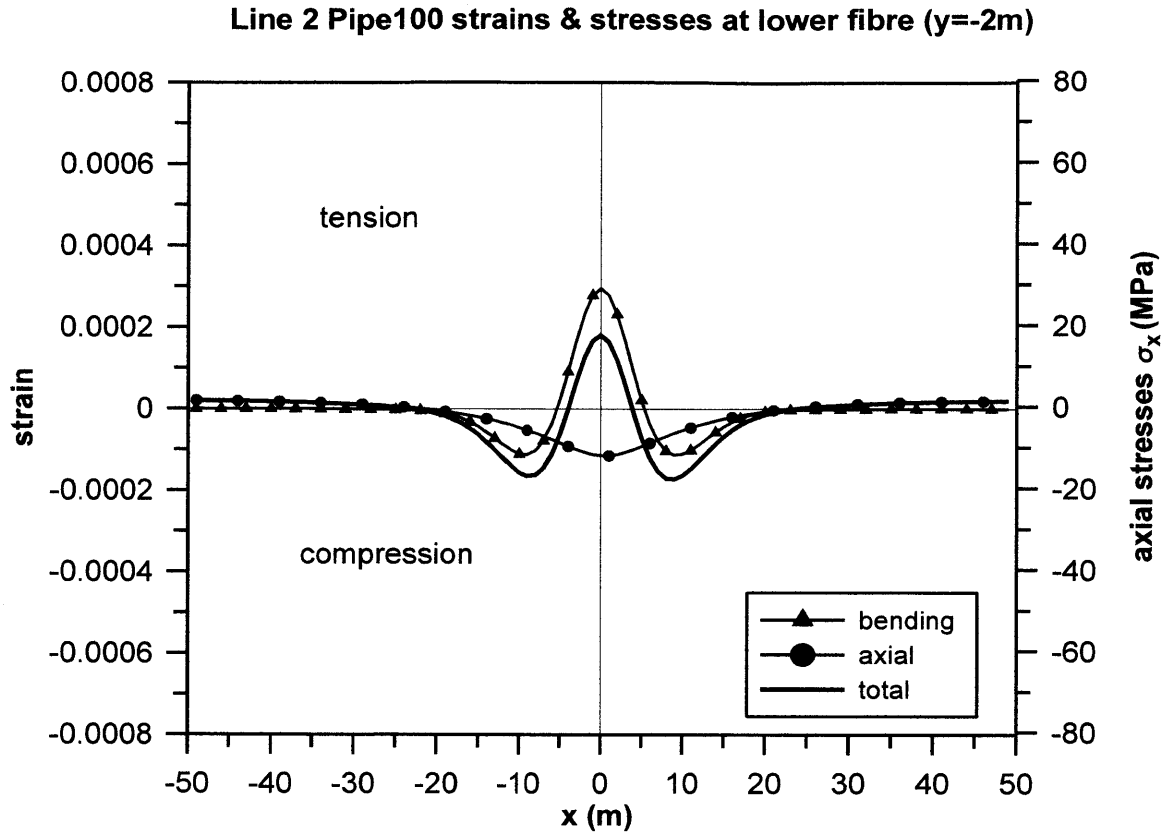
Line 2 Pipe100 strains & stresses at lower fibre (y=-2m)
strain
axial stresses σx (MPa)
tension
compression
bending
axial
total
x (m)
0.0008
0.0006
0.0004
0.0002
0
-0.0002
-0.0004
-0.0006
-0.0008
80
60
40
20
0
-20
-40
-60
-80
-50
-40
-30
-20
-10
0
10
20
30
40
50

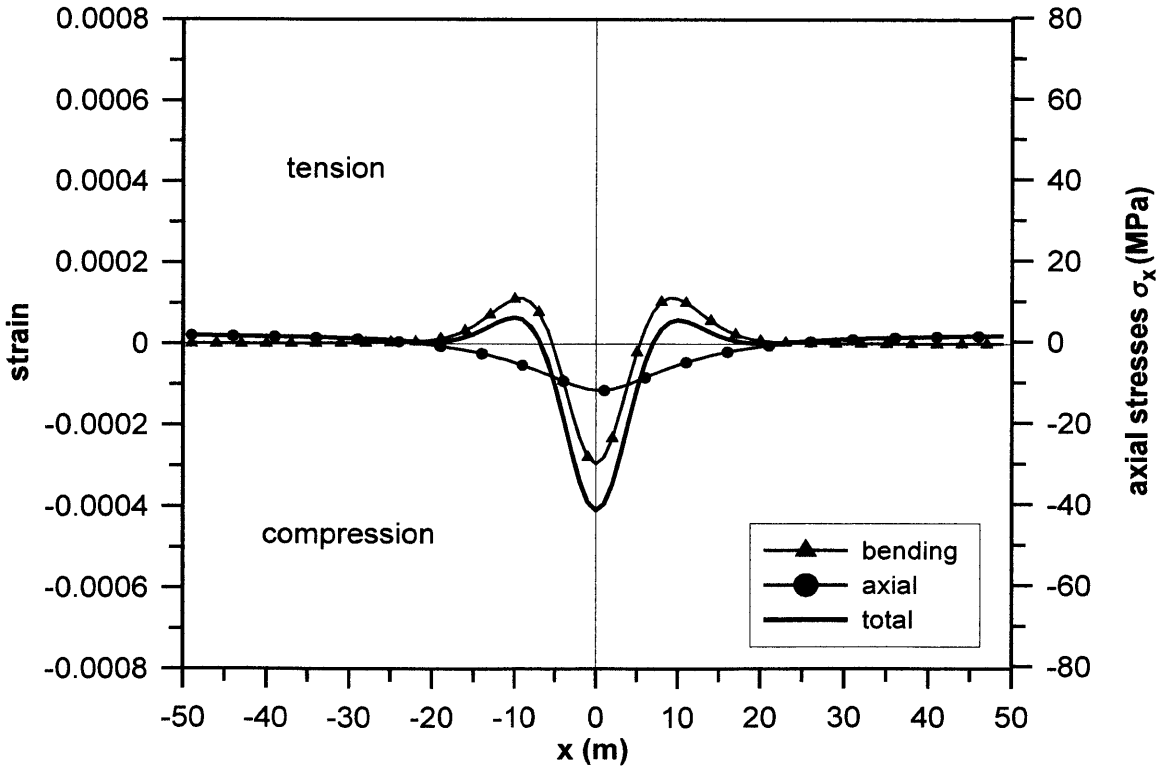
Line 2 Pipe100 strains & stresses at upper fibre (y=-2m)
strain
axial stresses σx (MPa)
tension
compression
bending
axial
total
x (m)
0.0008
0.0006
0.0004
0.0002
0
-0.0002
-0.0004
-0.0006
-0.0008
80
60
40
20
0
-20
-40
-60
-80
-50
-40
-30
-20
-10
0
10
20
30
40
50

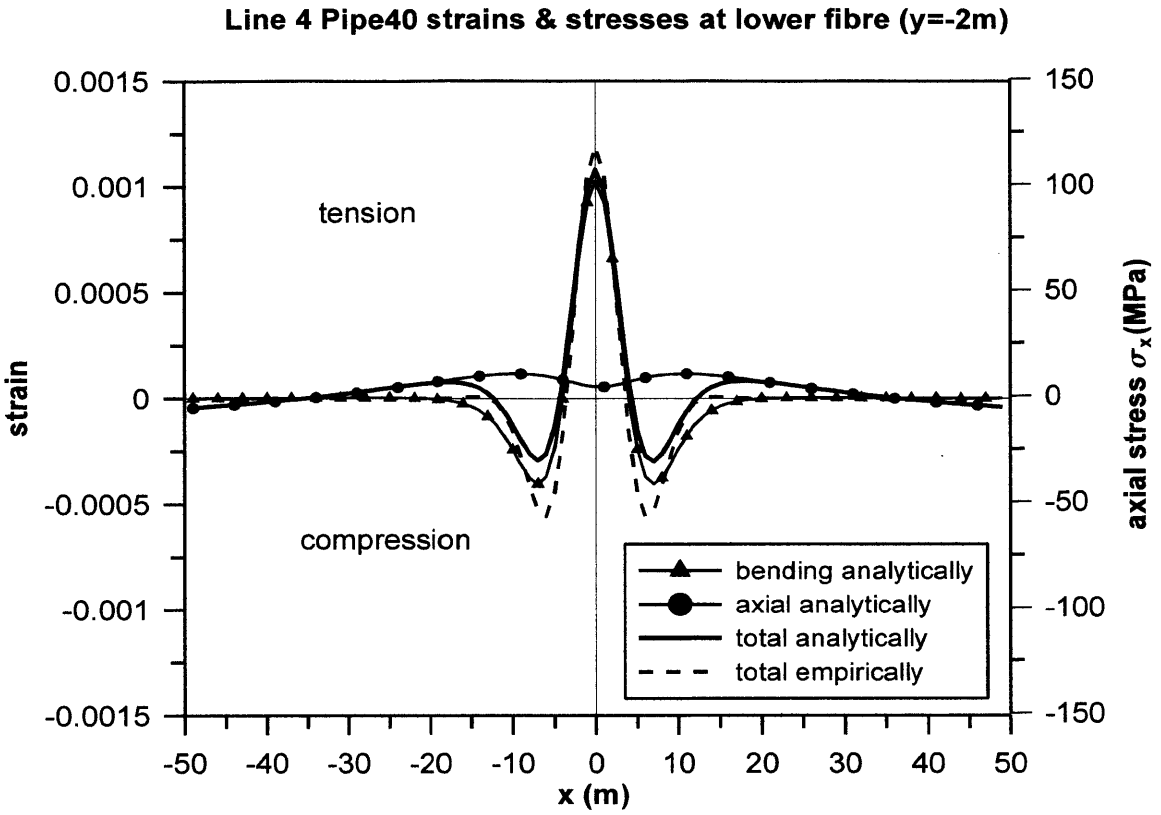
Line 4 Pipe40 strains & stresses at lower fibre (y=-2m)
strain
axial stress σ_x(MPa)
x (m)
tension
compression
bending analytically
axial analytically
total analytically
total empirically
0.0015
0.001
0.0005
0
-0.0005
-0.001
-0.0015
150
100
50
0
-50
-100
-150
-50 -40 -30 -20 -10 0 10 20 30 40 50

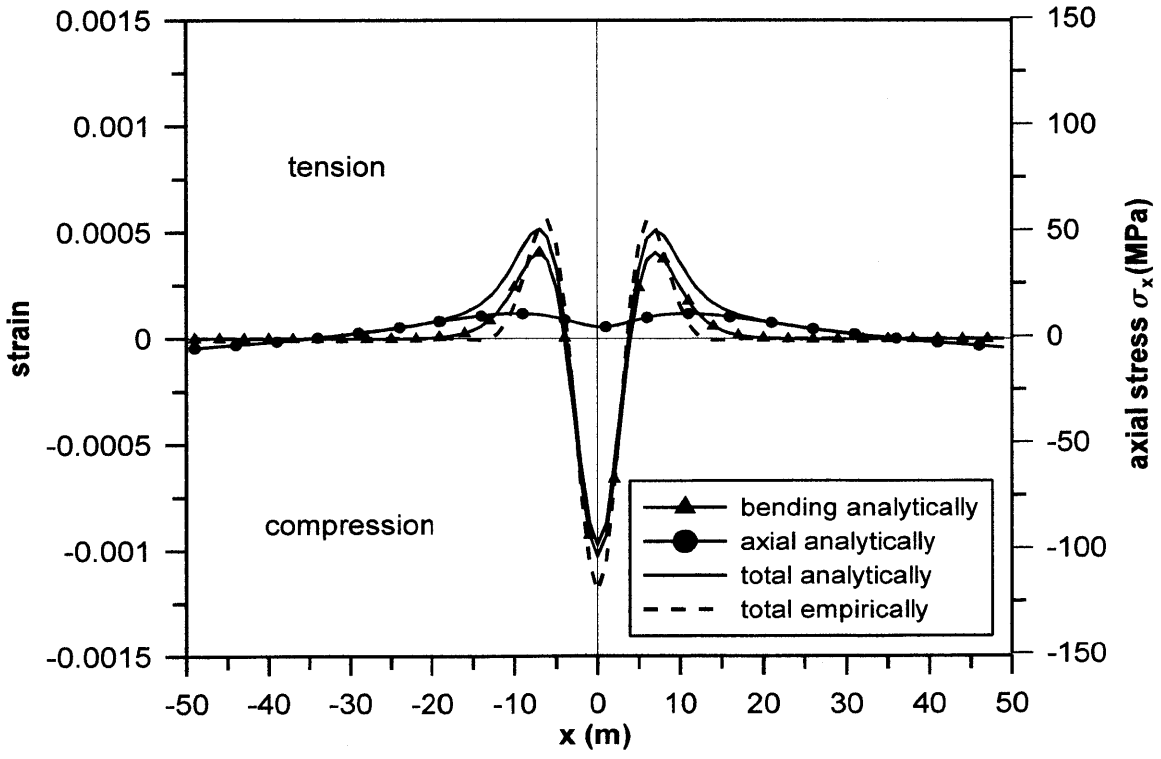
Line 4 Pipe40 strains & stresses at upper fibre (y=-2m)
strain
axial stress σ_x(MPa)
x (m)
tension
compression
bending analytically
axial analytically
total analytically
total empirically
0.0015
0.001
0.0005
0
-0.0005
-0.001
-0.0015
150
100
50
0
-50
-100
-150
-50 -40 -30 -20 -10 0 10 20 30 40 50

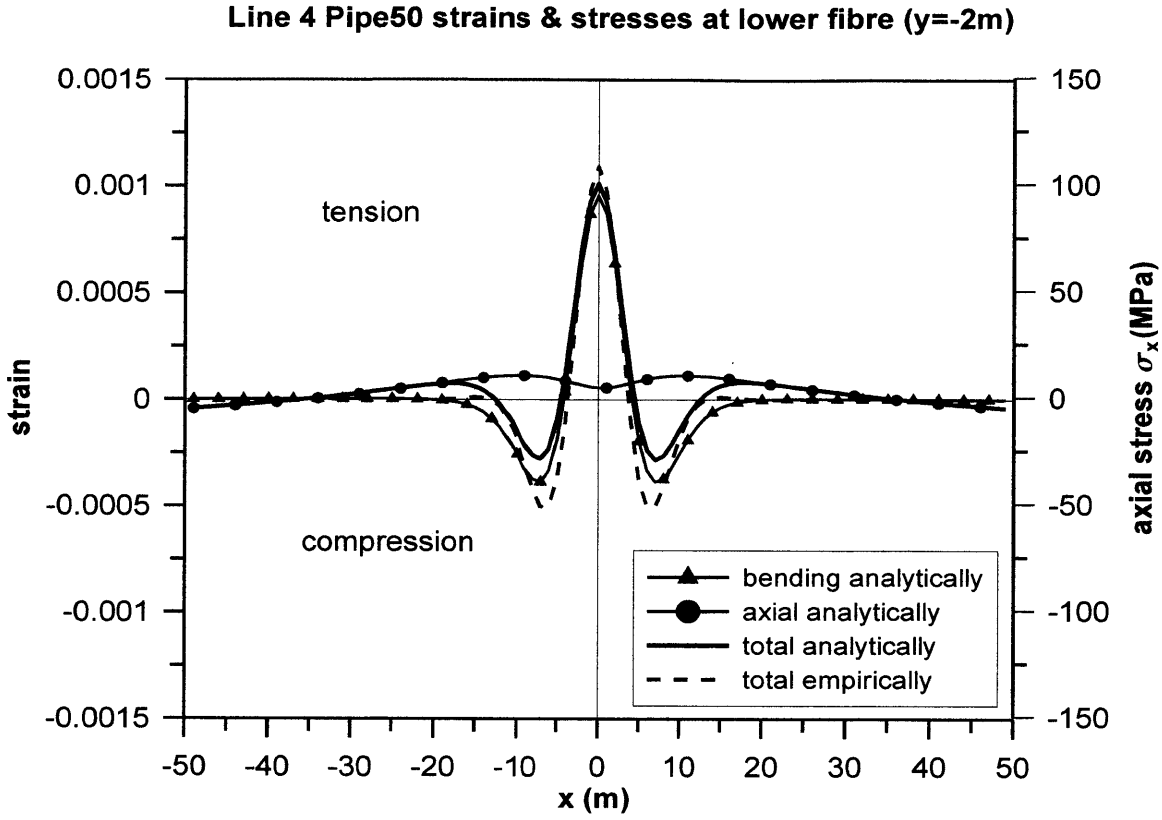
Line 4 Pipe50 strains & stresses at lower fibre (y=-2m)
0.0015
0.001
0.0005
0
-0.0005
-0.001
-0.0015
strain
150
100
50
0
-50
-100
-150
axial stress σ_x(MPa)
tension
compression
bending analytically
axial analytically
total analytically
total empirically
-50 -40 -30 -20 -10 0 10 20 30 40 50
x (m)

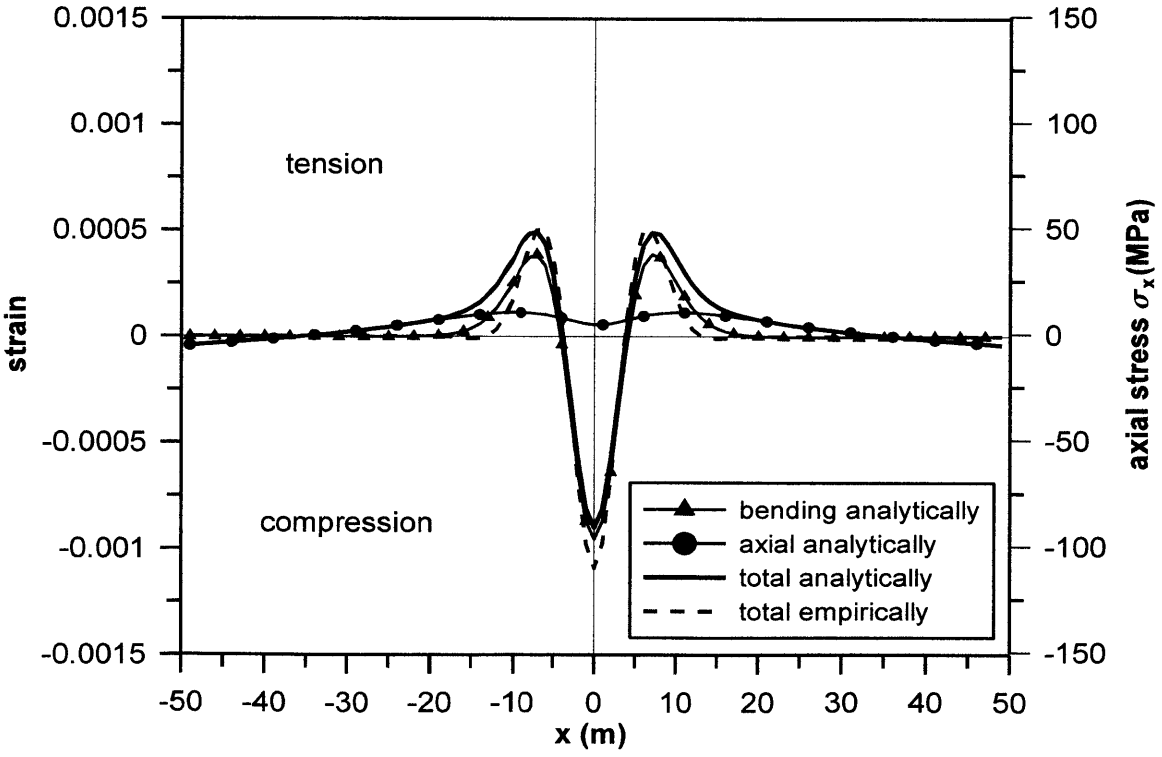
Line 4 Pipe50 strains & stresses at upper fibre (y=-2m)
0.0015
0.001
0.0005
0
-0.0005
-0.001
-0.0015
strain
150
100
50
0
-50
-100
-150
axial stress σ_x(MPa)
tension
compression
bending analytically
axial analytically
total analytically
total empirically
-50 -40 -30 -20 -10 0 10 20 30 40 50
x (m)

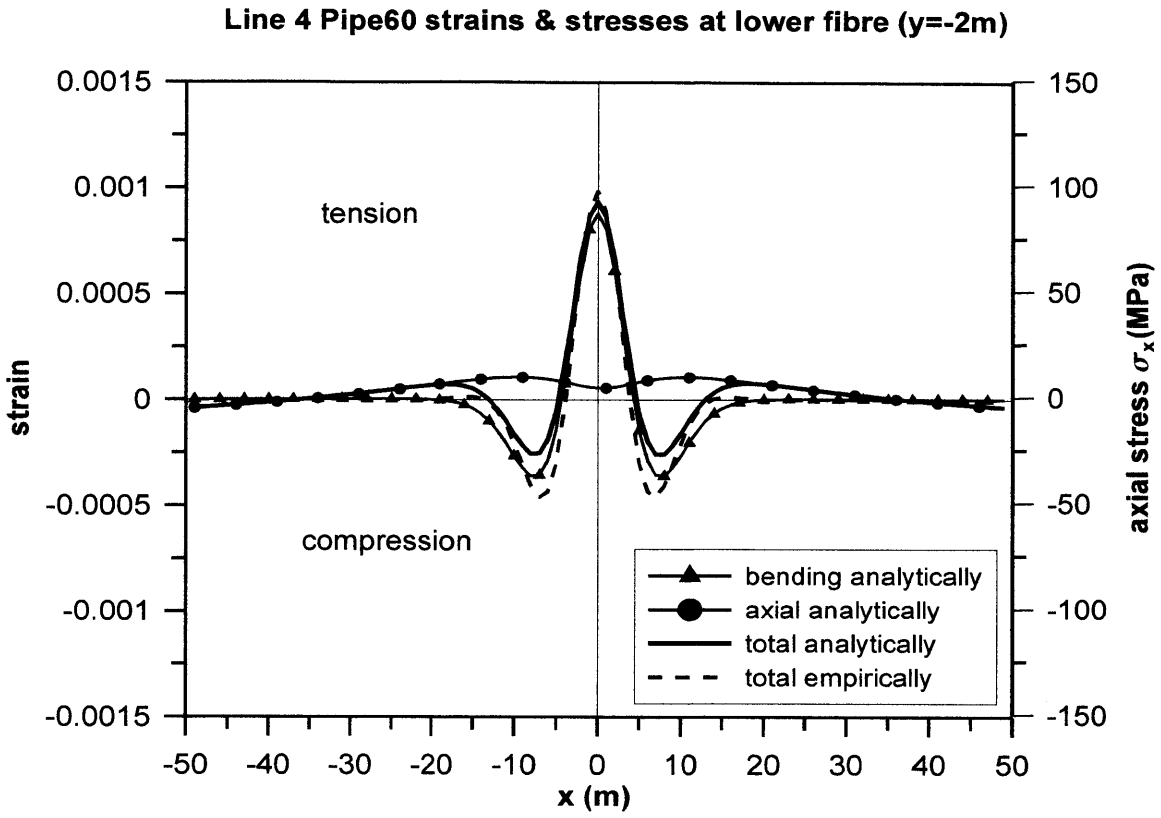
Line 4 Pipe60 strains & stresses at lower fibre (y=-2m)
strain
axial stress σ_x(MPa)
x (m)
tension
compression
bending analytically
axial analytically
total analytically
total empirically
0.0015
0.001
0.0005
0
-0.0005
-0.001
-0.0015
150
100
50
0
-50
-100
-150
-50 -40 -30 -20 -10 0 10 20 30 40 50

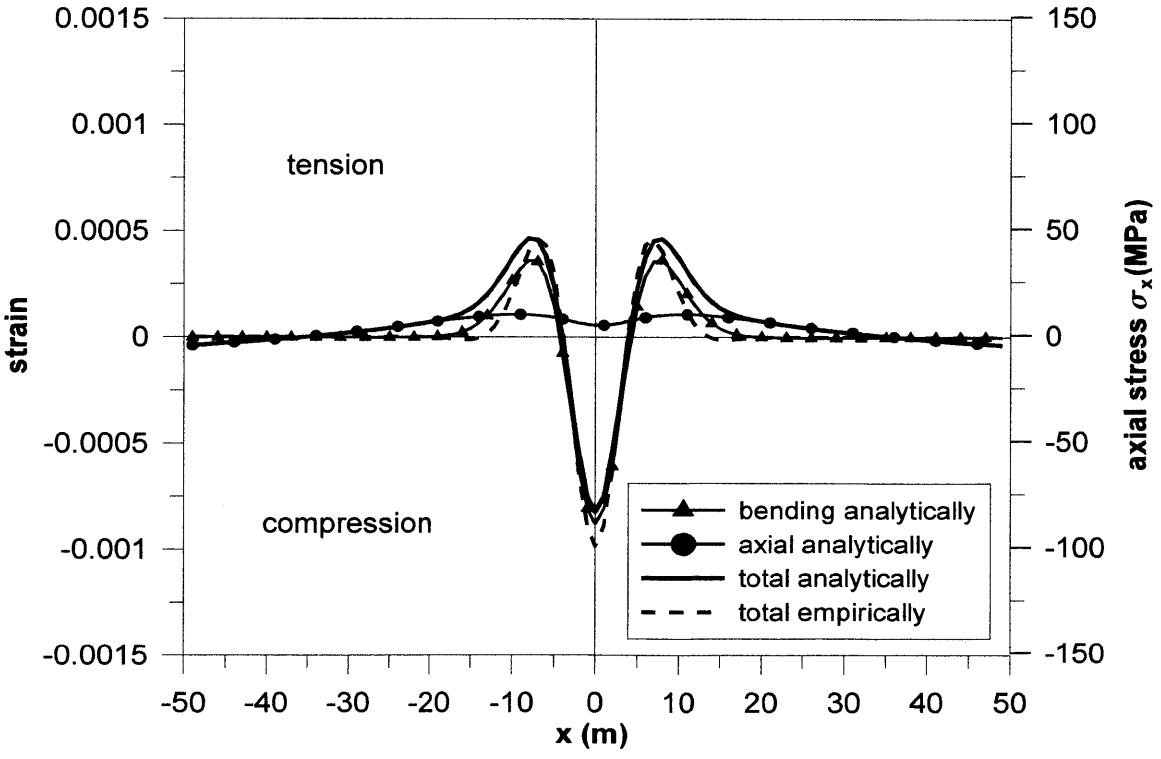
Line 4 Pipe60 strains & stresses at upper fibre (y=-2m)
strain
axial stress σ_x(MPa)
x (m)
tension
compression
bending analytically
axial analytically
total analytically
total empirically
0.0015
0.001
0.0005
0
-0.0005
-0.001
-0.0015
150
100
50
0
-50
-100
-150
-50 -40 -30 -20 -10 0 10 20 30 40 50

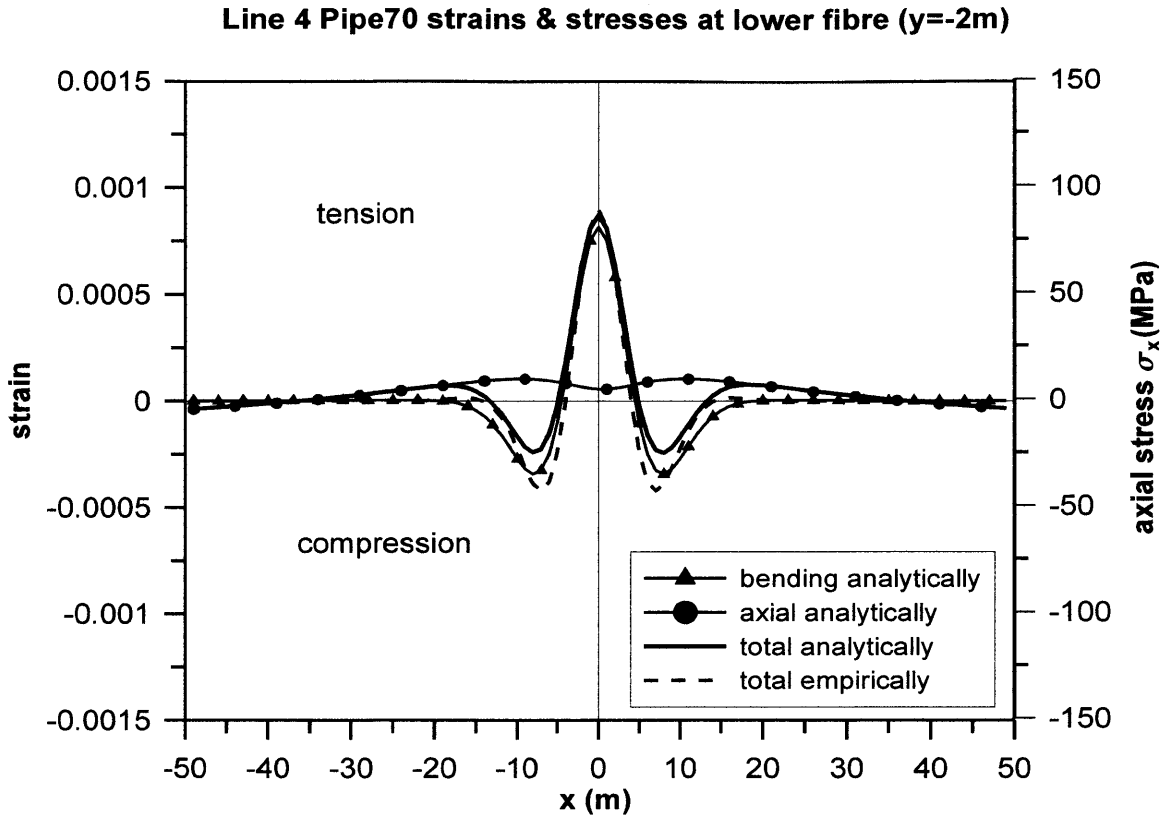
Line 4 Pipe70 strains & stresses at lower fibre (y=-2m)
strain
axial stress σ_x(MPa)
tension
compression
bending analytically
axial analytically
total analytically
total empirically
x (m)

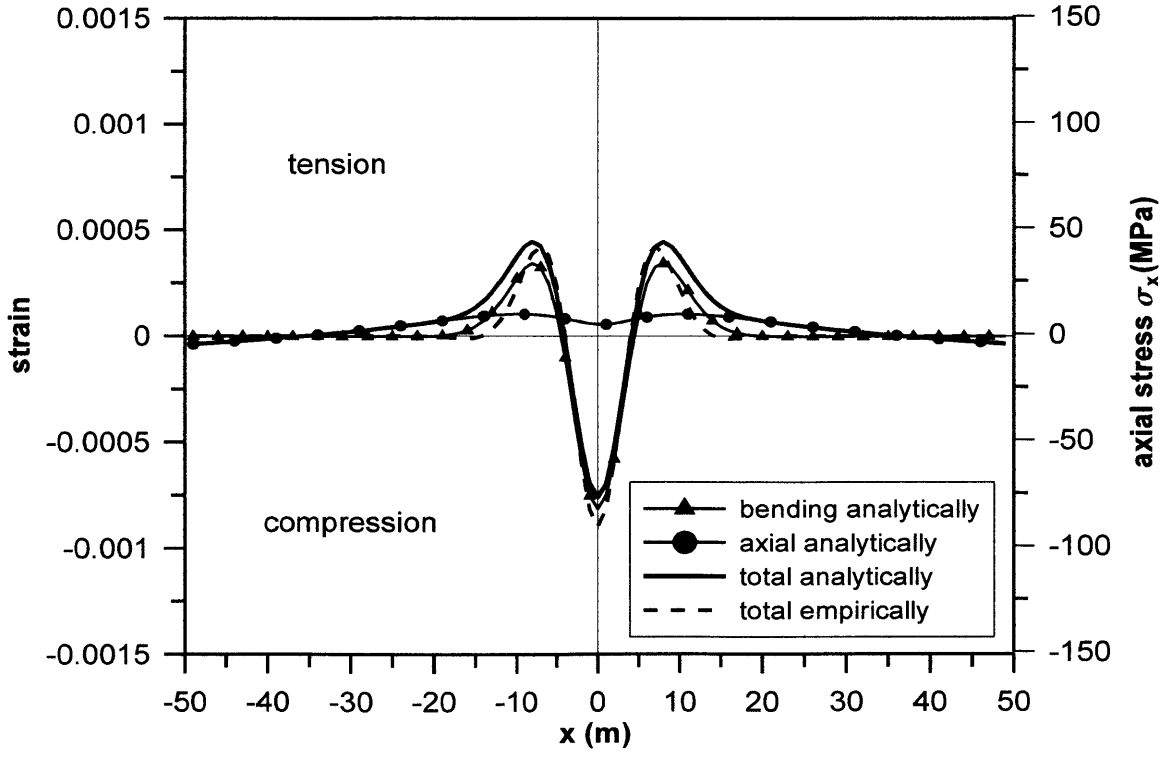
Line 4 Pipe70 strains & stresses at upper fibre (y=-2m)
strain
axial stress σ_x(MPa)
tension
compression
bending analytically
axial analytically
total analytically
total empirically
x (m)

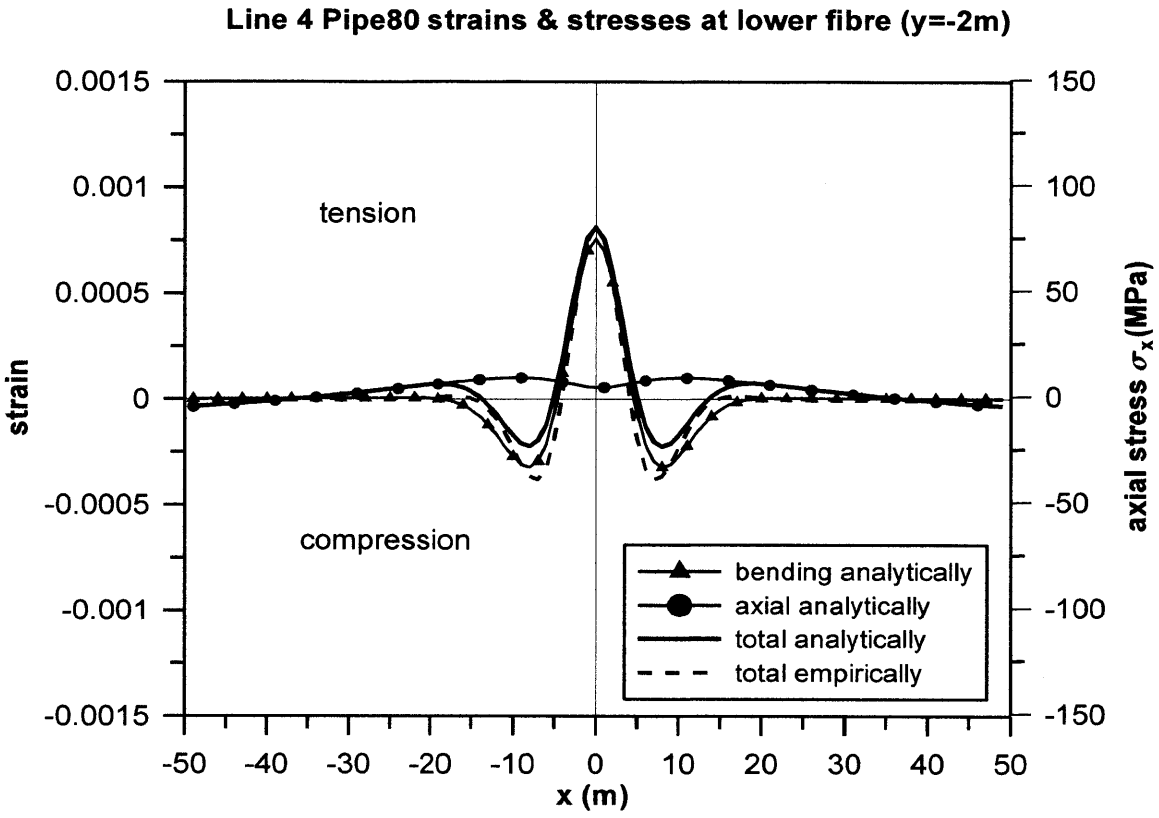
Line 4 Pipe80 strains & stresses at lower fibre (y=-2m)
strain
axial stress σ_x(MPa)
x (m)
tension
compression
bending analytically
axial analytically
total analytically
total empirically
0.0015
0.001
0.0005
0
-0.0005
-0.001
-0.0015
150
100
50
0
-50
-100
-150
-50 -40 -30 -20 -10 0 10 20 30 40 50

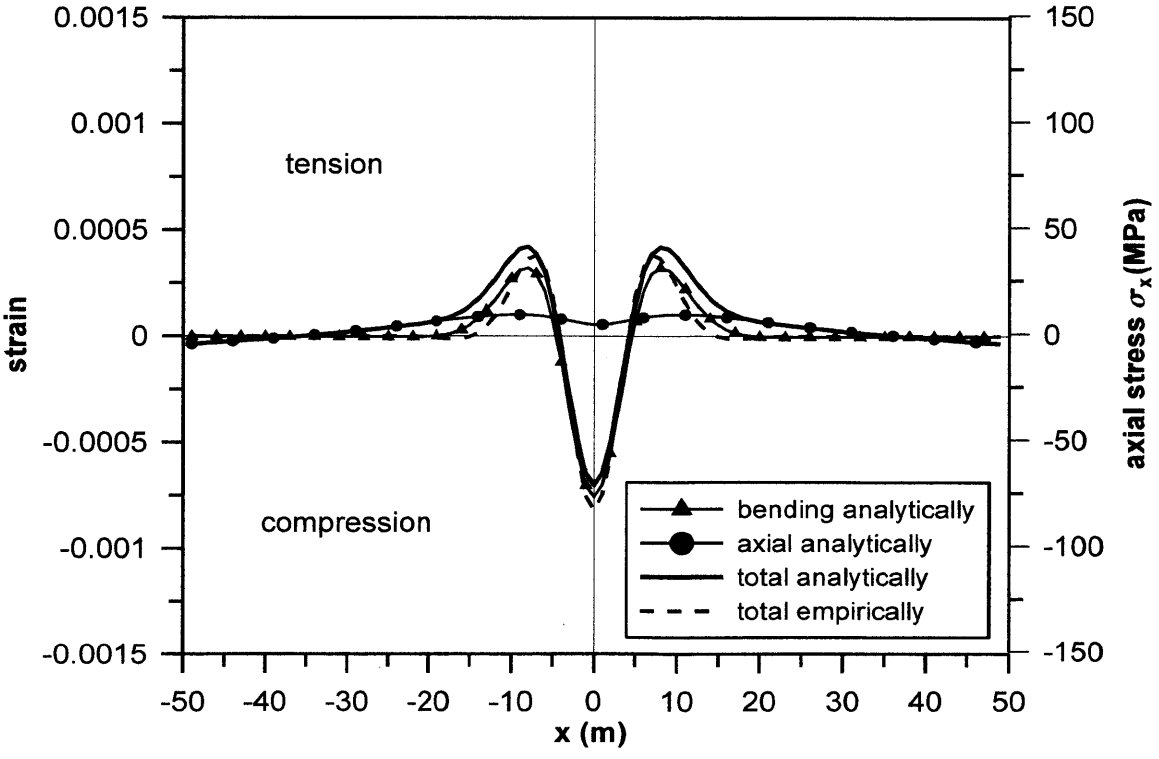
Line 4 Pipe80 strains & stresses at upper fibre (y=-2m)
strain
axial stress σ_x(MPa)
x (m)
tension
compression
bending analytically
axial analytically
total analytically
total empirically
0.0015
0.001
0.0005
0
-0.0005
-0.001
-0.0015
150
100
50
0
-50
-100
-150
-50 -40 -30 -20 -10 0 10 20 30 40 50

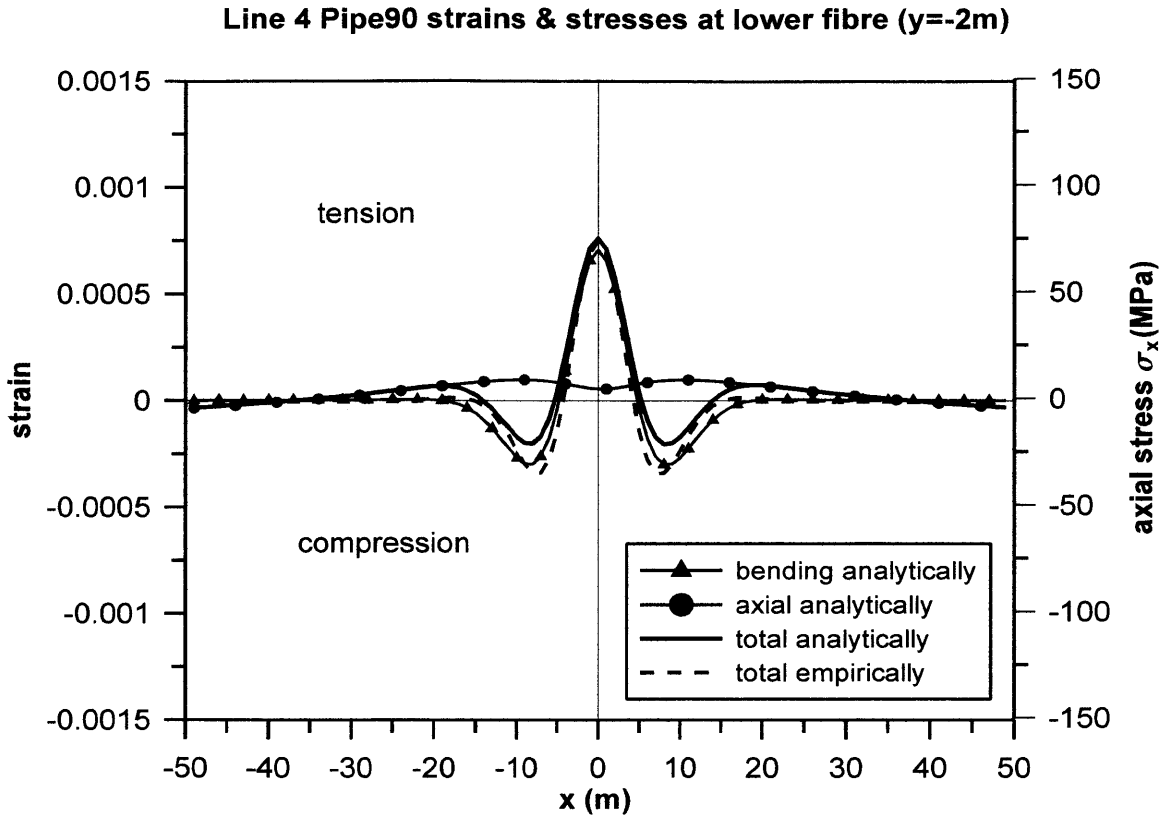
Line 4 Pipe90 strains & stresses at lower fibre (y=-2m)
strain
axial stress σ_x(MPa)
x (m)
tension
compression
bending analytically
axial analytically
total analytically
total empirically
0.0015
0.001
0.0005
0
-0.0005
-0.001
-0.0015
150
100
50
0
-50
-100
-150
-50 -40 -30 -20 -10 0 10 20 30 40 50

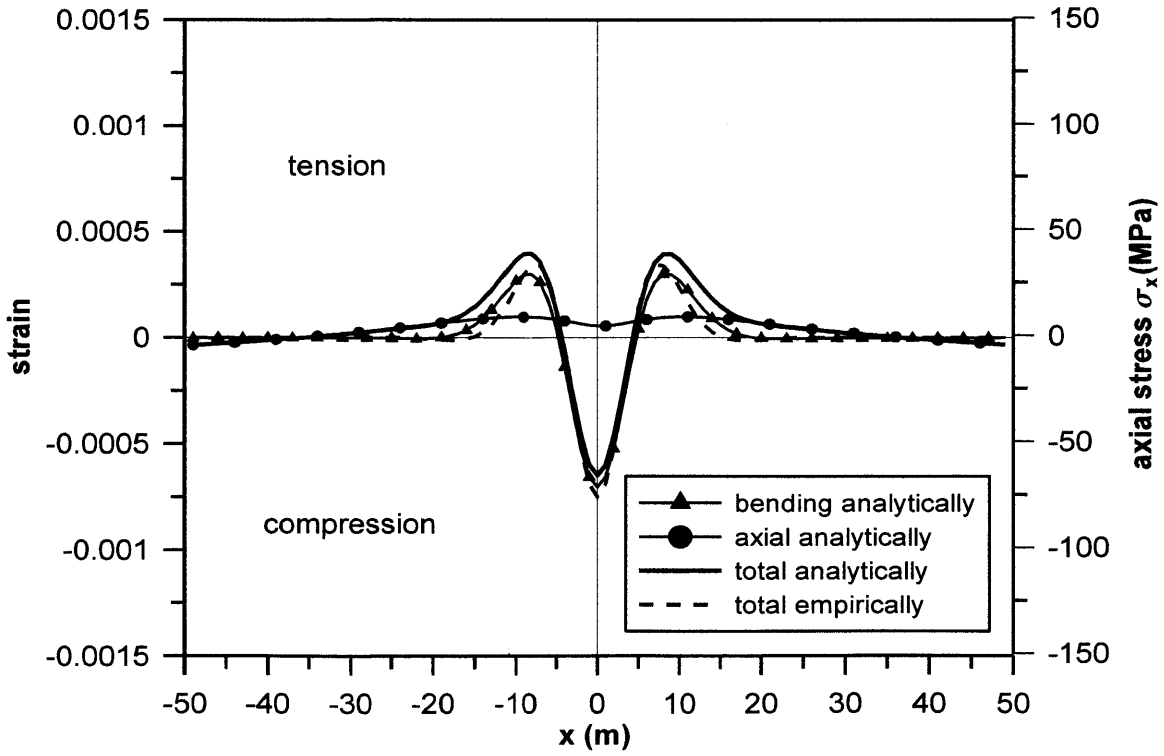
Line 4 Pipe90 strains & stresses at upper fibre (y=-2m)
strain
axial stress σ_x(MPa)
x (m)
tension
compression
bending analytically
axial analytically
total analytically
total empirically
0.0015
0.001
0.0005
0
-0.0005
-0.001
-0.0015
150
100
50
0
-50
-100
-150
-50 -40 -30 -20 -10 0 10 20 30 40 50

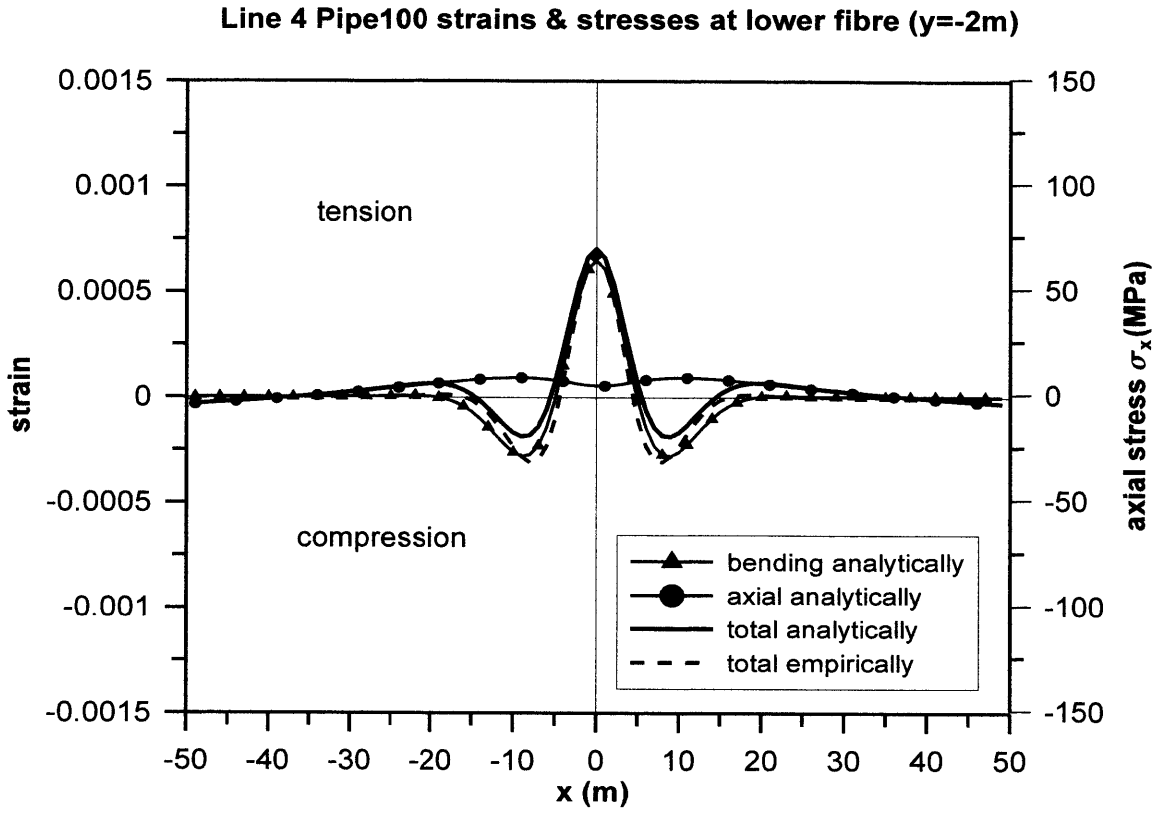
Line 4 Pipe100 strains & stresses at lower fibre (y=-2m)
strain
axial stress σ_x(MPa)
tension
compression
bending analytically
axial analytically
total analytically
total empirically
x (m)
0.0015
0.001
0.0005
0
-0.0005
-0.001
-0.0015
150
100
50
0
-50
-100
-150
-50 -40 -30 -20 -10 0 10 20 30 40 50

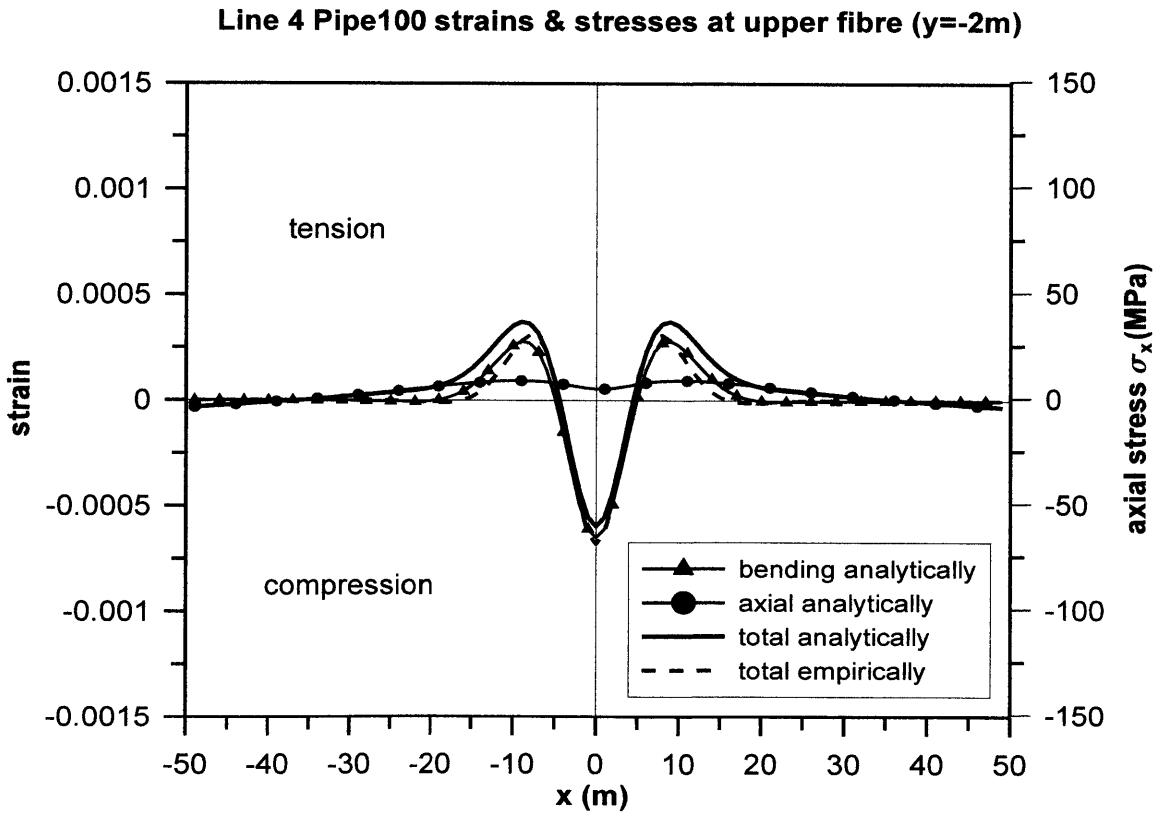
Line 4 Pipe100 strains & stresses at upper fibre (y=-2m)
strain
axial stress σ_x(MPa)
tension
compression
bending analytically
axial analytically
total analytically
total empirically
x (m)
0.0015
0.001
0.0005
0
-0.0005
-0.001
-0.0015
150
100
50
0
-50
-100
-150
-50 -40 -30 -20 -10 0 10 20 30 40 50